Proceedings

19th International Northern Research Basins Symposium and Workshop

Southcentral Alaska, USA – August 11–17, 2013

Editors:

Svetlana L. Stuefer and W. Robert Bolton

University of Alaska Fairbanks
Fairbanks, AK 99775, USA

Proceedings

19th International Northern Research Basins Symposium and Workshop

Southcentral Alaska, USA – August 11–17, 2013

ISBN: 978-0-615-86056-5

INE/WERC Report: 13.09

For additional copies of the proceedings, please contact:

Svetlana Stuefer
Dept. of Civil and Environmental Engineering
College of Engineering and Mines
University of Alaska Fairbanks
Fairbanks, AK 99775-5900, USA

Email: sveta.stuefer@alaska.edu

Preface

It is a pleasure to host the 19th International Northern Research Basins (NRB) Symposium and Workshop in the most northern state of the USA—Alaska. The subject of the 19th International NRB Symposium and Workshop—"Water Resources: Developments in a Changing Environment"—was broadly defined to accommodate topics on different aspects of hydrologic research and engineering in the Arctic. The symposium proceedings includes twenty-two papers and eighteen abstracts.

The organizing committee for the 19th International NRB created a program that provides settings for advancement and progress on hydrologic sciences in northern latitudes. Highlights of the symposium include a keynote speech on climate change in Alaska; an invited presentation about the proposed Susitna-Watana Hydroelectric Project; a field trip on the Susitna River; invited talks by state and federal authorities about hydrologic challenges in Alaska; and a visit to one of the most distinct areas in Alaska—the Kenai Fjords National Park, with its abundant wildlife and tidewater glaciers flowing down from the Harding Icefield.

The organizing committee would like to thank our invited speakers:

> John Walsh, Chief Scientist, International Arctic Research Center, for giving the keynote address: "Alaska in a Changing Climate: Wetter or Drier?"
>
> Wayne Dyok, Project Manager, Alaska Energy Authority, for presenting "Susitna-Watana Hydro: Clean, Reliable Power for 100 Years."
>
> Lynn Kent, Deputy Commissioner, Alaska Department of Environmental Conservation, for giving the state perspective on "Current Climate and Water Challenges in Alaska."
>
> Leslie Holland-Bartels, Regional Director for Alaska, U.S. Geological Survey, for presenting "A Federal Perspective of Water Resources Needs and Challenges of the North."

The Northern Research Basins Working Group was established in 1975 under the International Hydrological Program (IHP) by members from Canada, Denmark, Finland, Norway, Sweden, the USA, and the former USSR. Iceland joined in 1992, and the Russian Federation replaced the USSR in 1991. In addition, countries with polar research programs are eligible for associate membership. The objectives of the NRB Working Group have evolved over the years as follows:

1. To gain a better understanding of hydrologic processes, particularly those in which snow, ice, and frozen ground have a major influence on the hydrological regime, and to determine the relative importance of each component of the water balance.
2. To provide data for the development and testing of transposable models which may be applied to regional, national, and international water and land resource programs.
3. To relate hydrologic processes to the chemical and biological evolution of northern basins.
4. To assess and predict the effect of human activities on the hydrologic regime in northern environments.

5. To encourage the exchange of personnel (technicians, scientists, research officers, and others) among participating countries.
6. To provide information for the improvement and standardization of measurement techniques and network design in northern regions.
7. To encourage exchange of information on a regular basis, and
8. To set up task forces to promote research initiatives on topics of special interest to northern research basins.

To address these objectives, an international group of scientists, engineers, professors, and students from the circumpolar North meets every two years. During the meetings, the group discusses task forces to address specific questions about northern hydrology. Two task forces were discussed at the NRB meetings in Canada (2007) and in Norway (2009): "Predictions in ungauged basins" and "Observations of solid precipitation." A new possible task force, "Integration of cold regions science for societal needs," was suggested at the 18th NRB. The work on task forces continues between the meetings, with the results presented every two years at the NRB symposium during the task force workshop. The terms of reference for research task forces were formulated in the proceedings of the 9th International NRB Symposium and Workshop. A reprint of these terms is available in the conference program.

Acknowledgments
The organizers of the 19th International NRB Symposium and Workshop would like to thank the following organizations for their contributions and sponsorship:

Alaska Climate Science Center (AK CSC)
University of Alaska Fairbanks (UAF)
Institute of Northern Engineering (INE)
Water and Environmental Research Center (WERC)
International Arctic Science Committee (IASC)
Alaska Experimental Program to Stimulate Competitive Research (EPSCoR)

Without the generous support of these groups, this symposium would not have occurred. Special recognition is given to all who helped with the production of this symposium and workshop. Technical editor Grace Pedersen assisted with the formatting, compilation, and proofreading of the conference proceedings. Web designer Melanie Rohr created the logo, website, proceedings cover, and symposium program. Undergraduate student Emma Martin joined the organizers this summer and facilitated many logistical aspects of the symposium. Information technology specialist Peter Prokein managed the online services for registration fee payments. Fiscal officer Nomie Torres and grant manager Crystal Iacono provided prompt and efficient help with all fiscal matters. The work of all these individuals is extremely appreciated.

On behalf of the 19th International NRB organizing committee, I would like to welcome all participants and wish you all an excellent symposium!

Svetlana Stuefer
Chair, 19th International NRB Symposium and Workshop
Chief Delegate, U.S. Northern Research Basins Working Group

Symposium Organizing Committee

Detailed information about the 19th International NRB Symposium and Workshop can be found on the web at http://www.19thnrb.com/.

Table of Contents

Preface i

Symposium Organizing Committee iii

List of Participants ix

Symposium Papers 1

Hydrologic Connectivity and Dissolved Organic Carbon Fluxes in Low-Gradient High Arctic Wetland Ponds, Polar Bear Pass, Bathurst Island, Canada
Abnizova, A., Young, K.L., and Lafrenière, M.J. 3

Spatial and Temporal Variation in the Spring Freshet of Major Circumpolar Arctic River Systems: A CROCWR Component
Ahmed, R., Prowse, T.D., Dibike, Y.B., and Bonsal, B.R. 15

The Features of Suspended Sediment Yield in Rivers in Kamchatka, Far East Russia
Alekseevsky, N.I., and Kuksina, L.V. 25

Kenai Peninsula Precipitation and Air Temperature Trend Analysis
Bauret, S., and Stuefer, S.L. 35

An Analysis of Spatial and Temporal Trends and Patterns in Western Canadian Runoff: A CROCWR Component
Bawden, A.J., Burn, D.H., and Prowse, T.D. 45

Historical Changes and Future Projections of Extreme Hydroclimate Events in Interior Alaska Watersheds
Bennett, K.E., Cannon, A., and Hinzman, L. 57

Linking North Slope Climate, Hydrology, and Fish Migration
Betts, E.D., and Kane, D.L. 69

Input of Dissolved Organic Carbon for Typical Lakes in Tundra Based on Field Data of the Expedition Lena – 2012
Bobrova, O., Fedorova, I., Chetverova, A., Runkle, B., and Potapova, T. 77

Predicting Snow Density
Bruland, O., Færevåg, Å., Steinsland, I., and Sand, K. 83

Arctic Snow Distribution Patterns at the Watershed Scale
Homan, J.W., and Kane, D.L. 95

Modeling Groundwater Upwelling as a Control on River Ice Thickness
Jones, C., Kielland, K., and Hinzman, L. 107

Challenges of Precipitation Data Collection in Alaska
Kane, D.L., and Stuefer, S.L. 117

Water Temperature Variations in Two Finnish Lakes (Kallavesi and Inari) in 1981–2010
Korhonen, J. 127

Spatiotemporal Trends in Climatic Variables Affecting Streamflow Across Western Canada from 1950–2010: A CROCWR Component
Linton, H., Prowse, T., Dibike, Y., and Bonsal, B. 137

Scaling Runoff from Large to Small Catchments – Comparison of Theoretical Results with Measurements
Marchand, W.D., and Vaskinn, K. 149

Sediment Transport to the Kangerlussuaq Fjord, West Greenland
Mikkelsen, A., and Hasholt, B. 157

Synoptic Climatological Characteristics Associated with Water Availability in Western Canada: A CROCWR Component
Newton, B.W., Prowse, T.D., and Bonsal, B.R. 167

Winter Streamflow Generation in a Subarctic Precambrian Shield Catchment
Spence, C., Kokelj, S.A., Kokelj, S.V., and Hedstrom, N. 179

Water Balance Calculation over Surface Water Storage in the Dry Interior Climate of the Athabasca River Region in Western Canada: A CROCWR Component
Walker, G.S., Prowse, T.D., Dibike, Y.B., and Bonsal, B.R. 189

Forest Disturbance Effects on Snow and Water Yield in South-Central British Columbia
Winkler, R., Spittlehouse, D., Boon, S., and Zimonick, B. 201

Ecohydrology of Boreal Forests: The Role of Water Content
Young (formerly Cable), J.M., and Bolton, W.R. 213

Seasonal Stream Regimes and Water Budgets of Hillslope Catchments, Polar Bear Pass and Cape Bounty, Nunavut
Young, K.L., Lafrenière, M.J., Lamoureux, S., Abnizova, A., and Miller, E.A. 217

Symposium Abstracts 231

River Flow Transformation Processes in the Lena River Delta, Russia
Alekseevsky, N.I., Aibulatov, D.N., Kuksina, L.V., and Chetverova, A.A. 233

Hydrological Analysis of Catchments in the National Petroleum Reserve – Alaska Prior to Petroleum Development
Arp, C.D., and Whitman, M. 234

Macrodispersion of Groundwater Contaminants in Discontinuous Permafrost
Barnes, M.L., and Barnes, D.L. 235

Arctic Water Change: Limitations and Opportunities for Its Detection and Predictability
Destouni, G. 236

Response of Water Bodies in the Northwest Part of Russia to Climate Changes and Anthropogenic Impacts
Filatov, N.N., Efremova, T.V., Georgiev, A.P., Nazarova, L.E., Pal'shin, N.I., and Rukhovets, L.A. 237

The Interaction of Atmospheric, Hydrologic, Geomorphic, and Ecosystem Processes on the Arctic Coastal Plain
Hinzman, L.D., Wilson, C.J., Rowland, J.C., Hubbard, S.S., Torn, M.S., Riley, W.J., Wullschleger, S.D., Graham, D.E., Liang, L., Norby, R.J., Thornton, P.E., and Rogers, A. 238

Sensitivity of Yukon Hydrologic Response to Climate Warming: A Case Study for Community and Sectoral Climate Change Adaptation
Janowicz, J.R., Pomeroy, J.W., and Carey, S. 240

Thermokarst Lake Change in Western Siberia: From Spatiotemporal Landscape Dynamics to Hydrological Reflections
Karlsson, J.M., Lyon, S.W., and Destouni, G. 241

An Assessment of Suspended Sediment Transport in Arctic Alaska Rivers
Lamb, E., Toniolo, H., Kane, D., and Schnabel, W. 242

Greenland Freshwater Runoff. Part I: A Runoff Routing Model for Glaciated and Nonglaciated Landscapes (HydroFlow)
Liston, G.E., and Mernild, S.H. 243

Interactions between Vegetation, Snow, and Permafrost Active Layer
Marsh, P., Shi, X., Endrizzi, S., Baltzer, J., and Lantz, T. 244

Greenland Freshwater Runoff. Part II: Distribution and Trends, 1960–2010
Mernild, S.H., and Liston, G.E. 245

Climatic Redistribution of Canada's Western Water Resources (CROCWR)
Prowse, T.D., Bonsal, B.R., Burn, D.H., Dibike, Y.B., Edwards, T., Ahmed, R., Bawden, A.J., Linton, H.C., Newton, B.W., and Walker, G.S. 246

Permafrost Thaw Induced Changes to Surface Water Systems: Implications for Streamflow
Quinton, W.L., and Baltzer, J.L. 247

The Ecohydrology of Thawing Permafrost Plateaus
Quinton, W.L., and Baltzer, J.L. 248

Meteorology for Hydropower Production Scheduling
Sand, K., and Nordeng, T.E. 249

Delineation of Snow Patterns in Northern Alaska
Wagner, A.M., Hiemstra, C.A., and Sturm, M. 250

Winter Low Flow in the Mackenzie River Basin
Woo, M., and Thorne, R. 251

List of Participants

CANADA

Abnizova, Anna
Postdoctoral Fellow
Boreal Ecohydrology Research Group
Wilfrid Laurier University
75 University Ave W
Waterloo, ON, N2L 3C5
Email: anna_abnizova@yahoo.ca

Ahmed, Roxanne
M.Sc. Candidate
Water and Climate Impacts Research Centre
University of Victoria, Department of Geography
Victoria, BC, V8W 3R4
Email: roxannea@uvic.ca

Bawden, Allison
M.Sc. Candidate
Department of Civil and Environmental Engineering
University of Waterloo
Waterloo, ON, N2L 3G1
Email: abawden@uwaterloo.ca

Janowicz, Richard
Hydrology Manager
Water Resources Branch
Yukon Department of Environment
Box 2703
Whitehorse, YT, Y1A 2C6
Email: richard.janowicz@gov.yk.ca

Linton, Hayley
M.Sc. Candidate
Water and Climate Impacts Research Centre
University of Victoria, Department of Geography
Victoria, BC, V8W 3R4
Email: hayleylinton@gmail.com

Newton, Brandi
M.Sc. Candidate
Water and Climate Impacts Research Centre
University of Victoria, Department of Geography
Victoria, BC, V8W 3R4
Email: bwnewton@uvic.ca

Prowse, Terry
with guest,
Jennifer Prowse

Professor
Water and Climate Impacts Research Centre
University of Victoria, Department of Geography
Victoria, BC, V8W 3R4
Email: terry.prowse@ec.gc.ca

Spence, Chris

Research Scientist
National Hydrology Research Centre
Environment Canada
11 Innovation Blvd.
Saskatoon, SK, S7N 3H5
Email: chris.spence@ec.gc.ca

Walker, Gillian

M.Sc. Candidate
Water and Climate Impacts Research Centre
University of Victoria, Department of Geography
Victoria, BC, V8W 3R4
Email: walkerg@uvic.ca

Winkler, Rita

Research Hydrologist
Resource Science Department
BC Ministry of Forests and Lands
441 Columbia Street
Kamloops, BC, V2C 2T7
Email: rita.winkler@gov.bc.ca

Young, Kathy

Professor
Department of Geography
York University
4700 Keele Street,
Toronto, ON, M3J 1P3
Email: klyoung@yorku.ca; kathylyoung@gmail.com

DENMARK AND GREENLAND

Hasholt, Bent

Associate Professor Emeritus
Department of Geography and Geology
University of Copenhagen
Oester Voldgade 10
DK-1350 Copenhagen
Email: bh@geogr.ku.dk

FINLAND

Korhonen, Johanna
Hydrologist
Finnish Environment Institute (SYKE)
Box 140
00251 Helsinki
Email: johanna.korhonen@ymparisto.fi

NORWAY

Alfnes, Eli
Senior Hydrologist
Department of Hydrology
Statkraft Energi AS
P.O. Box 200 Lilleaker
Oslo, NO-0216
Email: eli.alfnes@statkraft.com

Bruland, Oddbjørn
Statkraft Energi AS
Sluppenveien 67006
Trondheim, N-7005
Email: Oddbjorn.Bruland@Statkraft.no

Marchand, Wolf-Dietrich
Area Manager Hydrology/Hydraulic
SWECO Norge AS
Professor Brochs gate 2
Trondheim, NO-7030
Email: wolf.marchand@sweco.no

Sand, Knut
with guest,
Evalena Ehrenpohl Sand
Hydrologist, Management Nordic (MNH)
Statkraft Energi AS
Sluppenveien 6
Trondheim, N-7034
Email: Knut.Sand@Statkraft.com

RUSSIAN FEDERATION

Bobrova, Olga
M.Sc. Candidate
Department of Land Hydrology
Saint-Petersburg State University
St. Petersburg, 196233
Email: helga.castor@gmail.com

Kuksina, Ludmila
Ph.D. Candidate
Faculty of Geography, Department of Hydrology
Moscow State University
GSP-1, 1 Leninskiye Gory
Moscow, 119991
Email: ludmilakuksina@gmail.com

UNITED STATES OF AMERICA

Bennett, Katrina
Ph.D. Candidate
International Arctic Research Center
University of Alaska Fairbanks
930 Koyukuk Drive, PO Box 757340
Fairbanks, AK 99775-7340
Email: kebennett@alaska.edu

Betts, Erica
Ph.D. Candidate
Water and Environmental Research Center
University of Alaska Fairbanks
Fairbanks, AK 99775
Email: edbetts@alaska.edu

Bolton, Robert
Research Assistant Professor
International Arctic Research Center
University of Alaska Fairbanks
Fairbanks, AK 99775-7340
Email: bbolton@iarc.uaf.edu

Hinzman, Larry
Director
International Arctic Research Center
University of Alaska Fairbanks
Fairbanks, AK 99775-7340
Email: lhinzman@iarc.uaf.edu

Homan, Joel
Ph.D. Candidate
Water and Environmental Research Center
University of Alaska Fairbanks
Fairbanks, AK 99775
Email: jwhoman@alaska.edu

Johnson, Crane
Hydraulic Engineer
Alaska District Headquarters
U.S. Army Corps of Engineers
Anchorage, AK 99506-0898
Email: Crane.Johnson@usace.army.mil

Jones, Chas
Ph.D. Candidate
International Arctic Research Center
University of Alaska Fairbanks
Fairbanks, AK 99775-7340
Email: chas.jones@iarc.uaf.edu

Kane, Douglas
Professor Emeritus
Water and Environmental Research Center
University of Alaska Fairbanks
Fairbanks, AK 99775-1760
Email: dlkane@alaska.edu

Liston, Glen
Senior Research Scientist
Cooperative Institute for Research in the Atmosphere
Colorado State University
Fort Collins, CO 80423-1375
Email: liston@cira.colostate.edu

Schnabel, William
Director
Water and Environmental Research Center
Institute of Northern Engineering
University of Alaska Fairbanks
Fairbanks, AK 99775-5910
Email: weschnabel@alaska.edu

Stuefer, Sveta
Assistant Professor
Department of Civil and Environmental Engineering
Water and Environmental Research Center
University of Alaska Fairbanks
Fairbanks, AK 99775-5860
Email: sveta.stuefer@alaska.edu

Wagner, Anna
Research Environmental Engineer
Cold Regions Research and Engineering Laboratory
P.O. Box 35170
Ft. Wainwright, AK 99703
Email: Anna.M.Wagner@usace.army.mil

Young, Jessie
Research Assistant Professor
International Arctic Research Center
University of Alaska Fairbanks
Fairbanks, AK 99775-7340
Email: jmcable@alaska.edu

Symposium

Papers

Hydrologic Connectivity and Dissolved Organic Carbon Fluxes in Low-Gradient High Arctic Wetland Ponds, Polar Bear Pass, Bathurst Island, Canada

Anna Abnizova[1*], Kathy L. Young[1], and Melissa J. Lafrenière[2]

[1]*Dept. Geography, York University, Toronto, ON, M3J IP3, CANADA*
[2]*Dept. Geography, Queen's University, Kingston, ON, K7L 3N6 CANADA*
**Corresponding author's email: abnizova@yorku.ca*

ABSTRACT
Arctic ponds are the dominant water bodies in wetland environments and have been recently recognized as "sentinels" of climate change due their sensitive hydrologic dynamics during the thaw season. They appear to emit significant amounts of greenhouse gases to the atmosphere from the mineralization of terrestrial dissolved organic carbon (DOC) transported via hydrological inputs from pond catchments. In this study, we evaluated the flow paths between the wetland ponds by examining their hydrologic dynamics and DOC concentrations and stores in response to hillslope-to-pond and pond-to-pond connectivity. This work in 2009 and 2010 at Polar Bear Pass, Nunavut, is based on observations of inflows from a late-lying snow bed into a wetland catchment, ensuing response in water levels and DOC of seven hydrologically connected ponds. Our findings illustrate an example of a water transport mechanism ("fill and spill") occurring along a hydrologic continuum and demonstrate its impact on DOC export, stores, and loads. Variability in precipitation and temperature during the snowmelt and post-snowmelt seasons produce direct responses in pond-to-pond connectivity and DOC dynamics. In particular, during snowmelt and heavy rainfall, DOC loads increase with increasing hydrological fluxes. Water level stability is observed in ponds situated further downslope from the late-lying snowbank, and they generally act as both receiving and storing units. Dissolved organic carbon stores in these ponds also decline as a result of dilution. The results from this study demonstrate the sensitivity of a wetland pond's hydrologic balance and DOC storage to its position in the landscape.

KEYWORDS
Arctic wetlands; arctic ponds; pond hydrology; thaw season; dissolved organic carbon loading

1. INTRODUCTION
The Canadian High Arctic is generally defined as a polar desert due to the small amounts of annual precipitation and cold temperatures. However, in the areas where water supplies exceed losses, arctic wetlands can be found. Presence of permafrost plays a crucial role in determining the relationship between hydrology and the mechanisms responsible for the transfer of water, nutrients, and carbon. This is due to its aquitard-type property, which limits water infiltration and subsurface flow often leading to overland (lateral) runoff (Judd & Kling 2002). In the presence of topographic depressions such as ponds or frost cracks, runoff dynamics can operate under a hydrologic process referred to as *fill and spill*. Specifically, water flows into a topographic depression allowing this landscape feature to act as a transient store. As the maximum storage levels in the depression are reached, new hydrologic connections may form as the water over-

fills this feature and spills out. This latter mechanism transforms these features into transition zones in the context of a hydrologic continuum (Bracken et al. 2013). This concept was initially coined by Spence and Woo (2003) after they showed the importance of lateral flows in water budget estimates for a subarctic valley in the Canadian Shield area. Since then, the concept of "fill and spill" has been widely applied in a wide range of environments (e.g., Tromp-van Meerveld & McDonnell 2006; Woo & Mielko 2007).

Arctic wetland and tundra ecosystems have been recognized as fundamental components in the global carbon cycle and store close to 50% of the global soil carbon (Tarnocai 2009). Arctic ponds, often the dominant terrain type in these areas, can be considered active processors of carbon, either channeling terrestrial dissolved organic carbon (DOC) to the atmosphere, or storing it in their sediments and water column (Kayranli et al. 2010; Carroll et al. 2011). Aquatic DOC also represents an important part of ecosystems and can be mineralized to CO_2, precipitated to sediments or incorporated into biological systems (Clair et al. 1999). It is the most abundant hydrologically transported component of carbon cycle (Schindler et al. 1997).

Hydrologically, high amounts of DOC in the northern wetlands are typically transported during the spring freshet and in response to heavy rainstorms during the thaw season (Clair et al. 1999; Lewis et al. 2012). Finlay et al. (2006) report that 55% of arctic river DOC flux occurs during snowmelt, and they consider this a significant portion of the annual carbon budget. Likewise, Lewis et al. (2012) suggest that snowmelt typically dominates the seasonal DOC flux in high arctic watersheds, and they found that storm events can generate disproportionately large DOC fluxes too. Aside from these studies, detailed information about the temporal trends in DOC loadings and their changes during transport from land to water bodies remains understudied (Finlay et al. 2006).

In this paper, we hypothesize that wetland ponds at Polar Bear Pass (PBP), especially ones adjacent to the hillslopes, play a dual role by acting as storage units and transit hydro-ecosystems by where water is transported downslope when their storage capacity is exceeded. We will apply the "fill and spill" concept (Spence & Woo 2003) to (1) assess the importance of hydroclimatic conditions in defining the degree of hillslope-to-pond and pond-to-pond connectivity, and (2) examine the response of water levels and DOC stores to these changes in connectivity for a series of ponds that follow a topographic gradient.

2. STUDY AREA AND METHODS

2.1 Polar Bear Pass

Polar Bear Pass, Bathurst Island, Nunavut, is one of the largest wetlands in the Queen Elizabeth Islands (75°72′N, 98°67′W). The wetland is situated in a broad valley (94 km^2 in area) and is characterized by wet meadows, two large lakes, and over 4000 tundra ponds with most ponds less than 1 ha (Abnizova et al. submitted). Vegetation cover in wet meadow areas is densely occupied by hydrophilic species of grasses and sedges (*Dupontia fisheri* and *Carex stans*), moss species such as *Orthothecium chryseum, Tomenthypnum nitens* (Sheard & Geale 1982a, b), shrubs such as *Salix arctica* and a variety of vascular plants. Hillslopes bound the wetland to the north and south (100 to 200 m a.s.l.), and they are sparsely vegetated with herbaceous perennials and lichens. Numerous stream valleys dissect the slopes, allowing the upland area (100 to 200 m a.s.l.) to be drained of seasonal snowmelt and rainwater. These waters are important in recharging the low-lying wetland (Young et al. 2010). The area experiences a polar desert

climatic regime (cold winters and cool, wet summers) much like Resolute Bay, the government weather station situated about 146 km to the southeast on Cornwallis Island (Young & Labine 2010).

We selected 7 wetland ponds with well-defined hydrologic linkages. They were located in fine-grained and ice-rich terrain, and they form a hydrologic chain; that is, they lie along a topographic gradient and are situated downslope from a lingering late-lying snow bed. It develops in the lee of the slope, depths can reach upwards of 2 m, and initially, it can extend well into the lowland (Figure 1). While snowmelt period in this wetland lowland is abrupt and typically lasts for just over one week, the late-lying snow bed continues to melt during the post-snowmelt period, and depending on climatic conditions, may supply the receiving areas with meltwater as long as 20 days (e.g., summer of 2009).

Study ponds situated particularly close to the hillslopes with late-lying snow beds have been classified as ponds with a strong hydrologic linkage and high catchment-to-pond connectivity. They will be referred to as P1–P7. To place our pond research into perspective with other ponds in the area, we also monitored an isolated pond (P8), one that depends solely on precipitation input to sustain it.

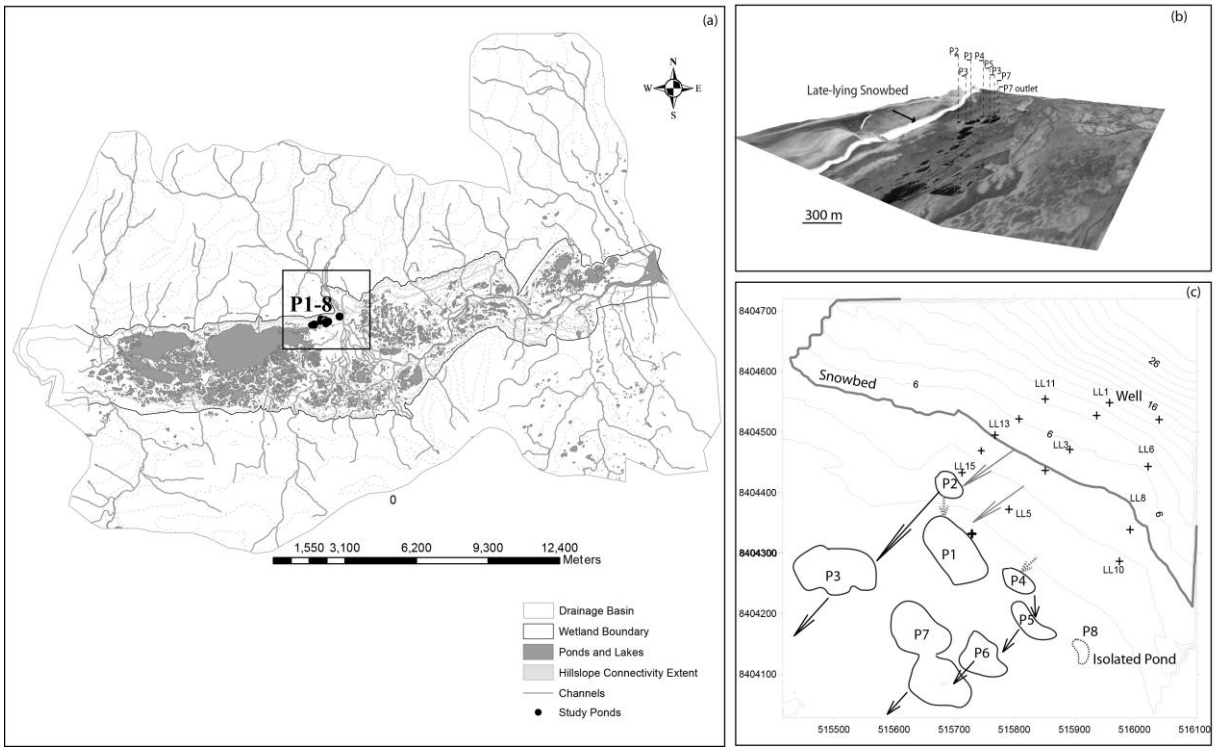

Figure 1: Topographic map of the study area showing the wetland and basin boundary of Polar Bear Pass, Bathurst Island, Nunavut. Contour lines are spaced at 30 m intervals in the drainage basin area and at 10 m interval in the wetland area. Study ponds are shown within a rectangle on the map (a), and on a 3D surface (b). A detailed terrain and topographic map (c) illustrates the study ponds, late-lying snow bed boundary, and catchment wells (+). Flow direction is also plotted. Solid grey lines indicate inflow into upslope ponds, solid black lines show inflow into downslope ponds, and dashed grey lines reveal the initial reduction in connectivity.

2.2 Field and Laboratory Methods

In 2007, a set of perforated and screened 5 cm diameter water wells were installed down to the permafrost table. Wells were placed in the center of each study pond, in the adjacent pond catchments, and along three transects downslope of the late-lying snow bed. Pond water levels were monitored continuously with electronic sensors and verified with manual measurements. Water tables in the catchment wells were monitored frequently, typically daily or every other day. Frost tables were monitored twice weekly beside wells. Water and frost tables were used to assess surface and groundwater inflow into the wetland ponds and provide estimates of DOC loadings from the late-lying snow bed catchment. The hydraulic conductivity of saturated soils was determined using bailing tests once or twice each season. Topographic surveys of the study area and ponds were conducted in 2007 and 2008 with a Total Survey Station Leica (±0.5 mm). Using the resulting bathymetric maps and pond water level data, the estimates of pond volume, and shrinkage/expansion of surface area were computed on a weekly basis.

Water samples for DOC were collected from each pond once a week from June to early September in 2009 and several times a week in 2010. To determine concentrations of DOC entering ponds from the catchment, water samples were also taken at the edge of the late-lying snow bed at the wells LL5 and P1A (Figure 1c). All samples were filtered in the field using pre-combusted GF/F filters (0.7 μm pore diameter) and a polyethylene syringe and stored in 40 mL glass acid-rinsed vials. Prior to the time of collection, the glass sample bottles were rinsed three times with filtered sample water. Each sample was then acidified to pH 2 by adding 2M HCl and stored in the dark at 4°C prior to analysis. Field measurements of pH (±0.2), conductivity (±0.001 μS/cm, dissolved oxygen (±0.01 mg/L), and water temperature (±0.15°C) were made on a weekly basis with a YSI 600R Multiparameter Sonde. Dissolved organic carbon analysis was conducted at the Facility for Biogeochemical Research on Environmental Change and the Cryosphere (FaBRECC) at Queen's University and Alfred Wegener Institute of Polar and Marine Research. Dissolved organic carbon levels were measured as non-purgeable organic carbon (NPOC) by high-temperature combustion (680°C) with a Shimadzu TOC-VCPH analyzer equipped with a high-sensitivity platinum catalyst.

3. RESULTS AND DISCUSSION

3.1 Pond Hydrology

Climatic conditions in 2009 and 2010 are shown in Figure 2. In 2009, mean air temperatures were lower than in 2010. In detail, average monthly temperatures in June, July, and August 2009 were 1.92°C, 5.02°C, and 4.50°C, respectively. Average monthly temperatures for June and July in 2010 were 3.06°C and 7.9°C. Rainfall amounted to 94.9 mm (June 1–August 31) in 2009 and 36 mm (June 1–July 31) in 2010 compared with 63.8 mm measured from June 1–July 31 in 2009.

Direct surface snow ablation measurements indicate that in 2009 the snow bed, pond, and wet meadow areas lasted for 14 days (Julian Days [JDAY] 152–165), 12 days (JDAY 152–163) and 10 days (JDAY 152–161), respectively. In 2010, direct monitoring of melt at the late-lying snow bed lasted for 19 days (JDAY 152–170), and 16 days in wet meadow and pond areas (JDAY 152–167). Overall, the late-lying snow bed persisted until JDAY 204 in 2009 and JDAY 185 in 2010.

As a result of variable climatic conditions in 2009 and 2010, the water tables of the study ponds in 2009 showed different seasonal dynamics (Figure 2). The presence of a late-lying snow bed in 2009 helped to sustain stable water levels in all connected upslope and downslope ponds. A significant rain event observed on JDAY 208, 2009 resulted in an increase of pond water levels, including the isolated pond. The "fill and spill" concept as described by Spence and Woo (2003) can be clearly seen in the water level dynamics of the transient (P5, P6) and downslope ponds (P3, P7). They possess more stable water levels than the upslope ponds (e.g., P1, P2, P3, P4), which receive inflows during the main snowmelt period, along with meltwater from the nearby a late-lying snow bed. Similarly, Woo and Mielko (2007) and Woo and Mielko (2008) show that lake connectivity and lake outflow were generated primarily during the snowmelt period and after large post-snowmelt rain events when a sufficient water level could rise above lake outlet elevations.

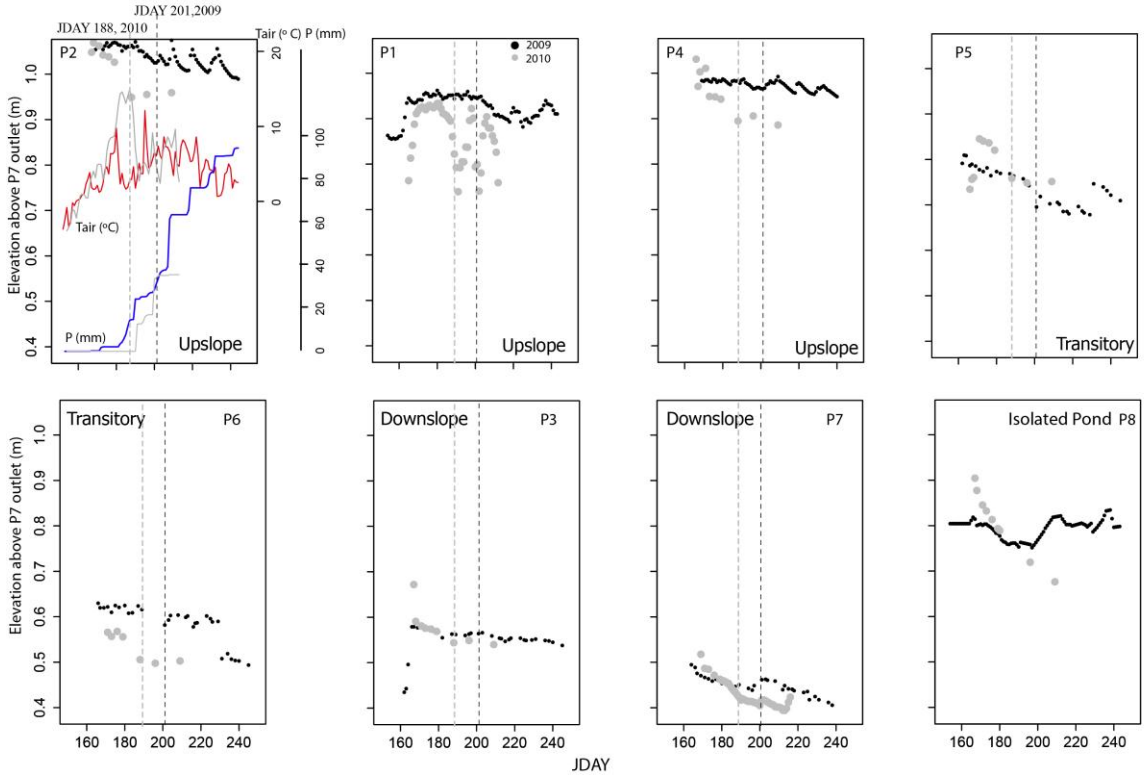

Figure 2: Seasonal water table of the study ponds in 2009 (black) and 2010 (grey) displayed according to their topographic elevation above P7 outlet (see Figure 1b). Seasonal mean air temperature and cumulative precipitation trends are shown for comparison in the upper left diagram. Black and grey dashed lines indicate the dates of loss in connectivity between ponds in 2009 and 2010 based on water level observations from P7 outlet.

In 2010, the late snowmelt and early post-snowmelt seasons were characterized by a lack of precipitation and elevated warm air temperatures. These favorable conditions enhanced evaporation losses from the ponds, and signaled a dramatic decline in water levels, resulting in a rapid loss of connectivity between them (JDAY 188). However, water level stability was retained by the end members in this hydrologic connectivity chain: specifically, P3 and P7. Pond connectivity to the late-lying snow bed in 2010 was of a shorter duration than in 2009. Again, this can be attributed to favorable climatic conditions in 2010.

In 2009, specific conductivity values in the upslope ponds showed an increasing trend, whereas one transient pond (P6, downslope of P5) and the downslope ponds showed an increasing tendency only after a loss in hydrologic connectivity amongst the ponds (Figure 3). Lower specific conductivity in the downslope ponds indicates a dilution process. In 2010, water conductivity began to rise earlier in contrast to the 2009 pattern. Only the downslope pond P7 showed the effect of dilution as a result of hydrologic connectivity.

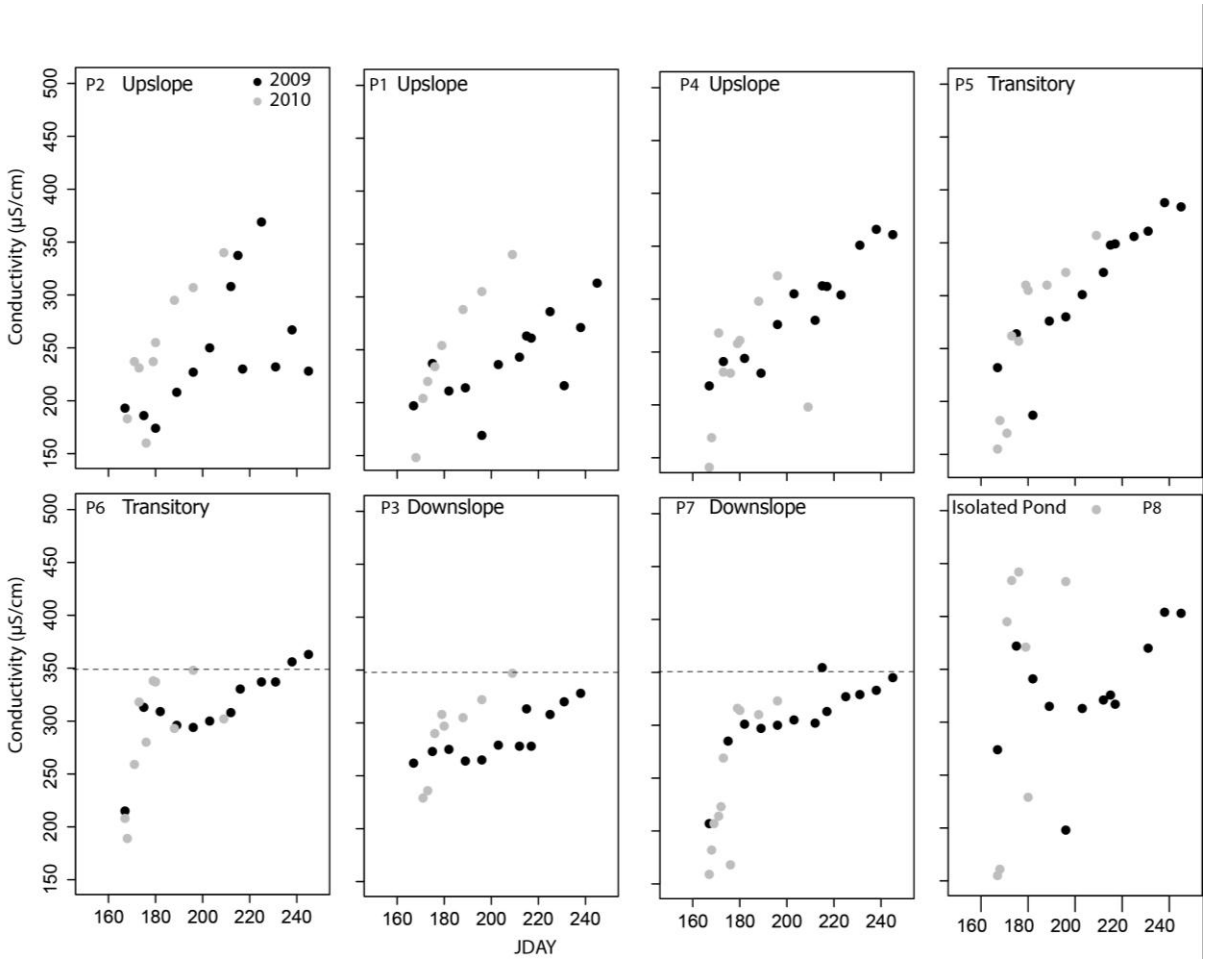

Figure 3: Specific electric conductivity in the study ponds during study seasons 2009 and 2010. Dashed grey line represents the diluted values of conductivity in the downslope ponds (below 350 µS/cm).

3.2 Pond Carbon Dynamics

Sampling for DOC in ponds was initiated right at the onset of the snowmelt in 2009 and represented the spring freshet period (JDAY 150 to JDAY 175, sample n = 3). Other measurements (n = 10) were conducted during the post-snowmelt period and included one measurement representative of a large rain event (22 mm). The results indicate that DOC levels were high in all ponds during snowmelt and right after the large rain event, with a downward trend in concentration for the downslope ponds in response to dilution clearly seen in DOC stores in P6 and P7 (Figure 4 and Figure 5). The elevated concentration of DOC in the isolated pond reveals an evapo-concentration process that is typical for small isolated ponds. Their pond

area and volumetric changes are sensitive to changing climatic conditions (Abnizova & Young 2010).

While arctic lakes and ponds generally have low DOC concentrations due to permafrost limiting the export of soil carbon and cold climate restricting productivity (Sobek et al. 2007), elevated DOC values in PBP ponds can be explained by the rich vegetation community in the pond catchments and strong hydrological inputs of carbon-rich waters during the melt season, especially in the connected ponds (Abnizova et al. 2012). At PBP, ponds receive additional water from late-lying snow beds, nearby ponds, and hillslope creeks. Overall, the connectivity gradient between these hillslope ponds resulted in a well-defined hydro-chemical and biogeochemical gradient.

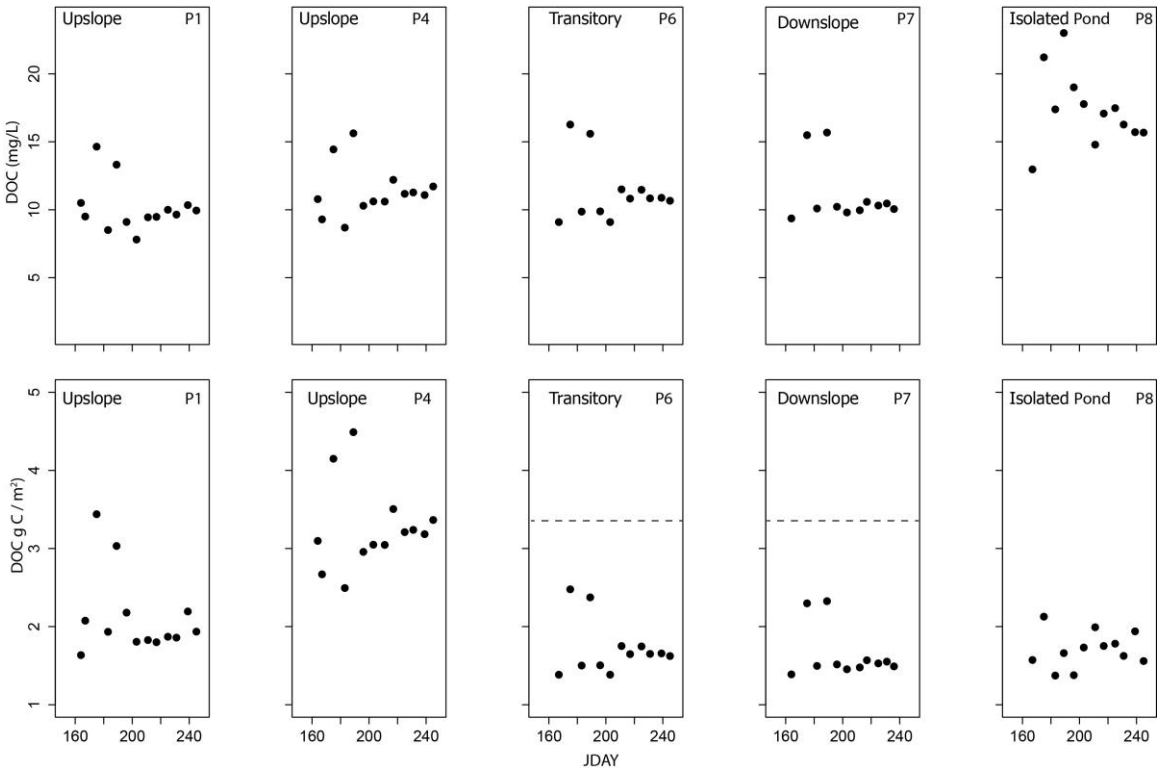

Figure 4: Dissolved organic carbon concentrations of water samples (upper panel) collected from the study ponds in 2009 compared with DOC stocks (gC/m^2) (lower panel) in the study ponds. Dashed grey line represents the diluted values of DOC stores in the downslope ponds (below 3.3 gC/m^2).

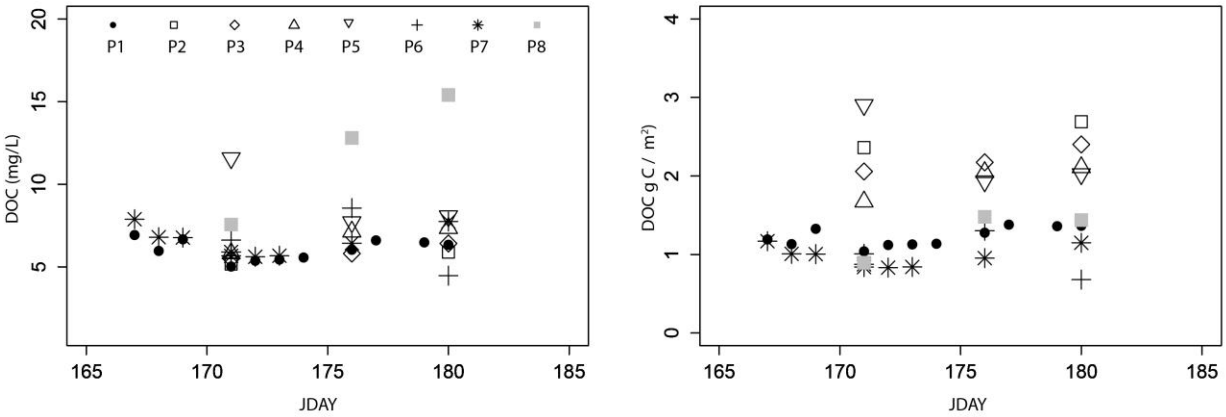

Figure 5: Dissolved organic carbon concentrations of water samples (left panel) collected from the study ponds in 2010 compared with DOC stocks (gC/m^2) (right panel) in the study ponds.

3.3 Seasonal Carbon Loadings

Analysis of carbon snowmelt loadings from the late-lying snow bed catchment identified different flux quantities during the study seasons, and these estimates were compared with 2008 field season values (Figure 6). In 2008 and 2009, the snowmelt flux was higher than in 2010. A second peak in DOC loadings (2008 and 2009) was observed during the latter part of the post-snowmelt period (JDAY 220). This secondary pulse followed an episode of sizable and frequent rainfall. These events helped to re-establish hydrologic connectivity in the catchment by raising soil moisture levels, promoting pond spillage, and lateral runoff, which eventually triggered elevated DOC concentrations. These findings are similar to several other studies (e.g., Kling 1995; Michaelson et al. 1998; Lewis et al. 2012).

This elevated flux of DOC from the snow bed catchment resulted from rainwater transport through wetland soils rich in carbon (Clair et al. 1999; Abnizova et al. 2012). Field observations indicated that the organic layer in the wet meadow can reach up to 15 cm in thickness. Examination of DOC loadings in 2010 suggests that DOC flux is reduced by a lower flow volume, which is in response to a lack of precipitation and warm air temperatures following snowmelt. A similar finding was observed in 2008 during a dry interval (JDAY 182–196), and this resulted in reduced DOC loadings. These relationships between seasonal climatic conditions (rainfall magnitude and frequency) and interaction with catchment hydrology dynamics appear important in defining (e.g., reducing or enhancing) the magnitude of DOC concentrations in arctic wetland ponds (Clark et al. 2007; Lewis et al. 2012).

While the seasonal estimates of DOC loadings from the wetland catchment to pond water is available from three study seasons, it is still challenging to provide reliable estimates for the site, since the magnitude of DOC concentrations and precipitation amounts can vary over space and time (Clark et al. 2007; Strack et al. 2008). This study, however, does suggest that during dry years with limited hydrologic connectivity, lower amounts of DOC will be available to pond ecosystems downslope of water sources (creeks, lingering snow beds). In this case, it is due to the disconnection between upland and downslope ponds.

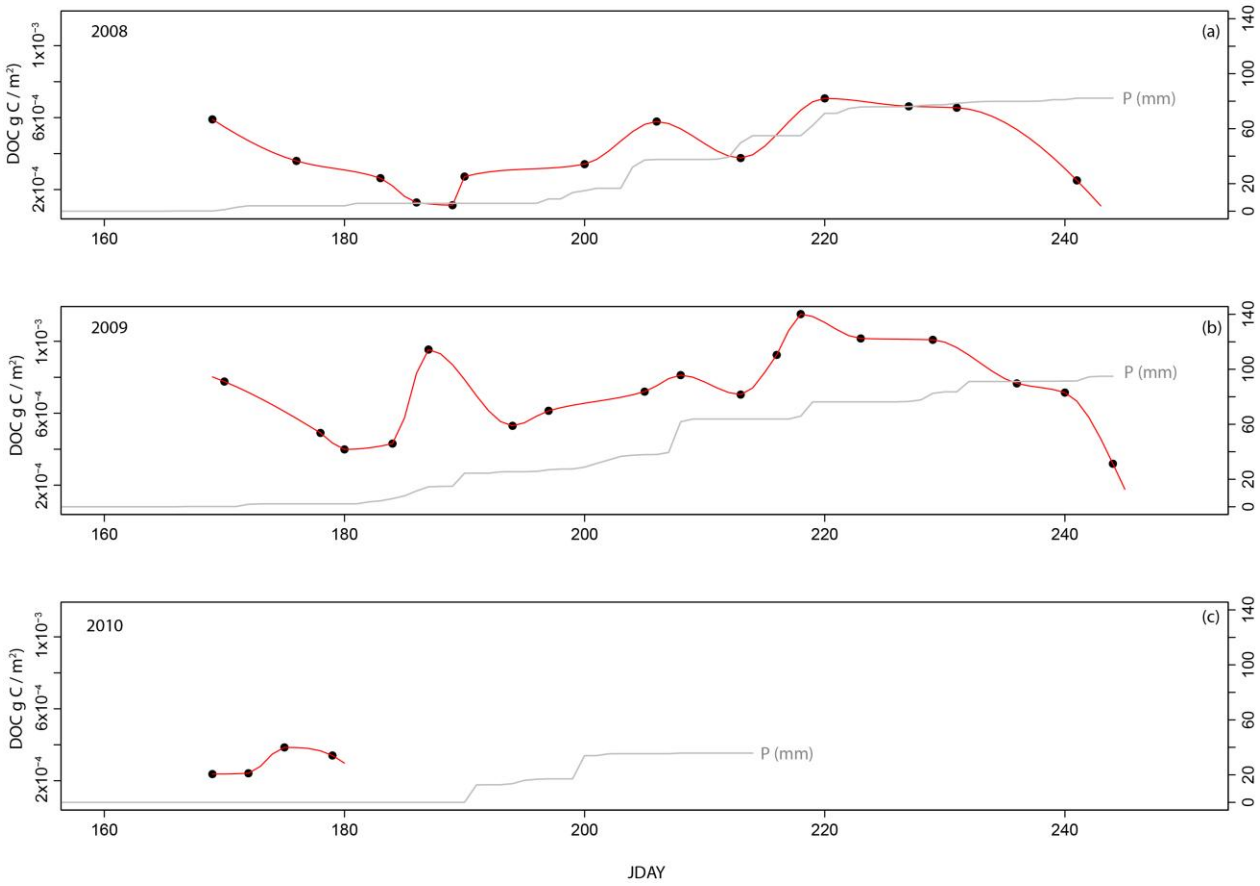

Figure 6: Yields of DOC in gC/m^2 day during 2008 – shown for comparison (a), 2009 (b), and 2010 (c). Estimates are based on inflow measurements from the upslope late-lying snow bed. Cumulative precipitation is plotted for all years.

4. CONCLUSIONS

The aim of this study was to understand the seasonal hydrology of tundra ponds lying along a hydrologic gradient and the seasonal dynamics of dissolved organic carbon flux and loadings into ponds. Our findings demonstrate that:

(1) Lateral hydrologic connectivity between wetland ponds plays an important role in water and carbon transport by either enhancing or limiting water and carbon fluxes into downslope ponds.

(2) Polar Bear Pass ponds situated near hillslopes with late-lying snow beds and along a topographic gradient typically play a *dual role* of receiving water and carbon (stores), and as transient units when water spills out of them and into other transient lower-lying ponds. Upslope ponds appear sensitive to seasonal dynamics in water and carbon fluxes from nearby hillslope water sources (late-lying snow bed), and respond with fluctuating water levels. In contrast, downslope transient ponds act as receiving, storing, or conduit units and show less sensitivity to upslope water source availability, as evidenced by steady water levels.

(3) Dissolved organic carbon stores are elevated in upslope ponds and decline along a hydrologic continuum.

(4) Carbon loadings from land to water follow highly seasonal patterns that are primarily driven by the snowmelt hydrology regime, and seasonal changes in precipitation and temperature (evaporation, ground thaw).

Future work analyzing surface and subsurface flow pathways, and their duration during both wet and dry seasons, will allow for a better prediction of hydrologic and biogeochemical transport in arctic wetlands, especially ones characterized by many small ponds and lakes.

ACKNOWLEDGMENTS

This research is partially supported by Natural Sciences and Engineering Research Council grants to K. Young and M. Lafrenière, and ArcticNet and International Polar Year funds. We are grateful for the continued logistical support from Polar Continental Shelf Program and Northern Student Training Program. We wish to thank many students for their dedication to fieldwork and Steve Koziar for DOC analysis in 2009 at the Facility for Biogeochemical Research on Environmental Change and the Cryosphere at Queen's University. Antje Eulenburg assisted in DOC and hydro-chemical analyses of water samples from the 2010 study season at the Alfred Wegener Institute for Polar and Marine Research, Potsdam Germany.

REFERENCES

Abnizova, A., Miller, E., Young, K.L. & Shakil, S. Seasonal variability in hydrological and physico-chemical characteristics of small water bodies across a High Arctic wetland, Nunavut Canada. *Arct. Antarct. and Alpine Res*. Submitted April 20, 2013.

Abnizova, A., Young, K.L. & Lafrenière, M.J. 2012 Pond hydrology and dissolved carbon dynamics at Polar Bear Pass wetland, Bathurst Island, Nunavut. *Ecohydrol*., doi: 10.1002/eco.1323, published online Oct. 11, 2012.

Abnizova, A. & Young, K.L. 2010 Sustainability of High Arctic ponds in a polar desert environment. *Arctic* 63(1), 67–84.

Bracken, L., Wainwright, J., Ali, G., Tetzlaff, D., Smith, M., Reaney, S. & Roy, A. 2013 Concepts of hydrological connectivity: Research approaches, pathways and future agendas. *Earth Sci. Rev.* 119, 17–34.

Carroll, M.L., Townshend, J.R.G., DiMiceli, C.M., Loboda, T. & Sohlberg, R.A. 2011 Shrinking lakes of the Arctic: Spatial relationships and trajectory of change. *Geophys. Res. Lett*. 38(20).

Clair, T.A., Ehrman, J.M. & Higuchi, K. 1999 Changes in freshwater carbon exports from canadian terrestrial basins to lakes and estuaries under a $2xCO_2$ atmospheric scenario. *Glob. Biogeochem. Cyc.* 13(4), 1091–1097.

Clark, J.M., Lane, S.N., Chapman, P.J. & Adamson, J.K. 2007 Export of dissolved organic carbon from an upland peatland during storm events: Implications for flux estimates. *J. Hydrol.* 347(3–4), 438–447.

Finlay, J., Neff, J., Zimov, S., Davydova, A. & Davydov, S. 2006 Snowmelt dominance of dissolved organic carbon in high-latitude watersheds: Implications for characterization and flux of river DOC. *Geophys. Res. Lett*. 33(10).

Judd, K.E. & Kling, G.W. 2002 Production and export of dissolved c in arctic tundra mesocosms: The roles of vegetation and water flow. *Biogeochem.* 60(3), 213–234.

Kayranli, B., Scholz, M., Mustafa, A. & Hedmark, S. 2010 Carbon storage and fluxes within freshwater wetlands: a critical review. *Wetlands* 30(1), 111–124.

Kling, G.W. 1995 Land-water interactions: The influence of terrestrial diversity on aquatic ecosystems. In: Chapin III, F.S. & Körner C. (eds.), *Arctic and Alpine Biodiversity: Patterns, Causes and Ecosystem Consequences.* Springer-Verlag Ecological Studies Series, Vol. 113, Springer Berlin Heidelberg, pp. 297–310.

Lewis, T., Lafrenière, M.J. & Lamoureux, S.F. 2012 Hydrochemical and sedimentary responses of paired High Arctic watersheds to unusual climate and permafrost disturbance, Cape Bounty, Melville Island, Canada. *Hydrol. Process.* 26, 2003–2018.

Michaelson, G.J., Ping, C.L., Kling, G.W. & Hobbie, J.E. 1998 The character and bioactivity of dissolved organic matter at thaw and in the spring runoff waters of the arctic tundra North Slope, Alaska. *J. Geophys. Res.-Atmos*. 103(D22), 28939–28946.

Michelutti, N., Douglas, M.S.V., Lean, D.R.S. & Smol, J.P. 2002 Physical and chemical limnology of 34 ultra-oligotrophic lakes and ponds near Wynniatt Bay, Victoria Island, Arctic Canada. *Hydrobiol.* 482(1-3), 1–13.

Schindler, D.W., Curtis, P.J., Bayley, S.E., Parker, B.R., Beaty, K.G. & Stainton, M.P. 1997 Climate-induced changes in the dissolved organic carbon budgets of boreal lakes. *Biogeochem*. 36(1), 9–28.

Sheard, J.W. & D.W. Gale. 1983a. Vegetation studies at Polar Bear Pass, Bathurst Island, N.W.T. Classification of plant communities, I. *Canadian Journal of Botany* 61, 1618–1636.

Sheard, J.W. & D.W. Gale. 1983b. Vegetation studies at Polar Bear Pass, Bathurst Island, N.W.T. Vegetation-environment relationships, II. *Canadian Journal of Botany* 61, 1637–1646.

Smol, J.P. & Douglas, M.S.V. 2007 From controversy to consensus: making the case for recent climate change in the arctic using lake sediments. *Frontiers in Ecol. and the Environ*. 5(9), 466–474.

Sobek, S., Tranvik, L.J., Prairie, Y.T., Kortelainen, P. & Cole, J.J. 2007 Patterns and regulation of dissolved organic carbon: An analysis of 7,500 widely distributed lakes. *Limnol. Oceanogr.* 52, 1208–1219.

Spence, C. & Woo, M.K. 2003 Hydrology of subarctic Canadian Shield: soil-filled valleys. *J. Hydrol.* 279(1-4), 151–166.

Strack, M., Waddington, J.M., Bourbonniere, R.A., Buckton, E.L., Shaw, K., Whittington, P. & Price, J.S. 2008 Effect of water table drawdown on peatland dissolved organic carbon export and dynamics. *Hydrol. Process.* 22(17), 3373–3385.

Tarnocai, C. 2009 The impact of climate change on Canadian peatlands. *Can. Water Resour. J.* 34(4), 453–466.

Tromp-van Meerveld, H.J. & McDonnell, J.J. 2006 Threshold relations in subsurface stormflow: 2. The fill and spill hypothesis. *Water Resour. Res.* 42, W02411.

Woo, M.K. & Mielko, C. 2007 An integrated framework of lake-stream connectivity for a semi-arid, subarctic environment. *Hydrol. Process.* 21(19), 2668–2674.

Woo, M.K. & Mielko, C. 2008 Flow connectivity of a lake-stream system in a semi-arid Precambrian shield environment. In: Woo, M.-k. (ed.), *Cold Region Atmospheric and Hydrologic Studies. The Mackenzie GEWEX Experience*, pp. 221–233. Springer, Berlin, Heidelberg.

Young, K.L., Woo, M.K. & Edlund, S.A. 1997 Influence of local topography, soils, and vegetation on microclimate and hydrology at a high arctic site, Ellesmere Island, Canada. *Arct. and Alp. Res*. 29(3), 270–284.

Spatial and Temporal Variation in the Spring Freshet of Major Circumpolar Arctic River Systems: A CROCWR Component

R. Ahmed[1*], T. D. Prowse[1], Y. B. Dibike[1], and B. R. Bonsal[2]

[1]*Water and Climate Impacts Research Centre, Environment Canada and University of Victoria, Victoria, BC, V8W 3R4, CANADA*
[2]*National Hydrology Research Centre, Environment Canada, Saskatoon, SK, S7N 3H5, CANADA*
**Corresponding author's email: roxannea@uvic.ca*

ABSTRACT
Terrestrial river runoff is the greatest source of freshwater input to the Arctic Ocean, providing more freshwater than direct surface precipitation and import of lower-salinity Pacific waters through the Bering Strait. In arctic-draining rivers, the annual spring flood provides as much as 60% of total annual flow volume. Meanwhile, rate of change in arctic climate is higher than other parts of the globe. A northward redistribution of precipitation, increased sea ice melting, glacial wastage, permafrost degradation, and an expected increase in river discharge may result in an intensification of the arctic hydrologic cycle. This corresponds to an earlier freshet onset followed by a more rapid snowmelt period and higher winter flow from greater subsurface infiltration into thawing permafrost. As part of a broad study investigating the Climatic Redistribution of Canadian Water Resources (CROCWR), this project aims to better understand climate-discharge relationships in Arctic river systems including the Mackenzie River in northwestern Canada. Historic daily discharge data for regions of the four major arctic-draining basins (Mackenzie, Ob, Lena, and Yenisei) have been analyzed to determine temporal and spatial variability and trends of the freshet period. This sets the background for further inquiry into relationships of freshet variability with climatic drivers and synoptic climatological patterns affecting water resources in western Canada.

KEYWORDS
Hydrology; spring freshet; Mann-Kendall; runoff

1. INTRODUCTION
The Arctic Ocean is largely an enclosed system, receiving freshwater from three main sources: continental river runoff, direct precipitation on the ocean surface, and import of lower-salinity Pacific waters through the Bering Strait (Aagard & Carmack 1989; Carmack 2000; Serreze et al. 2006). Other terrestrial and marine sources provide a minor contribution. Of these, river runoff comprises the greatest freshwater influx, providing as much as 50% or more compared with other sources based on varying definitions of Arctic Ocean contributing area (Prowse & Flegg 2000). Consequently, freshwater distribution and storage in the ocean is particularly sensitive to river discharge, especially since the Arctic Ocean receives ~11% of global river discharge while occupying only ~1% of global ocean volume (Aagard & Carmack 1989; Shiklomanov 1998). This is an important consideration, since stratification in the cold upper ocean is predominantly controlled by salinity, rather than temperature (Carmack et al. 2008). Stratification affecting freshwater export from the Arctic Ocean through the northern North Atlantic Ocean is an integral part of the global ocean circulation regime. A perturbation in the stratification of surface waters

can have effects on North Atlantic Deep Water (NADW) formation; this phenomenon, coupled with Atlantic meridional overturning circulation (AMOC), is a critical driving force in the global thermohaline circulation (e.g., Aagard & Carmack 1989; Anisimov et al. 2001; Dickson et al. 2002, 2000; Loeng et al. 2005; Proshutinsky et al. 2002; Serreze et al. 2006). Thus, there is a potential link between Arctic river discharge and oceanic heat transport to northern latitudes.

Recently, Arctic river discharge has undergone a change. During the period 1936 to 1999, discharge from Eurasian basins draining to the Arctic Ocean increased annually by 2.0 ± 0.7 km^3yr^{-1}, which resulted in a cumulative increase of 128 km^3 more freshwater released annually by the end of the period as compared with the beginning (Peterson et al. 2002). This increase was tempered by an overall yearly decrease in Canadian discharge to high-latitude seas (Labrador Sea, Eastern and Western Hudson Bay, Arctic Ocean, and Bering Strait) of -3.1 km^3 yr^{-1} during the period 1964–2003, although Canadian discharge directly to the Arctic Ocean showed a non-statistically significant increase (Déry 2005). Eurasian increases have been associated with variations in the North Atlantic Oscillation (NAO) climate index and increases in mean, surface air temperature, while North American decreases have been correlated with more intense positive phases of the Arctic Oscillation (AO) and negative phases of the Pacific Decadal and El Niño/Southern Oscillations (PDO/ENSO) (Déry 2005; Peterson et al. 2002).

Meanwhile, rate of change in Arctic climate is higher compared with other parts of the globe (ACIA 2005; White et al. 2007). The continuous decrease of snow and ice cover in the high latitudes enhance radiative feedbacks, causing an amplification of climate change effects in poleward regions (Polyakov et al. 2002; Serreze & Francis 2006). Northward migration of precipitation patterns, more profound sea ice melting, glacial wastage, permafrost degradation and an expected increase in river runoff all point to an intensification of the Arctic hydrologic cycle. Greater subsurface infiltration into thawing permafrost stocks is causing an increase in traditionally low winter flows, while the annual spring flood is occurring earlier in conjunction with a more rapid snowmelt period (ACIA 2005; Rawlins et al. 2010; Smith et al. 2007; Wu et al. 2005). In the major Arctic-draining rivers, this spring flood provides as much as 60% of total annual flow volume and is a major hydrologic event (Ahmed et al. 2012; Lammers et al. 2001). Seasonality and magnitude of this annual event play a role in the processes that govern freshwater storage and circulation in the Arctic Ocean.

Given the potentially major implications of spring discharge to the Arctic Ocean, there is an increased urgency to better understand the climate-discharge relationships in Arctic-draining rivers. Hydrological processes in the Arctic affect, and are affected by, midlatitude regions that extend far beyond what is traditionally considered within the Arctic domain (Francis & Vavrus 2012). Although Shiklomanov et al. (2007) found that peak spring discharge was generally decreasing in Eurasian basins and thus not a significant factor in increasing annual discharge, they stressed a need to investigate freshet volume versus peak-magnitude relationships with total annual discharge before ruling out spring discharge as a possible contributing factor for increased flow. As a step towards clarifying the role of spring discharge, this study analyzes trends in spring freshet volume, timing, and peak magnitude for four major circumpolar Arctic-draining rivers.

2. DATA AND METHODOLOGY

2.1 Study Area and Data

The study area of the four major circumpolar Arctic drainage basins is shown in Figure 1. Together, these rivers contribute almost 1900 km^3 of freshwater per year, or about 60% of annual flow volume from all Arctic contributing areas (Grabs et al. 2000; Prowse & Flegg 2000). Table 1 describes the number of stations per basin for which data were collected over each analysis period, but is not representative of the total number of stations with available daily discharge data. Stations with significant gaps in daily discharge data were eliminated from this analysis. Daily discharge data were obtained from the Environment Canada Hydrometric Database (HYDAT) for the Mackenzie River and from R-ArcticNET Russia v1.0 for the Lena, Yenisei, and Ob rivers.

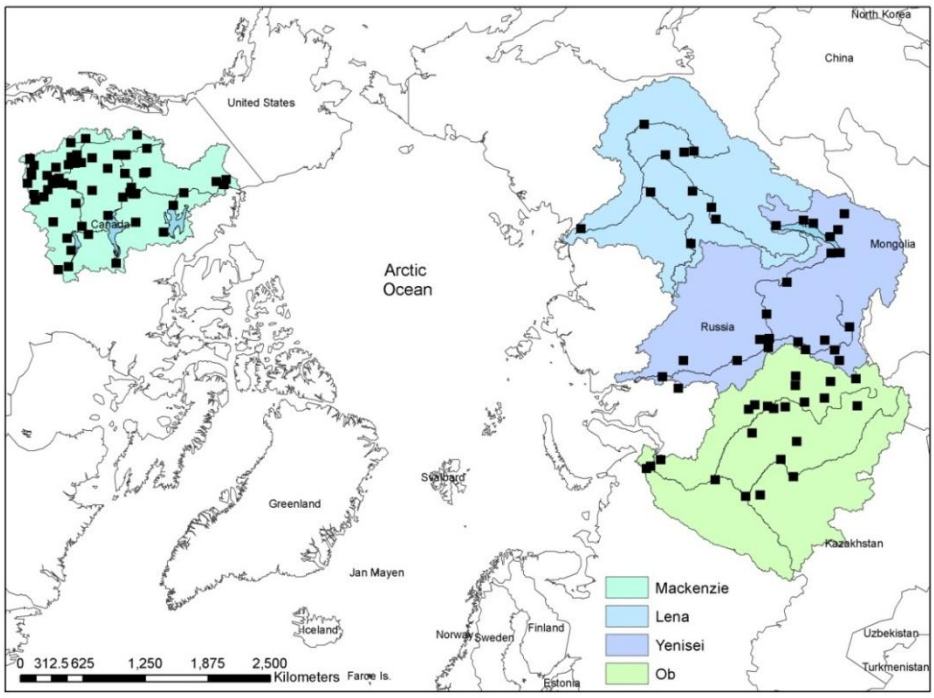

Figure 1: Map of the drainage basins of the Mackenzie, Lena, Yenisei, and Ob Rivers. Squares denote locations of gauging stations utilized in this study.

Table 1: Number of gauging stations used for each study basin per analysis period. Only stations with a sufficient amount of available daily gauged data were selected for this study.

Basin	Number of stations used							
	1940-2000	1955-2000	1962-2000	1962-2010	1973-2000	1973-2010	1980-2000	1980-2010
Mackenzie	N/A	N/A	18	18	56	56	62	62
Ob	12	23	24	N/A	24	N/A	24	N/A
Lena	2	6	10	N/A	10	N/A	10	N/A
Yenisei	13	21	22	N/A	22	N/A	22	N/A

2.2 Flow Estimation

Missing data were estimated using three different techniques. If there was an available upstream or downstream station along the river stem, measurements from that recording gauge were used, provided that it had a complete record over the period to be estimated. To account for missing or additional contributing area, the estimated river runoff rate was scaled such that

$$R_P = R_F A_P / A_F \quad (1)$$

where R denotes the runoff rate (m^3s^{-1}) over an area A (m^2) and subscripts P and F identify the partial and full records, respectively (Déry et al. 2005). Similarly, stations with partial records that had no upstream or downstream station along the same river stem were assessed for areal runoff scaling by comparing the hydrologic response to a nearby basin with similar hydroclimatic characteristics. Whenever possible, missing records were assigned values from basins with similar morphology and scaled by basin area in the same fashion as (1) (Gibson et al. 2006).

If there were no suitable stations to use for runoff scaling, then missing discharge values were estimated from the mean daily value of discharge over the entire evaluated time period, adjusted by the deviation in discharge from the mean of all rivers (evaluated over the same time period) for which data are available on the missing day (Déry et al. 2005). At least three rivers that do not have concurrent missing data were used for reconstruction in all cases. Here, data is reconstructed according to

$$R_P = \frac{R_1 + R_2 + \cdots + R_N}{\overline{R_1} + \overline{R_2} + \cdots + \overline{R_N}} \times \overline{R_P} \quad (2)$$

whereby R_P is the station with partial records for which missing data are to be reconstructed, $\overline{R_P}$ is the mean discharge for a specific day over the remaining time period, and $R_1 \ldots R_N$ and $\overline{R_1} \ldots \overline{R_N}$ are the time series of discharge for a particular day and the daily mean of the corresponding station for the evaluated time period, respectively.

2.3 Trend Detection

The Mann-Kendall (Kendall 1975; Mann 1945) trend test was used to detect trends in date of spring freshet, length of spring freshet, peak freshet magnitude, date of peak magnitude, freshet volume, April–July volume, April volume, May volume, June volume, and July volume. This nonparametric, rank-based test is often used for detecting trends in hydrologic time series that may be affected by seasonal climatic variability, missing data, or extremes (Hirsch & Slack 1984). Unfortunately, hydrological records for the Mackenzie River were more temporally limited than those for the Russian rivers, although there were a greater number of recording stations. Thus, trend analyses were conducted for eight separate time periods to incorporate the greatest number of stations per period.

Spring freshet was defined as the date at which cumulative departure from annual mean flow was most negative. This yielded the date when the flow on subsequent days was greater than the year average (Cayan et al. 2001). Visual inspection of the results verified that this was a reliable method for identifying the start date of spring freshet. The date of annual hydrograph centre of mass (Stewart et al. 2005) was used to define the freshet end date. Although this may not specifically reflect the end of spring runoff, it was adopted to provide a consistent metric for comparing trends in spring flows.

3. RESULTS

Table 2 summarizes the results of the trend analysis for two of the eight evaluated time periods. Only those results significant to at least the 10% significance level are presented here, although many stations exhibited either an increasing or decreasing trend not considered statistically significant. Figure 2 shows examples of spatial trend distribution for all stations, including those trends not considered statistically significant.

Table 2. Number of stations per analysis period that exhibited a significant trend at the 10% significance level. The arrow indicates the direction of the trend.

Freshet Measure	Analysis Period 1962-2000	Analysis Period 1980-2000
Freshet Date	↑5, ↓7	↑4, ↓13
Length	↑10, ↓9	↑9, ↓7
Peak Freshet Magnitude	↑2, ↓22	↑4, ↓5
Date of Peak Magnitude	↑7, ↓6	↑5, ↓1
Freshet Volume	↑7, ↓9	↑7, ↓4
April-July Volume	↑6, ↓15	↑10, ↓2
April Volume	↑33, ↓0	↑32, ↓0
May Volume	↑8, ↓19	↑9, ↓1
June Volume	↑4, ↓14	↑7, ↓3
July Volume	↑6, ↓11	↑12, ↓3

Freshet pulse dates are generally decreasing across North American and Russian stations in both time periods, although some stations displayed a tendency towards later freshet onset. A greater number of stations exhibited a significant decreasing trend in pulse dates in the 1980–2000 time period as compared with the 1962–2000 time period. Despite the generally earlier onset of freshet, there was no apparent spatially consistent tendency in the duration of freshet in either time period, indicating that an earlier freshet onset does not denote longer freshet duration. During 1962–2000, the maximum peak discharge recorded during the freshet significantly decreased in 22 out of 74 stations; meanwhile, during 1980–2000, only 5 out of 74 stations showed the same significant decrease, indicating that a decreasing tendency in freshet magnitudes may have slowed in the more recent time period.

Table 2 shows that, with the exception of April, the volume of freshwater recorded during the spring freshet periods as well as the higher-flow months of April to July tended to decrease in most stations, with fewer stations exhibiting an increase in volume. However, during the 1980–2000 time period, the exact opposite occurs, with a greater number of stations showing an increase in volume versus those showing a decrease. This suggests a dichotomy between the more recent time period and the longer-term trends. In both analysis time periods, no stations exhibited a tendency towards decreased April volume, indicating that the seasonality of the freshet may be evolving.

Figure 2 shows distinct differences in freshet volume trends between North America and Eurasia for the 1962–2000 analysis period. Stations in the Mackenzie basin generally displayed a decreasing tendency in freshet volume; meanwhile each Russian station with a significant trend showed an increasing tendency. These findings agree with those reported in Déry & Wood(2005) and Peterson et al. (2002), in which river discharge was found to be decreasing in 64 rivers in northern Canada, whilst increasing from the six largest Eurasian rivers. Figure 3 contains box plots of trend slopes for the 1962–2000 period, showing the spread of trend slopes for each of the freshet measures. The freshet date shows a greater occurrence of negative slopes, indicating a generally earlier freshet, although all of the timing measures have a median value close to zero, which is consistent with the results presented in Table 2 showing few stations with significant trends for the three timing measures. Freshet volume measures show a wide spread in trend slopes, with more stations exhibiting decreasing slopes with the exception of April, in which all stations displayed an increasing trend.

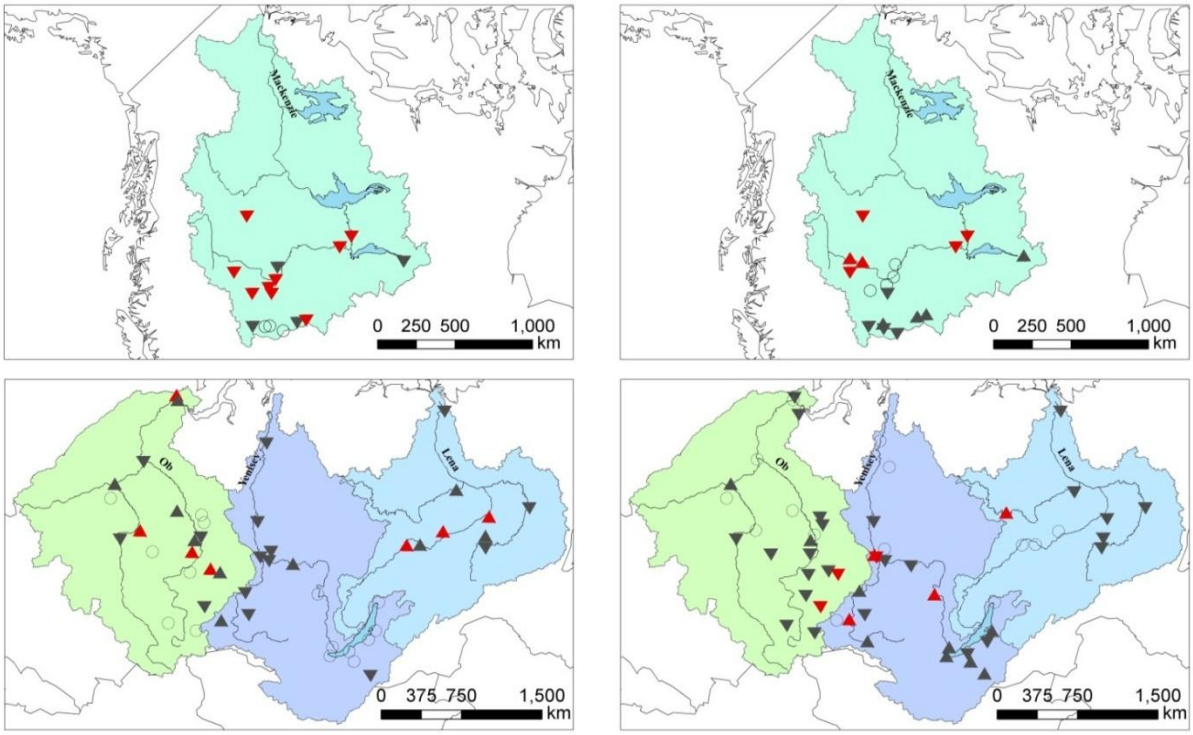

Figure 2: Spatial distribution of trends in (a) freshet onset dates and (b) freshet volume for 1962–2000 analysis period. Red triangles indicate trend is significant at 10% level; direction of arrow indicates direction of trend. Open circles denote stations which exhibited neither an increasing nor decreasing trend.

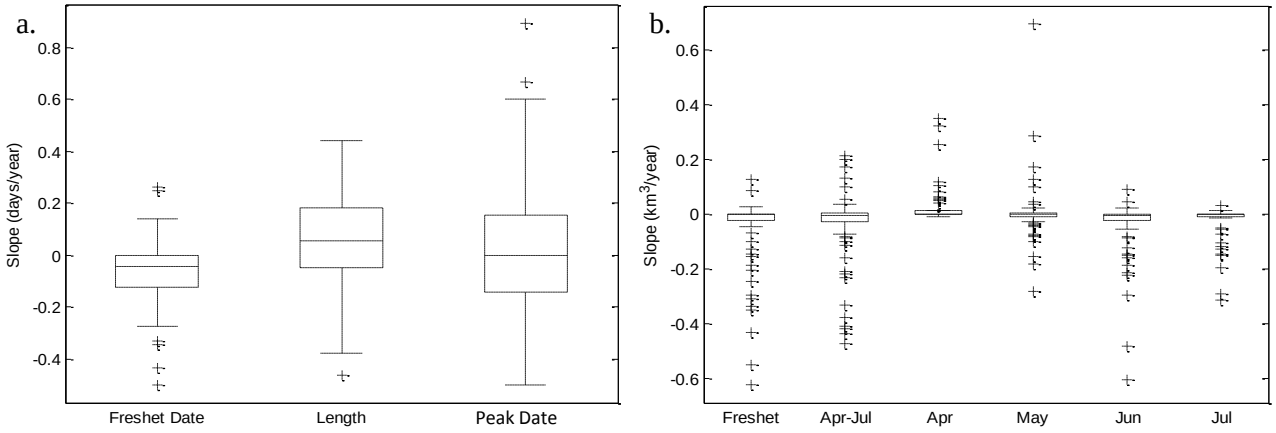

Figure 3: Box plots of trend slopes over the 1962–2000 period for (a) freshet timing measures and (b) freshet volume measures. The central mark is the median, the edges of the box are the 25th and 75th percentiles, and the whiskers correspond to approximately ±2.7 times the standard deviation.

Figure 4 shows the cumulative freshwater volume contribution during the spring freshet, recorded at the gauges nearest to each river's outlet into the Arctic Ocean. For these gauges, it was possible to record flow rates up to 2009, since more recent records were available. During 1980–2009, there was a significant increase in freshwater released into the Arctic Ocean regardless of trends recorded at individual stations in the river basin. The overall trend indicates that combined freshet flow contributions from the four major rivers have increased by an additional 90 km^3yr^{-1} over the 30-year period. Freshwater volume contribution also increased in the April–July time period, resulting in an additional 100 km^3yr^{-1} to be released by the end of the time period compared with the beginning.

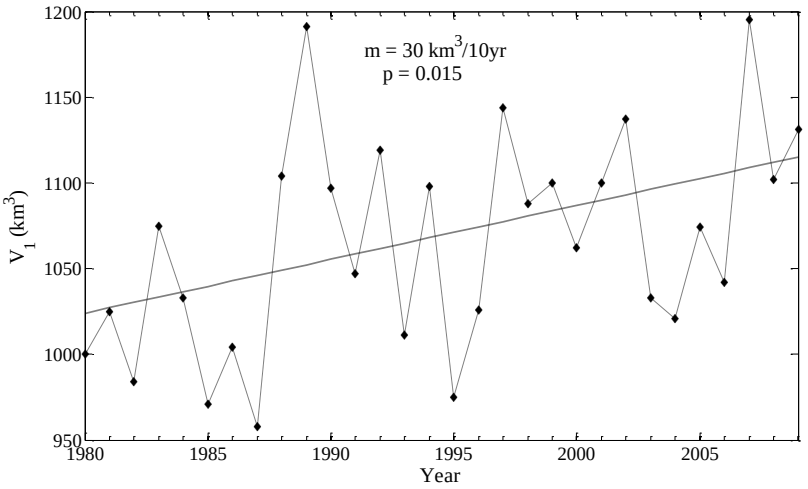

Figure 4: Trend in total Mackenzie-Lena-Ob-Yenisei spring freshet volume contribution during 1980–2009 as gauged at furthest downstream outlet stations. Here the trend is significant at 5% level, with an additional 90 km^3 of freshwater released by the end of the time period as compared with the beginning.

4. CONCLUSIONS

Spatial and temporal variations in spring freshet measures were examined for the four largest watersheds contributing freshwater to the Arctic Ocean. Overall, the spring freshet was found to occur earlier with an increasing length of duration, while peak discharge during the freshet tended to occur later and with decreased severity. The volume of freshwater released during April showed a strong increasing tendency in a large number of stations, suggesting a potential shift in the seasonality of high flow volumes in the nival river systems. Overall, freshwater volume released during the freshet or in the months of May through July showed an increase in the 1980–2000 analysis period, although the longer analysis period of 1962–2000 showed an overall decrease in volumes. This may be indicative of a regime shift in the shorter and more recent time period. Stations in the Mackenzie basin also exhibited a tendency towards decreased freshet volume, while Russian stations exhibited a tendency towards increased freshet volume.

Meteorological relationships with freshet metrics need to be explored, emphasizing the role of integrated multivariable effects (e.g., combined temperature and precipitation) controlling freshet generation. Although these major circumpolar rivers drain to the Arctic, they originate from basins with a diversity of hydrologic and climatic regimes. For example, 46% of their combined drainage area is located south of 55°N (Brooks 2012), well outside the Arctic or even sub-Arctic climatic regimes, and encompass a range of nival, pluvial, glacial and hybrid hydrologic regimes. Given the southerly extent of these basins where much of the flow originates, it is especially important to determine the midlatitude effects of climate and synoptic-scale atmospheric variability on spring-freshet metrics. Lastly, the effects of flow regulation on the timing and magnitude of freshet response also need to be more fully evaluated; the best possible approach being via hydraulic flow modeling that can remove the effect of regulation and thereby permit the controlling signals of climate to be better identified. Some of the above research recommendations are currently being undertaken, and will lead to an improved understanding of regional hydroclimatic controls of the seasonality and magnitude of spring freshet contributions to the Arctic Ocean.

ACKNOWLEDGMENTS

This work was partially supported by a Discovery Grant and ArcticNet funding from the Natural Sciences and Engineering Council of Canada (NSERC) to one of the co-authors. The authors would also like to acknowledge the Arctic Rapid Integrated Monitoring System (ArcticRIMS) and the Regional Hydrometeorological Data Network for the Pan-Arctic Region (R-ArcticNet) for freely providing data.

REFERENCES

A.C.I.A. 2005 *Arctic Climate Impact Assessment–Scientific Report*. Cambridge Univ. Press, NY.

Aagard, K. & Carmack, E.C. 1989 The role of fresh water in ocean circulation and climate. *J. Geophysical Research* 94, 14,485–14,498.

Ahmed, R., Prowse, T.D., Dibike, Y.B. & Bonsal, B.R. 2012 Temporal sequencing of annual spring runoff in major Arctic-draining rivers. In: Poster Session presented at American Geophysical Union Fall Meeting, Dec. 3–7, San Francisco, CA.

Anisimov, O., Fitzharris, B., Hagen, J.O., Jefferies, R., Marchant, H., Nelson, F., Prowse, T.D. & Vaughan, D.G. 2001 Polar regions (Arctic and Antarctic). In: McCarthy, J.J., Canziani,

O.F., Leary, N.A., Dokken, D.J. & White, K.S. (eds.), *Climate Change 2001: Impacts, Adaptation and Vulnerability*. Contribution of Working Group II to the Third Assessment Report of the Intergovernmental Panel on Climate Change. Cambridge University Press, Cambridge, pp. 803–841.

Brooks, R. 2012 Contributing river basin area by latitude. University of Victoria.

Carmack, E., Mclaughlin, F., Yamamoto-Kawai, M., Itoh, M., Shimada, K., Krishfield, R. & Proshutinsky, A. 2008 Freshwater storage in the Northern Ocean and the special role of the Beaufort Gyre. In: Dickson, R.R. et al. (eds.), *Arctic-Subarctic Ocean Fluxes: Defining the Role of the Northern Seas in Climate*. Springer, New York, pp. 145–169.

Carmack, E.C. 2000 The freshwater budget of the Arctic Ocean: Sources, storage and sinks. In: Lewis, E.L. (ed.), *The Freshwater Budget of the Arctic Ocean*. Kluwer, Dordrecht, Netherlands, pp. 91–126.

Cayan, D.R., Kammerdiener, S.A., Dettinger, M.D., Caprio, J.M. & Peterson, D.H. 2001 *Changes in the Onset of Spring in the Western United States*, 399–415.

Déry, S., Stieglitz, M., McKenna, E. & Wood, E.F. 2005 Characteristics and trends of river discharge into Hudson, James, and Ungava Bays, 1964–2000. *J. Climate* 18, 2540–2557.

Déry, S.J. 2005 Decreasing river discharge in northern Canada. *Geophys. Res. Lett.* 32, L10401.

Dickson, B., Osborn, T., Hurrell, J.W., Meincke, J., Blindheim, J., Adlandsvik, B., Vinje, T., Alekseev, G. & Maslowski, W. 2000 The Arctic Ocean response to the North Atlantic Oscillation. *J. Climate* 13, 2671–2696.

Dickson, B., Yashayaev, I., Meincke, J., Turrell, B., Dye, S. & Holfort, J. 2002 Rapid freshening of the deep North Atlantic Ocean over the past four decades. *Nature* 416, 832–7.

Francis, J.A. & Vavrus, S.J. 2012 Evidence linking Arctic amplification to extreme weather in mid-latitudes. *Geophys. Res. Lett.* 39, 1–6.

Gibson, J.J., Prowse, T.D. & Peters, D.L. 2006 Hydroclimatic controls on water balance and water level variability in Great Slave Lake. *Hydrol. Process.* 20, 4155–4172.

Grabs, W.E., Portmann, F. & De Couet, T. 2000 Discharge observation networks in Arctic regions: Computation of the river runoff into the Arctic Ocean, its seasonality and variability. In: Lewis, E. (ed.), *The Freshwater Budget of the Arctic Ocean*. Kluwer, Dordrecht, Netherlands, pp. 249–267.

Hirsch, R.M. & Slack, J.R. 1984 A non-parametric trend test for seasonal data with serial dependence. *Water Resources Research* 20, 727–732.

Kendall, M. 1975 *Rank Correlation Measures*. Charles Griffin, London.

Lammers, R.B., Shiklomanov, A.I., Vörösmarty, C.J., Fekete, B.M. & Peterson, B.J. 2001 Assessment of contemporary Arctic river runoff based on observational discharge records. *J. Geophysical Research* 106, 3321.

Loeng, H., Brander, K., Carmack, E., Denisenko, S., Drinkwater, K., Hansen, B., Kovacs, K., Livingston, P., Mclaughlin, F., Bellerby, R., Browman, H., Furevik, T., Grebmeier, J.M., Jansen, E., Jónsson, S. & Jørgensen, L.L. 2005 Ch. 9: Marine Systems. In: Symon, C., Arris,

L. & Heal, B. (eds.), *Arctic Climate Impact Assessment*. Cambridge University Press, New York, pp. 453–538.

Mann, H.B. 1945 Nonparametric tests against trend. *Econometrica: J. Econometric Soc.* 245–259.

Peterson, B.J., Holmes, R.M., McClelland, J.W., Vörösmarty, C.J., Lammers, R.B., Shiklomanov, A.I., Shiklomanov, I.A. & Rahmstorf, S. 2002 Increasing river discharge to the Arctic Ocean. *Science* 298, 2171–2173.

Polyakov, I.V., Alekseev, G., Bekryaev, R., Bhatt, U., Colony, R., Johnson, M., Karklin, V., Makshtas, A., Walsh, D. & Yulin, A. 2002 Observationally based assessment of polar amplification of global warming. *Geophys. Res. Lett.* 29, 1878.

Proshutinsky, A., Bourke, R.H. & McLaughlin, F. 2002 The role of the Beaufort Gyre in Arctic climate variability: Seasonal to decadal climate scales. *Geophys. Res. Lett.* 29, 15-1–15-4.

Prowse, T.D. & Flegg, P.O. 2000 Arctic river flow: A review of contributing areas. In: Lewis, E.L. (ed.), *The Freshwater Budget of the Arctic Ocean.* Kluwer, Dordrecht, Netherlands, pp. 269–280.

Rawlins, M.A., Steele, M., Holland, M.M., Adam, J.C., Cherry, J.E., Francis, J.A., Groisman, P.Y., Hinzman, L.D., Huntington, T.G., Kane, D.L., Kimball, J.S., Kwok, R., Lammers, R.B., Lee, C.M., Lettenmaier, D.P., McDonald, K.C., Podest, E., Pundsack, J.W., Rudels, B., Serreze, M.C., Shiklomanov, A., Skagseth, Ø., Troy, T.J., Vörösmarty, C.J., Wensnahan, M., Wood, E.F., Woodgate, R., Yang, D., Zhang, K. & Zhang, T. 2010 Analysis of the Arctic system for freshwater cycle intensification: Observations and expectations. *J. Climate* 23, 5715–5737.

Serreze, M.C., Barrett, A.P., Slater, A.G., Woodgate, R.A., Aagaard, K., Lammers, R.B., Steele, M., Moritz, R., Meredith, M. & Lee, C.M. 2006 The large-scale freshwater cycle of the Arctic. *J. Geophysical Research* 111, C11010.

Serreze, M.C. & Francis, J.A. 2006 The Arctic Amplification Debate. *Climatic Change* 76, 241–264.

Shiklomanov, I.A. 1998 Comprehensive Assessment of the Freshwater Resources of the World: Assessment of Water Resources and Water Availability in the World, WMO, UNDP, ed. WMO, Geneva.

Smith, L.C., Pavelsky, T.M., MacDonald, G.M., Shiklomanov, A.I. & Lammers, R.B. 2007 Rising minimum daily flows in northern Eurasian rivers: A growing influence of groundwater in the high-latitude hydrologic cycle. *J. Geophysical Research* 112, G04S47.

Stewart, I., Cayan, D. & Dettinger, M. 2005 Changes toward earlier streamflow timing across western North America. *J. Climate*, 1136–1155.

White, D., Hinzman, L., Alessa, L., Cassano, J., Chambers, M., Falkner, K., Francis, J., Gutowski, W.J., Holland, M., Holmes, R.M., Huntington, H., Kane, D., Kliskey, A., Lee, C., McClelland, J., Peterson, B., Rupp, T.S., Straneo, F., Steele, M., Woodgate, R., Yang, D., Yoshikawa, K. & Zhang, T. 2007 The arctic freshwater system: Changes and impacts. *J. Geophysical Research* 112, G04S54.

Wu, P., Wood, R. & Stott, P. 2005 Human influence on increasing Arctic river discharges. *Geophys. Res.Lett.* 32, L02703.

The Features of Suspended Sediment Yield in Rivers in Kamchatka, Far East Russia

N. I. Alekseevsky and L. V. Kuksina*

Dept. of Hydrology, Faculty of Geography, Moscow State University, Moscow, 119991, RUSSIA
**Corresponding author's email: ludmilakuksina@gmail.com*

ABSTRACT
The Kamchatka Peninsula is a specific region of sediment yield formation that is connected with active volcanism in the area. Volcanoes influence sediment influx through high liability of friable volcanic rocks to erosion. Mining in the Kamchatka region causes anthropogenic sources of mineral particle influx into river channels, but on most of the peninsula, natural factors of sediment yield fluctuations prevail (hydrological, hydrographical, orographical, climatic, lithological, and soil-vegetation factors). The main influence on sediment yield in mountain regions without areas of active volcanism is connected with catchment evaluation and the mean slope of the river. The suspended sediment yield of the plains increases due to catchment area and slope of river growth. In river basins with areas of active volcanism, the main factors of sediment yield formation are catchment area, water flow, friable volcanic deposits on the land, and drainage density on the flanks of the volcanoes.

KEYWORDS
Sediment yield; modern volcanic activity; multiple regression; potential washout; delivery coefficient; Kamchatka

1. INTRODUCTION
Transport of sediment and contaminants, and hence water quality, is strongly affected by the environmental features of the terrain. Sediment fluxes are sensitive to many influences (Syvitski 2003; Walling 2006); some of them lead to sediment load increase, whilst others cause decreased sediment flux. Whereas trends in the suspended sediment loads of the world's rivers due to human impacts have been studied recently (Walling & Fang 2003), there is still less concern about some specific natural drivers, namely, volcanoes, earthquakes (Dadson et al. 2004), and salmon impacts (Hassan et al. 2008).

Insufficient understanding of the interaction of numerous factors, including climate, precipitation (both average and peak), discharge (volume and velocity), basin geology, human impact, and the size of the drainage basin (Syvitski 2011) underlie wrong conclusions regarding seaward flux of fluvial sediment. Estimates of sediment transport rate are widely known to have large uncertainty (Schmelter et al. 2012). Sediment fluxes from small mountain rivers (e.g., western South and North America and most high-standing oceanic islands) have been greatly underestimated in previous global sediment budgets, perhaps by as much as a factor of three (Milliman & Syvitski 1992). In the case of volcanic environment, many sediment discharge drivers (e.g., loss of surface materials by erosional forces) are significantly increased in comparison with other mountains areas, a fact that could lead to more serious underestimates.

Kamchatka is a specific region due to conditions of river suspended-sediment yield formation. This fact is connected with variability of natural conditions including active volcanism in the region. At the same time, the region is one the most poorly studied hydrologically in Russia. Therefore, application of traditional approaches based on turbidity and sediment yield maps (Karaushev 1977; Dedkov & Mozgerin 1984) in this condition leads to underestimation of some factors of sediment yield formation and, as a result, to calculating errors.

The solution for the problem could be based on division of the Kamchatka region into districts that are characterized by similar conditions of sediment yield formation. Introduced zoning is the basis for creation of regression equations, considering the main factors of sediment yield formation in each divided region.

This task includes the following items:

(1) Analysis of suspended sediment yield scrutiny in Kamchatka;

(2) Analysis of natural factors of suspended sediment yield formation;

(3) Geographical demarcation of Kamchatka into zones with similar conditions of sediment yield formation;

(4) Revelation of determinative factors of sediment yield formation in each divided region; and

(5) Creation of regression equations for suspended sediment yield.

The assigned task is decided with the use of observation data on water flow and sediment yield from 63 permanent hydrological gauges in the period 1930–2010, fieldwork data in 2003–2012, GIS project "Factors of rivers sediment yield formation in Kamchatka."

2. METHODS

Kamchatka is characterized by poor examination of river sediment yield because of weak economic development of the region, difficulty with access, and low-developed infrastructure. Regular observations of suspended sediment yield were started in 1940 in the Kamchatka River and the Avacha River. The maximum density of sediment gauges is in the Kamchatka River basin, where from 1940–2011, observations were implemented in 35 gauges, or one gauge per 1530 km^2 at the average. Altogether, from 1940–2011, observations on sediment yield were carried out on 69 gauges, but observations at 6 of them are not representative, so we take into account the results from 63 gauges. The duration of observations varies from 6 to 71 years.

Sediment yield measurements in Kamchatka do not cover the whole year for most of the gauges. As a rule, observations are only carried out during high water and summer-fall low water periods, so it is necessary to recover gaps in series of observations; if not, average annual values of suspended sediment yield are two times greater. Recovery of gaps is implemented on the basis of relationship (Eq. 1)

$$T_m = f(Q_m), \quad (1)$$

where T_m is average monthly water turbidity, g/m^3, Q_m is average monthly water discharge, m^3/sec. Thereby, using series of water discharges which are longer than series of sediment yield, average monthly turbidity was recovered for 63 gauges in Kamchatka rivers. Relationships (Eq. 1) for all gauges have a high correlation coefficient of about 0.85–0.97.

But available data are not enough for a more or less reliable assessment of suspended sediment yield in rivers that are not covered by observations. That is why application of methods that allow us to estimate sediment yield from unstudied regions is necessary. The basis for implementation of this work is the division of Kamchatka into areas with similar factors of suspended sediment yield formation.

The main factors of sediment yield formation in Kamchatka are relief, climatic conditions (characterized by precipitation), and underlying surface (characterized by lithology and soil-vegetation cover).

The basis for zoning is relief, which causes a prevalence of erosion in mountain regions and accumulation in the plains, and changes from highlands and volcanoes to vast intermountain troughs, foothills, plains, and coastal lowlands. The main features of Kamchatka relief are conditioned by tectonic structure, but volcanic processes influence surface formation greatly, and relief is mostly volcanogenic in Kamchatka. The main relief elements stretch in a north–northwest direction along the peninsula longitudinal axis. The continental part of Kamchatka is characterized by a complicated distribution of mountain ranges and intermountain troughs.

Analysis of DEM allows us to divide Kamchatka into 11 orographic regions, divergent by relief, average height, and surface slopes. Plains occupy about 35% of Kamchatka. The western Kamchatka plain has the largest area.

Division into subregions was implemented by climatic features of the area, notably precipitation distribution. The amount of precipitation is dependent on altitude and remoteness from the sea coast. Subregion zoning was carried out by mapping average annual precipitation, constructed on the basis of data from 92 meteorological gauges. The least density of meteorological stations is in the northern (continental) part of Kamchatka; that is why division into subregions is almost impossible here, except Koryak Plateau, where the eastern edge is characterized by greater precipitation (700–1000 mm) than its central region (500–600 mm). Several subregions are demarked in the peninsula. Of particular importance for sediment yield formation is the rainfall-runoff erosivity factor, which characterizes erosive potential of precipitation (Litvin 2002; Wischmeier & Smith 1971). Its determination is based on the ratio of layer, rain intensity, and capacity of the different soil types to absorb and filter water. For the Kamchatka region, the distribution of the rainfall-runoff erosive index was acquired by a combination of maps (Larionov 1993) and new data on precipitation (until 2010).

Local features of sediment yield formation inside regions and subregions can be characterized by data on lithology of underlying bedrock and soil-vegetation cover. But division of the area into smaller sectors is inexpedient because of the poor network of sediment gauges, which does not allow coverage of these zones by observed data.

Therefore, based on the data on relief and distribution of average annual precipitation, the Kamchatka area was divided into 26 regions with similar conditions of sediment yield formation. These regions are characterized by a poor network of sediment gauges, which also is distributed unevenly. More than half of the gauges (the total amount is 63) are situated in the Kamchatka River basin. This fact required the generalization of sediment-yield formation factors. Regression relationships were elaborated for 11 combined regions, in which sediment yield depends on a complex of hydrological and landscape factors.

The available data enabled the construction of an elaborate regression model of suspended sediment yield

$$y_i = b_1 x_{1i} + b_2 x_{2i} + \cdots + b_p x_{pi} + b_0, \quad (2)$$

where y_i is the dependent variable value (specific sediment yield M_R, t/km^2·year), $x_{1i}, x_{2i}, \ldots x_{pi}$ are the independent variable values (specific discharge M_Q, l/sec·km^2); catchment area F, km^2; mean slope of catchment I_H, ‰; average slope of river $\bar{I}$, ‰; drainage density α, km/km^2; percentage of forest land f, %; rivers draining slopes and flanks of active volcanoes in catchment $\frac{F_{vol}}{F}$; coefficient of friable volcanic rocks presence in catchment $\frac{F_{friable}}{F}$), and b_0, b_1, …, b_p are unknown model parameters, estimated on the grounds of normal equations system (Lisicina 1974; Tkacheva 1974).

The efficiency of regression model estimates is characterized by $\frac{S}{\sigma}$, where S is the mean-square error of the forecast and σ is the mean square deviation. Mean-square error is estimated as (Apollov 1974)

$$S = \sqrt{\frac{\sum_{i=1}^{n} (M_{Rif} - M_{Rifor})^2}{n - m - 1}}, \quad (3)$$

where M_{Rif} is the actual specific sediment yield, t/km^2·year, M_{Rifor} is the estimated specific sediment yield, t/km^2·year, n is the series length, and m is the number of parameters in the design equation. The mean-square deviation is estimated as

$$\sigma = \sqrt{\frac{\sum_{i=1}^{n} (M_{Ri} - \overline{M_R})^2}{n - 1}}, \quad (4)$$

where M_{Ri} is the estimated specific sediment yield, t/km^2·year, $\overline{M_R}$ is the average estimated specific sediment yield, t/km^2·year, and n is series length. Results are considered good when $\frac{S}{\sigma}$ is less than 0.6, and satisfactory between 0.6 and 0.8 (Apollov 1974). The coefficient of multiple correlation error σ_R is simultaneously estimated as

$$\sigma_R = \frac{1 - R^2}{\sqrt{n - m}}, \quad (5)$$

where R is the coefficient of multiple correlation, n is series length, and m is number of parameters in the design equation.

3. RESULTS AND DISCUSSION

Zonation of sediment yield formation factors creates the necessary prerequisites for average annual turbidity and specific sediment yield mapping in Kamchatka. It is distorted under the influence of azonal factors such as relief, lithology, and economical activity. Mapping of sediment yield is implemented by division into districts with given range of sediment yield parameters variability (Karaushev 1977).

Thematic turbidity and specific sediment yield maps for Kamchatka are based on data from 63 sediment gauges in rivers with duration of observations from 6 to 71 years. All data used for mapping are representative. More than half of the gauges (54%) are situated on rivers with a catchment area of 500 km^2 and more, and 46% on rivers where the basin area is less than 500 km^2. The turbidity map contains 18 zones (instead of 4 marked out before [Karaushev 1977]); the average annual turbidity changes there from 10 to 1000 g/m^3 and more. The specific sediment yield map contains 13 zones with a variation range from 5–10 t/km^2 to 500 t/km^2 and more.

The turbidity of rivers in the western part of Kamchatka is considerably less than in rivers of the eastern regions. There are huge volcano massifs in the eastern part of Kamchatka, which are a constant source of mineral particle receipt by rivers. The most intense ashfalls occur here, and they impact the formation of soil and vegetation cover and determine the intensity of hillslope erosion.

Regions with minimum turbidity (10 g/m^3 and less) are in the southwest part of the peninsula, in the central part of the Central Range, and in the isthmus between the peninsula and continental Kamchatka. They are applied to areas with steady rock, and in spite of the high values of the rainfall-runoff erosivity factor, water turbidity does not reach great values. It is also determined by the high protectability of the vegetative cover.

Greater turbidity (11–50 g/m^3) characterizes the western and southeast parts of the peninsula and continental Kamchatka. Soils of this area have relatively high values of erodibility as long as bedrock has high and average resistance to erosion.

Considerable increasing of water turbidity characterizes eastern regions of the peninsula, where active volcanoes are situated. The content of suspended particles in water decreases with increasing distance from volcanic groups. The zone of maximum water turbidity coincides with the location of the Kliuchevskoy Volcano group. Close to volcanoes, water turbidity exceeds values of 1–10 kg/m^3 and, for some rivers, reaches values of 200 kg/m^3 and more. Such content of mineral particles is connected with low resistance of bedrock to erosion, maximum values of soil erosion, absence of vegetation, and high values of the rainfall-runoff erosivity factor. The suspended-sediment yield regime of rivers, draining slopes, and flanks of active volcanoes depends on volcanic eruptions. The maximum suspended sediment yield in the Kamchatka River was formed after major eruptions (Figure 1).

The distribution of specific sediment yield in Kamchatka coincides with turbidity distribution in total. Minimum values characterize continental Kamchatka and its western regions. Maximum values are observed in volcanic areas.

Specific suspended-sediment yield is determined by a complex influence of factors, detecting spatial variations of sediment yield and conditions of its transportation in the river network. It allows us to study suspended-sediment yield characteristics for unstudied river basins in relation to a combination of these factors (Karaushev 1977). Such research was implemented for the European part of the USSR and Siberia, Central Asia (Lisicina 1974: Tkacheva 1974), and Ukraine (Goreckaya 1974).

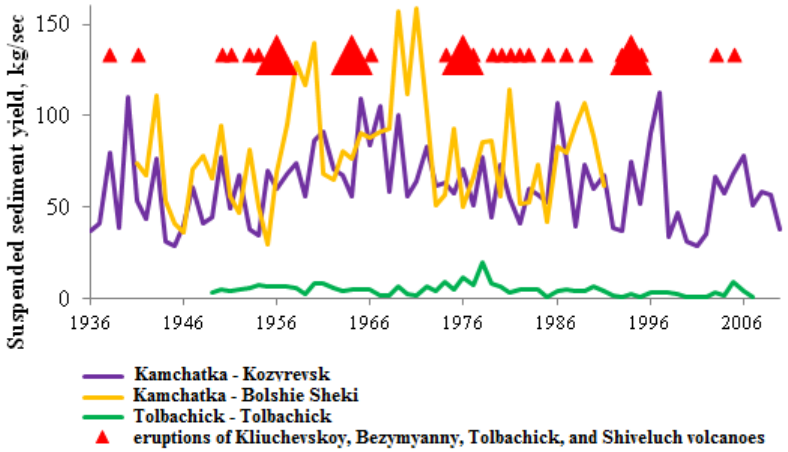

Figure 1: Correspondence between average annual suspended sediment yield and volcanic eruptions of the Kliuchevskoy Volcano group and Shiveluch Volcano.

Kamchatka was divided into 11 regions, characterized by similar conditions of suspended-sediment yield formation, for which regression relationships were elaborated (Table 1). These regions are as follows:

i. Northern, including river basins in continental part of Kamchatka
ii. The Kamchatka River basin (downstream)
iii. Downstream tributaries of the Kamchatka River
iv. River basins in the zone of active volcanism
v. River basins in the northwestern part of the peninsula
vi. Left-bank tributaries of the Kamchatka River in middle course
vii. River basins in the southwestern part of the peninsula
viii. River basins in the southeastern part of the peninsula
ix. Right-bank tributaries of the Kamchatka River in middle course
x. River basins in the eastern part of the peninsula
xi. The Kamchatka River basin (upstream)

Sediment yield is only a part of the total washout in river basins. To characterize the ratio between suspended sediment yield and potential washout in the region, we use the delivery coefficient K_d. Assessment of potential washout is implemented by the Wischmeier-Smith equation (Wischmeier & Smith 1971). Minimum values are in the continental part of Kamchatka, where the rainfall-runoff erosivity factor is the smallest in the region and soil-vegetation protection is high at the same time (Figure 2a). Maximum potential washout occurs in the western region, where the largest volcano groups are situated (see Figure 2a). Along with volcanic activity, the region is characterized by high values of the rainfall-runoff erosivity factor, poor vegetation, and high soil erodibility.

Table 1: Relationships (Eq. 2) for erosive regions on Kamchatka.

№	Dependency	Multiple correlation coefficient	Relative error %	S/σ
i	$M_R = b_{11}M_Q - b_{01}$	0.98	4.1 – 15.9	>0.8
ii	$M_R = b_{12}\alpha - b_{02}$	1.0	0 – 1.6	0.03
iii	$M_R = b_{13}M_Q + b_{23}f - b_{03}$	1.0	0.5 – 8.5	>0.8
iv	$M_R = b_{14}lgF + b_{24}\bar{I} + b_{34}f + b_{44}\frac{F_{vol}}{F} - b_{54}\frac{F_{friable}}{F} - b_{04}$	0.99	0.3 – 20.6	0.7
v	$M_R = b_{15}I_H - b_{05}$	0.88	5.0 – 69.0	>0.8
vi	$M_R = b_{16}M_Q - b_{06}$	0.83	20.0 - 700	>0.8
vii	$M_R = b_{17}lgF + b_{27}I_H - b_{07}$	0.87	0.5 – 143	0.7
viii	$M_R = b_{18}\bar{I} + b_{28}I_H - b_{08}$	0.98	1.3 – 45.5	0.4
ix	$M_R = b_{19}\alpha + b_{29}\bar{I} - b_{09}$	0.85	8.0 – 131	>0.8
x	$M_R = b_{110}f - b_{210}\bar{I} - b_{310}M_Q + b_{010}$	1.0	0.2 – 7.5	0.07
xi	$M_R = b_{111}M_Q + b_{211}f + b_{011}$	0.89	9.6 – 276	>0.8

Estimation of delivery coefficients shows that the ratio between suspended sediment yield and potential washout varies from part of a percent to 80%. The minimum values of K_d characterize river basins under the impact of ashfalls (Figure 2b). They are formed in conditions of maximum potential washout from volcanic areas and relatively small surface flow coefficients. The rate of flow is not enough for the transport of all the solid material. The maximum values of K_d are observed in river basins in the continental part of Kamchatka (see Figure 2b). In this region, potential washout is extremely small because of underlying surface properties (bedrock is resistant to erosion, and soils are hardly erodible) and climatic conditions (the rainfall-runoff erosivity factor is a minimum one). Rate of flow is also rather high for transport of the products of rock destruction.

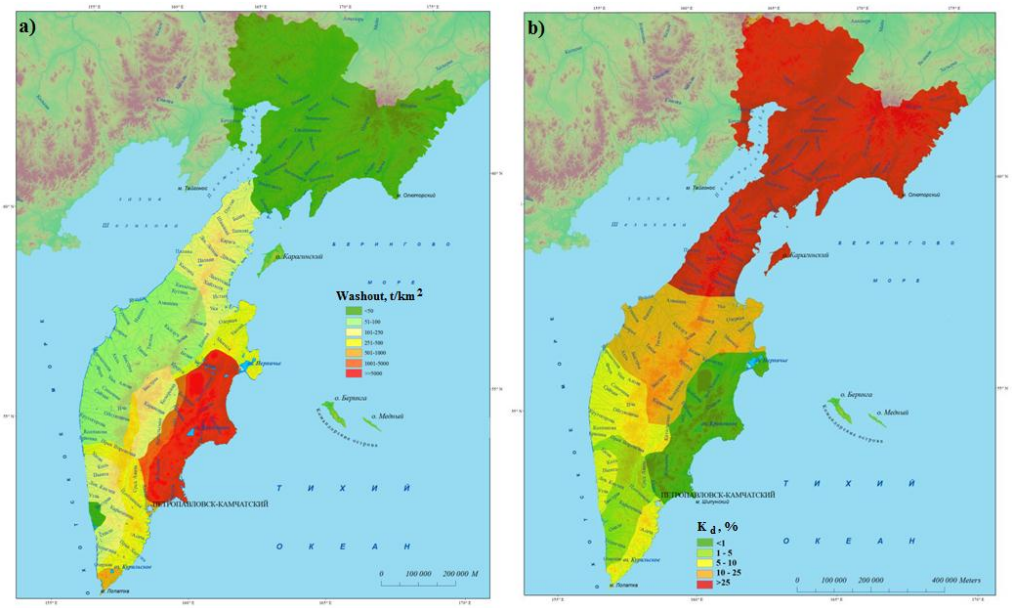

Figure 2: Distribution of potential sediments washout (a) and K_d (b) in Kamchatka.

4. CONCLUSION

Kamchatka is a specific region of conditions related to river sediment yield formation. The areas of modern volcanic activity on the eastern coast of the peninsula influence factors related to sediment formation such as relief, amount and distribution of precipitation, and soil-vegetation cover.

At the same time, Kamchatka is one of the least-studied regions of the territory of the Russian Federation. A poor network of sediment gauges requires elaboration of new approaches for sediment yield estimation in ungauged river basins. The solution for the problem could be based on the multiple regression method. These relationships were elaborated for 11 regions in Kamchatka with similar conditions of suspended sediment yield M_R formation. The main predictors of M_R are specific discharge, catchment basin, mean catchment evaluation, mean slope of catchment, average slope of river, drainage density, percentage of forest land, rivers that drain the slopes and flanks of active volcanoes in the catchment, and the coefficient of friable volcanic rocks present in the catchment.

The ratio between the potential washout of the region and its suspended sediment yield is characterized by a delivery coefficient. The minimum value characterizes volcanic areas (K_d is less than 1% there); maximum values are in the continental Kamchatka (K_d reaches 80% and more).

ACKNOWLEDGMENT

The study has been supported by the Russian Foundation for Basic Research (Project No. 12-05-00069-a).

REFERENCES

Apollov, B.A., Kalinin, G.P. & Komarov, V.D. 1974 Course of hydrological forecasts. St. Petersburg. In Russian.

Dadson, S.J., Hovious, N., Chen, H., Dade, W.B., Lin, J., Hsu, M., Lin, C., Horng, M., Chen, T., Milliman, J. & Stark C.P. 2004 Earthquake-triggered increase in sediment delivery from an active mountain belt. *Geology* 32, 733–736. In English.

Dedkov, A.P. & Mozzherin, V.I. 1984 Erosion and sediment yield on the Earth. Kazan. In Russian with an English summary.

Hassan, M.A., Gottesfeld, A.S. Montgomery, D.R., Tunnicliffe, J.F., Clarke, G.C. & Macdonald, S.J. 2008 Salmon-driven bed load transport and bed morphology in mountain streams. *Geophysical Research Letters* 35, doi: 10.1029/2007GL032997. In English.

Karaushev, A.V. (ed.) 1977 Sediment yield, its study and geographic distribution. St. Petersburg. In Russian.

Larionov, G.A. 1993 Soil erosion and deflation: the main regularities and quantitative evaluation. Moscow, MSU. In Russian.

Lisicina, K.N. 1974 Suspended sediment yield of the Siberian rivers. Regime, theory, estimation and measurement methods of sediments and waste waters 210: 48–72. In Russian.

Litvin, L.F. 2002 Geography of soil erosion in agricultural regions of Russia. Moscow. In Russian.

Milliman, J.D. & Syvitski, J.P.M. 1992 Geomorphic/tectonic control of sediment discharge to the ocean: the importance of small mountainous rivers. *Journal of Geology* 100, 525–544. In English.

Schmelter, M.L., Erwin, S.O. & Wilcock, P.R. 2012 Accounting for uncertainty in cumulative sediment transport using Bayesian statistics. *Geomorphology* 175–176, 1–13. In English.

Syvitski, J.P.M. 2003 Supply and flux of sediment along hydrological pathways: research for the 21st century. *Global and Planetary Change* 39, 1–11. In English.

Syvitski, J.P.M. 2011 Global sediment fluxes to the Earth's coastal ocean. *Applied Geochemistry* 26, 373–374. In English.

Tkacheva, L.G. 1974 Suspended sediment yield of the Central Asia rivers. Regime, theory, estimation and measurement methods of sediments and waste waters 210: 73–81. In Russian.

Walling, D.E. 2006 Human impact on land-ocean sediment transfer by the world's rivers. *Geomorphology* 79(3-4), 192–216. In English.

Walling, D.E. & Fang, D. 2003 Recent trends in the suspended sediment loads of the world's rivers. *Global and Planetary Change* 39, 111–126. In English.

Wischmeier, W.H. & Smith, D.D. 1978 *Predicting Rainfall Erosion Losses. A Guide to Conservation Planning.* USDA-Agric. Handbook No. 537, Washington, DC, 67 pp. In English.

Kenai Peninsula Precipitation and Air Temperature Trend Analysis

Samuel Bauret[1*] and Svetlana L. Stuefer[2]

[1]*Département de génie civil, Université de Sherbrooke, QC, J1K 2R1, CANADA*
[2]*Water and Environmental Research Center, Department of Civil and Environmental Engineering, University of Alaska Fairbanks, AK 99775, USA*
**Corresponding author's email: Samuel.Bauret@USherbrooke.ca*

ABSTRACT
This paper combines precipitation and temperature data from weather stations located throughout the Kenai Peninsula region of Alaska with trend testing to determine if there are significant variations of these climate indicators with time. More precisely, these indicators are the mean annual temperature (MAT), total annual precipitation, precipitation annual maximum, and frequency of occurrence in heavy precipitation events. In order to determine what constitutes a significant trend, statistical hypothesis testing with the Mann-Kendall trend test was used. Overall, the tests showed increases in MAT, decreases in total precipitation, and no trend in precipitation annual maximum or in frequency of heavy precipitation events. However, a seasonal shift in these events from late summer to mid-autumn is present. The combination of increasing temperatures and decreasing total precipitation may point towards the drying of ecosystems, such as wetlands. This study provides background information for the further analysis of social and environmental changes on the Kenai Peninsula within the framework of the Alaska ACE (Alaska Adapting to Changing Environments) project.

KEYWORDS
Kenai Peninsula; Mann-Kendall trend test; precipitation; air temperature

1. INTRODUCTION
Analysis of changes in precipitation and air temperature on the Kenai Peninsula was initiated for the Alaska ACE (Alaska Adapting to Changing Environments) project. Alaska ACE conducts biological, physical, and social research to determine the mechanisms by which communities adapt to environmental and social changes. The project includes three case study regions across the state of Alaska: Southcentral region (Kenai Peninsula), Southeast region (Alaska Panhandle) and Arctic region (north of the Brooks Range). Each region has unique hydrological and climate settings. This study focuses on the Southcentral region (Figure 1). The present climate of the Kenai Peninsula can be described as sub-Arctic maritime south and east of the Kenai Mountains (Figure 1) and sub-Arctic continental north and west of the Kenai Mountains (Shulski & Wendler 2007). The Kenai Peninsula is one of the more densely populated areas of the state, as well as one of the most visited by tourists, and as such is also one of the most vulnerable to the consequences of climate changes. These changes are generally associated with increases in surface air temperature. Analysis of mean annual air temperatures for the state of Alaska by Stafford et al. (2000) showed that the highest increases are found in the Interior region of Alaska (2.2°C), with a secondary high point on the Kenai Peninsula (2.0°C). Warming of the Kenai Peninsula is consistent with the thinning of glaciers on the Harding Icefield (Adalgeirsdottir et al.

1998; VanLooy et al. 2006) and drying of wetlands (Klein et al. 2004). Here, we identify and update changes in climate characteristics such as air temperature and precipitation specifically for the Southcentral region so that this information can be further used for the analysis of changes in ecosystems and communities of the Kenai Peninsula.

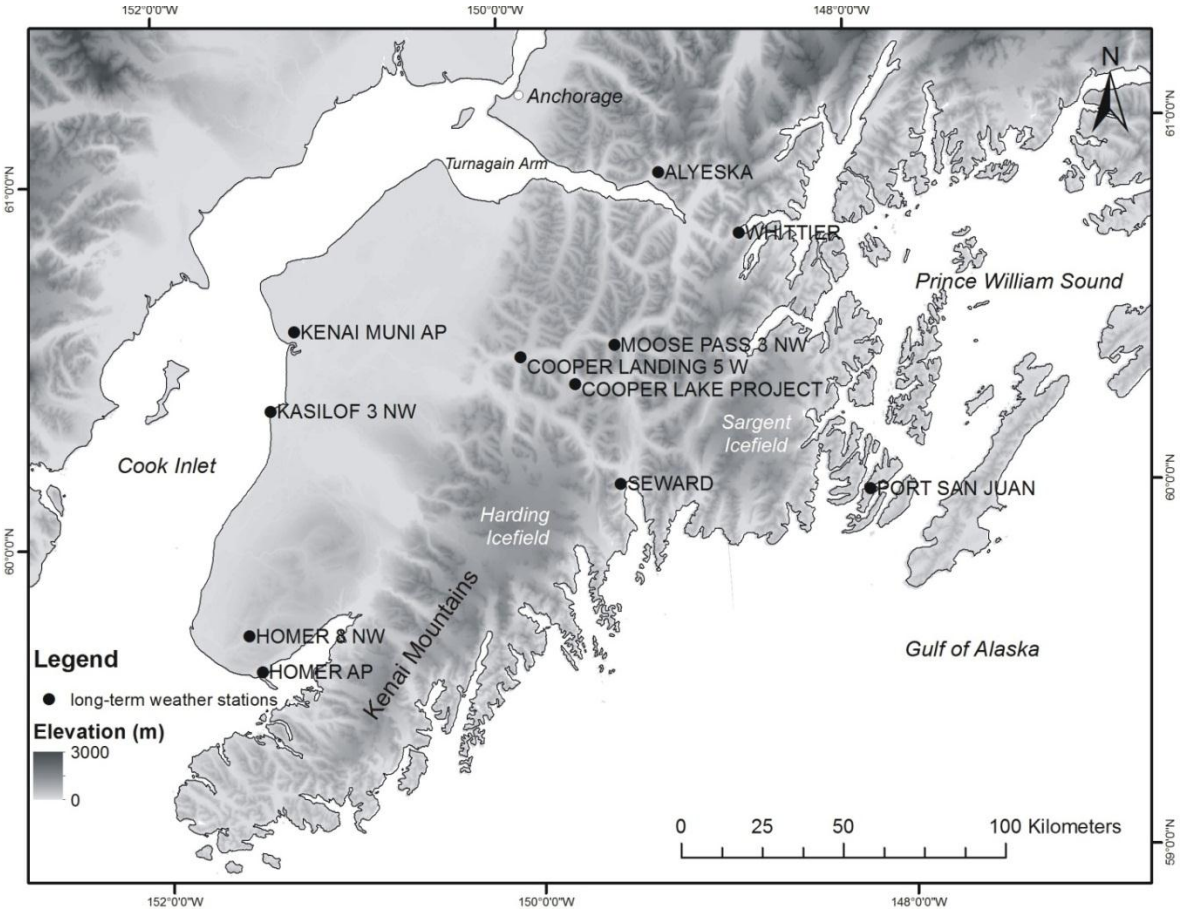

Figure1: Chosen gauging station locations in the Southcentral region of Alaska.

2. DATA AND METHODS

Weather data in the Southcentral region have been recorded for a relatively long time compared with most of the state. For example, the Kenai Municipal Airport and Seward weather stations have both accumulated over 100 years of precipitation data. Stations cover elevations from 10 m above sea level (Seward) to 153 m (Cooper Lake) and 327 m (Homer 8 NW) (Table 1).

Daily precipitation and daily high and low air temperature data are obtained from the Global Historical Climatology Network (GHCN). Annual mean air temperature and total annual precipitation were calculated from daily data. All stations retained for the study have record lengths in excess of 30 years. However, if many daily measurements are missing in one given year, that year can be rejected. Daily data were checked for outliers and gaps by plotting each station's data against time. Generally, the quality of the air temperature records is better than that of the precipitation records. This leads to an additional screening procedure for precipitation, described in the next section.

2.1 Precipitation Data Quality

Total annual precipitation is calculated by summing the precipitation depth measured every day over the course of a year. Unfortunately, much of the early data are missing for several stations. Missing values compromise a dataset's total sum more than they do its average. More specifically, extensive missing records can lead to a false interpretation of total annual precipitation during early years and can result in a significant positive trend. Presence of missing data was taken into account by adding the number of zero precipitation days to the number of days with recorded precipitation. Theoretically, this number should be 365 (or 366); however, in reality many days have no records. An order of reliability was assigned to each station based on the completeness of its data as follows:

Order 1- Stations having at least 30 years of data with 360 days of measurements each year
Order 2- Stations having at least 30 years of data with 350 days of measurements each year
Order 3- Stations having at least 30 years of data with 340 days of measurements each year
Order 4- Stations having at least 30 years of data with 330 days of measurements each year

Table 1 summarizes the order of reliability for each station. Stations that did not satisfy Order 4 were discarded and not used in the analysis of total annual precipitation. Analysis of missing data resulted in eliminating some of the early years and reduced the size of the dataset used to analyze the trend in total annual precipitation.

Table 1: Station list and summary of long-term precipitation and air temperature data.

Station Name	Elevation (m)	Air Temperature		Annual Total Precipitation and HPE			Precipitation AMS	
		Years	Last Year	Years	Last Year	Order of reliability	Years	Last Year
Homer AP	19	76	2012	71	2011	1	78	2010
Homer 8 NW	327	34	2011	32	2011	2	34	2010
Kasilof 3 NW	21	53	1996	32	1995	3	66	1997
Kenai Muni AP	27	76	2012	71	2011	1	77	2010
Cooper Landing 5 W	114	32	2011	-	-	-	36	2010
Cooper Lake	153	40	2001	31	2001	3	45	2003
Moose Pass 3 NW	140	30	2011	-	-	-	40	2004
Alyeska	82	36	2012	33	2011	4	46	2010
Whittier	18	44	2010	32	2010	1	58	2010
Seward	10	97	2012	70	2010	1	98	2008
Port San Juan	15	44	2010	32	2010	1	32	2006

In addition to the total annual precipitation, two more precipitation metrics were examined: annual maximum series (AMS) and frequency of occurrence of heavy precipitation events (HPE). Precipitation AMS were obtained from the *NOAA Atlas 14 Precipitation-Frequency Atlas of the United States, Volume 7: Alaska* (Perica et al. 2011). As part of the precipitation-frequency analysis, AMS selection included some additional screening procedures such as identifying co-located stations and merging the data together to extend the AMS record (Perica et al. 2011). Heavy precipitation events were retrieved from the GHCN data (for more details see Section 3.4). The study of HPE is also affected by precipitation data quality. The years rejected for the

study of total rainfall were therefore also rejected for the study of HPE. Annual maximum series is much less affected than the other two metrics, and temperature measurements are generally more reliable than precipitation.

3. RESULTS AND DISCUSSION

This section presents results of the analysis for four climate indicators: (1) mean annual air temperature, (2) total annual precipitation, (3) precipitation annual maximum series, and (4) frequency of occurrence of heavy precipitation events.

3.1 Mean Annual Temperature

Daily mean air temperature (MAT) is calculated as the average of daily low and high temperatures. The daily averages are then averaged over the entire year to obtain the MAT.

3.1.1 Visual interpretation

Mean annual temperature time series were plotted for each station. As an example, Figure 2 illustrates the MAT variability at Seward, the station with the longest continuous record (97 years) on the Kenai Peninsula. The Seward station highlights several warm years: in 1915, 1993, and 2005.

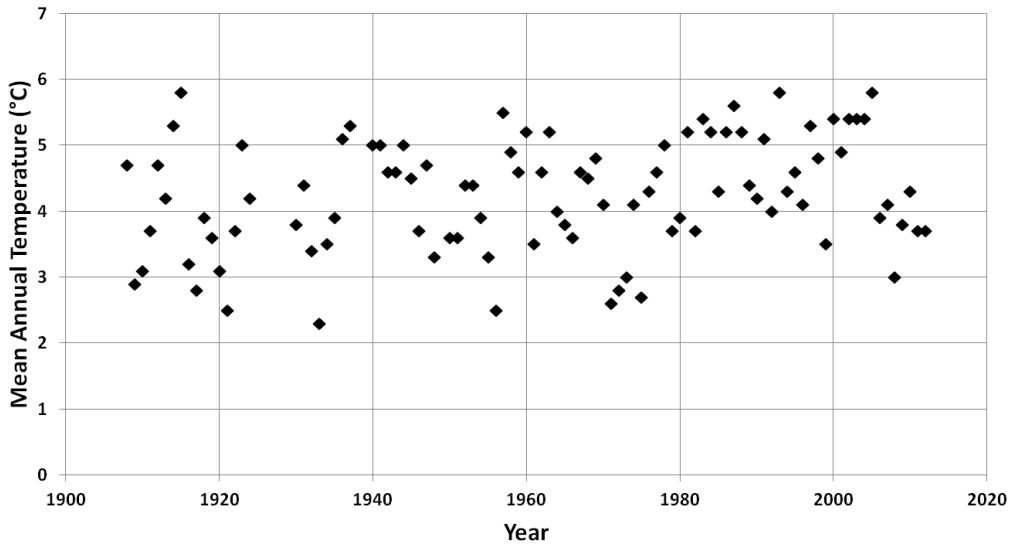

Figure 2: Seward mean annual temperature.

Data from other stations also indicate that the warmest MAT was observed in 1993 and 2005:

- 1993 was the warmest year for Port San Juan, Seward, Whittier, and Moose Pass 3NW.
- 2005 was the warmest year for most stations since 1993.

Data from several stations showed that the coldest MAT was recorded in 1971 and 1961:

- 1971 was the coldest year for Alyeska, Moose Pass 3NW, Cooper Lake, and Homer and amongst the lowest in all stations. This is also the year that the coldest temperature ever was recorded in the United States (-62.2°C near Prospect Creek, AK).
- 1961 was the coldest year in Whittier and Port San Juan, but not Seward.

There are some limitations to this list, associated with the missing records for some years. The years listed here may be the extremes for more stations than solely the ones listed. On the other hand, extremes may exist in other years that had to be rejected due to incomplete data. The data gap present in Whittier and Port San Juan (1966–1982) separates two agglomerations of data, with the latter being noticeably higher in both cases. Generally, the warmest and coldest years are the same for the stations south and east of the Kenai Mountains. Similarly, the warmest and coldest years are the same for the stations north and west of the Kenai Mountains (Figure 1).

3.1.2 Statistical test

The Mann-Kendall test is performed for the 20-, 30-, 40-, and 50-year time. For example, the "20 year" column in Table 2 refers to the latest 20 years of records. For the Kenai Municipal Airport, the 20-year period extends from 1993 to 2012. Similarly, for the "50 year" column, the period of record for this particular station is 1963–2012.

Table 2: Mann-Kendall test results for mean annual temperature.

Station Name	20 Year	30 Year	40 Year	50 Year
Homer AP	No Trend	No Trend	No Trend	**Sign. Increase**
Homer 8 NW	No Trend	No Trend	-	-
Kasilof 3 NW	No Trend	No Trend	No Trend	No Trend
Kenai AP	No Trend	No Trend	**Sign. Increase**	**Sign. Increase**
Cooper Landing 5 W	No Trend	No Trend	-	-
Cooper lake	**Sign. Increase**	**Sign. Increase**	No Trend	-
Moose Pass 3 NW	No Trend	No Trend	-	-
Alyeska	No Trend	No Trend	-	-
Whittier	No Trend	No Trend	**Sign. Increase**	-
Seward	No Trend	No Trend	No Trend	No Trend
Port San Juan	No Trend	No Trend	**Sign. Increase**	-

The trend test confirms that mean annual temperatures are on the rise in certain parts of the Kenai Peninsula. Homer and Kenai indicate a significant increase in MAT over the 50-year period. Two stations, located in the Prince William Sound area (Whittier and San Juan), show significant increase in MAT over the 40-year period. At the same time, Seward and Kasilof show no trend at the 5% significance level. Note that not a single test generated a significant decrease in temperatures, whether short-term (20 years) or long-term (50 years or more). Warming air temperatures were reported on the Kenai Watershed Forum (2012). One of the consequences of warmer temperatures is reflected in the study of drying wetlands by Klein et al. (2005). This study indicated that the Kenai Peninsula is becoming both woodier in its vegetation and drier.

3.2 Total Annual Precipitation

3.2.1 Visual interpretation

In 1986, total annual precipitation was well above the average for all stations on the Kenai Peninsula. In the case of Port San Juan and Whittier, 1986 is the wettest year in the entire record. For Homer 8NW and Seward, it is within the top five. As for dry years, 1996 was the driest year recorded for all stations adjacent to Prince William Sound, as well as for the Homer Airport and Homer 8NW.

3.2.2 Statistical test

The total annual precipitation dataset is sparser when compared with the previous indicator (MAT). This is because some of the years had to be discarded due to missing data (Table 1). Mann-Kendall test results are summarized in Table 3. In contrast to MAT, total annual precipitation is decreasing for more recent years (20 year and 30 year). The Mann-Kendall test shows that decrease in total annual precipitation is most pronounced at the Kenai Municipal Airport. Over the last 20 years, a decreasing trend in total precipitation can be seen at Whittier and Port San Juan, but it becomes non-significant over the longer periods. Most of the stations that have a reliability order of one, with one exception (Seward), confirm a decrease in total annual precipitation.

Table 3: Mann-Kendall test results for total annual precipitation.

Station Name	20 Year	30 Year	40 Year	50 Year
Homer AP	No Trend	**Sign. Decrease**	**Sign. Decrease**	No Trend
Homer 8 NW	No Trend	No Trend	-	-
Kasilof 3 NW	No Trend	No Trend	-	-
Kenai AP	**Sign. Decrease**	**Sign. Decrease**	No Trend	**Sign. Decrease**
Cooper Landing 5 W	-	-	-	-
Cooper Lake	No Trend	No Trend	-	-
Moose Pass 3 NW	-	-	-	-
Alyeska	No Trend	No Trend	-	-
Whittier	**Sign. Decrease**	No Trend	-	-
Seward	No Trend	No Trend	No Trend	No Trend
Port San Juan	**Sign. Decrease**	No Trend	-	-

3.3 Precipitation Annual Maximum Series

The annual maximum series (AMS) contain the maximum 24-hour precipitation of every year on record. These data are used to calculate precipitation frequency estimates that are used in hydrological design (Kane & Stuefer 2013). The goal is to analyze the variability of the severity of annual maximums in time. Again, the data are first plotted for every station (Figure 3) for visual interpretation.

3.3.1 Visual interpretation

Extreme rain events in 1986 and 1995 are readily visible at the Seward station (Figure 3). Below are the two most extreme rain events that were recorded by several stations on the Kenai Peninsula. Both of these events were also described in online news media:

- October 10, 1986: Kenai (109 mm), Seward (382 mm), Moose Pass 3 NW (63 mm), Homer 8 NW (79 mm)
- September 20, 1995: Whittier (277 mm), Seward (249 mm), Moose Pass 3 NW (89 mm), Cooper Lake (81 mm)

The following events were of similar importance, but more isolated:

- September 25, 1995: Cooper Landing (144 mm)
- October 23, 2002: Homer Ap (73 mm)
- November 24–25, 2002: Cooper Lake (95 mm), Cooper Landing (98 mm)

One major outlier was found in the data. This consisted of 80 inches at the Homer Airport on January 31, 1950. This data point was removed from the set before calculations.

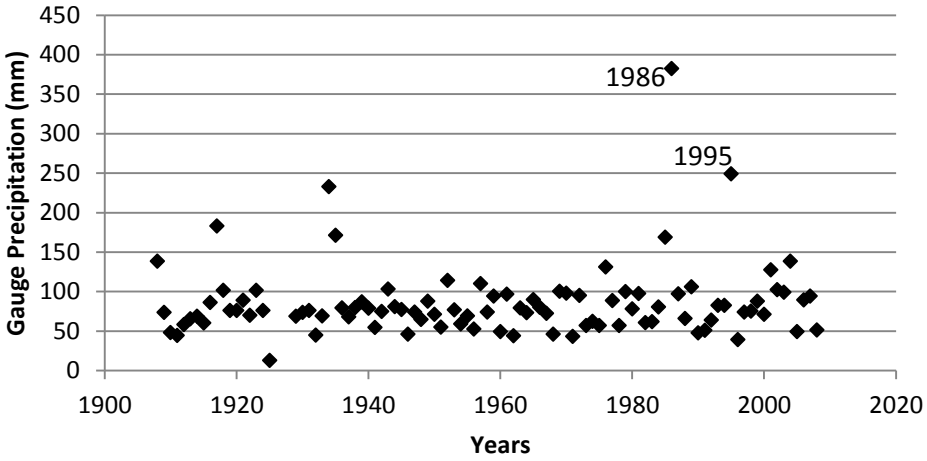

Figure 3: Seward precipitation AMS.

3.3.2 Statistical test

There is generally no trend for the AMS. A table need not be shown, as only one significant decrease was obtained from the Mann-Kendall test for the 30-year period at Homer Airport. These findings are consistent with NOAA's research results on precipitation frequency updates in Alaska (Perica et al. 2012). The mean and standard deviation from the AMS was also calculated for each station and used to select heavy precipitation events.

3.4 Frequency of Occurrence of Heavy Precipitation Events

Heavy precipitation events are defined as all daily precipitation exceeding a selected threshold. In order to calculate this threshold, we used the mean and standard deviation of each station's AMS (Figure 4).

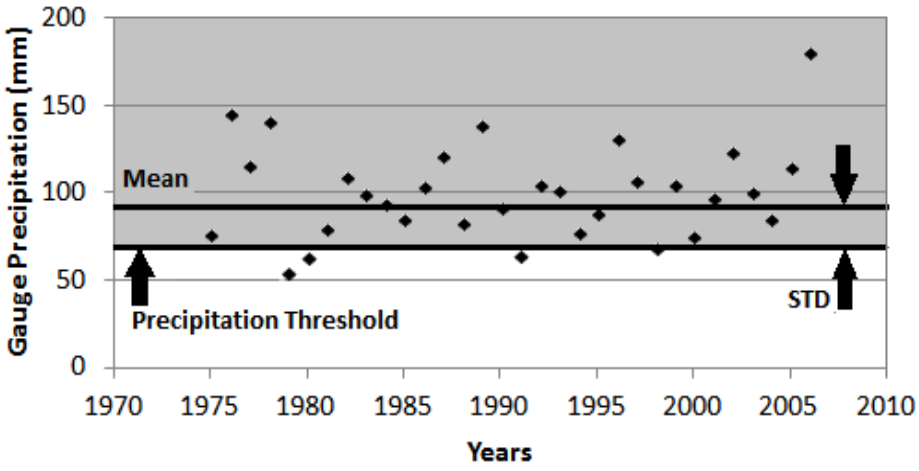

Figure 4: Approach to statistical testing: Selection of heavy precipitation threshold at Port San Juan.

The threshold is specific to each station, and computed by subtracting one standard deviation from the mean of annual maximum precipitation for each station (Table 4). Figure 4 illustrates selection of the precipitation threshold for Port San Juan (73.6 mm). Once the "heavy precipitation threshold" is identified, the number of events exceeding this threshold is counted for each year. In this manner, "occurrence of HPE" is represented for each station and used in subsequent statistical analysis.

3.4.1 Visual interpretation

Major outlier values in Whittier show a sequence of 3 nearly consecutive years (1985, 1986, and 1988) with HPE greater than 15, twice the mean (7.4). Annual maximum series analysis did not reveal high values for these particular years. This finding validates the need for checking heavy precipitation frequency, as AMS alone ignores events of similar magnitude occurring in the same year. The year of 1981 was a year of higher recurrence of heavy precipitation in many stations (Alyeska, Cooper Lake, Homer Airport); 2002 was also in the top 5 years for most stations.

3.4.2 Statistical test

Test results shown in Table 4 indicate no particular trend. Gray cells show insufficient data to conduct the test.

Table 4: Mann-Kendall trend test results for heavy precipitation events.

Station Name	HPE Threshold (mm)	20 Year	30 Year	40 Year	50 Year
Homer AP	20.5	No Trend	**Sign. Decrease**	No Trend	No Trend
Homer 8 NW	21.5	No Trend	No Trend	-	-
Kasilof 3 NW	14.3	No Trend	No Trend	-	-
Kenai AP	16.0	No Trend	No Trend	No Trend	No Trend
Alyeska	33.3	No Trend	**Sign. Increase**	-	-
Whittier	87.6	No Trend	No Trend	-	-
Seward	38.6	No Trend	No Trend	No Trend	No Trend
Port San Juan	73.6	No Trend	No Trend	-	-

No trend is present here, though the original dataset is greatly reduced and some stations' entire datasets had to be dismissed. Furthermore, to examine temporal distribution of the HPE during the year, the accumulated occurrence of the events for each month was graphed for the Kenai Airport Station (Figure 5) as a percentage of total HPE for each period (1899–1969 and 1970–2012). Since the Kenai Airport Station has a data gap from 1908 to 1942, both periods consist of roughly 40 years of data. Figure 5 shows that August and September had the most frequent occurrence of high precipitation events before 1970. The shift appears in late summer (July and August), when frequency of HPE occurrence decreases after 1970, and early fall (September and October) receives more frequent HPE. Therefore, the observed tendency is less frequent heavy rain in late summer and more heavy rainfall in the fall.

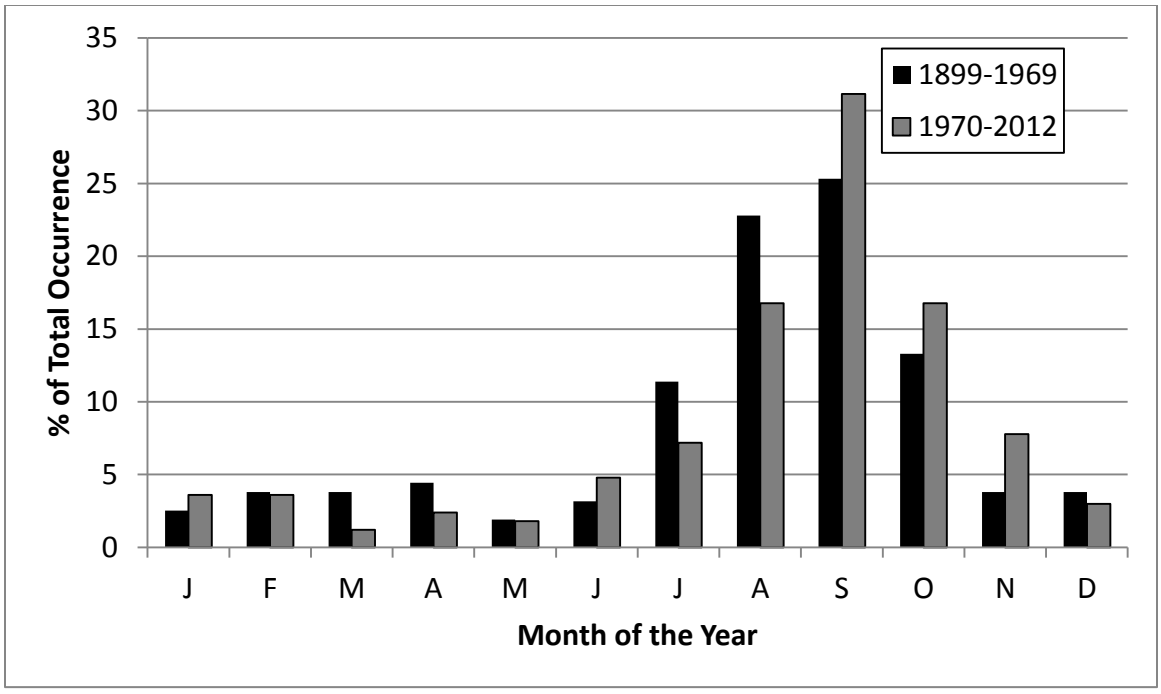

Figure 5: Monthly distribution of HPE occurrence at the Kenai Airport Station. Note that a gap in data is present from 1908 to 1942.

4. CONCLUSIONS

This study addressed the issue of climate change in the Kenai Peninsula from a hydrologist's or a meteorologist's perspective; it provides background information for the interdisciplinary group of scientists studying environmental and social changes in the Kenai Peninsula. The most reliable weather stations in this region were selected, and their measurements were analyzed through time. Analysis was focused on the climate indicators that have a direct impact on local communities: mean annual temperature, total annual precipitation, and extreme precipitation events, and how frequently they occur.

Mean annual temperatures are increasing at several stations across the region, especially when looking at the longer 40- and 50-year trends. However, the station with the longest record (Seward) does not show an increasing MAT trend at 5% significance level. The coldest MATs on the Kenai Peninsula were recorded in 1971, whereas the warmest MATs occurred in 1993 and 2005. In contrast to MAT, total annual precipitation shows a decreasing trend, however, long-term (40 or more years) reliable data are lacking. For many stations, 1986 was the wettest year, whereas 1996 was the driest year. When looking at the highest daily precipitation events for each year (AMS) and HPE, no trend was identified in these events over the period of record. However, a seasonal shift in heavy precipitation events from late summer to autumn exists. Future work will be directed towards identifying how observed changes in precipitation and air temperature affect lake and river hydrology, fish habitat, and local communities.

ACKNOWLEDGMENTS

This study was supported by the Alaska Experimental Program to Stimulate Competitive Research (EPSCoR), NSF grant OIA-12089927. It benefited from the collaboration, group

discussions, and field trips organized by the project leaders, with special thanks to Andrew Kliskey (UAA) and Robert Ruffner (KWF). Data formatting by CEE/UAF student Benjamin Glenn is greatly appreciated. On a more personal note, S. Bauret thanks the Civil Engineering Department at the Université de Sherbrooke (Québec), which encourages all of its students to engage in a study-abroad semester, which allowed him to discover Alaska. He also thanks the Québec Ministry of Education for the substantial scholarship that helped make this Alaska adventure possible.

REFERENCES

Adalgeirsdottir, G., Echelmeyer, K.A. & Harrison W.D. 1998 Elevation and volume changes on the Harding Icefield, Alaska. *J. Glaciol.* 44, 570–582.

Kane, D. & Stuefer, S. 2013 Challenges of Precipitation Data Collection in Alaska. *Proc. 19th NRB, Alaska*, this issue.

Kenai Watershed Forum 2012 *Stream Temperature Monitoring Network*, Available online: http://www.kenaiwatershed.org/research/temperature_monitoring.html, 23 March 2013.

Klein, E., Berg E.E. & Dial R. 2005 Wetland drying and succession across the Kenai Peninsula Lowlands, south-central Alaska. *Canadian Journal of Forest Research* 35(8), 1931–1941.

Mann, H.B. 1945. Nonparametric tests against trend. *Econometrica* 13, 245–259.

Perica, S., Kane, D., Dietz, S., Maitaria, K., Martin, D., Pavlovic, S., Roy, I., Stuefer, S., Tidwell, A., Trypaluk, C., Unruh, D., Yekta, M., Betts, E., Bonnin, G., Heim, S., Hiner, L., Lilly, E., Narayanan, J., Yan, F. & Zhao, T. 2012 Precipitation-Frequency Atlas of the United States, Alaska. *NOAA Atlas 14 Volume 7 Version 2.0, NOAA.* National Weather Service, Silver Spring, MD.

Shulski, M. & Wendler, G. 2007 *The Climate of Alaska*. University of Alaska Fairbanks, Fairbanks, Alaska.

Stafford, J.M., Wendler, G. & Curtis J. 2000 Temperature and precipitation of Alaska: 50 year trend analysis. *Theor. Appl. Climatol*. 67, 33–44.

VanLooy, J., Foster R. & Ford A. 2006 Accelerating thinning of Kenai Peninsula glaciers, Alaska. *Geophys. Res. Lett.* 33, L21307, doi: 10.1029/2006GL028060.

Western Regional Climate Center 2012 *Prospect Creek Camp, Alaska; Period of Record General Climate Summary – Temperature*. Available online: http://www.wrcc.dri.edu/cgi-bin/cliGCStT.pl?ak7778

An Analysis of Spatial and Temporal Trends and Patterns in Western Canadian Runoff: A CROCWR Component

Allison J. Bawden[1*], Donald H. Burn[1], and Terry D. Prowse[2]

[1]*Dept. of Civil & Environmental Engineering, University of Waterloo, Waterloo, ON, N2L 3G1, CANADA*
[2]*Water & Climate Impacts Research Centre, Environment Canada & University of Victoria, Victoria, BC, V8W 3R4, CANADA*
**Corresponding author's email address: abawden@uwaterloo.ca*

ABSTRACT
Climatic variability and change can have profound impacts on the hydrologic regime of a watershed. The Climatic Redistribution of Canada's Water Resources (CROCWR) project is concerned with quantifying changes in western Canadian water resources under past, present, and future climate through spatio-temporal analyses of runoff and its driving climatic and atmospheric forces (see also Linton et al. 2013; Newton et al. 2013). In this paper, annual and seasonal trends in western Canadian runoff are examined for the period of 1976–2010 using the Mann-Kendall (MK) test. Regional patterns of spatial variability are identified through principal component analysis (PCA) of the correlation matrix, and three hydrological regions are established representing watersheds in the upper, mid, and lower latitudes of the study region. Both watershed-scale and PCA trend results show increased runoff in the northernmost watersheds, while decreased water availability has resulted among the midlatitude basins. No consistent trend was found among all watersheds in the southern region. The results of this analysis will provide water resource managers with an indication of the direction and magnitude of changing water availability in western Canada.

KEYWORDS
Hydrology; climate change; trend analysis; principal component analysis

1. INTRODUCTION
Global climate has experienced a great deal of variability over the past century, differing widely from region to region. A number of studies (e.g., Zhang et al. 2007; Min et al. 2008) have documented temperature warming and increased precipitation at higher latitudes, and contrasting precipitation decreases in more southerly latitudes, over the past 50 years. The implications of climate change stretch beyond the scope of meteorological variability, however. In particular, a recent report of the Intergovernmental Panel on Climate Change (Bates et al. 2008) stressed that future climate is likely to intensify the hydrologic cycle and hence may affect water security in certain locations. For some regions, this will mean enhanced access to water resources, but because the effects will not be spatially uniform, other locations will experience reduced access (Prowse 2008). In areas that rely primarily on glaciers and seasonal snowpack for their water supply, for instance, the consequences of climate change on future water availability are likely to be severe. Under a warmer climate, less precipitation will fall as snow and snowmelt will occur earlier in the year, contributing to an earlier occurrence of peak runoff, away from summer when demand is highest (Barnett et al. 2005). Increased discharge has already been recorded in regions that spatially align with noted increases in temperature and precipitation—namely, the northern

high latitudes—and studies have attributed these increases to local warming effects, including intensified precipitation minus evaporation (Zhang et al. 2013). Global scale studies using hydrologic and general circulation models (GCMs) have also predicted changes in water distribution that will see further heightened runoff at high latitudes and decreased runoff in the midlatitudes (Barnett et al. 2005; Prowse 2008).

Because of the geographic nature of these changes, some large regions will contain zones of diametrically opposed responses, and will thus be affected by a greater need for effective water management. One of these regions is western Canada. An area of highly contrasting topography and hydroclimatic regimes, western Canada spans the mid to high latitudes of the Northern Hemisphere, stretching from south of 50°N to the North Pole. Coupled with the fact that the area is home to many of the world's largest rivers—a combination of both heavily regulated and pristine aquatic environments—western Canada is a critical region in which the impacts of climate change and variability on water supply can, and should, be assessed.

A number of recent studies have examined historical and/or modeled future changes in different measures of water availability in some of Canada's western drainage basins. In the high latitudes, Déry and Wood (2005) investigated trends in streamflow in the Canadian Arctic and found generally decreasing discharge that they related to various large-scale atmospheric phenomena. For Rocky Mountain rivers, Rood et al. (2008) identified earlier timing of spring peak flows and a decrease in summer month discharge. St. Jacques et al. (2010) also found that, even by eliminating the effects of the Pacific Decadal Oscillation, a major controlling factor of streamflow in the northern Rockies, overall runoff in this mountainous region has still declined over the past 60 years. For the alpine-fed Liard and Athabasca River basins, Burn et al. (2004) identified a general trend toward earlier onset of spring runoff; increasing winter flows and earlier occurrence of the spring freshet were similarly identified for the larger Mackenzie River basin by Abdul Aziz and Burn (2006).

In British Columbia, Fleming et al. (2005) noted different trend responses to climatic warming in annual streamflow volume for catchments with and without a glacial cover. Déry et al. (2009) indicated that an earlier onset of the spring melt, in addition to decreases in summer streamflow and a delay in the onset of fall discharge, are common to pluvial, nival, and glacial rivers in this region.

In rivers feeding the western Prairies, Schindler and Donahue (2006) found drastic reductions in summer discharge since the early 20th century, ranging from 20% in basins where human impact has been minimal to 84% in regions where damming and large water withdrawals have occurred. For the South Saskatchewan River basin, Tanzeeba and Gan (2011) used four IPCC emissions scenarios and four GCMs to model future climate and water availability; their results suggested that enhanced evaporation caused by rising temperatures will offset increases in precipitation, contributing to reduced mean annual maximum flows. Similarly, Kienzle et al. (2011) simulated a range of climate change conditions for the upper North Saskatchewan River basin and found that, under all climate change scenarios, a shift in the future hydrologic regime will include earlier spring runoff and peak flow, increases in both high and low flow magnitudes, and significantly greater discharge between October and June, with correspondingly less from July to September.

Despite results from studies isolated to one or a few western Canadian watersheds, knowledge of how water availability in this region as a whole has changed is still lacking. This paper attempts

to quantify the spatio-temporal climatic redistribution of Canada's western water resources for the 1976–2010 period through an analysis of runoff in 25 conterminous western Canadian watersheds.

2. DATA AND METHODOLOGY

2.1 Study Area and Runoff Data

The CROCWR study region includes 25 watersheds that span the majority of the western Canadian provinces and territories and contains many of Canada's largest rivers. Watersheds were delineated using a series of latitude-longitude points that correspond to 37 hydrometric gauging stations from the Water Survey of Canada (WSC) HYDAT database. Daily streamflow data for each watershed were computed based on defined input and output stations, and monthly runoff values were calculated by dividing by watershed drainage area. Annual and seasonal runoff records were created from the monthly time series. Seasons were defined as winter (January to March), spring (April to June), summer (July to September), and fall (October to December) based on a review of the watershed hydrographs. Annual series were created based on the hydrologic year (October to September). A map of the CROCWR region is shown in Figure 1. Details of the CROCWR watersheds are provided in Table 1.

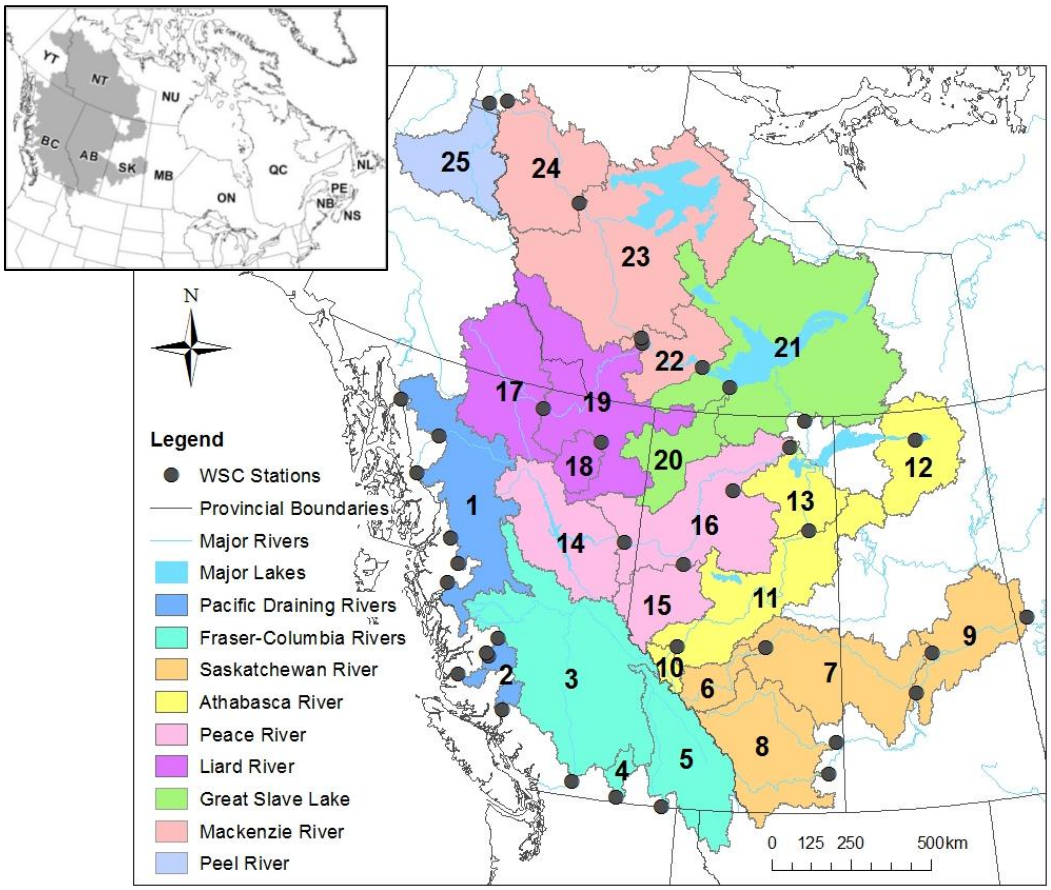

Figure 1: Map of the CROCWR study area, including 37 WSC gauging stations used to define watersheds. Numbers correspond to watershed information detailed in Table 1. Inset map shows location of CROCWR region within Canada.

Table 1: Details of the CROCWR study area.

Watershed	Area (km^2)
Pacific Basins	
1 North Pacific	1,990
2 South Pacific	5,720
Fraser-Columber Rivers	
3 Fraser	217,000
4 Okanagan	7,590
5 Columbia	155,000
Saskatchewan River	
6 Upper North Saskatchewan	28,100
7 Lower North Saskatchewan	102,900
8 Upper South Saskatchewan	104,250
9 Lower South Saskatchewan	117,000
Athabasca River	
10 Upper Athabasca	9,770
11 Lower Athabasca	123,230
12 East Lake Athabasca	50,700
13 West Lake Athabasca	35,800
Peace River	
14 Upper Peace	101,000
15 Smoky River	50,300
16 Lower Peace	141,700
Liard River	
17 Upper Liard	104,000
18 Fort Nelson	20,300
19 Lower Liard	150,700
Great Slave Lake	
20 Hay	51,700
21 Great Slave	322,300
Mackenzie River	
22 Upper Mackenzie	15,000
23 Mid-Mackenzie	324,500
24 Lower Mackenzie	84,600
Peel River	
25 Peel	70,600

2.2 Trend Detection

Time series of runoff data were analyzed for trend using the MK non-parametric test (Mann 1945; Kendall 1975). The MK test is a rank-based statistical tool frequently applied in hydro-meteorological studies for identification of significant monotonic trends in a dataset.

Following the method of Burn et al. (2004a), the data used in this analysis were first corrected for serial correlation by means of the Trend Free Pre-Whitening approach developed by Yue et al. (2002). The magnitude and direction of the MK trends were estimated using the Theil-Sen robust slope estimator (Sen 1968).

Before studying trend in a time series, it is important to assess the relative homogeneity of the data in order to identify the presence of change points (Reeves et al 2007). Continuity, or a lack of change points, is often necessary in order to draw accurate conclusions from trend analysis. The presence of change points in the data was assessed using the Pettit test (Pettit 1979).

2.3 Hydrological Regionalization

Principal component analysis was used to classify distinct areas of runoff variability within the CROCWR region. In PCA, the dominant patterns, or modes, of spatial variability are expressed as the principal components (PCs) of a correlation or covariance matrix. The correlation matrix was specified in the PCA to avoid loadings being focused exclusively in regions of high runoff (Maurer et al. 2004); the results therefore represent patterns of spatially coherent runoff anomalies (Lins 1997).

PCA produces a new dataset of mutually orthogonal eigenvectors with corresponding eigenvalues listed in decreasing order of importance. The time series related to the first few eigenvectors represent a large fraction of variability of the original dataset. The eigenvectors illustrate how geographical areas of runoff vary together. In some cases, spatial patterns become more easily interpretable and physically meaningful when the eigenvectors are subjected to a rotation. The orthogonal varimax rotation, commonly used in PCA on hydroclimatic data, was used in this study. Orthogonal rotation of the eigenvectors results in redistribution of the variances among the rotated modes (Jonsdottir & Uvo 2007).

3. RESULTS AND DISCUSSION

3.1 Trend Analysis

The results of MK trend detection for 1976–2010 annual runoff are presented in Figure 2. Application of the Pettit test showed no consistent shift among all basins for a common year. Watersheds that did experience change points generally tended to exhibit trends in the direction of the shift significant at the 5% or 10% significance level.

Some potentially misleading conclusions can be drawn from Figure 2, highlighting the importance of performing trend analyses on variables representing shorter periods of time within the year (e.g., seasons or months) in order to better grasp the patterns of changing inter- and intra-annual runoff. Nevertheless, the annual results provide a general summary of the seasonal results and are therefore presented.

As Figure 2 shows, changing water availability is not as simple and clear-cut as "higher latitudes are becoming wetter, while mid- and lower latitudes are getting drier." Although a general discrepancy in runoff trends did exist between northern and southern basins for the 1976–2010 period, there are some important and complicating exceptions.

Unlike the majority of the other CROCWR watersheds located north of 60°N, the Mid-Mackenzie and Peel River basins exhibited decreasing tendencies in annual runoff for the 1976–2010 period. The presence of negative trend slopes for annual runoff in these basins is not, however, representative of the changes that occurred throughout the majority of the year. For the Mid-Mackenzie River basin, runoff increased slightly during the fall and winter seasons (0.1 to 0.2 mm/yr), but decreases in summer and spring (-0.2 to -0.4 mm/yr) were marginally stronger, contributing to an overall decrease in annual runoff (-0.5 mm/yr). The stronger decreasing slope for annual runoff is not illustrative of what occurred during each of the seasons. For the Peel

River basin, the decreasing annual runoff slope of -0.3 mm/yr was strongly influenced by a decreasing tendency in spring (-0.9 mm/yr), despite the watershed having experienced an increasing tendency in summer runoff (0.4 mm/yr) and increasing trends significant at the 5% level in fall and winter runoff (0.2 to 0.4 mm/yr).

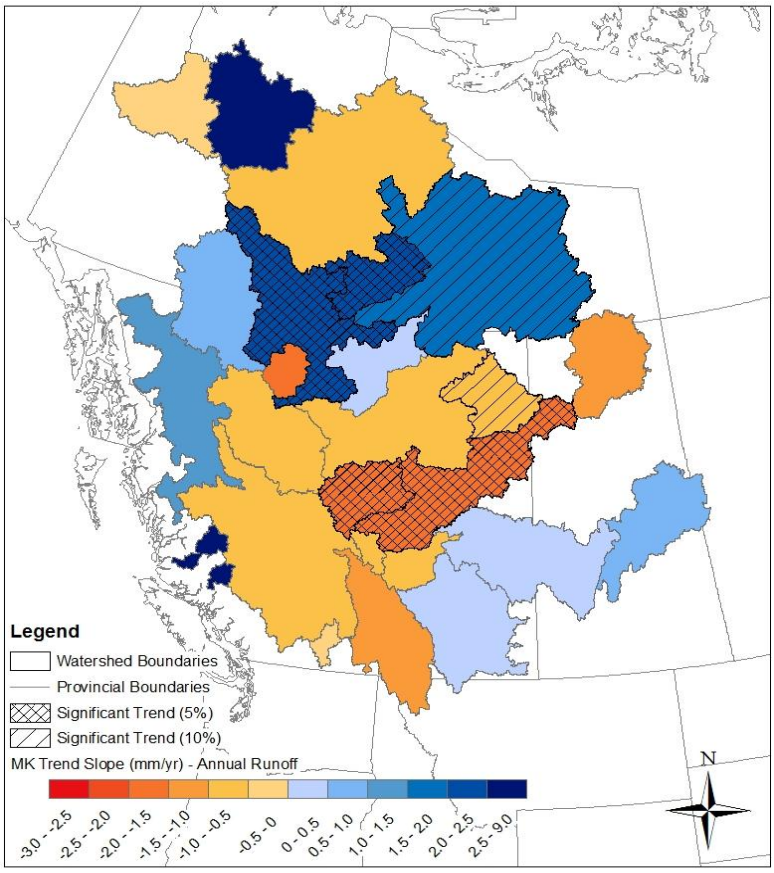

Figure 2: Annual runoff trend slopes for the 1976–2010 period. Positive (negative) slopes indicate increasing (decreasing) tendencies. Significant trends (hatched) are shown at both the 5% and 10% significance levels.

Within the mid- to lower-latitude watersheds, primarily decreasing trends and tendencies in annual runoff were experienced, particularly in and around the Lower Athabasca River basin. There are two notable exceptions to this observation, however. The Lower North Saskatchewan and Upper and Lower South Saskatchewan River basins incurred increasing tendencies (and significant increasing trends, in some cases) both annually and during all seasons. In addition, the North and South Pacific basins along the west coast both experienced higher magnitude increasing tendencies for all variables (with the exception of fall for the North Pacific basin), suggesting that degree of latitude is not always indicative of expected trend direction.

The fall and winter seasons exhibited the clearest difference in trend slopes between northern and more southern basins, when all watersheds poleward of 60°N displayed increasing trends or tendencies, with the opposite true for most of the southern basins. These results support the hypothesis that water availability is increasing at higher latitudes during the cold seasons.

Summer trend results, although generally weaker in magnitude, mirrored annual trends the closest, indicating that changes in summer have had a very strong influence on overall annual water availability. The most complicating season was spring, where the general north–south divergence was completely dissolved. During spring, all of the most southern basins experienced slight increasing tendencies in runoff.

The influences of latitude and longitude, mean elevation above sea level, and drainage area on watershed runoff (mean and trend) were examined. Table 2 presents the results of correlation analysis, and reveals a clear positive relationship between average runoff and mean watershed elevation; no significant correlation was found between runoff trend (MK slope) and elevation, however. Results from Table 2 also support projections of increasing runoff with latitude as a (albeit weak) significant positive relationship existed between runoff trend and degree of latitude for all hydrologic variables considered, except spring runoff (which, as discussed above, did not follow the general trend pattern of the other seasons). As expected, watershed area had no influence on either runoff or trend, since the influence of area was removed via the calculation of runoff depth from streamflow. It is noteworthy that all correlations between runoff (mean and trend) and longitude were negative, perhaps implying a shift in runoff from east to west. Future work will examine this relationship further. In addition, percent glacial coverage over the watershed would be another useful factor to explore (e.g., Déry et al. 2012).

Table 2: Pearson's correlation (*R* value) between topography and 1976–2010 runoff (mean and trend). Significant correlations are **bolded** (10%) and **underlined** (5%).

		Topographical Parameter			
1976-2010 Runoff Characteristic		Latitude	Longitude	Mean Elevation	Drainage Area
Annual	Mean Runoff	-0.22	**-0.43**	**0.59**	-0.17
	Runoff Trend	**0.42**	**-0.37**	-0.22	0.02
Winter	Mean Runoff	-0.32	-0.21	**0.55**	-0.07
	Runoff Trend	**0.53**	**-0.42**	-0.21	0.03
Spring	Mean Runoff	-0.18	**-0.53**	**0.62**	-0.13
	Runoff Trend	0.14	-0.23	-0.05	0.09
Summer	Mean Runoff	-0.17	**-0.42**	**0.53**	-0.21
	Runoff Trend	**0.45**	-0.30	-0.32	0.02
Fall	Mean Runoff	-0.26	-0.31	**0.53**	-0.14
	Runoff Trend	**0.43**	**-0.38**	-0.15	-0.04

Note: Latitude and longitude are defined as decimal degrees from the Equator and Prime Meridian, respectively. Degrees of latitude are positive in the Northern Hemisphere; degrees of longitude are negative in Canada, where the west has lower values than the east. Latitude and longitude values at the centroid of each watershed were used.

3.2 Principal Component Analysis

Rotated PCA (rPCA) revealed three distinct regions of coherent hydrological variability: the northern or "upper region" (UR), the midlatitude or "middle region" (MR), and the southern or "lower region" (LR) of the CROCWR study area. Although the boundaries of the regions (and hence the watersheds included) varied slightly from season to season and annually, the presence of each region was common to each of the variables. The first three rPCs accounted for 52.4% of

variance in annual runoff, 46.4% in winter runoff, 51.9% in spring runoff, 55.3% in summer runoff, and 47.7% in fall runoff. Figure 3 shows rPCA results for annual runoff. Factor loadings with magnitudes of 0.32 to 0.55 were considered significant but weak; loadings of 0.55 to 0.78 were considered fair; and 0.78 to 1.0 were considered strong.

While the UR was generally consistent and discernible for all variables, with largest contribution of the northern watersheds occurring in the summer, the LR and MR tended to shift east-west with the seasons. For annual runoff, the LR consisted of the 11 lowest-latitude watersheds; the easternmost Saskatchewan River basins were excluded from the LR during winter, spring, and summer, and the area extended northwest into the North Pacific basin on the west coast during winter and spring. The LR was least clearly defined during the fall, when significant negative loadings from the Saskatchewan River system occurred and no prominent contributions existed from the other low-latitude basins.

For annual runoff, the MR included mainly the watersheds that displayed decreasing runoff trends and tendencies annually, including the Peace-Athabasca River system. This region was fairly consistent among each season, with the smallest contribution occurring in winter and the largest area covered in spring. The Great Slave Lake and Upper Mackenzie River basins contained negative loadings for annual, spring, and summer runoff, indicating a strong opposing response for this region north of Lake Athabasca.

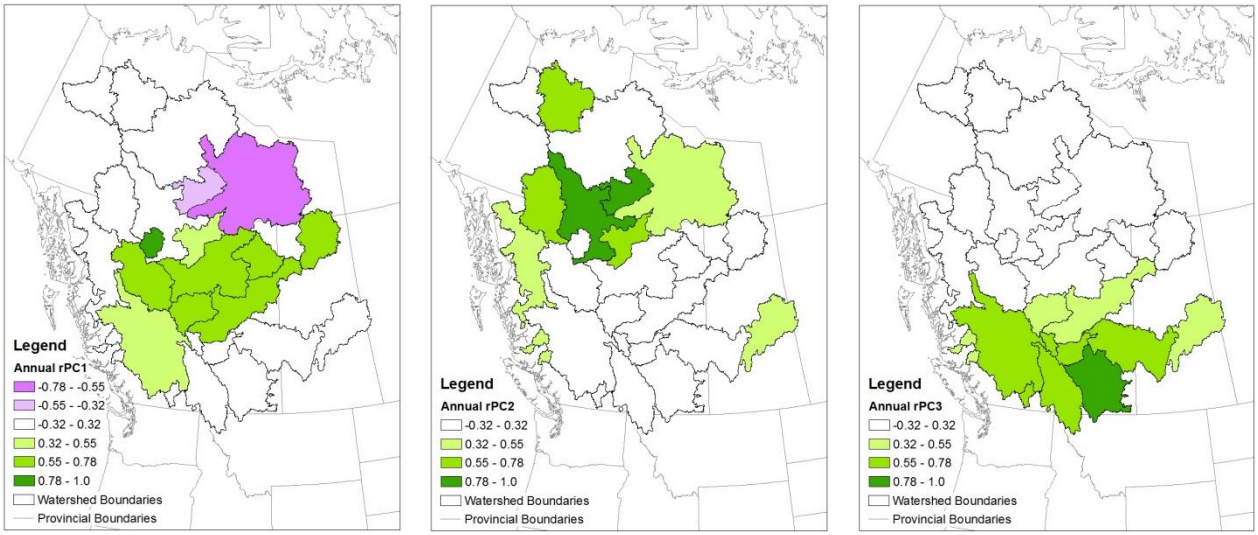

Figure 3: Annual runoff factor loadings for the first three rPCs; loadings over |0.32| were considered significant. From left to right: rPC1, rPC2, and rPC3 describe the middle, upper, and lower CROCWR regions, respectively. rPC1 accounted for 18.8% of the total variance in annual runoff, while rPC2 accounted for 16.3%, and rPC3 accounted for 17.3%.

For each variable, the runoff data matrix was projected onto the rPC loadings matrix to obtain time series for each rPC. Mann-Kendall trend analysis was performed on the rPC scores, providing a source of comparison between the watershed-scale trend results. Figure 4 shows plots of the first three rPC scores for annual runoff. Table 3 provides rPC score trend results for each variable.

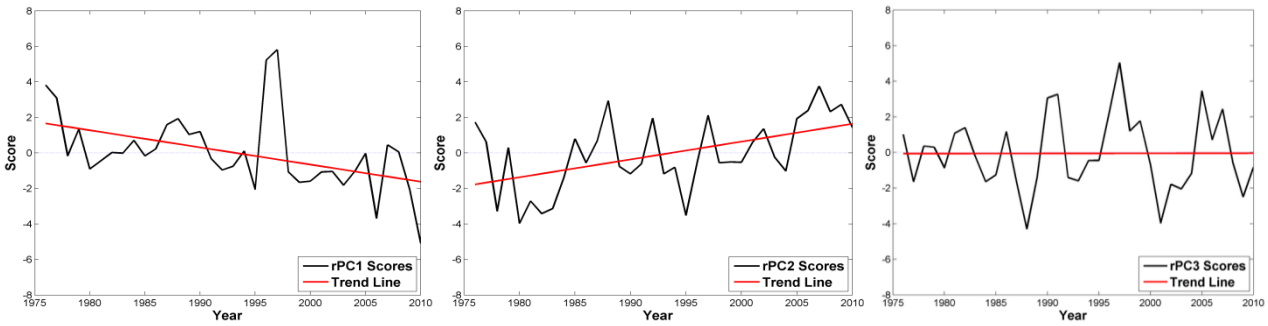

Figure 4: Time series of annual runoff scores for the first three rPCs: rPC1 corresponds to the MR, rPC2 corresponds to the UR, and rPC3 corresponds to the LR of the CROCWR study area. Trend lines for the 1976–2010 period are shown in red.

Table 3: MK trend slope values for the first three rPCs for each variable. Results are presented by region with corresponding rPC in square brackets ([ ]). Significant trends are **bolded** (10%) and **underlined** (5%).

	Trend Slope (runoff anomaly/yr) [PC#]					
	Upper Region		Middle Region		Lower Region	
Annual	**0.1**	[2]	**-0.1**	[1]	0	[3]
Winter	**0.1**	[2]	0	[3]	0	[1]
Spring	0	[2]	-0.1	[1]	0	[3]
Summer	**0.1**	[2]	-0.1	[1]	0	[3]
Fall	**0.1**	[3]	**-0.1**	[1]	**-0.1**	[2]

Regional trend analysis on rPC scores confirmed predictions that the higher latitudes have generally experienced increased runoff, especially during the cold seasons, while changes at the mid and lower latitudes were not as pronounced. For all seasons except spring, significant increasing trends were detected for the UR. In addition, the MR saw reduced runoff year-round, with significant results occurring annually and during the fall. The LR experienced no trend for all variables except fall, which exhibited a significant decreasing trend; the overall lack of change in the LR was likely caused by the fluctuating definition of the region in terms of which watersheds were included during each season, and the contrasts in runoff trends among the individual watersheds.

4. CONCLUSIONS

Trends and variability in western Canadian runoff were analyzed for the period of 1976–2010. Overall, runoff was found to have increased in most watersheds north of the 60th parallel, especially in the winter, while midlatitude watersheds generally experienced decreased runoff, implying a northward shift in water availability from adjacent southerly basins. The lowest-latitude watersheds showed an even mix of both increasing and decreasing tendencies, suggesting the prediction that "low latitudes are becoming drier" is not applicable in all cases. For example, both the Pacific Coast and western Prairies displayed increases in runoff for all seasons, implying this is not strictly a seasonally dependent observation. Correlation analysis showed a significant yet weak relationship between runoff trends and latitude ($R \approx 0.5$), the

result of which was largely affected by these conflicting increasing and decreasing trends in the southern CROCWR basins.

Principal component analysis on runoff data revealed three regions of coherent hydrologic behaviour: the northern or UR, midlatitude or MR, and southern or LR. Consistent with the results of watershed-scale trend analysis, the UR experienced increased runoff, the MR experienced decreased runoff, and the LR experienced a mix of seasonally dependent increasing and decreasing trends for all runoff variables analyzed.

As the 21st century progresses, it is likely that increasing temperatures in the high latitudes will create stronger contrasts between water resources in the Arctic and midlatitudes, creating a greater need for revised water management and a potential for additional water diversion systems in western Canada.

ACKNOWLEDGMENTS

This research was funded by the Natural Sciences & Engineering Research Council of Canada, the Ontario Student Assistantship Program, and the University of Waterloo. Streamflow data were provided by Environment Canada's Archived Hydrometric Database (available online: http://www.wsc.ec.gc.ca/applications/H2O/index-eng.cfm).

REFERENCES

Abdul Aziz, O.I. & Burn, D.H. 2006 Trends and variability in the hydrological regime of the Mackenzie River Basin. *Journal of Hydrology* 319, 282–294.

Barnett, T.P., Adam, J.C. & Lettenmaier, D.P. 2005 Potential impacts of a warming climate on water availability in snow-dominated regions. *Nature* 438(17), 303–309.

Bates, B. et al. 2008 *Climate Change and Water*. Technical paper of the Intergovernmental Panel on Climate Change, IPCC Secretariat, Geneva 210.

Burn D.H., Abdul Aziz, O.I. & Pietroniro, A. 2004 A comparison of trends in hydrological variables for two watersheds in the Mackenzie River Basin. *Canadian Water Resources Journal* 29(4), 283–298.

Déry, S.J. & Wood, E.F. 2005 Decreasing river discharge in northern Canada. *Geophysical Research Letters* 32(L10401), 1–4.

Déry, S.J., Hernandez-Henriquez, M.A., Owens, P.N., Parkes, M.W. & Petticrew, E.L. 2012 A century of hydrological variability and trends in the Fraser River Basin. *Environmental Research Letters* 7(024019), 1–10.

Déry, S.J., Stahl, K., Moore, R.D., Whitfield, P.H., Menounos, B. & Burford, J.E. 2009 Detection of runoff timing changes in pluvial, nival, and glacial rivers of western Canada. *Water Resources Research* 45(W04426), 1–11.

Fleming, S.W. & Clarke, G.K.C. 2003 Glacial control of water resources and related environmental responses to climatic warming: empirical analysis using historical streamflow data from Northwestern Canada. *Canadian Water Resources Journal* 28(1), 69–86.

Jonsdottir, J.F. & Uvo, C.B. 2007 Long term variability in Icelandic hydrological series and its relation to variability in atmospheric circulation over the North Atlantic Ocean. *International Journal of Climatology* 29(10), 1369–1380.

Kendall, M.G. 1975 *Rank Correlation Measures*. Charles Griffin, London.

Kienzle, S.W., Nemeth, M.W., Byrne, J.M. & MacDonald, R.J. 2011 Simulating the hydrological impacts of climate change in the upper North Saskatchewan River basin, Alberta, Canada. *Journal of Hydrology* 412, 76–89.

Lins, H.F. 1997 Regional streamflow regimes and hydroclimatology of the United States. *Water Resources Research* 33(7), 1655–1667.

Linton, H.C., Prowse, T.D., Dibike, Y. & Bonsal, B.R., 2013 Spatiotemporal trends in climatic variables affecting streamflow across western Canada from 1950–2010: A CROCWR component. *Proc. of the Northern Research Basin Symposium (unpublished), August*..

Mann, H.B. 1945 Non-parametric tests against trend. *Econometrica* 13, 245–259.

Maurer, E.P., Lettenmaier, D.P. & Mantua, N.J. 2004 Variability and potential sources of predictability of North American runoff. *Water Resources Research* 40, W09306.

Min, S.K., Zhang, X. & Zwiers, F. 2008 Human induced Arctic moistening. *Science* 320, 518–520.

Newton, B.W., Prowse, T.D. & Bonsal, B.R., 2013 Synoptic climatological characteristics associated with water availability in western Canada: A CROCWR component. *Proc. of the Northern Research Basin Symposium* (unpublished), *August*.

Pettitt, A.N. 1979 A non-parametric approach to the change-point problem. *Applied Statistics* 28(2), 126–135.

Prowse, T.D. 2008 Climatic Redistribution of Water Resources in Western Canada. *Western Watershed Stewardship Council Meeting*, October 29.

Reeves, J., Chen, J., Wang, X.L., Lund, R. & Lu, Q. 2007 A review and comparison of changepoint detection techniques for climate data. *Journal of Applied Meteorology and Climatology* 46, 900–915.

Rood, S.B., Pan, J., Gill, K.M., Franks, C.G., Samuelson, G.M. & Shepherd, A. 2008 Declining summer flows of Rocky Mountain rivers: Changing seasonal hydrology and probable impacts on floodplain forests. *Journal of Hydrology* 349, 397–410.

Sen, P.K. 1968 Estimates of the regression coefficient based on Kendall's tau. *Journal of the American Statistical Association* 63, 1379–1389.

St. Jacques, J. M., Sauchyn, D.J. & Zhao, Y. 2010 Northern Rocky Mountain streamflow records: Global warming trends, human impacts or natural variability? *Geophysical Research Letters* 37(L06407), 1–5.

Tanzeeba, S. & Yew Gan, T. 2012 Potential impact of climate change on the water availability of the South Saskatchewan River Basin. *Climatic Change* 112, 335–386.

Yue, S., Pilon, P.J., Phinney, B. & Cavadias, G. 2002 The influence of autocorrelation on the ability to detect trend in hydrological series. *Hydrological Processes* 16(9), 1807–1829.

Zhang, X., He, J., Zhang, J., Polyakov, I., Gerdes, R., Inoue, J. & Wu., P. 2013 Enhanced poleward moisture transport and amplified northern high-latitude wetting trend. *Nature Climate Change Letters* 3, 47–51.

Zhang, X., Zwiers, F.W., Hegerl, G.C., Lambert, F.H., Gillett, N.P., Solomon, S., Stott, P.A. & Nozawa, T. 2007 Detection of human influence on twentieth-century precipitation trends. *Nature Letters* 448(26), 461–465.

Historical Changes and Future Projections of Extreme Hydroclimate Events in Interior Alaska Watersheds

Katrina E. Bennett[1*], Alex Cannon[2], and Larry Hinzman[1]

[1]*International Arctic Research Centre, University of Alaska Fairbanks, Fairbanks, AK 99775, USA*
[2]*Pacific Climate Impacts Consortium, University of Victoria, Victoria, BC,, V8W 3R4, CANADA*
**Corresponding author's email: kebennett@alaska.edu*

ABSTRACT
Climate change will shift the frequency, intensity, duration, and persistence of extreme hydroclimate events and may have particularly disastrous consequences in vulnerable systems such as the warm permafrost-dominated interior region of Alaska. This work focuses on recent research results from trends and generalized extreme value analyses at two Interior Alaska river basins for 1951–2012. Trends analysis of maximum streamflow for the Chena and Salcha Rivers indicates a strong (> +50%) and statistically significant increase in 12-day flow events during the late fall/winter and during the snowmelt period (late April), followed by a significant decrease in the 12-day flow events during the post-snowmelt period (late May/June). The March-April-May seasonal (and annual on the Chena only) trends, however, illustrate significant decreases (> -50%) in maximum streamflow on both systems, which indicates the importance of trends analysis across multiple time scales. Generalized extreme value analysis highlights that changes in the winter and spring are non-linear and non-stationary in nature and may be indicative of shifting regimes linked to climate variability. Exploration based on a study of Environment Canada's CMIP-5 ClimDEX indices of temperature and precipitation for Alaska suggests that the driving climate factors are projected by a subset of global climate models to increase by the 2080s, which may indicate a future with continued increases in extreme hydroclimate events for Alaska's interior basins. Adequate representation of extremes is required to accurately understand and model these changing patterns, and provide adequate warning to Alaska communities of such events.

KEYWORDS
Extreme events; streamflow; boreal forest; sub-Arctic; Interior Alaska

1. INTRODUCTION
Extreme hydroclimatic responses in regional-scale Interior Alaska watersheds are influenced by both climate change and natural climate variability, and lead to unanticipated shifts in water storage that may impact statewide and global freshwater resource availability and quality. The signal of mean change has been well documented in previous work (Hinzman et al. 2005) and includes shifts in snow cover extent (Brown 2010); permafrost distribution (Osterkamp 2005); lake and river freeze-up and breakup (Magnuson et al. 2000); glacial mass-balance (Moore et al. 2009); and regional synoptic and river discharge (Dery & Wood 2005). However, analysis of extreme events, including changes in streamflow in the Arctic and sub-Arctic region of Alaska, has been limited. Some of the limitations of the work are due to short, low-quality records of streamflow available for comprehensive study, and because understanding of hydroclimatologic regimes, snowmelt and freeze-thaw dynamics, and antecedent moisture storage conditions

driving events at the regional-scale in Alaska watersheds remains unclear (Woo et al. 2008). This paper seeks to expand our understanding of historical changes (1951–2012) in hydroclimate extremes through the examination of maximum streamflow changes in terms of non-parametric (trends) and non-stationary (generalized extreme value, GEV) analytical approaches at two Interior Alaska watersheds. The results are also discussed with respect to an ensemble of future (2080s) global climate model (GCM) projections of extreme indices of temperature and precipitation for the region nearby Fairbanks, Alaska.

2. STUDY AREA

The Salcha (5740 km^2) and the Chena (5350 mi^2) River basins are meso-scale headwater systems to the Tanana River basin (Figure 1), which drains eventually into the Yukon River, entering the Bering Sea via Norton Sound. The Salcha River (USGS 15484000, gauged since 1948) and the Chena River (USGS 15514000, gauged since 1947) are snowmelt-dominated systems with rainfall peaks in August corresponding to convective systems that are common in Interior Alaska (Figure 1). Average mean temperatures are -2.5°C and annual precipitation total is ~270 mm (Fairbanks International Airport climate station, 1970–2000). Salcha has 67% of its basin at "high elevation" (above 600 m), with 32% of its slopes facing north; the Chena has 33% of its basin at high elevation, with 16% of the watershed comprised of north-facing aspect slopes.

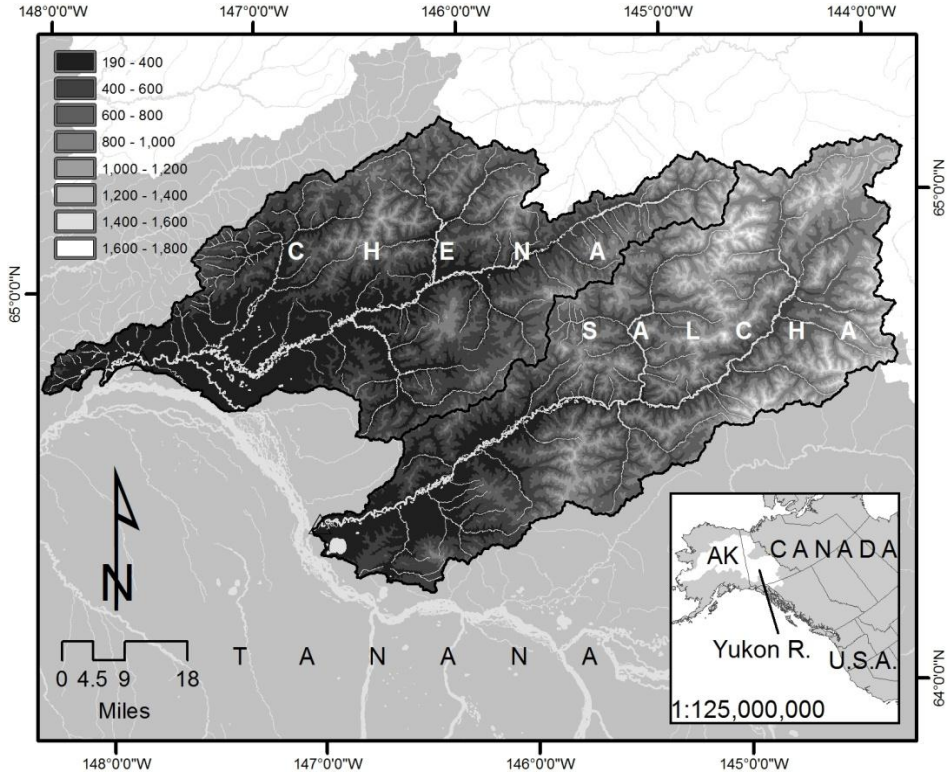

Figure 1: Salcha and Chena River basins, Interior Alaska, USA. The inset illustrates the Yukon River basin and Alaska in the context of Canada and the USA.

Discontinuous permafrost underlies both basins, with north-facing slopes dominated by permafrost, black spruce, and bog mosses. South-facing slopes exhibit seasonally frozen ground and are forested predominantly by birch, alder, and shrub understory. Tussock tundra is found at low elevations. Soils are primarily organic over silty eolian deposits, underlain by igneous

gravelly colluviums. High-elevation rock outcrops exist above 1000 m (National Elevation Dataset, USGS).

3. METHODS

3.1 Trends Analysis

Trend analysis was completed for the maximum 12-day, monthly, seasonal (December-January-February, DJF; March-April-May, MAM; June-July-August, JJA; and September-October-November, SON), and annual time series from 1951–2012. Trends were analyzed using an approach developed by Yue et al. (2002) as outlined in Wang and Swail (2001), where the trend magnitude is calculated using the Theil-Sen approach (Sen 1968; Theil 1950a, b, c). The time series is then pre-whitened, and the non-parametric Mann-Kendal test for significance is calculated. The analysis was carried out using the R-project's (http://www.r-project.org/) zyp package (Bronaugh & Werner 2009).

3.2 GEV Analysis

The study of extremes in the field of hydrology can be approached from the extreme value theorem, which allows for the fitting of extreme values by the generalized extreme value (GEV). The approach is grounded in the theory of extremal limits that states that a sufficiently long time series of block maxima will approach the GEV distribution asymptotically at large sample sizes (Coles 2001). One of the primary reasons to utilize a GEV-based approach is that it is suited to analysis of non-stationary hydroclimatic extremes (Milly et al. 2008). The parameters in the GEV distribution can be allowed to change with time (or with covariates that are time-dependent), hence allowing the efficient detection of trends in extremes within the extreme value theorem framework.

The GEV approach applied in this study utilizes the R-project's GEVcdn package as described in Cannon (2010, 2011). Generalized extreme value analysis was applied only to the monthly, seasonal, and annual maximum streamflow data. The approach defines a technique to model the GEV distribution as a function of covariates using a conditional density network that is a probabilistic extension of the multilayer perceptron (MLP) neural network. The cumulative distribution of a GEV follows as,

$$F(y;\mu,\sigma,\kappa) = \exp\left[-\left\{1-\kappa\frac{(y-\mu)}{\sigma}\right\}^{1/\kappa}\right], \kappa \neq 0, 1-\kappa\frac{(y-\mu)}{\alpha} > 0$$

$$F(y;\mu,\sigma) = \exp\left[-\exp\left\{\frac{-(y-\mu)}{\sigma}\right\}\right], \kappa = 0$$

where μ is the location parameter, and signifies the distribution center; the scale parameter, σ, determines the size of the deviations around μ; and κ is the shape parameter that determines the tail behavior of the distribution (normally Fréchet, Weibull or Gumbel type, Cannon 2010; Katz 2013). To avoid problems with maximum likelihood (ML) estimation of the shape parameter, a penalized version of ML that applies a prior distribution to the shape parameter that is representative of natural processes (Cannon 2010; Coles & Dixon 1999; Martins & Stedinger 2000) is used here. In addition, the shape parameter is kept constant in all candidate models.

The work presented herein details results from five different candidate models. The initial model is stationary (S), in which parameters are not allowed to vary in time. In the remaining models, the location and scale parameters are allowed to vary in time by specifying either a linear or non-linear hidden-layer activation function $m(\cdot)$ in the conditional density network model architecture. In the linear GEV model, $m(\cdot)$ is the identify function, whereas $m(\cdot)$ is the hyperbolic tangent function in non-linear models. A linear non-stationary (LNS) version of the GEV framework assumes that the location and scale parameters are allowed to vary linearly with time. This version of the GEV essentially follows El Adlouni et al. (2007),

$$\mu(t) = \beta_1 + \beta_2 t$$

$$\log(\alpha(t)) = \delta_1 + \delta_2 t$$

where β_1, β_2, δ_1, and δ_2 are parameters estimated from data. In the non-linear models, the number of hidden-layer nodes controls the degree of non-linearity that can be represented (Cannon 2010). Three non-linear non-stationary candidate models of increasing complexity are analyzed by changing the number of nodes from one to three (NLNS1, NLNS2, and NLNS3, respectively).

To determine which one of the candidate model approaches is most applicable, the Akaike Information Criteria, corrected for small sample sizes (AICc) and the Bayesian Information Criteria (BIC) statistics are applied (Burnham et al. 2011). Statistics such as AICc and BIC can be used to determine information loss; AICc includes a correction factor for small samples. BIC tends to be most parsimonious in terms of its tendency towards models that are not overfit. Hence, BIC is focused upon in results reporting. These two statistics identify the best model when minimized. Only the model that is minimized is reported in Table 1.

3.3 ClimDEX Indices

The Expert Team on Climate Change Detection and Indices (ETCCDI) developed a set of indices that could be used for analysis of extreme events (see Zhang et al. 2011). The purpose of the ETCCDI indices was to have a set of reproducible, common index variables that could be easily calculated based on available daily climate data such as air temperature and precipitation (Zhang & Zwiers 2013). Three ClimDEX indices are presented here; the minimum of the daily minimum temperatures in a month or year (TNn), the maximum of the daily maximum temperatures within a month or year (TXx), and the maximum consecutive 5-day precipitation total in a month (Rx5, Table 2).

The dataset was developed based on the R-projects's package climdex.pcic, and downloaded from Environment Canada's ClimDEX portal (http://www.cccma.ec.gc.ca/data/climdex/). The GCMs on the portal were based on data availability in the CMIP5 database as of September 2012 (Kharin et al. 2013; Sillmann et al. 2013a, b). Datasets were extracted for the three grid cells nearby Fairbanks, Alaska, and processed from monthly statistics to seasonal and annual differences from 1971–2000. Data averaged from the 2071–2100 (centered on the 2080s), model simulation run one, and representative concentration pathway (RCP) 8.5 are reported here. Results from six GCMs are analysed as an ensemble. GCMs in the ensemble are CanESM2, CCSM4, CNRM-CM5.1, IPSL-CM5A-LR, MPI-ESM-LR, and MRI-CGCM3. See Bennett & Walsh (in prep., *Journal of Climate*) for more details.

Table 1: The Salcha and the Chena River basin trend statistics for month, season, and annual. Statistical significance of the trend is in brackets. Bold values indicate statistical significance of trend <0.10 (90% confidence interval). Models that minimize AICc and BIC are listed below trend results. S = stationary; LNS = linear non-stationary; and NLNS = non-linear non-stationary, with 1, 2, and 3 pertaining to the number of model nodes.

Stations		Jan	Feb	Mar	Apr	May	Jun	Jul	Aug	Sep
Salcha 15484000	Trends	**45 (0.01)**	**45 (0.05)**	42 (0.15)	**98 (0.00)**	**-59 (0.00)**	-19 (0.46)	7 (0.87)	-19 (0.21)	-19 (0.3)
	AICc	NLNS3	LNS	NLNS3	NLNS1	NLNS2	NLNS2	NLNS2	S	NLNS1
	BIC	NLNS3	LNS	NLNS3	NLNS1	NLNS2	S	S	S	S
Chena 15514000	Trends	19 (0.16)	16 (0.36)	13 (0.36)	**69 (0.00)**	**-73 (0.00)**	-18 (0.47)	1 (0.67)	-12 (0.22)	-29 (0.17)
	AICc	NLNS1	NLNS1	NLNS3	NLNS2	NLNS3	NLNS2	S	NLNS2	NLNS1
	BIC	S	S	NLNS3	NLNS2	NLNS3	NLNS2	S	S	NLNS1

		Oct	Nov	Dec	DJF	MAM	JJA	SON	ANN
Salcha 15484000	Trends	0 (0.76)	**45 (0.00)**	**56 (0.00)**	**51 (0.02)**	**-55 (0.01)**	-3 (0.81)	-19 (0.3)	-21 (0.19)
	AICc	S	LNS	NLNS2	NLNS3	NLNS2	S	NLNS1	NLNS2
	BIC	S	LNS	NLNS2	NLNS2	NLNS2	S	S	S
Chena 15514000	Trends	-12 (0.44)	**27 (0.08)**	**27 (0.04)**	24 (0.14)	**-73 (0.01)**	-16 (0.27)	-27 (0.21)	**-49 (0.01)**
	AICc	NLNS2	LNS	NLNS3	NLNS3	NLNS3	S	NLNS1	NLNS3
	BIC	S	LNS	NLNS2	LNS	NLNS2	S	S	NLNS3

4. RESULTS

Streamflow on the Salcha and Chena Rivers illustrates a dual peak that is indicative of snowmelt/rainfall-dominated systems (Figure 2, panels a, c). The snowmelt peak is the largest annual contribution to flow, followed by a secondary maximum flow peak in late June that is only apparent on the Salcha River. The June peak is indicative of late melt associated with high-elevation snowpacks in the upper reaches of the watershed. The rainfall peak in both systems occurs in mid-August and is associated with convective storm systems that bring intense rainfall to the region and run quickly off the landscape, generating peak flows and sometimes flooding events.

The 12-day and monthly trends (Figure 2, Table 1) illustrate a strong and significant increase in maximum flows in November and December at both sites that continue through the winter (January and February) at the Salcha River basin. This change is also observed as a strong increase in DJF seasonal trends on the Salcha. At both sites, a strong and significant increase in April flows is noted; 12-day trends illustrate that the change is actually occurring in late April as opposed to earlier April when ice cover may influence the gauge. Late May through early June 12-day trends highlight declining flows in both systems. These changes show up as large flow reductions in May at a monthly time scale and in MAM seasonal flows. The annual flow trends

in these two systems are dominated by this May/June decline, although only the trend on the Chena is significant at the 99% confidence interval (CI, Table 1, Figure 2). Annual streamflow or seasonal (MAM) trends do not reflect the April flow increases indicative of shifts in the spring freshet.

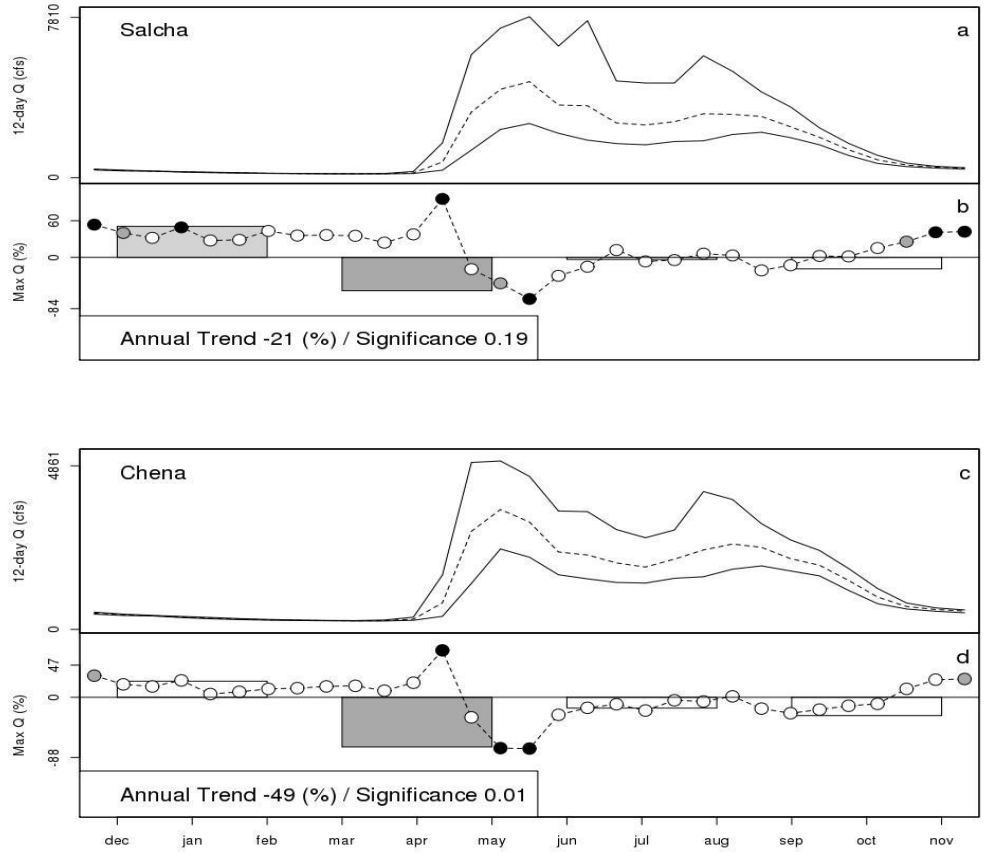

Figure 2: The Salcha River (a, b) and the Chena River (c, d) maximum, mean (dashed) and minimum 12-day flows are illustrated in the top panels (a, c). The trend statistics are illustrated in the bottom panels (b, d); 12-day flows are shown with circles, the seasonal results are shown with boxes that indicate trend size and direction, and the annual trend and significance is reported in text in the bottom left-hand corner. Grey and black circles and boxes are the 95% and 99% CI, and white are not significant.

The AICc and BIC results for the GEV model candidates illustrate that for the five different models, the stationary (S) and the non-linear, non-stationary (NLNS) models of intermediate complexity (2 nodes) are the most commonly selected as the best performing models (Table 1). Considering BIC results only, the months of July to October (excluding September) appear to be mostly associated with stationary models, while the more dynamic periods of the year appear to best represented by the non-stationary, non-linear models. Annually, the Salcha River system is best modeled by the stationary model, whereas the maximum streamflow in the Chena is better captured by non-linear non-stationary models.

ClimDEX indices of temperature extremes (TNn and TNx), and 5-day precipitation (Rx5), illustrate projections in extreme events for the overall forcing mechanisms that drive streamflow.

Broadly, increasing temperatures and precipitation are projected by the 2080s (Table 2) for the region nearby Fairbanks, Alaska. The extreme minimum temperatures are changing more than extreme maximum temperatures, and changes are most apparent in the winter and spring seasons. TXx is changing the most in the spring and autumn. The across-GCM standard deviations are greatest during the winter for TNn, although the projected changes are much larger than the variation across models, pointing to coherence in the projections. Rx5 is projected to increase the most in the summer and the autumn seasons, with the ensemble projected changes more than 2–3 times that of the across-model standard deviations (Table 2, Bennett & Walsh 2013 in prep. for the *Journal of Climate*).

Table 2: ClimDEX indices for minimum of the daily minimum temperatures (TNn), maximum of the daily maximum temperatures (TXx), and 5-day precipitation (Rx5), seasonal and annual statistics. Results, centered on the 2080s, are shown as an average of 6 GCMs differenced from the 1971–2000 time period for the 3 grid cells nearby Fairbanks, Alaska. See text for more details.

	DJF	MAM	JJA	SON	ANN
			TNn		
2080s Difference	12.81	10.29	4.67	9.36	13.39
2080s Standard Deviation	2.8	2.81	1.34	1.25	2.94
			TXx		
2080s Difference	4.21	5.21	3.9	4.42	3.71
2080s Standard Deviation	1.47	2.13	2.53	1.36	2.87
			Rx5		
2080s Difference	2	4	8	8	12
2080s Standard Deviation	2	2	3	3	5

5. DISCUSSION

Snowmelt-dominated systems in Interior Alaska appear to be changing in response to large shifts in snowpack and groundwater (i.e., baseflow) that are linked to warming winter minimum temperatures and increasing summer and fall precipitation (Hinzman et al. 2005; Zhang et al. 2000). The winter baseflow increase has been related to thawing permafrost in the Northwest Territories of Canada (St. Jacques & Sauchyn 2009) and in the Yukon River basin of Alaska and Canada (Walvoord & Striegl 2007). The Salcha River system, with a greater percentage of its basin at high elevation and 32% at a north-facing aspect, could be experiencing changes in winter baseflow as a result of shifts in the permafrost. Increasing trends in maximum streamflow occurring in November and through the winter could also be indicative of increased fall rains that result in higher streamflow volumes leading into winter. Fall rains would be amplified in the higher elevation Salcha River system, compared with the lower elevation Chena River basin.

Although ice affects many of the rivers in Interior Alaska, the Chena River basin is the USGS's index gauge owing to open-water conditions along the Chena that exist through the winter. The proximity of the Salcha River basin to the Chena index station also increases confidence in winter streamflow changes. This study looked only at maximum streamflow. In the winter

months of the year, maximum and minimum streamflow is very similar, and trends are similar in direction and magnitude although not identical (results not shown).

Increases observed in 12-day and monthly April maximum streamflow indicate that over 1951–2012, strong and significant changes have occurred in the timing of snowmelt that is indicative of a regime shift (Euskirchen et al. 2007). A decline in May/early June streamflow is indicative of a shift away from the normally high freshet streamflow volumes of the historical period towards relatively lower streamflow volumes associated with freshet tails. In the case of the Salcha River, which has a large percentage of its basin at mid to high elevation, the freshet has likely experienced a reduction in magnitude along with an extension in the melt season, with the lower elevation areas melting out earlier, but the higher elevation zones still retaining their melt regimes but with less overall snowpack. This change may lead to the increased possibility for ice-jamming events on the Salcha River, as the overall freshet period has been extended by a number of weeks. This is probably also why the trend results for the Chena are stronger and more significant during May and annually, as compared with the Salcha, while Salcha has changed more in April versus the Chena.

Changes in trends examined on a 12-day, monthly, seasonal, and annual time scale illustrate the importance of examining trend results across various time scales. The changes in terms of April flows are apparent only at the 12-day and monthly time scale. Even the monthly trend results do not show that the greatest increases are occurring in the last week of April, at a time when, in normal years, ice effects on the gauges have passed. The large declines in May/June flows, on the other hand, are indicative of an overall annual trend in decreasing streamflow volumes.

Generalized extreme value results highlight the importance of understanding the type of analysis used for examining changes in streamflow. During the summer (June for Salcha, July and August for both basins), late fall (September for Salcha only, October, and November for both basins), and winter (February for both basins, and January for the Chena only), it appears that stationary and linear non-stationary models may perform best. This is indicative of a stable or shifting system in which the time-dependent signal is linear in nature. However, during the months of March to May for both basins, June and September for Chena only, and January on the Salcha, non-linear non-stationary models perform best. This indicates that the trend occurring over the time period is non-linear. These months are broadly the time periods when increased baseflow (hypothesized to be occurring due to thawing permafrost) and changes in snowpack are shifting. These changes may also be linked to non-linear features of the climate system such as large-scale teleconnections patterns or changes in atmospheric moisture cycling. Modeling approaches that consider patterns in extremes in these months should take into account the non-stationary and non-linear shifts that may represent dynamic alterations of the streamflow system and indicate a large change in terms of the regime.

Future projections to the 2080s in extreme temperature and precipitation indices indicate that Alaska watersheds nearby Fairbanks are moving towards warmer (less cold) extreme minimum temperatures in winter and spring, and towards more wet summers and autumns, with increases in 5-day precipitation events. These changes may result in shifts in streamflow towards "true" snowmelt-rainfall dominant systems. In low- to mid-elevation sites such as the Chena and the Salcha River basins, these changes are likely to be the more extreme along the continuum of change, as indicated from other work in the Pacific Northwest on shifting in snowmelt-rainfall systems (Elsner et al. 2010).

6. CONCLUSIONS

This paper illustrates findings from trends and GEV analysis undertaken for two Interior Alaska river basins over 1951–2012. The Salcha and the Chena Rivers are representative of headwater systems in Interior Alaska that are primarily snowmelt/rainfall-dominated and are underlain by discontinuous permafrost that is close to freezing (i.e., warm). Historical changes in these meso-scale watersheds are illustrative of broader scale shifts occurring across the North American boreal forest.

Trend results for 1951–2012 indicate strong and significant changes in maximum streamflow. Notable changes are occurring during winter and in April and May/early June. Winter streamflow is increasing in these systems due to changes in temperature and precipitation that are driving permafrost shifts (St. Jacques & Sauchyn 2009; Walvoord & Striegl 2007). April maximum streamflow increases are strong and statistically significant, while May/early June shows declines in streamflow in both systems. Differences in basin geometry between the two systems are likely reasons between the different trend results. Winter baseflow increases are strongest in the Salcha River, which has a large percentage of its watershed at high elevation and north facing, and thus has more permafrost potential and receives more precipitation. High-elevation snowpacks are likely not changing as much relative to the lower-elevation areas that comprise a larger percentage of the Chena River system. Thus, snowpack at the Salcha River system is experiencing not only a decrease in snowmelt magnitude, but also an extension of its melt period. The Chena River system experienced maximum streamflow increases during April that were reflective of the earlier melt, and larger relative declines in May/early June compared with the Salcha system. The Salcha River basin retained its upper elevation snowpack in April, resulting in an extended melt period.

Generalized extreme value analysis indicates that, in general, the changes occurring in these basins that are related to baseflow and snowpack shifts are best represented by non-linear non-stationary models and may be related to features of the climate system such as large-scale teleconnections patterns or changes in atmospheric moisture cycling. Modeling approaches that consider changes during these months should take into account the non-stationary and non-linear shifts that may represent dynamic alterations of the system and indicate a large change in terms of the streamflow regime. Covariates representing variations in large-scale climate models could potentially be incorporated into the non-stationary GEV framework to examine this in more detail.

An ensemble of GCMs project future changes (2080s) of extreme indices of temperature and precipitation for the Fairbanks area on the order of +13°C (+4°C), and +12 mm for monthly minimum (maximum) of the daily minimum (maximum) and daily 5-day precipitation events. The seasons of the largest projected change are winter and spring for temperature, and fall for precipitation. These projected changes coincide with the largest historical shifts in extreme maximum streamflow related to snowpack and baseflow shifts. Future projections in extreme temperature and precipitation indicate continued and increasing change in terms of extreme hydroclimate events in these snowfall-rainfall and warm-permafrost watersheds of Interior Alaska.

REFERENCES

Bennett, K.E. & Walsh, J. 2013 (in prep. for the Journal of Climate) Spatial and temporal changes in indices of extreme precipitation and temperature for Alaska.

Bronaugh, D. & Werner, A. 2009 Package 'zyp'. *CRAN Repository*.

Brown, R.D. 2010 Northern Hemisphere snow cover variability and change, 1915–97. *J. Clim.* 13**,** 2339–2355.

Burnham, K.P., Anderson, D.R. & Huyvaert, K.P. 2011 AIC model selection and multimodel inference in behavioral ecology: some background, observations, and comparisons. *Behav. Ecol. Sociobiol.* 65**,** 23–35.

Cannon, A.J. 2010 A flexible nonlinear modelling framework for nonstationary generalized extreme value analysis in hydroclimatology. *Hydrol. Process.* 24**,** 673–685.

Cannon, A.J. 2011 GEVcdn: An R package for nonstationary extreme value analysis by generalized extreme value conditional density estimation network. *Computers & Geosciences* 37**,** 1532–1533.

Coles, S. 2001. *An Introduction to Statistical Modeling of Extreme Values.* Springer Verlag.

Coles, S.G. & Dixon, M.J. 1999 Likelihood-based inference for extreme value models. *Extremes* 2**,** 5–23.

Dery, S.J. & Wood, E.F. 2005 Decreasing river discharge in northern Canada. *Geophys. Res. Lett.* 32.

Elsner, M.M. et al. 2010 Implications of 21st century climate change for the hydrology of Washington State. *Clim. Change* 102**,** 225–260.

Euskirchen, E., McGuire, A. & Chapin, F.S. 2007 Energy feedbacks of northern high-latitude ecosystems to the climate system due to reduced snow cover during 20th century warming. *Global Change Biol.* 13**,** 2425–2438.

Hinzman, L.D. et al. 2005 Evidence and implications of recent climate change in northern Alaska and other Arctic regions. *Clim. Change* 72**,** 251–298.

Katz, R.W. 2013 Statistical methods for nonstationary extremes. *Extremes in a Changing Climate*. Springer, pp. 15–37.

Kharin, V., Zwiers, F. Zhang, X. & Wehner, M. 2013. Changes in temperature and precipitation extremes in the CMIP5 ensemble. *Clim. Change* 1–13.

Magnuson, J.J. et al. 2000 Historical trends in lake and river ice cover in the Northern Hemisphere. *Science* 289**,** 1743.

Martins, E.S. & Stedinger, J.R. 2000 Generalized maximum-likelihood generalized extreme-value quantile estimators for hydrologic data. *Water Resour. Res.* 36**,** 737–744.

Milly, P.C.D., Betancourt, J., Falkenmark, Hirsch, R.M., Kundzewicz, Z.W., Lettenmaier, D.P. & Stouffer, R.J. 2008 Stationarity is dead: Whither water management. *Science* 319**,** 573–574.

Moore, R. et al. 2009 Glacier change in western North America: influences on hydrology, geomorphic hazards and water quality. *Hydrol. Process.* 23**,** 42–61.

Osterkamp, T. 2005 The recent warming of permafrost in Alaska. *Global Planet. Change* 49**,** 187–202.

Sen, P.K. 1968 Estimates of the regression coefficient based on Kendall's tau. *J. Amer. Statistical Assoc.* 63**,** 1379–1389.

Sillmann, J., Kharin, V., Zhang, X., Zwiers, F. & Bronaugh, D. 2013a: Climate extremes indices in the CMIP5 multi-model ensemble. Part 1: Model evaluation in the present climate. *J. Geophys. Res.: Atmos.*

Sillmann, J., Kharin, V., Zwiers, F., Zhang, X. & Bronaugh, D. 2013b: Climate extreme indices in the CMIP5 multi-model ensemble. Part 2: Future climate projections. *J. Geophys. Res.: Atmos.*

St. Jacques, J.-M. & Sauchyn, D.J. 2009 Increasing winter baseflow and mean annual streamflow from possible permafrost thawing in the Northwest Territories, Canada. *Geophys. Res. Lett.* 36**,** L01401.

Theil, H. 1950a A rank-invariant method of linear and polynomial regression analysis, III. *Nederlands Akad. Wetensch. Proc.* 53**,** 1397–1412.

Theil, H. 1950b A rank-invariant method of linear and polynomial regression analysis, II. *Nederlands Akad. Wetensch. Proc.* 53**,** 521–525.

Theil, H. 1950c A rank-invariant method of linear and polynomial regression analysis, I. *Nederlands Akad. Wetensch. Proc.* 53**,** 386–392.

Walvoord, M.A. & Striegl, R.G. 2007 Increased groundwater to stream discharge from permafrost thawing in the Yukon River basin: Potential impacts on lateral export of carbon and nitrogen. *Geophys. Res. Lett.* 34**,** L12402.

Wang, X.L. & Swail, V.R. 2001 Changes in extreme wave heights in northern hemisphere oceans and related atmospheric circulation regimes. *J. Clim.* 14**,** 2204–2221.

Woo, M.K., Kane, D.L., Carey, S.K. & Yang, D.Q. 2008 Progress in permafrost hydrology in the new millennium. *Permafrost and Periglacial Processes* 19**,** 237–254.

Yue, S., Pilon, P., Phinney, B. & Cavadias, G. 2002 The influence of autocorrelation on the ability to detect trend in hydrological series. *Hydrol. Process.* 16**,** 1807–1829.

Zhang, X. & Zwiers, F.W. 2013 Statistical indices for the diagnosing and detecting changes in extremes. *Extremes in a Changing Climate*. Springer, pp. 1–14.

Zhang, X., Vincent, L.A., Hogg, W.D. & Niitsoo, A. 2000 Temperature and precipitation trends in Canada during the 20th century. *Atmosphere-Ocean.* 38**,** 395–429.

Zhang, X. et al. 2011 Indices for monitoring changes in extremes based on daily temperature and precipitation data. *Wiley Interdisciplinary Reviews: Climate Change* 2**,** 851-870.

Linking North Slope Climate, Hydrology, and Fish Migration

Erica D. Betts* and Douglas L. Kane

Water and Environmental Research Center, University of Alaska Fairbanks, Fairbanks, AK 99775, USA
**Corresponding author's email: edbetts@alaska.edu*

ABSTRACT
Arctic grayling are a species that have a life history strategy specifically adapted to the extreme climate of the North. They migrate to spawning grounds just after breakup in the spring, migrate to feeding sites in early summer, and finally in the fall migrate back to their overwintering sites. The Kuparuk River is a perennial stream originating in the foothills of the Brooks Range on the North Slope of Alaska. Sections of the Kuparuk are intermittent, in that during low flows in the system these reaches appear dry. Water reappears downstream of these dry reaches, and it is believed that water continues to flow below the channel surface through an unfrozen thaw bulb beneath these reaches. These dry reaches create a barrier to fish migration. The impacts of a warming Arctic may have implications for the flow of water through this unfrozen layer beneath the river and, consequently, the flow of water within the channel. A better understanding of this phenomenon is crucial to understanding the impacts of a changing climate on hydrology and, ultimately, fish populations in the Arctic.

KEYWORDS
Arctic grayling; hyporheic flow; hydrology; North Slope; fish migration; overwintering

1. INTRODUCTION
Climate change is expected to occur at a higher rate in the Arctic than in the lower latitudes. The Arctic Climate Impact Assessment found that for the area north of 60°N, the projected mean annual temperature increase will be approximately twice the projected increase in the global mean annual temperature (Prowse et al. 2006a). The Arctic is already experiencing the evidence of these changes as witnessed by changes in precipitation and rates of evapotranspiration (ET). This measure of surface water balance (precipitation minus potential evapotranspiration) declined significantly in the Alaska Arctic between 1960 and 2001, showing a decrease in water availability with time (Hinzman et al. 2005). A change in water availability has implications for fish and wildlife species directly and/or through modifications to critical habitat. Although precipitation is expected to increase with climate change, this increase is expected to be smallest in the summer (Prowse et al. 2006b). When combined with an expected increase in evapotranspiration, the future surface water balance could see a further decline. Increases in evapotranspiration result from increases in air/water temperature, longer ice-free seasons, an increase in transpiring vegetation, and finally increased permafrost thaw, which decreases surface water levels (Prowse et al. 2006b).

The research presented here is an attempt to predict how future changes in the surface water balance may impact fish species in the Arctic. Specifically, this research will assess the occurrence of barriers to fish migration to overwintering sites. A major limiting factor for fish species on the North Slope is the ability to find adequate overwintering habitat (Craig 1989). The Arctic is a landscape dominated by cold winters. Species that exist in this environment have

evolved to withstand such harsh winters. For fish, the main strategies are to leave the system altogether or find adequate overwintering sites. Overwintering sites consist of those waterways or bodies that do not freeze solid in winter and that have an adequate dissolved oxygen supply. Because climate change alters temperature, it has implications for the changing of seasons. Currently, as temperatures increase in the spring, ice and snowmelt and breakup occur. Waterways become engorged as a whole winter's worth of snow and ice melts and flows into and through waterways to the Arctic Ocean. During this period, fish leave their overwintering sites in search of feeding and spawning grounds. The North Slope of Alaska experiences most of its precipitation in the winter. The result is a continual drying during the summer and a decrease in hydrologic connectivity (Bowling et al. 2003). Late summer rains are common and allow hydrologic connectivity to be reestablished. Fish that may have been stranded in water bodies that were good feeding, spawning, or rearing grounds but not good for overwintering can now move to overwintering sites. Hydrologic linkages between smaller streams and ponds to larger rivers and lakes is reestablished only with an increase in precipitation in late summer/early fall along with shorter, cooler days. These linkages allow fish to leave their feeding grounds and migrate to their overwintering sites (Morris 2003). Researchers on the North Slope have reported incidences of fish becoming stranded and unable to migrate as a result of low or no flow in streams and rivers (Martin et al. 2009). A formal study of this phenomenon has not occurred on the North Slope.

This project will assess the impact of climate change on the ability of Arctic grayling to access adequate overwintering sites in the Upper Kuparuk River basin on the North Slope of Alaska. The premise is that the establishment of hydrologic connectivity in late summer/early fall is important for many species of fish on the North Slope. Arctic grayling are the species being studied due to the existence of long-term research on this species in the Upper Kuparuk (Buzby 2004). The Upper Kuparuk is one of the most widely studied watersheds on the North Slope (Kane et al. 2000; Kane et al. 2003; McNamara et al. 1998) and as such provides a long history of hydrologic data. Figure 1 highlights the relationship between Arctic grayling migration and the typical hydrologic regime found in the Kuparuk River basin.

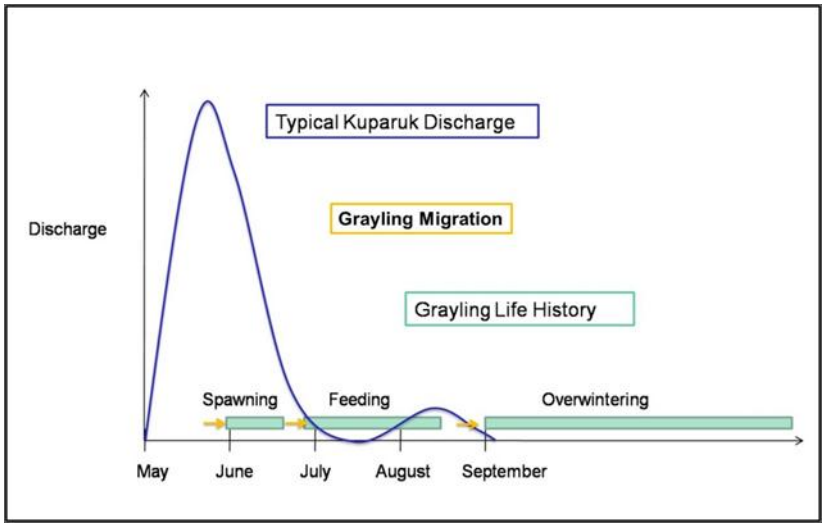

Figure 1: Relationship between timing of Arctic grayling migrations and typical hydrologic flow regime in nonglacial-fed arctic rivers.

Grayling leave overwintering sites after breakup in the spring. From overwintering sites, they migrate to spawning sites and then spend the rest of the summer feeding. As discussed previously, water levels drop during this period and can lead to fish becoming stranded. Late summer rain along with lower ET rates typically allow for increased connectivity in late summer/early fall, when grayling migrate back to their overwintering sites.

2. METHODS

The first step in this research is to identify locations that may present barriers to fish migration. The Upper Kuparuk represents a simplified case for studying hydrologic connectivity, in that connectivity is analyzed along the river itself as opposed to looking at the complex linkages between a river and connecting ponds, lakes, and wetlands. Arctic grayling overwinter in the headwater lake of the Kuparuk and migrate downstream as far as 60 km to spawn. Feeding sites exist within the river along this 60 km reach. Barriers to fish migration occur when sections of this reach run dry. Flow has not been recorded to cease completely through this reach. Instead it is believed that flow occurs below the surface of the river through these sections during periods of low flow in the system. In areas underlain by permafrost, there exists an area of melted permafrost below the river. This thaw bulb varies in thickness depending on the time of year, the water temperature, and the type of substrate. Water can flow within a stream channel or below the channel within this thaw bulb. This subsurface flow does not generally penetrate into deep groundwater due the permafrost layer below. In instances of low flow, the water in a river can appear to stop flowing at one location only to seemingly continue spontaneously a few meters or even miles downstream. What occurs is that the water is flowing entirely underground for that stretch of the river. This type of event may not typically be modeled in a routine hydrologic model, but for the purposes of fish migration, such an event is critical. Some research has been done on hyporheic flow in the Upper Kuparuk (Zarnetske et al. 2007; Zarnetske et al. 2008), but the research sites studied did not include those sections that lose surface water flow.

Critical reaches were identified as those sections of the river that have been documented as running dry during the summer. Interviews with researchers on the North Slope identified two locations along the Kuparuk as well as two locations on Oksrukuyik (Ox) Creek, a nearby stream. It was decided to include one Ox Creek location for comparison. The two locations on the Kuparuk are referred to as the Lower (KUP) and Upper (UK) Kuparuk sites due to their relative upstream and downstream positions. Because the length and exact location of these sites was unclear, temperature sensors were placed on the riverbed along these reaches to identify the presence or absence of surface water for the first field season. Pressure transducers were installed within the study reaches, but only one per site. Aerial photography was obtained using low-flying aircraft during a dry spell, which allowed for further identification of the location and length of these dry reaches. The second year of data collection allowed for better placement of pressure transducers and discharge measurements. Figure 2 shows the location of pressure transducers and temperature loggers along the Kuparuk River and Oksrukuyik Creek.

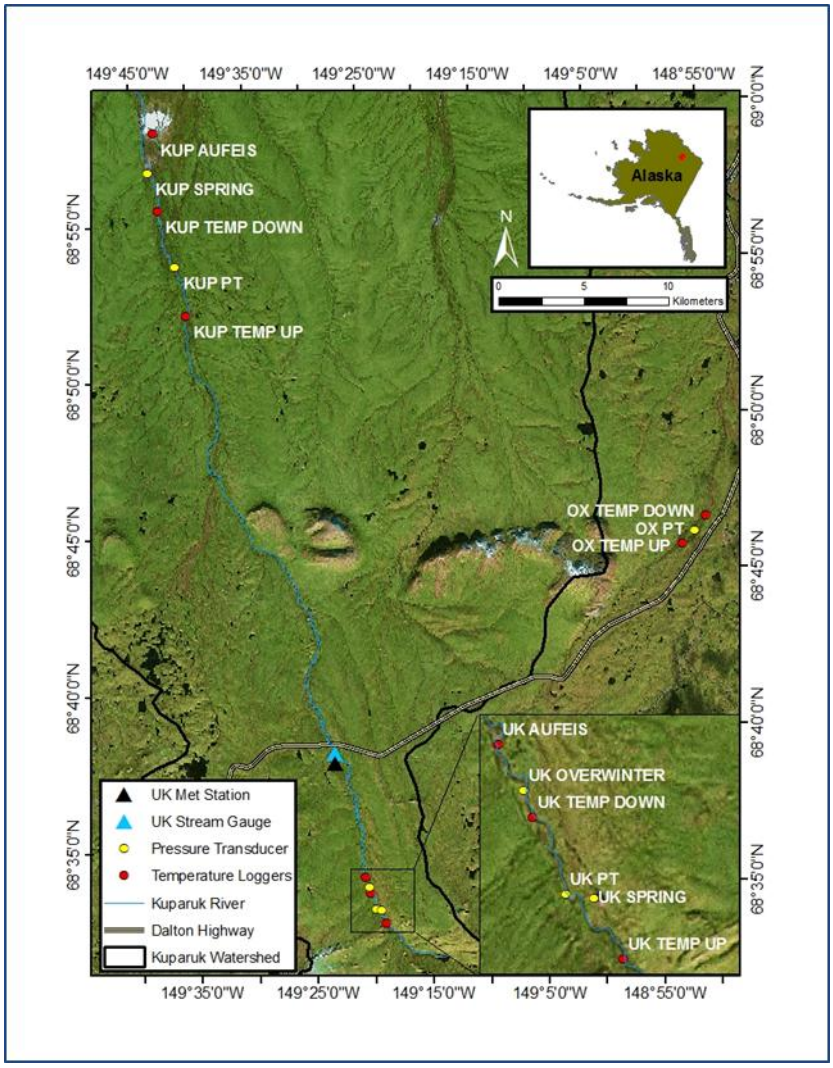

Figure 2: Research location: Kuparuk watershed, North Slope of Alaska. Image shows location of pressure transducers, temperature loggers, and meteorological stations. Research was conducted at three sites: Upper Kuparuk (UK), Lower Kuparuk (KUP), and Oksrukuyik Creek (OX).

A staff gauge is located on the Upper Kuparuk near the Dalton Highway bridge. This gauging site has been in place since 1996. Stage data collected at critical reaches were compared with stage data collected at this gauge site for the same years, 2010 and 2011. A statistical relationship was established between stage at each reach and stage at the gauging site on the Upper Kuparuk. This relationship was then used to derive historical stage values at the critical reaches based on the stage values measured at the gauge site. The results of this recreated historical dataset are discussed below.

3. RESULTS AND DISCUSSION

Stage data collected at the Upper and Lower Kuparuk sites were compared with data from the Upper Kuparuk Stream Gauge. Data from 2010–2012 were used to establish a statistical relationship between the sites. Based on this relationship, a longer historical dataset was created

for the Upper and Lower Kuparuk sites. This dataset provided information regarding the timing and frequency of dry periods over the past 15 years. Field notes of observations from researchers working in this area of Alaska were used to confirm as many dates as possible. Figure 3 displays the timing of "no flow" events at the Upper Kuparuk site as identified by the recreated dataset. The shaded area indicates the critical migration period for Arctic grayling. Dry spells occurring during this period impede fish from migrating to their overwintering site.

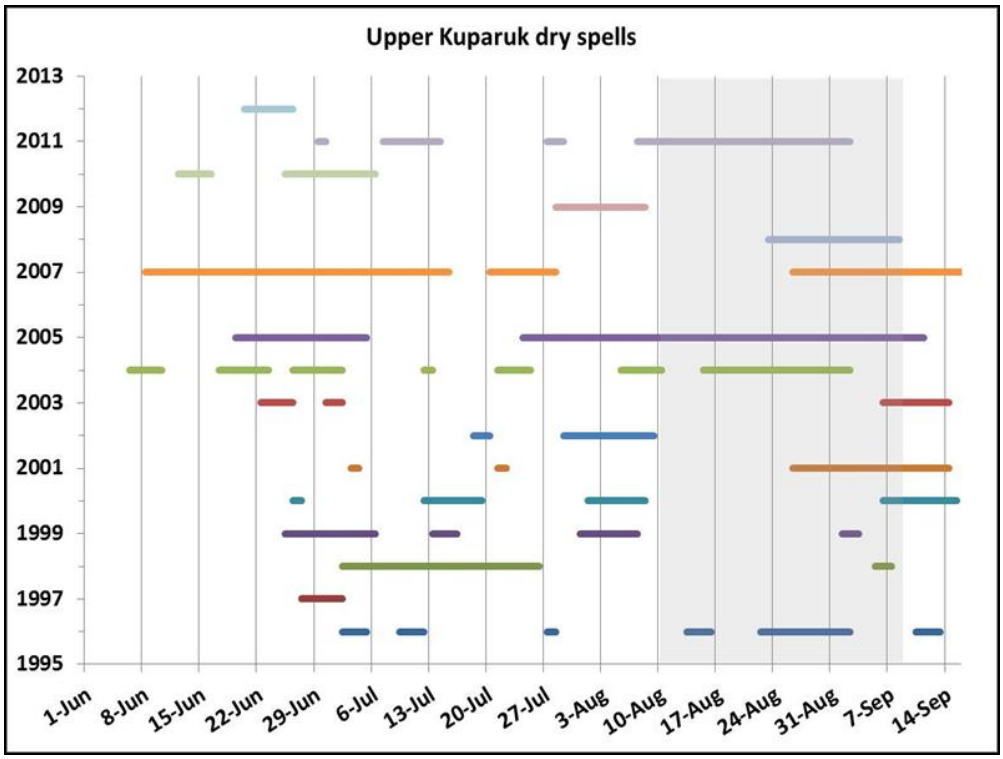

Figure 3: The recreated dataset showing dry spells per year. The shaded region indicates the time period during which Arctic grayling migrate to their overwintering site.

Figure 4 displays the data in terms of total number of days with no flow. This gives a picture of how often such events occur on average in any given year. Notice the particularly high number of days in 2004, 2005, and 2007. The green triangles represent the actual measured values in the Upper Kuparuk, while the blue diamonds represent the estimated values.

Figure 5 shows the timing of dry events as a monthly average. It is interesting to note that there is no statistically significant difference in the likelihood of a dry event occurring in any given month during the summer. This is particularly interesting given that the monthly precipitation average tends to increase in the summer through August, when it begins to decline again (Kane et al. 2004; Martin et al. 2009).

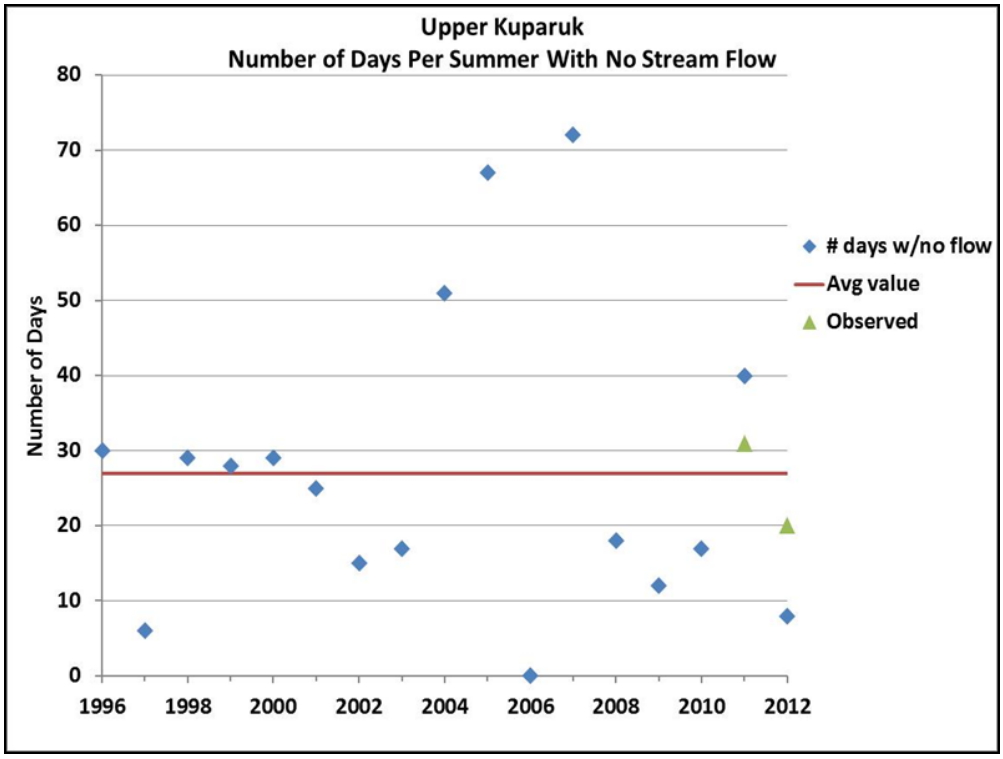

Figure 4: Estimated number of days per summer with no above-surface stream flow based on 15 years of data. Observed values for 2011 and 2012 are also shown.

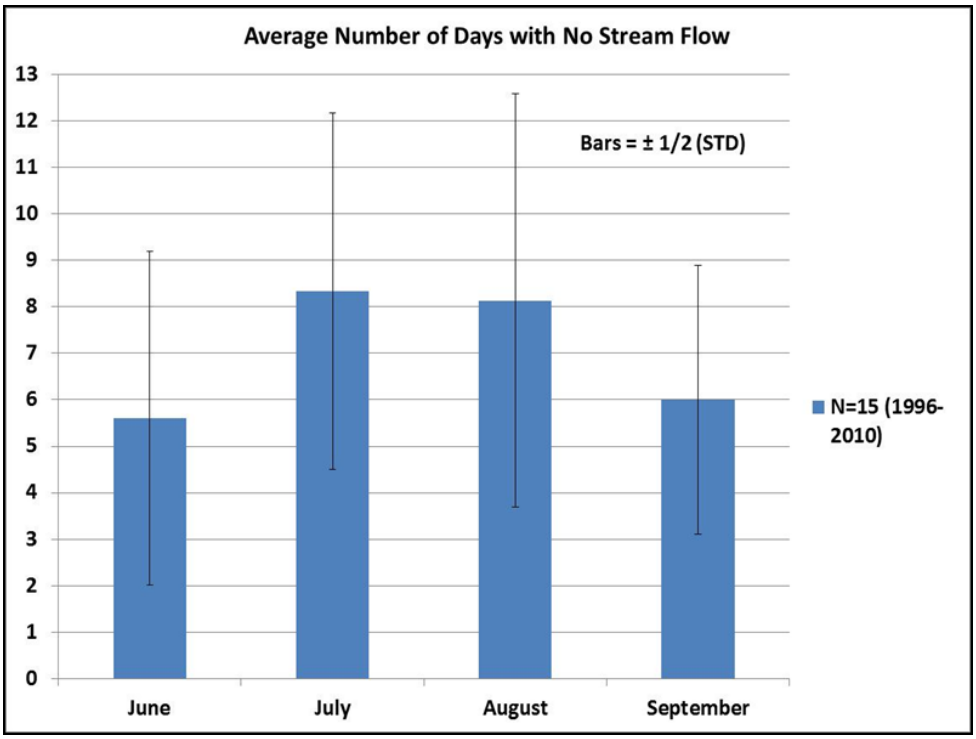

Figure 5: Average number of days per month with no flow at Kuparuk dry site.

The summer of 2011 provided a good opportunity for studying dry spells, as over 30 days were recorded as no-flow events at both the Upper and Lower Kuparuk sites. Of particular importance was the occurrence of nearly 2 weeks of no flow during fall grayling migration. Researchers were able to measure the impact of this barrier on tagged grayling in the Upper Kuparuk. Results show that nearly 75% of the biomass accumulated during the previous two months was lost during this two-week period (Deegan 2012).

4. CONCLUSIONS

This research provides a first look at the issue of hydrologic connectivity on the North Slope as defined by the needs of a resident fish species. The results of this effort indicate that no-flow events are a common occurrence in this system. Results of concurrent research also show that dry spells that occur during critical migration periods can have a very negative impact on grayling fitness. The implications of this research in light of climate change are that higher summer temperatures leading to higher rates of evapotranspiration will lead to a greater occurrence of these dry spells. Precipitation rates are expected to increase with higher temperatures, but the nature of this increase is less clear. Large rain events would favor increased runoff as the primary mechanism for water to leave the system, while smaller, more frequent rain events favor evapotranspiration (Hinzman and Kane 1992).

It is possible that a change in the hydrologic regime of the North Slope will have impacts on fish species. The life history strategies adopted by Arctic grayling and other species in the Arctic are the result of adaptation to the physical processes at work in the region (Bryant 2009). The timing of spring melt, the timing of freeze-up, and the amount and timing of precipitation are all factors to which species have become adapted. The Arctic is already witnessing a change in these environmental conditions. The rate of this change and the ability of species to adapt will have implications for the numbers and types of species that remain in the region.

ACKNOWLEDGMENTS

Funding for this research was provided by the U.S. Fish and Wildlife Service, a grant from the National Fish and Wildlife Fund, and a fellowship from the World Wildlife Fund. Special thanks go to Joel Homan, John Mumm, and Nathan Stephen for help in the field. Amy Tidwell and Douglas Kane provided valuable input into the design of this project.

REFERENCES

Bowling, L.C., Kane, D.L., Gieck, R.E. & Hinzman, L.D. 2003 The role of surface storage in a low-gradient arctic watershed. *Water Resources Research* 39(3).

Bryant, M.D. 2009 Global climate change and potential effects on Pacific Salmonids in freshwater ecosystems of southeast Alaska. *Climatic Change* 95(1-2), 169–193.

Buzby, K.M. & Deegan, L.A. 2004 Long-term survival of adult Arctic grayling (*Thymallus arcticus*) in the Kuparuk River, Alaska. *Can. J. Fish. Aquat. Sci.* 61, 1954–1964.

Craig, P.C. 1989 *An Introduction to Anadromous Fishes in the Alaskan Arctic.* Biological Papers of the University of Alaska 24, pp. 27–54.

Deegan, L.A. 2012 Fishscape: Seasonality and Synchronicity of Ecological Processes. *Arctic LTER Spring Meeting, Woods Hole Marine Biological Lab, March 23–25*.

Hinzman, L.D. & Kane, D.L. 1992 Potential response of an arctic watershed during a period of global warming. *Journal of Geophysical Research* 97, 2811–2820.

Hinzman, L.D., Bettez, N.D., Bolton, W.R., Chapin, F.S., Dyurgerov, M.B., Fastie, C.L. et al. 2005 Evidence and implications of recent climate change in northern Alaska and other arctic regions. *Climatic Change* 72, 251–298.

Kane, D.L., Hinzman, L.D., McNamara, J.P., Zhang, Z. & Benson, C.S. 2000 An overview of a nested watershed study in Arctic Alaska. *Nordic Hydrology* 31(4/5), 245–266.

Kane, D.L., McNamara, J.P., Yang, D., Olsson, P.Q. & Gieck, R.E. 2003 An extreme rainfall/runoff event in Arctic Alaska. *Journal of Hydrometeorology* 4, 1220–1228.

Kane, D.L., Gieck, R.E., Kitover, D.C., Hinzman, L.D., McNamara, J.P. & Yang, D. 2004 *Hydrologic Cycle on the North Slope of Alaska*. Int. Association of Hydrological Sciences Publication 290, pp. 224–236.

Martin, P.D., Jenkins, J.L., Adams, F.J., Jorgenson, M.T., Matz, A.C., Payer, D.C. et al. 2009 *Wildlife Response to Environmental Arctic Change: Predicting Future Habitats of Arctic Alaska.* Report of the Wildlife Response to Environmental Arctic Change (WildREACH): Predicting Future Habitats of Arctic Alaska Workshop, 17–18 November 2008. Fairbanks, Alaska, U.S. Fish and Wildlife Service, 138 pp.

McNamara, J.P., Kane, D.L. & Hinzman, L.D. 1998 An analysis of streamflow hydrology in the Kuparuk River Basin, Arctic Alaska: A nested watershed approach. *Journal of Hydrology* 206, 39–57.

Morris, W. 2003 *Seasonal Movements and Habitat Use of Arctic Grayling (Thymallus arcticus), Burbot (Lota lota), and Broad Whitefish (Coregonus nasus) within the Fish Creek Drainage of the National Petroleum Reserve-Alaska, 2001–2002*. Technical Report No. 03-02. Alaska Department of Natural Resources.

Prowse, T.D., Wrona, F.J., Reist, J.D., Gibson, J.J., Hobbie, J.E., Levesque, L.M.J. & Vincent, W.F. 2006a Climate change effects on hydroecology of Arctic freshwater ecosystems. *AMBIO* 35(7), 347–358.

Prowse, T.D., Wrona, F.J., Reist, J.D., Hobbie, J.E., Levesque, L.M.J. & Vincent, W.F. 2006b General features of the Arctic relevant to climate change in freshwater ecosystems. *AMBIO* 35(7), 330–338.

Zarnetske, J.P., Gooseff, M.N., Brosten, T.R., Bradford, J.H., McNamara, J P. & Bowden, W.B. 2007 Transient storage as a function of geomorphology, discharge, and permafrost active layer conditions in Arctic tundra streams. *Water Resources Research* 43.

Zarnetske, J.P., Gooseff, M.N., Bowden, W.B., Greenwald, M.J., Brosten, T.R., Bradford, J.H. & McNamara, J.P. 2008 Influence of morphology and permafrost dynamics on hyporheic exchange in arctic headwater streams under warming climate conditions. *Geophysical Research Letters* 35.

Input of Dissolved Organic Carbon for Typical Lakes in Tundra Based on Field Data of the Expedition Lena – 2012

Olga Bobrova[1*], Irina Fedorova[2,1], Antonina Chetverova[1,2], Benjamin Runkle[3], and Tatyana Potapova[1]

[1]*Department of Land Hydrology, St. Petersburg State University, St. Petersburg, 199178, RUSSIA*
[2]*Otto-Shmidt Laboratory, Arctic and Antarctic Institute, St. Petersburg, 199397, RUSSIA*
[3]*Inst. of Soil Science, University of Hamburg, Hamburg, 20146, GERMANY*
**Corresponding author's email: helga.castor@gmail.com*

ABSTRACT

Interest in the problem of the formation of arctic river carbon runoff is growing due to the influence of global warming on the emission of greenhouse gases. Last summer (in August 2012), measurements were carried out on the catchment of Fish Lake on Samoilovsky Island in the Lena River delta. Fish Lake is a thermokarst polygonal lake, and the landscape of its catchment is typical for arctic tundra. These measurements were done in order to study the input of dissolved organic carbon (DOC) to the lake from the active layer of the catchment. The depth of the active layer was 20 to 60 cm: 20–30 cm on polygon rims and 30–60 cm in polygon centers and near the lake. Measured soil moisture values were 28%–72%. In general, the mean concentration of DOC for the catchment was 25 mg/l. The DOC in pore water was 8 to 51 mg/l, depending on the position of the point on a polygon. The highest values were in the dry centers of the polygons. In water bodies, such as the polygon ponds and Fish Lake, DOC concentration was 5 to 7 mg/l. These measurements are essential in calculating the input of DOC in the lake during one month. Considering that water runoff from the catchment of Fish Lake is 32 m^3 per day (Ogorodnikova 2011), DOC runoff to the lake is about 800 g per day. Thus, the preliminary flow rate for the Lena River delta (493 g/km^2*day) can be obtained. To expand this estimate for the tundra zone and the whole Arctic, additional measurements should be conducted.

KEYWORDS

Arctic; permafrost; dissolved organic carbon; DOC; Lena

1. INTRODUCTION

On the Lena River delta at the Samoilovsky research station, measurements of different components of the carbon cycle were carried out for several years as part of the Russian-German expeditions. In August 2012, during the "Lena 2012" expedition on Samoilovsky Island in the Lena River delta, investigations were carried out at Fish Lake to study the input of dissolved organic carbon (DOC) in the water of the lake from its catchment. Special attention was paid to the flow of carbon from the active layer of permafrost. Study of processes on small catchments will help further assess the patterns of runoff of dissolved carbon in the entire Lena River delta and the Arctic as a whole. Samoilovsky Island is located near the splitting of the Olenekskaya, Trofimovskaya, and Bykovskaya channels (Figure 1). Fish Lake is a thermokarst polygonal lake, typical for polygonal tundra; its surface is 0.5 km^2 and its catchment area is 1.62 km^2.

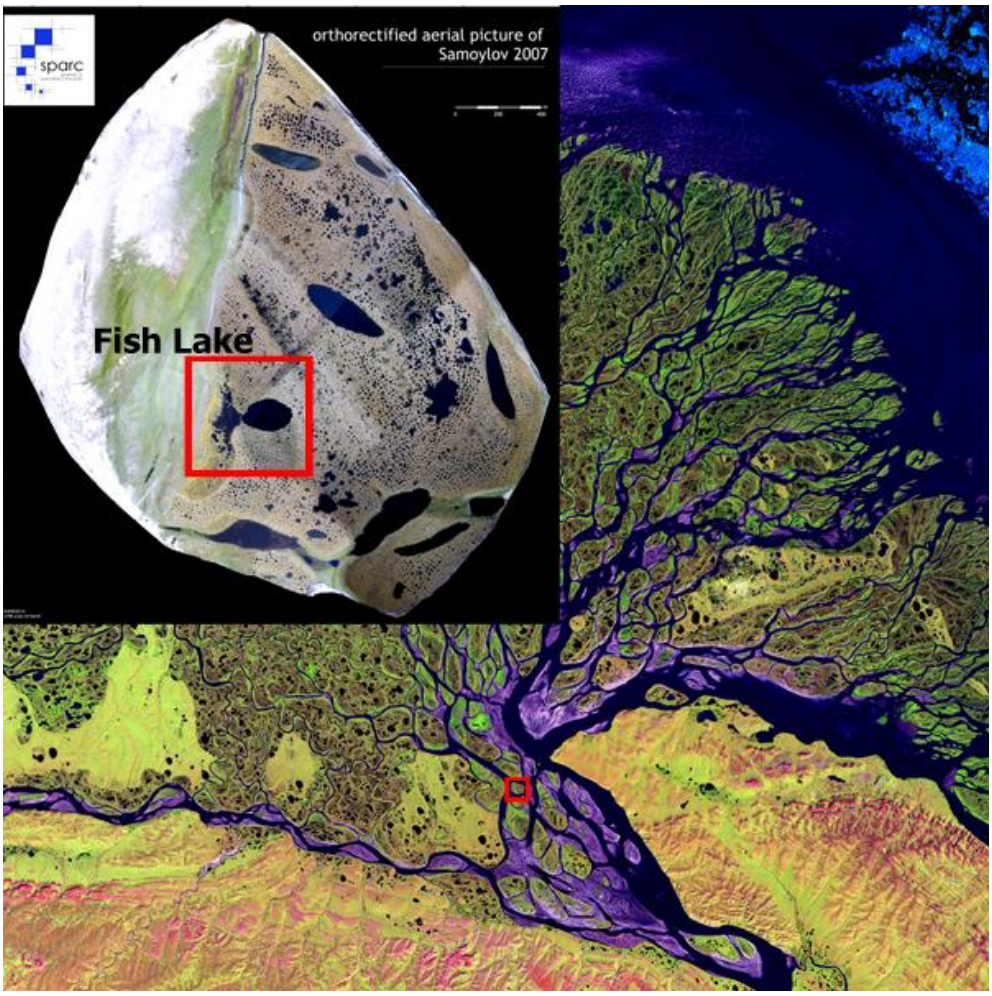

Figure 1: Lena River delta, Samoilovsky Island and the position of Fish Lake.

2. METHODS

Measurements of the concentration of DOC were made in the pore water of seasonal thawing at 21 points in the catchment area of the lake (Figure 2). The depth of seasonal thawing and humidity were also measured at the same points. The points were selected in different parts of the polygons to account for the heterogeneity of the landscape in the catchment area. Samples were taken at a depth of seasonal thawing using a special device: a thin metal tube with holes at the bottom and a valve at the top. Samples were collected in plastic bottles, 120 ml each, and stored at a temperature of 0°C when the analysis could not be performed immediately. If the sample was muddy, it was filtered before analysis. Samples were analyzed in the field using a Spectro::lyser probe. The measures are based on the water absorption of radiation at wavelengths from 220 to 790 nm at intervals of 2.5 nm.

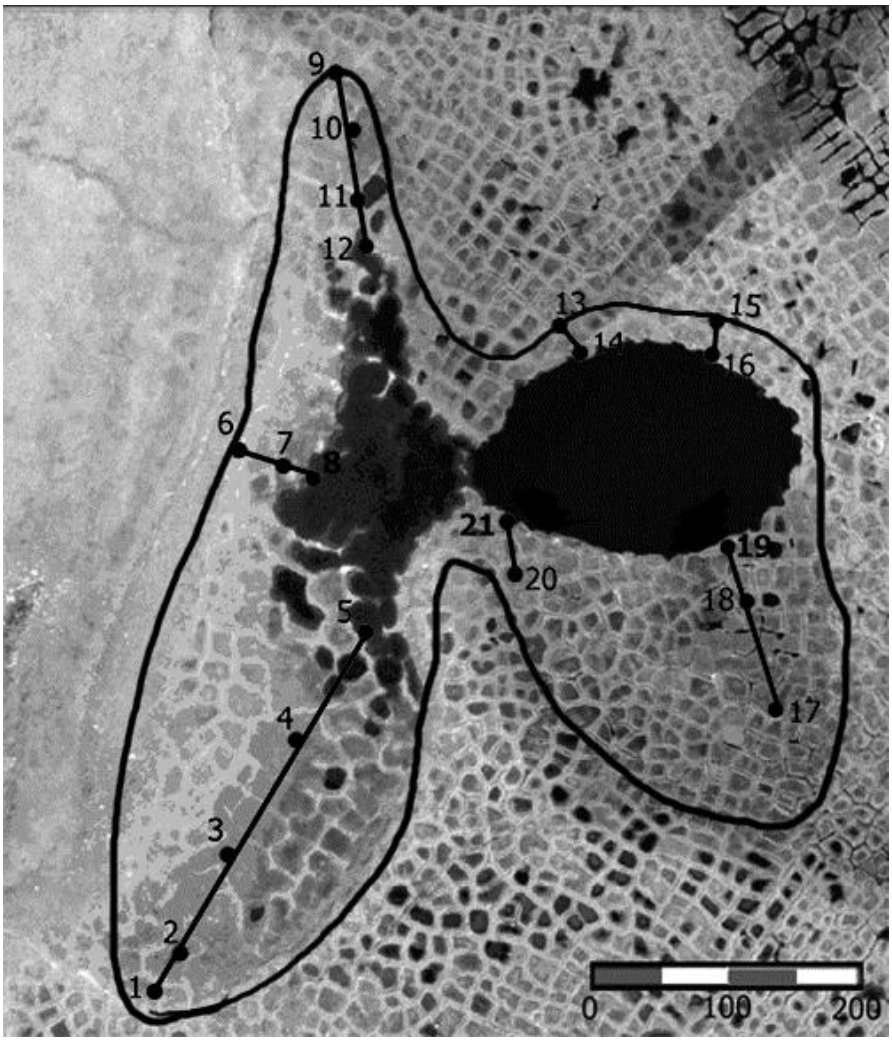

Figure 2: Sampling points at the Fish Lake catchment.

Soil moisture was measured at the same points where the DOC samples were collected to calculate the input of DOC to Fish Lake from the catchment area by groundwater flow. The measurement was performed by the dielectric method, using a portable device. At each step, three measurements were taken at points located in an equilateral triangle with its center at the point of sampling.

Some samples were transported to St. Petersburg for analysis for permanganate oxidation (PO). Permanganate oxidation is the parameter that was measured at the stations of the regular hydrologic network in the former USSR, thus the correlation between PO and DOC is important for the comparison of old and new data.

3. RESULTS AND DISCUSSION

The depth of the active layer was between 20 and 60 cm: 20–30 cm on the polygon rims and 30–60 cm in the polygon centers and near the lake. During the month when the measurements were made, the depth increased 10% to 15%. Measured soil moisture value was 28% to 72%. The centers of the polygons were wettest, and several whole polygons in the lower part of the

catchment near the lake were documented to have 60% to 72% moisture content. The mean concentration of DOC for the catchment was 25 mg/l. Dissolved organic carbon in the pore water was 8 to 51 mg/l, depending on the position of the point on a polygon. This result is similar to the ones reported by Moore et al. (2003), where the concentration of DOC in the pore water was 20 to 60 mg/l.

Bauer and Bianchi (2011) write about a slightly lower concentration of DOC in arctic catchments with permafrost: 5 to 27 mg/l. The highest DOC values were obtained in the dry centers of polygons, which can be explained by the accumulation of DOC in those spots. In the water bodies of the delta-like polygon ponds, Fish Lake, and the delta channels, DOC concentration was 5 to 7 mg/l. For the arctic deltas, a DOC concentration of about 10 to 44 mg/l was mentioned by Lobbes at al. (2000). However, their work analyzed samples that were taken in summer after the maximum discharge, when the concentration of the organic elements in the water could have been higher due to erosion of the catchment by meltwater. According to the data of Cauwet and Sidorov (1996), the highest concentration of organic carbon in the Lena River is observed in June after the spring flood. The values of DOC concentration in pore waters, thaw depth, and moisture of the active layer enable calculation of the input of DOC in the lake during one month. Considering that water runoff from the catchment of Fish Lake is 32 m^3 per day (Ogorodnikova 2011), DOC runoff to the lake is about 800 g per day.

Thus, preliminary flux rates of DOC for the Lena River delta (493 g/km^2*day) can be evaluated. This value should be considered as very low. In the work of Moore et al. (2003), DOC flux rates from the wetland catchments were reported between 8 and 57 kg/km^2*day (for the sampling period from 18 June to 1 October). Such a difference can be explained by the shallow thaw depth of the Fish Lake catchment as well as the small inclination of the catchment.

The values of the permanganate oxidation were 15 to 22 mg/l for the delta channels and the lakes on Samoilovsky Island (including Fish Lake) and 45 to 48 mg/l for the pore waters at the Fish Lake catchment. These values are higher than the values for the Lena River in the Hydrological Yearbook (1960–1975): 5 to 20 mg/l for August.

4. CONCLUSION

The concentration of DOC in the pore water of the active layer was 8 to 51 mg/l, which correlates with the results of other research in the Arctic. The runoff of the DOC at Fish Lake was calculated using the mean concentration, the depth of the active layer, soil moisture, and water runoff from the catchment. Dissolved organic carbon runoff to the lake is evaluated at about 800 g per day, which means that the flow rate is 493 g/km^2*day. These results can be used for preliminary estimation of the input of DOC to water bodies of the arctic tundra. However, for the tundra zone and the Arctic as a whole, these measurements should be expanded.

ACKNOWLEGMENT

This work was performed as part of the project “Samoilovsky Island Research Station” for the program “Laptev Sea System” and as preparation for the new Russian-German project about carbon in permafrost (CryoCarb), which starts in October 2013.

REFERENCES

Bauer, J.E. & Bianchi, T.S. 2011 Dissolved organic carbon cycling and transformation. In: Wolanski, E. & McLusky, D.S. (eds.), *Treatise on Estuarine and Coastal Science*, Vol. 5, pp. 7–67.

Cauwet, G.I. & Sidorov, I. 1996 The biogeochemistry of Lena River: Organic carbon and nutrients distribution. *Marine Chemistry* 53, 211–227.

Hydrological Yearbook 1960–1975, Volume 8, Issue 0-7. Basins of the Laptev, East Siberian and Chukchotskoye Seas, St. Petersburg, Gidrometetizdat, 1960–1975.

Lobbes, J.M., Fitznar, H.P. & Kattner, G. 2000 Biogeochemical characteristics of dissolved and particulate organic matter in Russian rivers entering the Arctic Ocean. *Geochimica et Cosmochimica Acta* 64(17), 2973–2983.

Moore, T.R., Matos, L. & Roulet, N.T. 2003 Dynamics and chemistry of dissolved organic carbon in Precambrian Shield catchments and an impounded wetland. *Canadian Journal of Fisheries and Aquatic Sciences* 60, 612–623.

Ogorodnikova, N.N. 2012 (graduate work) Calculating the depth of seasonal thawing of permafrost in the delta of the Lena river (for example Samoilovsky Island). St. Petersburg State University.

Predicting Snow Density

Oddbjørn Bruland[1,2a*], Åshild Færevåg[2b], Ingelin Steinsland[2b], and Knut Sand[1]

[1]*Statkraft, Trondheim, 7037, NORWAY*
[2]*Norwegian University of Science and Technology,*
[a]*Department of Hydraulic and Environmental Engineering, N-7490, NORWAY*
[b]*Department of Mathematical Sciences, Trondheim, N-7490, NORWAY*
**Corresponding author's email: Oddbjorn.Bruland@Statkraft.no*

ABSTRACT
Snow density is an important measure in hydrological applications. It is used to convert snow depth to the snow water equivalent (SWE). A model developed by Sturm et al. (2010) predicts snow density by using snow depth, snow age, and snow class defined by location. In this work, the model is extended to include seasonal weather variables and variables concerning location. The model is tested and fitted for 4040 Norwegian snow depth and density measurements in the period 1998 to 2011. A Bayesian modeling framework is chosen. The final model improved the snow density predictions for the Norwegian data compared with the model of Sturm et al. (2010). In addition, year-specific measurements are performed in different areas and included in the model by using random effects. The associated reduction in the prediction error is computed, indicating a significant improvement by utilizing information of annual snow measurements.

KEYWORDS
Snow density; snow storage; hydropower

1. INTRODUCTION
About 60% of the precipitation in Norway falls as snow, and the snow storage is essential in connection with risk of flooding, avalanche warning, climate research, and hydropower production. In hydropower production, where snow represents energy storage, exact estimates of snow storage are important for planning power generation. With an approximated value of snow storage of 1 billion US$ in an average year, small errors in snow storage estimates represent large values. Even though variability of the snow depths is higher than the variability of snow density, the amount of snow depth data possible to collect by snow radar reduces the error of the average areal snow depth estimates and leaves snow density estimates as the major source of error in the calculation of snow storage.

The density of snow is a result of climate during the snow accumulation period and the overlaying weight of snow. Different models have been developed to calculate snow density. Steppuhn (1976) indicated that there are correlations between snow depth and density, but only found a weak correlation at snow depths deeper than 85 cm. Elder et al. (1998) found that a linear model based on net solar radiation, elevation, and slope could explain 70% of the variation in observed snow densities. CROCUS (Brun et al. 1989), Alpine 3D (Lehning et al. 2006), and SnowTran3D (Liston & Elder 2006) are all models describing snow density as a function of snow depth, snow age, and snow metamorphism. However, these models are all complex with an extensive need of detailed information and, thus, are computationally intensive for large

domains. Sturm et al. (2010) developed a model that estimates the local snow bulk density with respect to snow depth, snow age, and snow climate class from Sturm et al. (1995). They found that the relative error in SWE using this density model was not much higher than the range of SWE that would be encountered at a single site due to local real variability. This, the simplicity of the method, and the low requirements of input data make the method presented in Sturm et al. (2010) interesting for testing in operational applications in the hydropower sector of Norway.

In Norway, there are big differences in local climate and topography, and it is a question whether climate classes used in the model by Sturm et al. cover the variations found in Norway. Statkraft has an extensive dataset, later called the Norwegian dataset, of snow surveys including more than 35,000 snow density observations from 982 locations all around Norway. The main objective of this study is to test how well the model by Sturm et al., with its defined climate classes, will reproduce these observations. We also want to test whether a new climate classification, use of observed weather, and other explanatory variables can be found to improve the model to a level where it reproduces the observations with satisfactory quality and thus can be used for operational purposes in the hydropower sector. In this study, a selection of 4040 Statkraft snow density observations from different areas in Norway in the period 1998 to 2011 is used to fit the model to Norwegian conditions (Færevåg 2013).

The aims of the study are (i) to describe and test a method that predicts the snow bulk density in conjunction with snow depth, climate, and location; (ii) to develop the model by means of weather data; (iii) to fit and test different models by using Norwegian data; (iv) to include random year and area effect to see if performing multiple area- and year-specific measurements provides better predictions; and (v) to look at the associated reduction in error by collection of year-specific snow density measurements.

2. BACKGROUND

Observed snow densities vary normally between 0.1 g/cm^3 for new fallen snow to 0.5 g/cm^3 and sometimes higher for wind-packed, icy, or wet snow.

In Statkraft's 37,000 observations of snow densities in Norway, the average is 0.33 g/cm^3 with a standard deviation of 0.07 g/cm^3. The distribution of Statkraft's snow density observations are given in Figure 1..

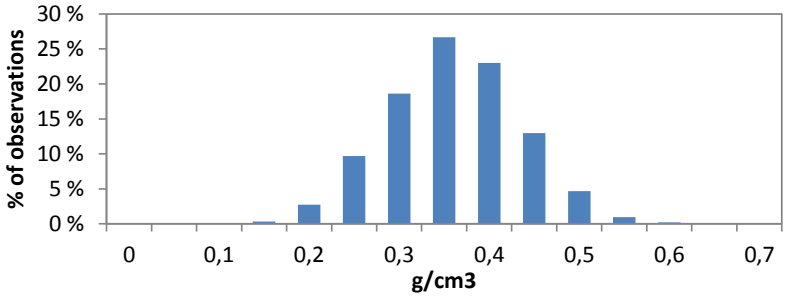

Figure 1: Distribution of snow density observations in Norway.

The highest observed densities in the Norwegian dataset are 0.656 g/cm^3, and the lowest are 0.52 g/cm^3, and 95% of the observations are between 0.20 g/cm^3 and 0.48 g/cm^3. These densities are higher than the densities reported by Sturm et al. (2010) from an Alaska dataset, where 95% of

the densities ranged between 0.12 and 0.42 g/cm^3. The snow density in the Norwegian dataset shows the average observed densities from November to May and the corresponding snow depths in the Norwegian dataset (Figure 2).

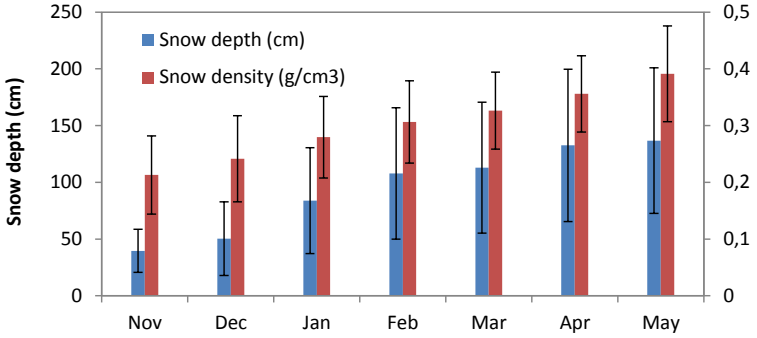

Figure 2: Average snow density during the winter in Norway (from Statkraft observations from 1930 to 2013).

The densities ρ_0 are clearly correlated both to age and snow depth, and the model given by Eq. (1) explains 29% of the observed variance in snow densities.

$$\rho_0 = \frac{1}{1000}(224{,}552 + 0.651846 \cdot DOY + 0.485908 \cdot h_s)\,, \qquad (1)$$

where ρ_0 is snow bulk density in g/cm^3 and *DOY* is number of days from 1 October (-92) to 30 June (+181) and h_s is snow depth in cm.

Sturm et al. (2010) developed a model that estimates the snow bulk density based on data from the United States, Canada, and Switzerland. It uses snow depth, snow age, and snow class as input variables.

Snow class is found by a classification system for seasonal snow cover proposed in Sturm et al. (1995). It has six classes, where each class is defined in terms of physical characteristics of the snow and the snow layers. The classes are also derived by using three different climate variables—wind, precipitation, and air temperature—given by the weather stations at the different locations, in a binary classification system. The snow class distribution in Scandinavia is shown in Figure 3. In Norway, tundra and maritime snow are dominant.

In the model by Sturm et al. (2010), bulk density is a function of snow depth (h_s), the day of year (DOY), and the snow class parameters k_1, k_2, ρ_0, and ρ_{max},

$$\rho_{h_i,DOY_i} = (\rho_{max} - \rho_0)[1 + exp(k_1 \cdot h_i + k_2 \cdot \mathrm{DOY}_i)] + \rho_0 \qquad (2)$$

where $0 < \rho_0 \leq \rho_{max} < 1$, k_1 and k_2 are the densification parameters for depth and day of year (DOY), and ρ_{max} is maximum bulk density and ρ_0 is the initial density of the individual snow layer. The snow class parameters are given in Table 1. The snow season begins early in October. Day of year represents the effect of snow aging and the number of days in the winter season, and runs from 1 October (-92) to 30 June (+181).

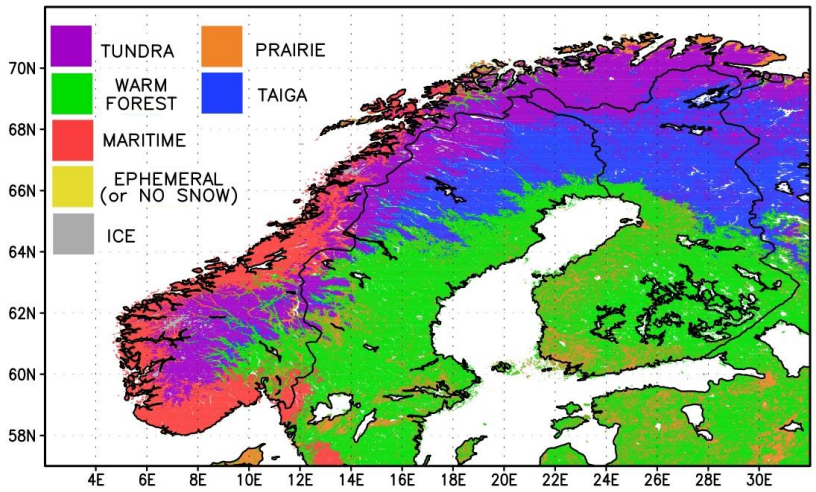

Figure 3: Snow class distribution in Norway. Source: Liston & Hiemstra 2011).

Table 1: Model parameters for each snow class (Sturm et al. 2010).

Snow class	ρ_{max}	ρ_0	k_1	k_2
Tundra	0.3630	0.2425	0.0029	0.0049
Maritime	0.5979	0.2578	0.0010	0.0038
Prairie	0.5940	0.2332	0.0016	0.0031
Alpine	0.5975	0.2237	0.0012	0.0038
Taiga	0.2170	0.2170	0.0000	0.0000

3. DATA AND MODELING

3.1 Snow Data

In further analysis and model development, snow depth and snow density observations from 244 locations within 17 different areas in Norway were selected from the Statkraft dataset. The selection covers most prevailing climates in Norway, with coastal humid climate in the southwest, to dry, cold climate in the inland, and cold, coastal climate further north. The meteorological information was obtained from meteorological stations within the areas and covers data both from the Norwegian Meteorological office (Met.No) and Statkraft's meteorological station network (Figure 4).

Normally, the average snow density or a density found by using the snow depth/snow density relation is used to calculate an area's snow water equivalent (SWE). The average error when estimating a snow density based on mean values is 9.9%. Using the regression between depth and density does not improve the estimates. Figure 5 shows that the error has increased over the years and decreases with snow depth and number of observations for both methods. The errors are largest for densities below 0.1g/cm^3 and above 0.5 g/cm^3.

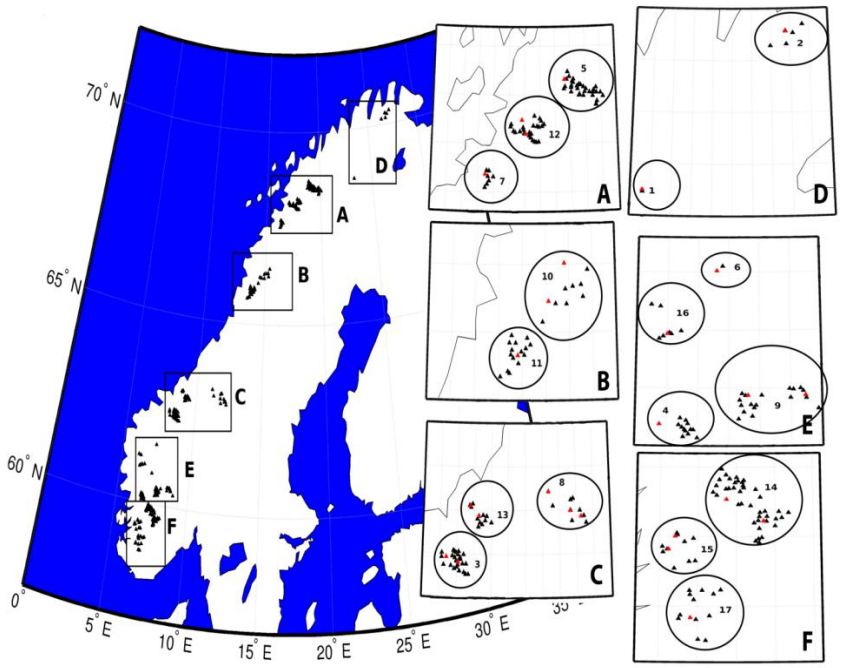

Figure 4: Locations of the 17 study areas grouped in 6 main groups (A–F). Red triangles mark the position of meteorological stations.

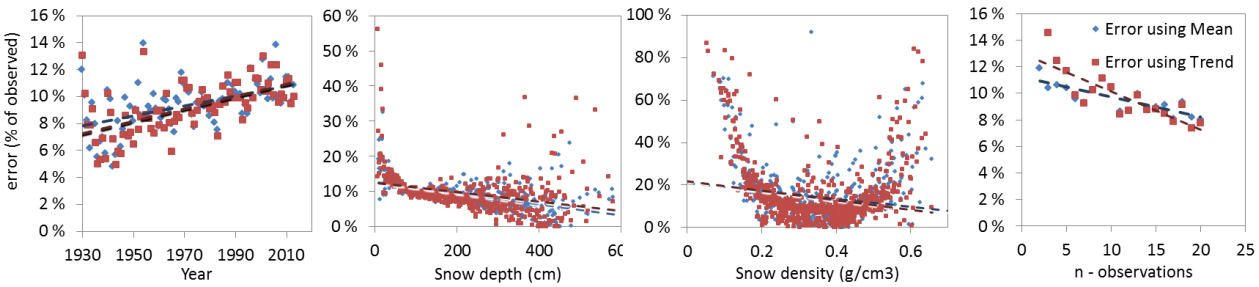

Figure 5: Snow density estimation errors based on traditional methods estimated from the Norwegian dataset.

Table 2 displays the characteristics of the snow data and climate for each of the measurement areas along with number of locations in each area and the number of snow measurements used in each area. The year-to-year variation in snow densities for an area is illustrated in Figure 6.

The temperature normally decreases with elevation, and the temperatures for the different locations are calculated from weather stations data nearby using Eq. (3).

$$T = T_0 + a(h - h_0), \quad (3)$$

where T is the air temperature to be found for the location at elevation h (masl); T_0 and h_0 are the air temperature and elevation (masl) of the representative weather station; and a is the temperature gradient. The precipitation measurements are corrected for wind loss using local wind measurement and corrections suggested by Førland et al. (1996).

Table 2: Number of sub-locations, mean depth, snow density, and snow water equivalent (SWE), total number of measurements (*n*), and information about the climate for the period November–April for each measurement area.

Id	Area	No. of locations	Depth (cm)	Density (g/cm3)	SWE (mm)	*n*	Temp			Wind		Precip
							Mean	Max	Min	Mean	Max	Total
1	Adamselv	5	74.1	0.345	26.4	42	-5.7	15.0	-26.0	4.5	21.1	49
2	Alta	1	51.7	0.266	13.4	18	-8.4	11.3	-38.8	2.2	16.7	101
3	Aura/Grytten	24/3	119.3	0.349	43.2	439	-0.9	20.0	-30.0	2.5	19.6	437
4	Tysso-Folgefonn	12	219.5	0.390	87.7	168	-2.1	15.0	-23.7	2.8	27.0	912
5	Innset	32	90.5	0.282	27.1	556	-5.8	15.0	-40.0	2.2	13.9	366
6	Jostedalen	1	190.3	0.327	64.1	39	-2.6	12.2	-25.3	1.6	22.0	631
7	Kobbelv	7	162.5	0.414	68.8	188	-3.8	12.8	-30.9	5.1	27.7	514
8	Nea-Nidelv	10	108.8	0.338	36.6	144	-4.1	16.9	-34.5	2.7	19.9	273
9	Nore	19	81.8	0.295	25.2	306	-6.4	16.2	-39.2	2.8	26.1	276
10	Rana	9	107.4	0.315	35.3	254	-4.4	14.5	-46.7	1.2	17.7	457
11	Røssåga	15	103.3	0.353	37.7	273	-3.0	15.0	-26.9	1.6	9.8	1145
12	Skjomen	24	123.6	0.34	43.4	324	-3.4	18.9	-25.7	3.0	50.0	273
13	Svorka/Trollheim	3/9	126.5	0.376	50.3	243	-1.8	18.1	-34.4	1.6	50.0	599
14	Tokke	40	99.9	0.306	31.9	535	-3.4	17.6	-34.9	1.8	24.6	604
15	Ulla-Førre	10	138.6	0.398	57.6	243	-0.7	21.7	-26.5	3.6	29.9	1143
16	Vik/Høyanger	5/2	184.8	0.384	75.4	191	-3.4	14.4	-45.0	4.4	23.2	668
17	Sira-Kvina	13	82.3	0.339	28.8	77	-3.0	16.2	-29.0	2.2	11.5	658
Total		244	118.2	0.337	42.5	4040	-3.7	21.7	-46.7	2.7	50.0	536

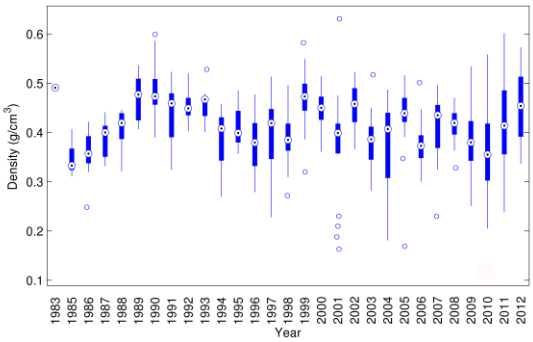

Figure 6: Observed snow density in the area Ulla-Førre in the period 1983–2012.

3.2 Model

The expected snow density following Sturm et al. (2010) is given by

$$E(Y_i) = (\rho_{max} - \rho_0)\left[1 - exp\left(\sum_{p=1}^{p} -k_p, x_{p,i}\right)\right] + \rho_0, \quad (4)$$

where k_p is the P number of originally unknown model parameters to be estimated, and $x_{p,i}$ is the explanatory variable for observation i belonging to an explanatory parameter p. It is the variables x_1, x_2,..., x_9 that will be used in the model in different compositions to improve the performance of the model.

All accumulation of weather data is summarized hourly from the accumulation start date $A_0(i)$ to the day of measurement i, DOY(i). The accumulation starts from the time t corresponding $t = A_0$. The accumulation start date (A_0) is found by using a degree-day model calibrated within HBV models established for catchments in the vicinity.

The explanatory variables and their correlation to density are summarized in Table 3.

Table 3: Summary of the nine explanatory variables constructed for the model.

Covariate	Name	Restrictions	Correlation to density
x1	Snow depth	-	0.48
x2	Snow age (DOY)	-	0.39
x3	Elevation (masl)	-	0.20
x4	Temperature	After and during snowfall/rain	0.16
x5	Wind	During snowfall	0.24
x6	Snow and wind	Snowfall and wind	0.29
x7	Precipitation	Ratio as snow	-0.05
x8	Precipitation	Ratio as mixed snow/rain	0.07
x9	Precipitation	Ratio as rain	0.03

The snow density conditions for each of these areas and years can vary among each other. The variability can be caused by various effects that are not explained by the weather variables or the other covariates.

We can try to assess this variation among different areas by using random effects.

$$E(Y_i) = (\rho_{max} - \rho_0)\left[1 - exp\left(\sum_{p=1}^{p} -k_p, x_{p,ik}\right) - \epsilon_{jk}\right] + \rho_0, \quad (5)$$

where $Y_{i,jk}$ is the response variable for observation i in area j in year k, and $x_{p,i}$ are the explanatory variables. The j different areas are likely to have different overall response for each year k. The model accounts for this by including a term ϵ_{jk}. ϵ_{jk} is the random effect for area j in year k. The random effects are estimated from annual measurements and give input of the specific year's condition.

4. RESULTS

Markov Chain Monte Carlo (MCMC) simulations are applied for Bayesian estimation by simulating the posterior distribution of the parameters of the model by using the software WinBUGS and OpenBUGS. The model performance is based on their predictive ability. The mean error (ME), the mean absolute error (MAE), the root mean squared error (RMSE), and the continuous ranked probability score (CRPS) are used to evaluate the models

4.1 Model Selection

First, the model is found that predicts the snow density best without random effects. Afterwards, this model is tested with and without year- and area-specific measurements.

The models are tested for Norwegian snow depth data to see which model provides reliable estimates of the bulk density. Equation (2) is applied to each observation using the different covariates, to estimate the bulk density. Snow density is also calculated by the Sturm et al. model in Eq. (4), which uses the parameters in Table 1 defined by the snow classes. The snow classes for each of the 244 locations are found by the snow classification scheme illustrated in Figure 3. All the models are compared with each other, and in addition versus the Sturm et al. model, based on the predictive distribution and the true measurement. Ten different models with different combinations of the explanatory variables were tested. The models are listed in Table 4.

Table 4: Different test models. x_1: snow depth, x_2: day of year, x_3: elevation, x_4: accumulated wind, x_5: accumulated plus degrees, x_6: accumulated snow when there is wind, x_7: ratio light snow, x_8: ratio mixed snow and rain, x_9: ratio rain.

Model	x_1	x_2	x_3	x_4	x_5	x_6	x_7	x_8	x_9
A	x						x	x	x
B	x			x	x	x			
C	x			x	x		x	x	x
D	x			x	x				
E	x		x	x	x				
F	x		x	x		x			
G	x	x		x	x				
H	x		x	x					
I	x		x	x	x	x			
J	x	x	x	x	x	x	x	x	x

The performances of the different selected combinations are presented in Table 5. Model B and C score best in the MAE, but Model E has a better score in CRPS.

Since we are considering a predictive distribution, this model was chosen based on the lowest CRPS. The only difference between Model D and E is that the covariate elevation (x_3) is included in Model E. The CRPS implies a slightly better estimate for E. All models except Model J, where all parameters are included, performed better than the Sturm et al. model.

Table 5: Various evaluation criteria: Mean absolute error, root mean square error, continuous ranked probability score, and weighted scores of MAE and RMSE. Different models are tested against measured densities using the test dataset. The framed value indicates the best score for the different evaluation criteria.

Model	MAE	Weighted MAE	RMSE	Weighted RMSE	CRPS
A	0.0508	0.0537	0.0607	0.0648	0.03776
B	0.0465	0.0491	0.0567	0.0602	0.07472
C	0.0460	0.0487	0.0556	0.0590	0.03440
D	0.0460	0.0486	0.0555	0.0589	0.03440
E	0.0462	0.0488	0.0558	0.0590	0.03418
F	0.0493	0.0520	0.0596	0.0632	0.07675
G	0.0467	0.0490	0.0561	0.0590	0.03451
H	0.0477	0.0504	0.0572	0.0608	0.03538
I	0.0465	0.0490	0.0567	0.0600	0.06931
J	0.1487	0.1497	0.1577	0.1593	0.08074
Sturm	0.0617	0.0636	0.0719	0.0743	0.06170

In Figure 7 snow density estimates, the Sturm et al. model and the posterior mean from Models A, E, G are plotted together with the observed snow density.

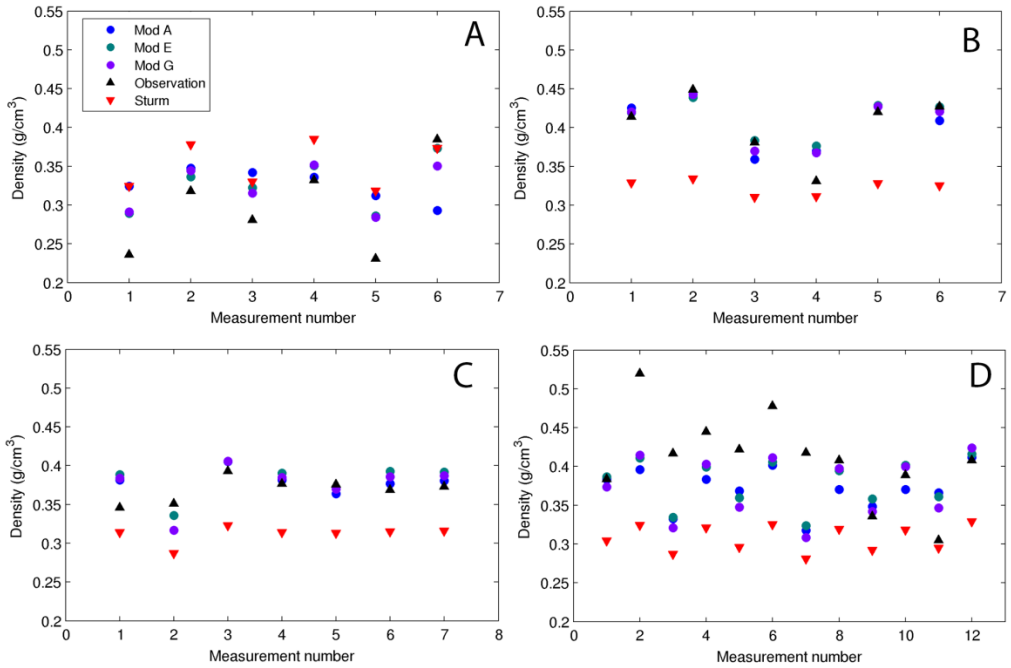

Figure 7: Posterior mean estimates and observed density in four different locations for four different models without random effects. (a) Vinjerui: area 14, maritime, (b) Illekleiv: area 4, tundra, (c) Stordalen: area 3, tundra, (d) Stearuvuggi: area 7, tundra.

Based on Model E, the model parameters are estimated (Table 6). The summary statistics, the empirical mean, and the standard deviation are displayed for each model parameter.

Table 6: Mean and standard deviation (std dev) of estimated model parameters and number of samples.

Variable	Mean	std dev	Sample size
ρ_0	0.1481	0.0148	10000
ρ_{max}	0.4720	0.0128	10000
k_1	0.00503	5.48E-4	10000
k_3	0.00018	4.63E-5	10000
k_4	0.00477	6.82E-4	10000
k_5	0.00042	7.41E-5	10000

To improve the predictions, it is possible to collect annual measurements in every area. Here, the snow density is treated differently across areas and differently among years following a random effects specification,

$$E(Y_{ijk}) = (\rho_{max} - \rho_0)\left[1 - exp\left(-k_1 x_{1,ijk} - k_2 x_{2,ijk} - k_3 x_{3,ijk} - k_4 x_{4,ijk} - k_5 x_{5,ijk} - \epsilon_{jk}\right)\right] + \rho_0, \qquad (6)$$

where *Yijk* is the estimated snow density for snow measurement *i* in area *j* for year *k*. $i \in (1,...,n)$, $j \in (1,...,17)$ and $k \in (1998,...,2012)$, and ϵ_{jk} is the random effect of area *j* in year *k*.

Two methods are used, and Figure 8 displays the reduction in the error as a function of $n = \{0,5,10,15,25\}$ number of annual measurements in year 1998. This supports the idea that multiple annual measurements give a better result, but the error reduction stagnates after $n = 10$ to 15 measurements.

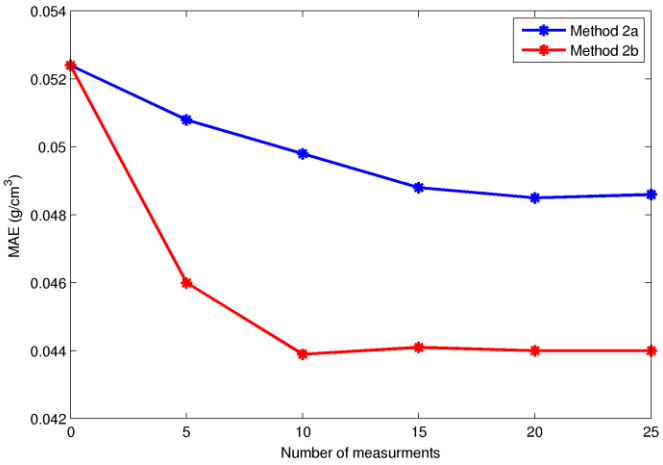

Figure 8: Error reduction in absolute error by collection of $n = \{0,5,10,15,20,25\}$ number of year specific measurements. Data from year 1998.

5. DISCUSSION AND CONCLUSION

Sturm et al. (2010) presented a methodology to estimate the snow density based on climate, snow depth, and snow age, where the model parameters were found on the basis of a dataset from Alaska and Canada. Snow densities predicted from this model were compared with a

Norwegian dataset, provided by Statkraft, and covering most areas in Norway for the years back to 1930. By using the snow classification dataset in Sturm et al. (1995), most of the 244 locations were classified as maritime (58) and tundra (175) snow class, and a few were classified as taiga snow. In most cases, the model underestimated the Norwegian snow densities.

Apart from snow depth, the model of Sturm et al. (2010) does not include the variability in the density due to yearly variability in the climate. Using the snow classes to predict the snow density means that if depths measured on the same date in various years are equal, then the estimated density will be equal too. Based on the previous work of Sturm et al. (2010), a new model that directly includes the seasonal variability in the weather is developed. This model is also an extension of the model of Sturm et al. (2010), using other explanatory variables and new model parameters.

Several models consisting of different explanatory variables were tested against Norwegian snow data. The final model included the following predictor variables: (1) measured snow depth, (2) elevation (masl) at the location, (3) temperature – accumulated plus degrees, and (4) wind – accumulated wind speeds above 2 m/s when the temperature is below the freezing point. These variables need to be known for each location where snow density is to be predicted. The predictors are estimated based on weather data from weather stations near the measurement locations.

The extended model includes the seasonal variability by the variables wind and temperature. The day of the year (DOY) is excluded from the model. This variable was highly correlated with snow density, but gave worse predictions. This might be explainable, since the effect of age is already embedded in the measurement of snow depth and the accumulation of weather variables. The elevation of the location did not influence the model much, but was chosen based on the CRPS score. An explanation can be that the effect of location altitude is already explained in the model through the correction of temperature due to altitude.

Even if the variability among areas and years is considered by using weather variables, it is conceivable that some other kind of variation in the properties of the snow densities does not emerge through the explanatory variables. Thus, a random year-area effect is added to the model. This random effect is estimated by year-specific measurements in different ways. The best predictions came from a model with random effects. This model used information from year- and area-specific measurements already in the beginning while estimating model parameters from the training dataset in the MCMC simulation. The use of year- and area-specific measurements assisted in bias removal and improved the model. The result does not necessarily get better after more than 10 observations.

The snow density prediction model developed in this study can be useful for estimating snow density instead of taking manual measurements. As the model takes wind speeds, temperature, elevation, and snow depth as input variables, it is easy to use and is applicable wherever weather stations are available and representative. This model is compared with the original model it is based on (Sturm et al. 2010), and gives more reliable predictions. Analyses show that information gained by collecting about 10 annual snow densities in each area can improve the predictions significantly.

REFERENCES

Brun, E., Martin, E., Simon, V., Gendre, C. & Coleou, C. 1989 An energy and mass model of snow cover suitable for operational avalanche forecasting. *Journal of Glaciology*, 333–342.

Elder, K., Rosenthal, W. & Davis, R.E. 1998 Estimating the spatial distribution of snow water equivalence in a montane watershed. *Hydrological Processes* 1793–1808.

Essery, R., Li, L. & Pomeroy, J. 1999 A distributed model of blowing snow over complex terrain. *Hydrological Processes*, 2423–2438.

Færevåg, Å. 2013 (May 8). Predicting Snow Density. Trondheim, Norway. Retrieved from http://urn.kb.se/resolve?urn=urn:nbn:no:ntnu:diva-20666

Førland, E.J., Allerup, P., Dahlström, B., Elomaa, E., Jónsson, T., Madsen, H. et al. 1996 *Manual for Operational Correction of Nordic Precipitation Data*. Oslo: Met.No.

Gneiting, T. & Raftery, A. 2007 Strictly proper scoring rules, prediction, and estimation. *Journal of the American Statistical Association* 102, 359–378.

Gneiting, T., Balabdaoui, F. & Raftery, A.E. 2007 Probabilistic forecasts, calibration and sharpness. *Journal of the Royal Statistical Society Series B: Statistical Methodology* 102, 243–268.

Jacobsen, M. 2005 *Fundamentals of Atmosphere Modeling*. Cambridge University Press, Cambridge.

Lehning, M., Völksch, I., Gustafsson, D., Nguyen, T.A., Stähli, M. & Zappa, M. 2006 ALPINE3D: A detailed model of mountain surface processes and its application to snow hydrology. *Hydrological Processes*, 2111–2128.

Liston, G.E. & Elder, K. 2006 A distributed snow-evolution modeling system (SnowModel). *American Meteorological Society*, 1259–1276.

Liston, G.E. & Hiemstra, C.A. 2011 The changing cryosphere: Pan-Arctic snow trends (1979–2009). *Journal of Climate* 24, 5691–5712.

Liston, G. & Sturm, M. 1998 A snow-transport model for complex terrain. *Journal of Glaciology*, 498–516.

Spiegelhalter, D.J., Thomas, A., Best, N.G. & Lunn, D. 2003 WinBUGS user manual (version 1.4).

Steppuhn, H. 1976 Areal water equivalents for prarie snowcovers by centralized sampling. *44th Annual Western Snow Conference, Calgary, Alberta* (pp. 63–68).

Sturm, M., Tara, B. & Liston, A.G. 2010 Estimating snow water equivalent using snow depth data and climate classes. *Journal of Hydrometeorology* 11, 1380–1394.

Arctic Snow Distribution Patterns at the Watershed Scale

Joel W. Homan* and Douglas L. Kane

Water and Environmental Research Center, University of Alaska Fairbanks, Fairbanks, AK 99775, USA
**Corresponding author's email: jwhoman@alaska.edu*

ABSTRACT
Watershed-scale hydrologic models require good estimates of the spatially distributed snow water equivalent (SWE) at winter's end. Snow on the ground in treeless arctic environments is susceptible to significant wind redistribution, which results in heterogeneous snowpacks with greater quantities of snow collection in depressions, valley bottoms, and leeward sides of ridges. In the Arctic, both precipitation and snow gauges are poor indicators of the actual spatial snowpack distribution, particularly at winter's end. Snow distribution patterns are similar from year to year because they are largely controlled by the interaction of topography, vegetation, and consistent weather patterns. From one year to the next, none of these controls radically change. Consequently, shallow and deep areas of snow tend to be spatially predetermined, resulting in depth (or SWE) differences that may vary as a whole, but not relative to each other, from year to year. Our aim was to identify snowpack distribution patterns and establish their stability in time and space at a watershed scale in the Arctic. Snow patterns were established by (1) numerous field survey points from end-of-winter field campaigns, and by (2) differentiating snowpacks that characterize small-scale anomalies (local scale) from snowpacks that represent a large-scale area (regional scale). We concluded that SWE values within plus or minus one standard deviation of the record average SWE represent the regional-scale snowpack. Removing local-scale influences provides a more accurate representation of the regional snowpack, which will aid in forecasting snowmelt runoff events.

KEYWORDS
Arctic snow distribution; watershed scale; heterogeneous snowpacks; snow water equivalent

1. INTRODUCTION
Snow hydrology is an important component of the Arctic hydrologic cycle. The total water content of the snowpack at the end-of-winter within the Arctic has comprised between 30% and 40% of the annual precipitation (Kane et al. 1991; Kane et al. 2008b), and on average, about two-thirds of the snow water equivalent (SWE) leaves the catchment as runoff (Kane et al. 2000; 2004; 2008a). On the other hand, the average runoff ratio for rainfall events is roughly one-third for most summer precipitation events (Kane et al. 2012). The high runoff ratio in spring is mostly due to permafrost and frozen subsurface conditions of the active layer. The low runoff ratio of the summer months is partially due to evapotranspiration (ET) over the basin and surface storage availability on the Coastal Plain, where there are many ponds, lakes, and wetlands. The disparity in the watershed areas that contribute to runoff (potentially the entire basin for snowmelt and only part of the basin for rainfall) also affect the runoff ratios. Heterogeneous snowpacks resulting from snow redistribution is also a major factor in increasing the snowmelt runoff. Much of the redistributed snow accumulates in depressions, valley bottoms, and leeward sides of ridges. Drift formation in depressions generally results in proportionally higher water content

close to or within drainage channels, which potentially increases runoff. The combination of above-average water content close to the drainage channels, reduced time of transport of hillslope meltwater due to water tracks, and a completely frozen active layer that limits subsurface meltwater storage produces a higher runoff ratio during snowmelt than is observed for rainfall runoff events. Some extreme summer storms, however, have produced flows greater than the largest measured snowmelt flood, but only for small high-gradient headwater basins. For large arctic rivers, the spring snowmelt floods dominate and can be expected every year.

In the Alaska Arctic, where snow accumulation may last for nine months and then ablate in a relatively short time, typically 10 days just before the solstice, the end-of-winter SWE plays a significant hydrologic role in watersheds (Kane & Hinzman 1988). The task of accurately quantifying solid precipitation in the Arctic is made difficult because it is a remote, sparsely inhabited, and severely cold environment. An additional problem is that often the quality of precipitation measurements from meteorological stations is poor. For instance, in the Alaska Arctic, snowfall precipitation has been shown to be underestimated by a factor of two or three when windy conditions prevail (Benson 1982). Redistribution of snow by wind can create complex snow distributions resulting in heterogeneous or even patchy snowpacks (Elder et al. 1991; Seyfried & Wilcox 1995; Prasad et al. 2001; Winstral et al. 2002; Anderton et al. 2004; DeBeer & Pomeroy 2009). The number of wind events, wind magnitude and direction, vegetation, and topography are all factors that are important to the end-of-winter snowpack distribution. Difficulties in measuring falling solid precipitation, as well as quantifying snow redistribution and winter-long sublimation, make ground-based snow surveys at winter's end the most reliable observational method.

The primary goal of this study is to provide better data for input into hydrologic models. Specifically, we intend to improve our understanding of watershed-scale spatial variability of solid precipitation at winter's end in the central region of the Alaska Arctic including the Dalton Highway corridor. Snow survey data used for this investigation were collected from 2000 to 2011 by faculty, staff, and students of the Water and Environmental Research Center (WERC) at the University of Alaska Fairbanks.

Warm season precipitation patterns within a section of the study area (Kuparuk River Watershed) were evaluated in 1993 and 1994 by Kane et al. (2000). Their findings indicate a direct correlation between rainfall and elevation, with increasing precipitation from lower to higher elevations. While the summer precipitation patterns were evident with elevation, the distribution of winter SWE was less conclusive. Most of the uncertainties arise from a sparse observational network and the short period of observation. This paper presents new findings using a long-term (2000–2011) snow dataset.

2. STUDY DOMAIN

The study domain covers a 200 by 240 km region of Alaska's Arctic Slope that is bound by the Brooks Range on the south and the Arctic Ocean on the north, and includes the Chandler, Anaktuvuk, Itkillik, Kuparuk, Putuligayuk (Put), Sagavanirktok (Sag), Kadleroshilik (Kad), and Shaviovik River basins (Figure 1). All of the watersheds drain north and eventually empty into the Arctic Ocean. The Putuligayuk lies entirely within the Coastal Plain region; the Kuparuk and Kadleroshilik Rivers emanate from the Foothills; the Sagavanirktok, Shaviovik, Kavik, Itkillik, Anaktuvuk, and Chandler Rivers originate in the Brooks Range.

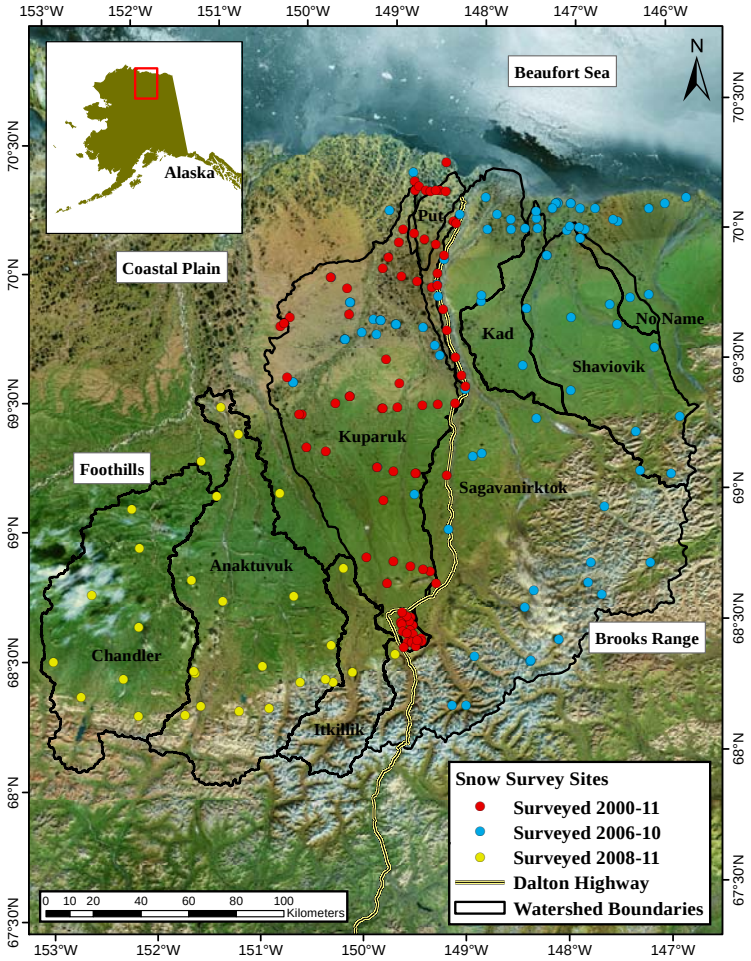

Figure 1: Site map showing snow survey locations within several Central Alaska North Slope watersheds.

The southern and northern boundaries of the domain are at 68°10′N and 70°15′N latitude, respectively. The western and eastern boundaries of the domain are at 153°00′W and 146°45′W longitude, respectively. Elevation within the study area ranges from sea level to 2675 m (0 to 8025 ft). The topography is characterized by a flat northern portion (generally referred to as *Coastal Plain*) and by gently rolling hills and valleys (*Foothills*) and mountain ridges (*Mountains*) of the Brooks Range to the south.

The entire study area is underlain by continuous permafrost (250 to 300 m in the Brooks Range and up to 600 m along the coast) and is snow-covered 7 to 9 months of the year (Osterkamp 1984). The region is mostly treeless (some patches of trees in riparian areas in the Foothills). Vegetation consists of alpine communities in the mountainous region, tussock tundra in the Foothills, and sedge tundra on the Coastal Plain (Walker et al. 1989; CAVM Team 2003). Willow and birch shrubs are common in riparian areas, and shrub height is variable, from approximately 30 cm to over 1 m. In response to climate warming in the Arctic, there is an increase in the abundance and extent of shrubs in tundra areas (Sturm et al. 2001; Sturm et al. 2005; Tape et al. 2006).

3. SURVEY LOCATIONS

From 2000 to 2011, over 1000 snow surveys were conducted at roughly 200 locations. The snow survey dataset is a collection of results from numerous research projects, so the exact number of sites surveyed and their locations changed yearly. The distribution of snow survey sites is shown on a map of Alaska's central North Slope (Figure 1). The color coding classifications best describe the timing and duration of surveys, but does not mean the sites were visited every year within this classification. Ideally, sites would have been surveyed every year throughout the duration of the projects. Weather conditions, however, play a large role in the feasibility of reaching most of the remote survey sites, which are accessible only by snow machine and/or helicopter. High winds, fog, whiteout, and flat light conditions prevented some of the sites from being surveyed every year, although the goal was to monitor them.

The snow surveys were conducted under a variety of projects, but regardless of the project, the snow survey sites were chosen to represent a wide range of snowpacks. Surveying along a uniform grid would have been inadequate at a watershed scale because the Arctic snowpack is very heterogeneous (Kane et al. 1991; Homan et al. 2010; Sturm & Wagner 2010), with relatively shallow snow on hilltops, along ridges, and on steep slopes, while deeper snow accumulates in valley bottoms, water tracks, and leeward slopes. Elevation, terrain, vegetation cover, and spatial distribution were all considered during the survey site-selection process. Snowmelt studies have shown that areas with deeper snow take several days or weeks longer to completely melt compared with areas of shallower snow (Hinzman et al. 1991). In the end, the snow survey sites were positioned to represent both "regional" and "local" snow conditions in order to capture a greater spatial variability of the snowpack. The "regional-scale" sites are characteristic of larger-scale snow conditions (hundred meters to a kilometer), while "local-scale" sites represent more limited features such as wind-scoured ridges or snowdrift deposits within depressions such as streams and water tracks.

4. SNOW SURVEY METHODS

The snow surveys include gravimetric snow density sampling and snow depth measurements collected over an area of 25 m by 25 m; this technique is often referred to as double sampling. The snow depth of the snowpack in Alaska is more variable than the density (Benson & Sturm 1993; Sturm et al. 2010). Usually, double sampling yields an areal SWE estimate with a lower variance than is possible using collected snow cores only. Rovansek et al. (1993) showed that double sampling provides improved SWE estimates. The WERC uses an optimal ratio of 10; that is, 50 depths accompany 5 snow cores at each survey site.

Snow cores are sampled using a fiberglass tube ("Adirondack") with an inside area of 35.7 cm^2 (diameter = 6.7 cm). The advantage of the Adirondack for shallow snowpack is that its diameter is larger than many other types of snow tubes (like the Mt. Rose); thus, it provides a larger sample of the shallow Arctic snowpack.

The WERC uses constant 50 m lengths for the snow depth course, with a 1 m sampling interval along an L-shaped transect (Kane et al. 2012). Twenty-five depth measurements are made on each leg of the L; this strategy is used to account for the presence of snowdrifts in the area of measurement. The directions of measurement are chosen randomly. Snow depth measurements are made using a T-shaped graduated rod (T-probe). The SWE is defined as follows: SWE = SD * (ρ_s / ρ_w), where ρ_s is average snow density from the 5 snow core samples, ρ_w is water density, and SD is an average of 50 snow depths (Kane et al. 2012; Stuefer et al. 2013).

5. RESULTS

Winter in the Alaska Arctic starts with snowfall and ends with snowmelt and subsequent runoff. But what happens to the snow during the eight-to-nine-month-long cold season in between? In the Arctic, snow can fall any day of the year, but snow accumulation typically begins in September or early October and continues throughout the entire winter, with no significant midwinter melt. Snow accumulation occurs during a few large events, many small events, or somewhere in between, but more commonly from a variety of event sizes. It is incorrect to assume that snowfall at a given location is equivalent to snow accumulation recorded during field measurements or by a precipitation gauge, or that a location's measured accumulation can be easily extrapolated to another location. Snow on the ground in treeless arctic environments is susceptible to significant wind redistribution, which is normally accompanied by in-transit sublimation. As a result, from both transport and sublimation the end-of-winter snowpack is very heterogeneous (Table 1).

Table 1: Average end-of-winter (2000–2011) snowpack characteristics for the study domain.

	Depth (cm)	Density (kg/m^3)	SWE (cm)
Max	165	415	42
Min	0	0	0
Average	40	250	10

5.1 Snowpack Distribution

Though the snowpack itself may be heterogeneous, the redistribution of snow has been found to have some consistencies: snow removal from hilltops, ridges, and windward slopes, while accumulating in valley bottoms, water tracks, and leeward slopes. To identify snowpack distribution patterns, SWE measurements from the long-term (2000–2011) snow dataset were used (Figure 1, Table 2). We suspected SWE would increase with increasing elevation as rainfall has been determined to do, so the study domain was divided into three physiographic regions: *Coastal Plain* (<150 m), *Foothills* (150–600 m), and *Mountains* (>600 m) (Table 3). The SWE was subsequently evaluated against corresponding survey site elevations (Figure 2). The dataset illustrates that SWE values measured within the Coastal Plain increase with increasing elevation, but they decrease with increasing elevation in the Foothills and Mountains regions. Overall, the survey data demonstrate a slight decrease in SWE with increasing elevation. More specifically, there is a decrease of only 13 mm of SWE for every 1000 m of elevation gain. This is a significant difference compared with summer precipitation, which increases more than 200 mm for the same 1000 m elevation gain (Kane et al. 2000). Essentially, the present dataset illustrates that the average SWE is relatively independent of elevation on Alaska's central North Slope, with roughly an average of 10 cm from the Coastal Plain to the Mountains.

All of the measured SWE values represent a certain percentage of Alaska's central North Slope. Some might characterize small-scale anomalies (local scale), while others might signify a large-scale area (regional scale). Since we are interested in identifying snowpack distribution patterns at a watershed scale, snow survey sites that represent local-scale snowpacks needed to be identified and removed. After analyzing the long-term dataset, we concluded that SWE values within plus or minus one standard deviation of the record average SWE represent the regional-scale snowpack. Using the record average SWE and the standard deviation, we separated the SWE measurements into local- and regional-scale classifications.

Table 2: Summary of sites surveyed and yearly and record average SWE and standard deviations (Stdev).

	Yearly Data												Record
	2000	2001	2002	2003	2004	2005	2006	2007	2008	2009	2010	2011	2000-2011
Sites Surveyed	58	75	68	71	45	60	118	140	112	143	102	77	1069
Average SWE	11.37	10.06	9.72	11.89	10.48	10.30	8.80	9.31	8.30	12.64	10.11	11.90	10.41
Stdev	3.95	3.87	3.59	3.63	3.75	4.43	3.38	4.28	4.54	6.13	4.15	6.57	4.36
+ 1 Stdev	15.31	13.93	13.31	15.51	14.22	14.74	12.18	13.59	12.84	18.78	14.27	18.47	14.77
- 1 Stdev	7.42	6.19	6.13	8.26	6.73	5.87	5.42	5.03	3.76	6.51	5.96	5.32	6.05

Table 3: Snow surveys separated into physiographic regions. The percentage of surveys completed within each region and the average elevation of the regions are also provided.

	Surveys	%	Average Site Elev. (m)
All	1069		401
< 150 m	410	38%	50
150 - 600 m	296	28%	292
> 600 m	363	34%	885

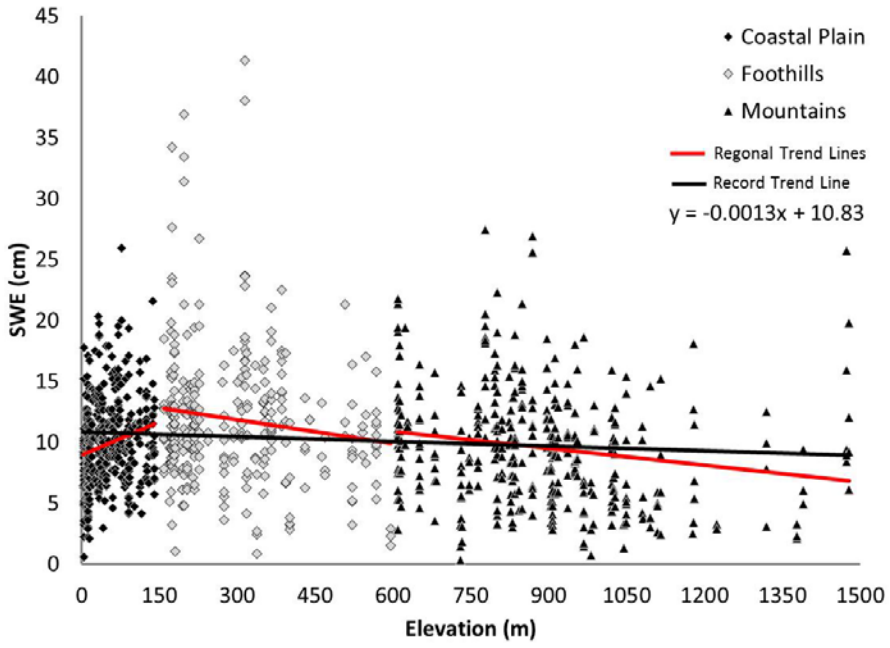

Figure 2: Complete record (2000–2011) of 1069 SWE values divided into physiographic regions plotted against survey site elevation. Record averaged SWE from the Coastal Plain to the Brooks Range is 10.41 cm, with an average standard deviation of 4.36 cm.

Snow water equivalent measurements greater than one standard deviation characterize areas of increased snow accumulation (drifted landscapes), while SWE values less than one standard deviation suggest that the location has experienced snow removal (wind swept) (Figure 3,

Table 4). Both snow-drifted and wind-scoured areas represent local-scale features, so SWE measurements greater or less than one standard deviation of the record average SWE were removed from the dataset. In all, 30% of the SWE measurements represented local-scale snowpacks (Table 5). The plus or minus one standard deviation outliers were almost evenly split with respect to total numbers, with 46% representing drifting landscapes and 54% characterizing wind-swept regions. However, there was a great percentage of drifting outliers in the Foothills and wind-swept outliers in the Mountains.

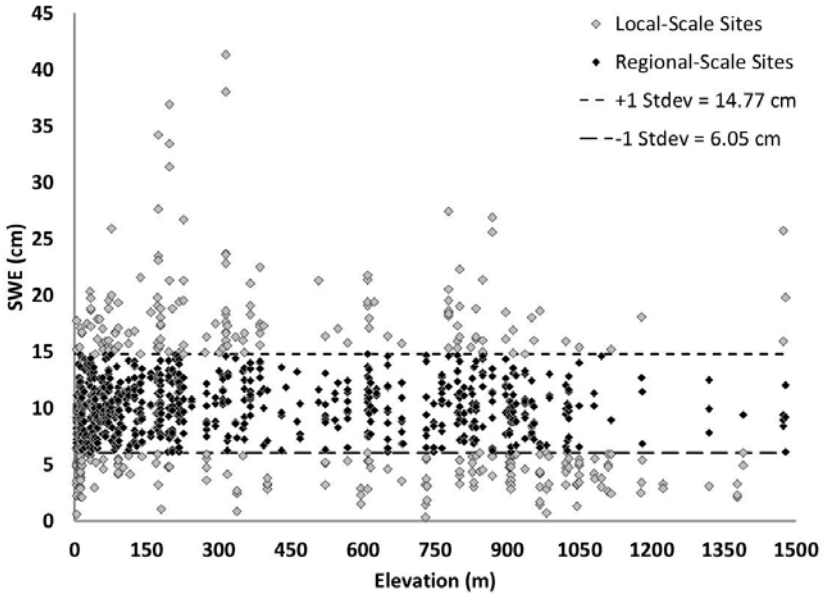

Figure 3: SWE measurements that deviate by ±1 standard deviation represent local-scale snow conditions. Measurements above 1 standard deviation indicate drifting deposition, while measurements below 1 standard deviation suggest wind scouring. SWE measurements within 1 standard deviation of the record SWE represent the regional snowpack and have an average of 10.13 cm.

Table 4**:** Number of snow survey sites that represent the regional-scale snowpack (SWE within ±1 standard deviation of the record average SWE), along with the number of sites that characterize local-scale snowpacks (SWE outside the range of ±1 standard deviation of the record average SWE). New yearly average SWE values were calculated only using SWEs that represent regional-scale snowpacks.

	Yearly Data												Record
	2000	2001	2002	2003	2004	2005	2006	2007	2008	2009	2010	2011	2000-2011
Regional-Scale Sites w/in Record Stdev (+/- 1) (14.77 > SWE > 6.05)	43	58	53	56	35	41	88	101	75	85	72	39	747
Removed Local-Scale Sites	15	17	15	15	10	19	30	39	37	58	30	38	322
% of Sites Removed	26%	23%	22%	21%	22%	32%	25%	28%	33%	41%	29%	49%	29%
Adjusted SWE	10.79	10.22	9.51	10.79	10.27	9.73	9.49	9.63	9.23	10.91	10.14	10.78	10.13
Stdev	2.31	2.40	2.45	1.95	1.94	2.36	2.15	2.18	1.87	2.41	2.00	2.25	2.19
Change in SWE	5%	-2%	2%	9%	2%	6%	-8%	-3%	-11%	14%	0%	9%	2%

Table 5: Number of snow survey sites that represent regional- and local-scale snowpacks separated into physiographic regions. Local-scale survey sites are further divided into ±1 standard deviation outliers. Associated percentages are also provided.

	Surveys	Regional-Scale Sites Within +/- 1 Std		Local-Scale Outliers		Outliers > 1 Std (SWE > 14.77)		Outliers < 1 Std (SWE < 6.05)	
All	1069	747	70%	322	30%	149	46%	173	54%
< 150 m	410	325	79%	85	21%	38	45%	47	55%
150 - 600 m	296	205	69%	91	31%	64	70%	27	30%
> 600 m	363	217	60%	146	40%	47	32%	99	68%

As we had hoped, the extreme high and low SWE measurements that represent local-scale snow conditions were evenly distributed above and below plus or minus one standard deviation, and essentially cancel out one another. The extreme values, however, had a small effect on the slope of the record trend line, because the survey sites that result in high and low SWE values are generally concentrated at different elevations. For example, the Mountains region normally has more hilltops, ridges, and steep slopes, which are characteristically sites of snow removal, while the Foothills region has more valley bottoms, water tracks, and vegetation for the snow to cumulate. By using all of the SWE measurements, the snowpack distribution patterns can be obscured by local-scale influences. The removal of survey sites that represent local-scale anomalies provides a more accurate representation of the regional snowpack. The removal of local-scale SWE values affected the record average SWE very little, only changing it from 10.41 to 10.13 cm.

5.2 Discussion

Many of the snow-surveyed sites constantly represent either regional- or local-scale snowpacks (Table 6). By sampling only locations that consistently provide SWEs that characterize the regional average snowpack, we improve our point-source sampling strategy so that we get more information from data that are more representative. This selective sampling method only works in areas with previous data collection. In the future, we intend to determine whether site-specific characteristics, such as slope, aspect, and vegetation, can aid in survey site selection in different, previously unsurveyed areas. In doing so, slope, aspect, and vegetation cover will be compared at regional- versus local-scale sites. We want to determine what characteristics each of the two groups (regional vs. local) has and why.

Table 6: Example survey sites that generally represent regional- and local-scale snowpacks.

Snow Survey Site ID	Elev (m)	# of Yrs Surveyed	Yrs w/in +/- 1 Stdev	% of Yrs w/in +/- 1 Stdev
Generally within +/- 1 Stdev. Represents **Regional Scale** Snowpack				
WestDock	5	12	10	83%
FranklinBluff	71	12	11	92%
H02	172	10	10	100%
UK09	763	10	10	100%
UK15	951	10	10	100%
Generally **NOT** within +/- 1 Stdev. Represents **Local Scale** Snowpack				
Happy	314	12	0	0%
UK08-UH	968	12	2	17%
Ukmet	778	12	3	25%
P01	12	10	4	40%
UK04-GCL	908	12	5	42%

6. CONCLUSIONS

The presently collected long-term snow dataset provides a rare opportunity to explore spatial- and temporal-scale variations over a large-scale area in the Alaska Arctic. Using this dataset, we identified a snowpack distribution pattern at a regional scale. More specifically, we determined that SWE measurements within plus or minus one standard deviation of the record average SWE closely represented the regional snowpack, while SWE values outside the one standard deviation range characterized local-scale anomalies. These extreme high and low SWE measurements that represent local-scale snow conditions were evenly distributed above and below the plus or minus one standard deviation and essentially cancel out one another. This made it possible to remove the survey sites that represented local-scale snowpacks, so the data being used more directly represented the regional average snowpack. The removal of local-scale SWE measurements had little effect on the record average SWE, which we concluded was relatively independent of elevation on Alaska's central North Slope, with roughly an average of 10 cm from the Coastal Plain to the Mountains. The lack of variability in SWE with change in elevation was unexpected and inconsistent with summer precipitation patterns.

REFERENCES

Anderton, S.P., White, S.M. & Alvera, B. 2004 Evaluation of spatial variability in snow water equivalent for a high mountain catchment. *Hydrological Processes* 18(3), 435–453. doi: 10.1002/hyp.1319

Benson, C.S. 1982 *Reassessment of Winter Precipitation on Alaska's Arctic Slope and Measurement on the Flux of Wind Blown Snow*. Report UAG R-288, Geophysical Intitute, University of Alaska, 26 pp.

Benson, C.S. & Sturm, M. 1993 Structure and wind transport of seasonal snow on the Arctic Slope of Alaska. *Annals of Glaciol.* 18, 261–267.

CAVM Team 2003 Circumpolar Arctic Vegetation Map. Scale 1:7,500,000. Conservation of Arctic Flora and Fauna (CAFF) Map No. 1. U.S. Fish and Wildlife Service, Anchorage, AK.

DeBeer, C.M. & Pomeroy, J.W. 2009 Modelling snow melt and snowcover depletion in a small alpine cirque, Canadian Rocky Mountains. *Hydrological Processes* 23(18), 2584–2599.

Elder, K., Dozier, J. & Michaelsen, J. 1991 Snow accumulation and distribution in an alpine watershed. *Water Resources Research* 27(7), 1541–1552.

Hinzman, L.D., Kane, D.L. & Gieck, R.E. 1991 Regional snow ablation in the Alaskan Arctic. In: Prowse, T.D. & Ommanney, C.S.L. (eds.), Northern Hydrology: Selected Perspectives, *Proc. of Northern Hydrology Symposium, Saskatoon, Saskatchewan,* 121–139.

Homan, J.W., Luce, C.H., McNamara, J.P. & Glenn, N.F. 2010 Improvement of distributed snowmelt energy balance modeling with MODIS-based NDSI-derived fractional snow-covered area data. *Hydrological Processes*. doi: 10.1002/hyp.7857

Kane, D.L., Gieck, R.E. & Hinzman, L. 2008a Water balance for a low-gradient watershed in Northern Alaska. In*:* Kane, D.L. & Hinkel, K.M. (eds.) *Proc. 9th International Conference on Permafrost.* University of Alaska Press, Fairbanks.

Kane, D.L., Gieck, R.E., Kitover, D.C., Hinzman, L.D., McNamara, J.P. & Yang, D.Q. 2004 Hydrological cycle on the North Slope of Alaska. In: Kane, D.L. & Yan, D. (eds.) *Northern Research Basins Water Balance.* IAHS Publ. 290. IAHS, Wallingford, pp. 224–236.

Kane, D.L. & Hinzman, L.D. 1988 Permafrost hydrology of a small arctic watershed. *Proc. 5th International Conference on Permafrost, Trondheim, Norway*, 590–595.

Kane, D.L., Hinzman, L.D., Benson, C.S. & Liston, G.E. 1991 Snow hydrology of a headwater arctic basin. 1. Physical measurements and process studies. *Water Resources Research* 27(6), 1099–1109.

Kane, D.L., Hinzman, L.D., Gieck, R.E., McNamara, J.P., Youcha, E.K. & Oatley, J.A. 2008b Contrasting extreme runoff events in areas of continuous permafrost, Arctic Alaska. *Hydrology Research* 39(4), 287–298.

Kane, D.L., Hinzman, L.D., McNamara, J.P., Zhang, Z. & Benson, C.S. 2000 An overview of a nested watershed study in Arctic Alaska. *Nordic Hydrology* 31(4-5), 245–266.

Kane, D.L., Youcha, E.K., Stuefer, S., Toniolo, H., Schnabel, W., Gieck, R.E., Myerchin-Tape, G., Homan, J.W., Lamb, E. & Tape, K. 2012 *Meteorological and Hydrological Data and Analysis Report for the Foothills/Umiat Corridor and Bullen Projects: 2006–2011*. University of Alaska Fairbanks, Water and Environmental Research Center, Report INE/WERC 12.01, Fairbanks, AK, 260 pp.

Osterkamp, T.E. 1984 *Temperature Measurements in Permafrost.* Report FHWQ-AK-RD-85-11, Alaska DOTPF. Fairbanks, Alaska, 87.

Prasad, R., Tarboton, D.G., Liston, G.E., Luce, C.H. & Seyfried, M.S. 2001 Testing a blowing snow model against distributed snow measurements at Upper Sheep Creek, Idaho, United States of America. *Water Resources Research* 37(5), 1341–1356.

Rovansek, R.J., Kane, D.L. & Hinzman, L. 1993 Improving estimates of snowpack water equivalent using double sampling. *Proc. 61st Western Snow Conference*, 157–163.

Seyfried, M.S. & Wilcox, B.P. 1995 Scale and the nature of spatial variability – Field examples having implications for hydrologic modeling. *Water Resources Research* 31(1), 173–184.

Stuefer, S., Kane, D.L. & Liston, G.E. 2013 In situ snow water equivalent observation in the U.S. Arctic. *Hydrology Research*.

Sturm, M., Douglas, T., Racine, C. & Liston, G.E. 2005 Changing snow and shrub conditions affect albedo with global implications. *J. Geophys. Res.* 110(G1), G01004.

Sturm, M., Racine, C. & Tape, K. 2001 Climate change: Increasing shrub abundance in the Arctic. [10.1038/35079180]. *Nature* 411(6837), 546–547.

Sturm, M., Taras, B., Liston, G.E., Derksen, C., Jonas, T. & Lea, J. 2010 Estimating snow water equivalent using snow depth data and climate classes. *J. Hydrometeorol.* 11(6), 1380–1394.

Sturm, M. & Wagner, A.M. 2010 Using repeated patterns in snow distribution modeling: An Arctic example. *Water Resources Research* 46(12), W12549.

Tape, K., Sturm, M. & Racine, C. 2006 The evidence for shrub expansion in Northern Alaska and the Pan-Arctic. *Global Change Biology* 12(4), 686–702.

Walker, D.A., Binnian, E., Evans, B.M., Lederer, N.D., Nordstrand, E. & Webber, P.J. 1989 Terrain, vegetation and landscape evolution of the R4D research site, Brooks Range Foothills, Alaska. *Holarctic Ecology* 12(3), 238–261.

Winstral, A., Elder, K. & Davis, R.E. 2002 Spatial snow modeling of wind-redistributed snow using terrain-based parameters. *J. Hydrometeorol.* 3(5), 524.

Modeling Groundwater Upwelling as a Control on River Ice Thickness

Chas Jones[1*], Knut Kielland[2], and Larry Hinzman[1]

[1]*International Arctic Research Center, University of Alaska Fairbanks, Fairbanks, AK 99775, USA*
[2]*Institute of Arctic Biology, University of Alaska Fairbanks, Fairbanks, AK 99775, USA*
**Corresponding author's email: chas.jones@iarc.uaf.edu*

ABSTRACT
The Tanana River flows through Interior Alaska, a region characterized by discontinuous permafrost. Studies link degrading permafrost to increased winter river discharge due to increasing groundwater input. In winter, Interior Alaska rivers are exclusively fed by groundwater, which serves as an external source of heat. In fact, some portions of rivers fed by groundwater maintain thin ice throughout the winter, or remain altogether ice-free, despite very cold air temperatures. These ice conditions represent a significant danger to winter travellers that use rivers for wintertime travel, particularly in this largely roadless area. We developed a deterministic model to explore how fluctuations in groundwater discharge control ice thickness on the Tanana River. The model allows us to examine how local changes in groundwater characteristics affect ice dynamics by addressing two questions: What are the dominant factors controlling seasonal ice dynamics on the Tanana River? What are the rates of change in ice thickness resulting from observed and projected changes in these factors? Ice melt is amplified by increased hydraulic gradient, increased groundwater upwelling, increased air temperature, increased groundwater temperature, or increased snow depth. A warming climate in regions with discontinuous permafrost is expected to increase groundwater input into rivers, decrease the temperature gradient between the atmosphere and the ice/water interface, and increase snow depths. All these changes contribute to decreased ice thickness and thus more hazardous conditions for winter travellers. The model illustrates the physical mechanisms, which corroborates reports from Alaskans that ice conditions have become more dangerous in the spring, and further suggests that permafrost degradation could contribute to the degradation of river ice in a warming climate.

KEYWORDS
Groundwater; heat transfer; permafrost; ice; river; surface water

1. INTRODUCTION
Historically, many villages and towns in Alaska were founded along waterways that provided relatively easy access throughout most of the year. During Alaska winters, frozen river systems are frequently used as transportation networks by people using snow machines, dog sleds, cross-country skis, snowshoes, and in some places even as ice roads. Frozen rivers can be navigated easily because there are few barriers or obstructions to inhibit travellers. We worked with several non-academic, local collaborators who have had extensive experience traveling on Alaska rivers in all seasons. Their observations on the Tanana River mirror those found by Herman-Mercer et al. (2011), who reported that rural Alaskans have observed that thin ice is becoming more

common on the Yukon River in recent winters. These areas are dangerous for winter travellers in Alaska who regularly use rivers for wintertime travel.

In collaboration with rural Alaskans, we explore how changes in hydrology will affect residents of Interior Alaska by examining the thermal balance between groundwater discharge and winter air temperatures in areas that have dangerous ice conditions in the Tanana River of Alaska. We initiated field studies in locations identified by local residents as having thin or no ice in most years. We developed a numeric model that allowed us to explore the relationship between seasonal groundwater flows and ice thickness under changing environmental conditions by examining three primary research questions: (1) What physical factors have the greatest influence on seasonal dynamics between river ice thickness and groundwater upwelling on the Tanana River? (2) How do variations in environmental conditions change the capacity of groundwater to melt river ice? (3) How might environmental conditions in a warmer climate affect river ice thickness on the Tanana River?

Heat provided by groundwater upwelling can degrade river ice from below. Under certain conditions, the groundwater heat flux exceeds atmospheric heat losses, and dangerous ice conditions can be maintained for extended periods despite very cold air temperatures. In recent decades, there have been reports that thin ice and open water may be more prevalent on Interior Alaska rivers in winter (Campbell & Althoff 2013; Herman-Mercer et al. 2011). These conditions can be caused by a number of factors including fast-moving turbulent water, warm air temperatures, external heat sources (power plant or sewage emissions), or groundwater upwelling in shallow areas. In this paper, we examine how changes in groundwater hydrology may affect river ice dynamics.

Ice-rich permafrost is an effective barrier to water transport and recharge (Burt & Williams 1976; Horiguchi & Miller 1980; Kane & Stein 1983), but warming temperatures have caused permafrost degradation across the Arctic (Hinzman et al. 2005; Jorgenson et al. 2001; Serreze et al. 2000). Permafrost degradation has been described as a potential mechanism for increased hydrologic connectivity between surface and groundwater systems observed through drainage of lakes (Yoshikawa & Hinzman 2003); increased daily summer and winter minimum flows (Smith et al. 2007); and increases in winter river baseflow (Walvoord & Striegl 2007). During winter conditions in Alaska, ice-covered rivers are fed entirely by groundwater; therefore, increased winter baseflow is indicative of increased groundwater input.

The Tanana Flats, which lies to the south of the Tanana River downstream of Fairbanks, has a high groundwater table and is reported to have experienced extensive permafrost degradation since the 1700s (Jorgenson et al. 2001). Much of the Tanana River neighboring the Flats appears to be fed by groundwater upwelling. Assuming that observations of our local collaborators and Herman-Mercer et al. (2011) are correct, the increased observations of thin ice and open water on the Tanana are hypothesized to be caused by increased winter groundwater flow caused by permafrost degradation intensified by a warming climate.

2. METHODS

We modeled the thermal balance between groundwater discharge and ice-free areas in the Tanana River near Fairbanks, Alaska, USA, a region that is characterized by discontinuous permafrost (Jorgenson et al. 2008). Our study area was located in Hot Cake Slough on the Tanana River, which is located in the Bonanza Creek Long-Term Ecological Research (LTER)

area approximately 9 miles southwest of Fairbanks (64°43′26″N, 148°7′22″W). This region is bordered by the Tanana Flats to the south, an area with a high water table largely fed by groundwater.

Our objective was to better understand how groundwater upwelling influences river ice thickness and how the potential ice melt rate (by groundwater) is affected by changing various environmental parameters (hydraulic conductivity, upwelling rate, ice thickness, snow depth, air temperature, and water depth). Thus, we developed a conceptual model (Figure 1) that illustrates how groundwater controls river ice thickness under specific conditions. Based upon this conceptual model, we created a numerical model using MATLAB (version 2011b) to estimate the potential ice melt rate by groundwater under static environmental conditions (assumes constant air temperature, wind velocity, snow depth, snow density, upwelling rate, groundwater temperature, and water column temperature).

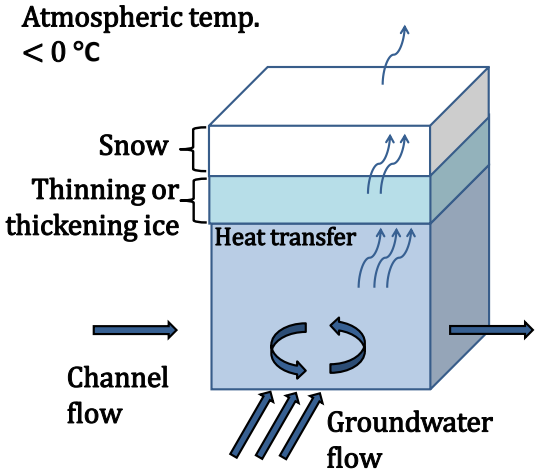

Figure 1: Conceptual model of heat transfer and changing ice conditions.

The conceptual model (Figure 1) shows a system where water flows laterally into and out of a control volume cell, while groundwater flows into the cell vertically. The cell is capped by a top layer of ice and snow with a specified initial thickness (d_{ice} and d_{snow}, respectively). The atmosphere above the ice and snow is set to a constant temperature (T_{air}) and wind velocity (V_{wind}). The boundary between the ice and the water is assumed to be 0°C, and heat is conducted from the water to the atmosphere (through the snow and ice) when the air temperature is less than 0°C.

The initial inflows and outflow have a specified volumetric flow rate (Q) and temperature (T), and a calculated volumetric heat content [H, relative to the freezing point of water (T_{melt})], which are subscripted by source in the equations [inflow (*in*), groundwater (*GW*), or outflow (*out*)]. H_{in}, H_{GW}, and H_{out} are calculated using Eq. (1), which references the density of water (ρ_{H_2O}) and the specific heat capacity of water (C_{p,H_2O}).

$$H = \rho_{H2O}\, C_{p,H2O} Q\, (T - T_{melt}) \qquad (1)$$

The groundwater inflow is assumed to be thoroughly mixed with the lateral inflow. The temperature of the lateral outflow is assumed the same as the lateral inflow, but the volumetric flow out of the cell is equal to the sum of the lateral and groundwater inflows. The total sum of

heat available to be conducted through the ice and snow (H_{loss}) or to melt ice (H_{melt}) is calculated according to Eq. (2).

$$H_{melt} = H_{in} + H_{GW} - H_{out} - H_{loss} \quad (2)$$

The heat lost through conduction through the ice, snow, and air boundary layer is partially dependent upon the thickness and thermal conductivity of the ice and snow (k_{ice}, k_{snow}, respectively) and the wind velocity according to the relationships denoted in Eq. (3). The k_{snow} was calculated from field measurements of snow density using equations presented by (Sturm et al. 1997), and the thermal transmittance of the boundary layer component is estimated using an approach discussed in Starosolszky (1968).

$$H_{loss} = \frac{T_{melt} - T_{air}}{\frac{d_{ice}}{k_{ice}} + \frac{d_{snow}}{k_{snow}} + \frac{1}{10 + V_{wind}}} \quad (3)$$

The potential ice melt ($\dot{d}_{\text{melt}}$) rate is calculated from the H_{melt} in combination with the latent heat of fusion for water (λ_{fusion}) and the density of ice (ρ_{ice}) using Eq. (4).

$$\dot{d}_{melt} = \frac{\Delta d_{ice}}{t} = \frac{H_{melt}}{\lambda_{fusion}\, \rho_{ice}} \quad (4)$$

The model modifies the ice thickness in the subsequent cell by subtracting Δd_{ice} from d_{ice} over the amount of time necessary for water to flow across the surface of the cell. After determining the ice thickness in the subsequent cell, the model calculates the potential rate of ice melt for that cell using the revised water flow rate and ice thickness assuming that the groundwater inflow is the same in every cell.

3. RESULTS

Model results indicate that the groundwater upwelling rate and its associated energy flux increases linearly as the hydraulic conductivity of a system increases under a constant temperature (Figure 2). At a groundwater upwelling temperature of 4.0°C, the heat flux could melt up to 17 mm/day under conditions without atmospheric heat losses, that is, if 100% of the groundwater heat was used to melt river ice (Figure 3).

Our results indicate that under field conditions with the measured upwelling rate (0.312 m^3/m^2 day), the potential ice melt is increased by increasing air temperature, hydraulic conductivity, groundwater upwelling, or snow depth. Figure 4 illustrates the linear relationship between atmospheric temperature and potential ice melt. Given our measured upwelling rate (0.312 m^3/m^2 day), at -10°C, the potential ice melt rate would be positive, but at -20°C, the potential ice melt rate is negative (indicating that there would be ice growth). This assumes that there was no accumulated water depth and a small layer of ice covering the water surface.

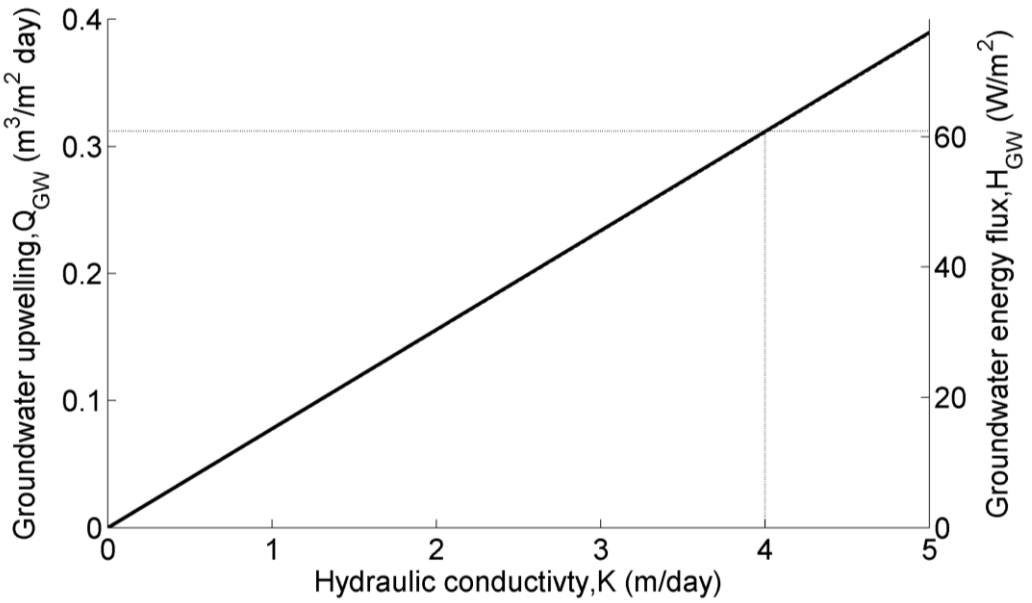

Figure 2: Hydraulic conductivity relative to the groundwater upwelling rate and its associated heat flux at a groundwater temperature of 4°C at our measured vertical hydraulic gradient.

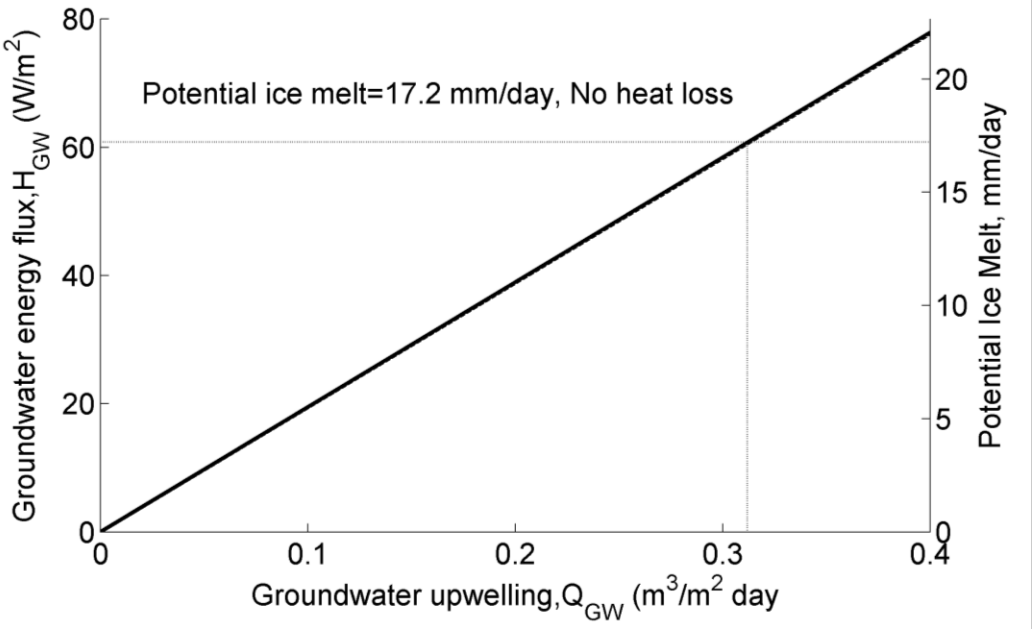

Figure 3: The potential heat flux associated with groundwater upwelling with a temperature of 4°C and the potential ice melt rate associated with that heat flux, assuming a system with no atmospheric heat losses or gains (perfectly insulated from the atmospheric temperature).

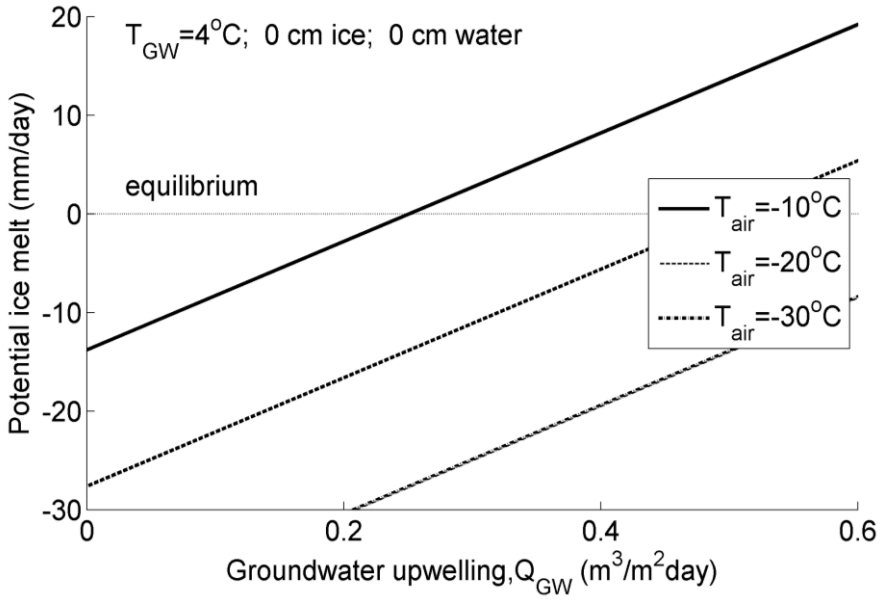

Figure 4: Groundwater upwelling effects on ice melt rates under decreasing air temperatures.

Figure 5 illustrates the modeled response to snow depth. At -27°C with no snow, the potential ice melt rate is negative (indicating conditions favoring ice growth), but with 5 cm snow at the same air temperature, the system is at thermal equilibrium with no ice growing or degrading. With 10 cm of snow, the insulating effects of the snow allow for some degradation of ice conditions (up to 5 mm/day of ice melt).

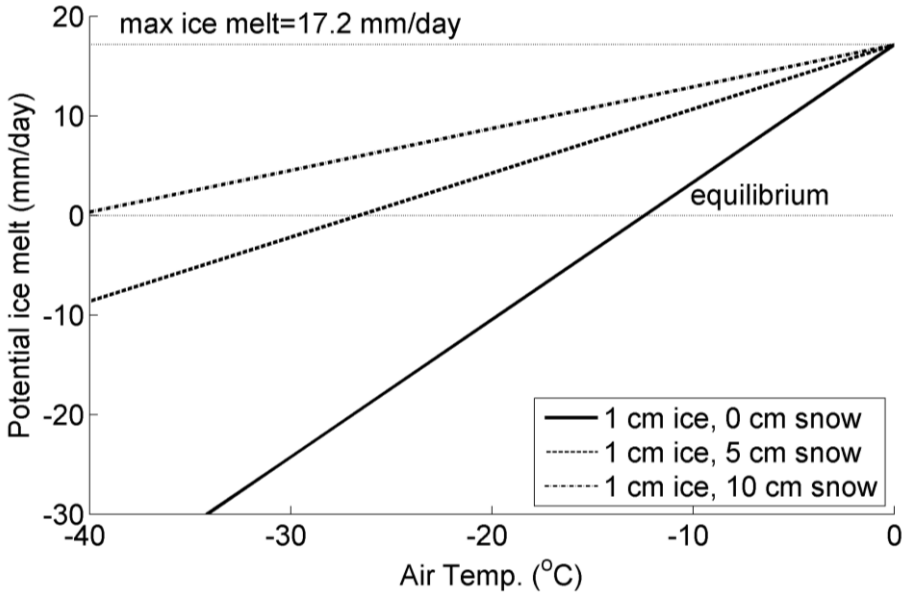

Figure 5: Potential ice melt rate at varying temperatures under different snow depths.

Figure 6 demonstrates how relatively large increases in the initial ice thickness has a relatively small effect on the potential ice melt rate when compared to similar increases in snow depth.

Under a constant snow depth, the change in potential ice melt is relatively small with even 25 cm increases in the initial ice thickness. In addition, under 20 cm or more of snow, there is a small increase in the potential ice melt rate.

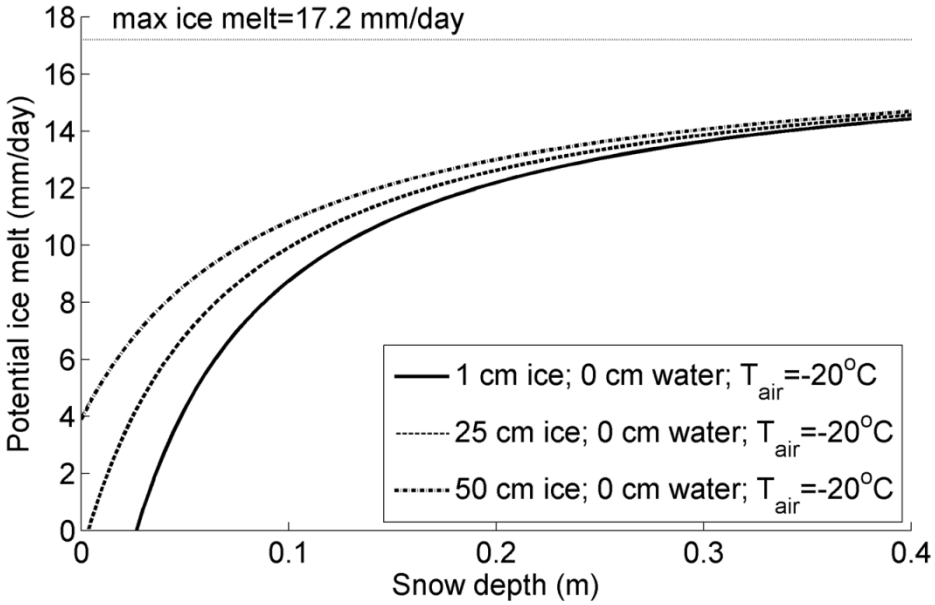

Figure 6: Potential ice melt rate at varying snow depths under three initial ice thicknesses.

4. DISCUSSION

Preliminary modeling results indicate that the wintertime groundwater–river system can be modeled and produces interesting and reasonable results. Figure 7 summarizes the model results. Increases in piezometric head (groundwater pressure) or hydraulic conductivity would increase the groundwater upwelling rate and the groundwater heat flux. The increased heat energy would lead to an increased rate of ice melt or degradation. Increases in the snow depth would increase thermal insulation over the ice and would decrease heat loss from the groundwater and river water, thus causing more heat energy to be available for degradation of the ice thickness. Increases in air temperature would decrease the temperature gradient between liquid water and the air, therefore decreasing the heat losses and increasing the ice melt rate. Finally, any increases in groundwater temperature would increase the groundwater heat flux and would increase the ice melt rate.

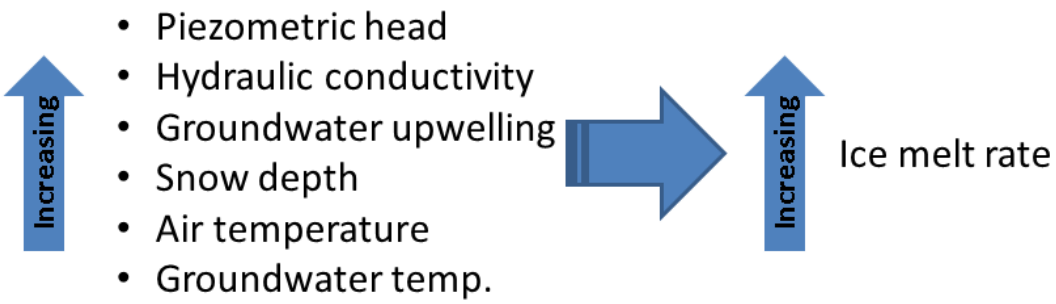

Figure 7: Summary of the factors that affect ice melt rate associated with groundwater flow into a hydrologic system with flowing water, based on numeric modeling results.

Increased air temperatures associated with climate change are warming permafrost, which is transforming some discontinuous permafrost areas to non-permafrost. These areas are expected to increase rates of exchange between surface water and groundwater. In areas with positive groundwater pressure, upwelling rates are expected to increase. Walvoord and Striegel (2007) estimate that winter groundwater discharge in the Tanana River has increased by approximately 20% between 1963 and 2005. Additionally, under an altered climate, increased winter air temperatures would be expected to decrease the temperature gradient. Increased snow depths in the area might also be expected. Thus, a future climate scenario might include estimates based upon these concepts to determine how ice conditions might be affected by groundwater upwelling in the region under an altered climate with degraded permafrost.

5. CONCLUSIONS

Rural Alaskans have indicated that travel conditions have gotten more dangerous in recent memory. Our modeling results illustrate a potential mechanism to account for changing travel conditions on side-sloughs of the Tanana River and other rivers in Interior Alaska. Degrading permafrost conditions have been reported as having increased groundwater upwelling, which could degrade ice from below and generate hazardous ice conditions on shallow channels. These hazardous areas are typically areas that appear to be safe for river travel, but in actuality are not safe. These areas could have stretches of thin ice that are difficult to predict without a better understanding of the potential mechanisms causing its existence. On the Tanana River, between Fairbanks and Nenana, field efforts show that dangerous areas are most commonly found along the southern river bank, which borders the Tanana Flats. The Tanana Flats is an area characterized by an extensive network of wetlands, bogs, and ponds, which are indicative of an area with substantial groundwater upwelling.

ACKNOWLEDGMENTS

This research is supported by a number of programs including the National Science Foundation grant with the Institute of Arctic Biology, University of Alaska Fairbanks; Resilience and Adaptation Program, University of Alaska Fairbanks; International Arctic Research Center, Alaska EPSCoR; Alaska Climate Science Center, Water and Environmental Research Center; and the USGS National Initiative for Water Research.

REFERENCES

Burt, T.P. & Williams, P.J. 1976 Hydraulic conductivity in frozen soils. *Earth Surface Processes* 1, 349–360.

Campbell, C. & Althoff, R. 2013 Personal interview.

Herman-Mercer, N., Schuster, P.F. & Maracle, K.B. 2011 Indigenous observations of climate change in the lower Yukon River basin, Alaska. *Human Organization* 70.

Hinzman, L.D., Bettez, N.D., Bolton, W.R., Chapin, F.S., Dyurgerov, M.B., Fastie, C.L., Griffith, B., Hollister, R.D., Hope, A., Huntington, H.P., Jensen, A.M., Jia, G.J., Jorgenson, M.T., Kane, D.L., Klein, D.R., Kofinas, G.P., Lynch, A.H., Lloyd, A.H., McGuire, A.D., Nelson, F.E., Oechel, W.C., Osterkamp, T.E., Racine, C.H., Romanovsky, V.E., Stone, R.S., Stow, D.A., Sturm, M., Tweedie, C.E., Vourlitis, G.L., Walker, M.D., Walker, D.A., Webber, P.J., Welker, J.M., Winker, K.S. & Yoshikawa, K. 2005 Evidence and implications

of recent climate change in northern Alaska and other arctic regions. *Climatic Change* 72, 251–298.

Horiguchi, K. & Miller, R.D. 1980 Experimental studies with frozen soil in an "ice sandwich" permeameter. *Cold Regions Science and Technology* 3, 177–183.

Jorgenson, M.T., Racine, C.H., Walters, J.C. & Osterkamp, T.E. 2001 Permafrost degradation and ecological changes associated with a warming climate in central alaska. *Climatic Change* 48, 551–579.

Jorgenson, M.T., Yoshikawa, K., Kanevskiy, M., Shur, Y.L., Romanovsky, V.E., Marchenko, S., Grosse, G., Brown, J. & Jones, B.M. 2008 Permafrost Characteristics of Alaska.

Kane, D.L. & Stein, J. 1983 Water movement into seasonally frozen soils. *Water Resources Research* 19, 1547–1557.

Serreze, M.C., Walsh, J.E., Chapin, F.S., Osterkamp, T.E., Dyurgerov, M.B., Romanovsky, V.E., Oechel, W.C., Morison, J., Zhang, T. & Barry, R.G. 2000 Observational evidence of recent change in the northern high-latitude environment. *Climatic Change* 46, 159–207.

Smith, L.C., Sheng, Y. & MacDonald, G.M. 2007 A first pan-Arctic assessment of the influence of glaciation, permafrost, topography and peatlands on northern hemisphere lake distribution. *Permafrost and Periglacial Processes* 208, 201–208.

Starosolszky, O. 1968 Ice in Hydraulic Engineering. Tromso, Norway.

Sturm, M., Holmgren, J., Konig, M. & Morris, K. 1997 The thermal conductivity of seasonal snow. *Journal of Glaciology* 43, 26–41.

Walvoord, M.A. & Striegl, R.G. 2007 Increased groundwater to stream discharge from permafrost thawing in the Yukon River basin: Potential impacts on lateral export of carbon and nitrogen. *Geophysical Research Letters* 34, L12402.

Yoshikawa, K. & Hinzman, L.D. 2003 Shrinking thermokarst ponds and groundwater dynamics in discontinuous permafrost near Council, Alaska. *Permafrost and Periglacial Processes* 14, 151–160.

Challenges of Precipitation Data Collection in Alaska

Douglas L. Kane* and Svetlana L. Stuefer

Water and Environmental Research Center, University of Alaska Fairbanks, Fairbanks, AK 99775, USA
**Corresponding author's email: dlkane@alaska.edu*

ABSTRACT
One of the basic tools of hydrologic engineering for runoff prediction is either precipitation intensity-duration-frequency (idf) (or depth-duration-frequency (ddf)) datasets. Recently, we (Perica et al. 2012) completed a revised precipitation frequency analysis for the whole of Alaska. Now we can reflect on some of the shortcomings of the precipitation data-collection program in the state of Alaska that were revealed by the frequency exercise for this northern remote area. Extreme topography, extensive spatial coverage, and wide-ranging climate results in annual precipitation values ranging from 120 in. (3050 mm) to 10 in. (254 mm). Although the number of stations used in the recent study compared with the 1963 original study increased substantially (517 versus 261), the fact that we only used data from about 30% of our present and historical stations implies that we can improve our data collection effort. The following is a discussion of some of the limitations and impediments encountered during the comprehensive precipitation frequency analysis for Alaska.

KEYWORDS
Precipitation; frequency analysis; duration analyses, annual precipitation maxima; hydrology; Alaska

1. INTRODUCTION
Next to air temperature, precipitation is the most widely observed and used environmental variable. Yet, it is recognized that we do a poor job in the Arctic of measuring both liquid and solid precipitation forms (Goodison et al. 1998; Yang et al. 1998; Yang et al. 1999; Yang et al. 2000). No precipitation gauge that is used extensively in the world measures the equivalent of 100% of the actual precipitation. Still we use those historical measurements of precipitation to generate either intensity-duration-frequency (idf) or depth-duration-frequency curves (ddf) and utilize the results in a number of engineering drainage and flood design applications.

Precipitation stations in Alaska have historically been sparse. A closer look at the distribution of stations would also reveal that a very large majority of the stations are still at low elevations along the coast or on major tributaries. Alaska is a very large state (1,480,000 km^2; 570,000 mi^2); it spans approximately 20° latitude (~51° N to 70° N) and 57° longitude (~130° W to 173° E), an expanse almost equivalent to the Lower 48. This can result in five to seven regional climate categories, depending on the criteria used. We described six regional climates in this paper (Arctic, Interior, West Coastal, Southwest Islands, Bristol Bay/Cook Inlet, and South/Southeast Coast) that range from Arctic to maritime.

Significant precipitation data collection in Alaska was initiated around 1900. The first precipitation frequency atlas for Alaska was published in the 1960s (Miller 1963; Miller 1965). It was based on precipitation measurements for varying durations from 234 daily stations, 9 hourly

stations, 18 6-hour stations, and 33 Canadian stations. The two major difficulties encountered in this early study were the lack of data in remote and mountainous areas of Alaska's broad reach and the absence of computers for use in the analysis and spatial distribution of results.

For the latest precipitation frequency estimation (Perica et al. 2012), there was the potential of using data from 1689 stations: 913 daily stations, 667 hourly stations, 73 15-minute stations, and 36 *n*-minute stations. Sixty daily stations and 10 hourly stations in Canada, along the Alaska-Canadian border, were also used. In the final 2012 idf analyses, 396 daily and 121 hourly Alaska stations were used.

The biggest advantage of the 2012 analysis versus the 1963 results is the additional 50 years of collected precipitation data; however, some of the earlier stations were discontinued during the intervening 50 years and some new stations were initiated. In 1963, the maximum record length was about 50 years, while in the most recent study it was over 100 years. The average record length for the 2012 study (Perica et al. 2012) was 32 years for daily stations (n = 396) and 18 years for durations between 1 hr and 24 hr. Stations with 5 years of data were included in the 1963 study, while in the recent study all stations with 15 years were retained (including some with as few as 9 to 10 years in remote areas). Because of the copious stations and the longer duration (stations established earlier) of stations in the Lower 48 relative to Alaska, NOAA/NWS uses the minimum criteria of 30 data years for precipitation frequency estimation.

In most idf/ddf analyses in the U.S., there are enough National Oceanic and Atmospheric Administration/National Weather Service (NOAA/NWS) stations to do an adequate job. However, because of the sparseness of stations in Alaska, data from any source were considered for use in the Alaska precipitation frequency analyses (assuming it passed quality checks). Data from the following sources were collected: Alaska Department of Transportation and Public Facilities; Environment Canada; USDC Midwestern Region Climate Center; USDC National Climate Data Center; National Interagency Fire Center; USDC Western Region Climate Center; USDA National Resource Conservation Service; USDI Geological Survey; Federal Aviation Administration; and University of Alaska Fairbanks. Data from Environment Canada were collected along the eastern boundary; all other boundaries (south, west, and north) of Alaska are open water (with scattered islands).

So, what could we do in terms of precipitation data collection in Alaska that would increase the value of this dataset that has been building for over 100 years?

2. HURDLES AND ISSUES CONFRONTED

The following is a short discussion of some of the problems encountered when performing the recent precipitation frequency estimation. Clearly, some of these problems were already known and even existed when the first precipitation frequency analysis was carried out. Because of the lack of precipitation data for Alaska, we collected any data we could find; these included data from research projects by various groups. The main advantage of research precipitation measurements was that they were often made in remote areas lacking previous measurements. The primary disadvantage is that the record length of these datasets is often too short to use in the analysis. In many cases, it is likely that the people collecting this data had no idea that their data could potentially be used for precipitation frequency analysis.

2.1 Density of Stations

The density of precipitation stations in Alaska is at least an order of magnitude less than in the contiguous states; this is mainly due to sparseness of populated centers, rugged terrain, climate extremes, and the vast size of the state (1,480,000 km^2, 570,000 mi^2). For example, in California (424,000 km^2, 163,700 mi^2), where a precipitation frequency analysis was recently completed, there is approximately one precipitation gauge for every 50 km^2, while in Alaska there is one every 880 km^2. Thus, the California density is approximately 18 times greater. There were almost 1700 potential precipitation stations for use in the recent precipitation frequency estimation for Alaska (Perica et al. 2012); however, only 396 daily and 121 hourly stations were used (one station every 2860 km^2). The distributions of these daily and hourly (including sub-hourly) stations in Alaska and Western Canada are shown in Figures 4.4.2 and 4.4.3 in Perica et al. (2012).

It is clear that the density of the precipitation data network in Alaska is far less than what is preferred; however, even this marginally sparse dataset provided a markedly improved analysis of the precipitation characteristics of Alaska. The criteria for precipitation frequency analysis used by NOAA/NWS were relaxed on station duration and percentage of missing data to increase the number of stations that could be used in the analysis. Also, use was made of data collected by any agency as long as the data met certain quality criteria for use.

2.2 Stations with Elevation

The populated centers of Alaska are generally located along the coast or at low elevations on major drainages. Not surprisingly, this is where a majority of existing and historical meteorological stations that are collecting precipitation data have been established. Over 50% of Alaska land area is above 1000 ft (~305 m) elevation, 30% is above 2000 ft (~610 m) elevation, and 10% is above 4000 ft (1220 m) elevation (Figure 1). In the 1963 analysis, there was approximately one station for every 10,000 mi^2 (28,500 km^2) above 1000 ft (~305 m); in the 2012 analysis, this statistic had improved by about a factor of 5 (one station every 2100 mi^2 (5500 km^2)). While the number of stations at higher elevation has improved with time, it is still dramatically low. It should be noted that most runoff originates in the unpopulated headwaters of the catchments at high elevations, so it is important to have good estimates of precipitation at high elevation. In the 2012 analysis, 134 stations were above 1000 ft (305 m) and 10 were above 3000 ft (915 m). In 1963, there were 26 above 1000 ft (305 m) and none above 3000 ft (315 m).

2.3 Proximity

In a state with very few stations, it is surprising to find some precipitation stations that are located near each other. On examination, however, very few Alaska stations are located close to one another and collecting data at the same time. The exceptions were in populated centers like Anchorage and Fairbanks, where stations with overlapping data were in operation although separated only by 5 to 10 mi (8 to 16 km). What generally happened was that a station was moved within proximity to the original location. In some cases, overlapping data were collected at both sites for a year or two and then terminated at the original site. In order to get a longer record in these cases, co-located datasets were combined, thus effectively reducing the number of useable stations, but extending the record length.

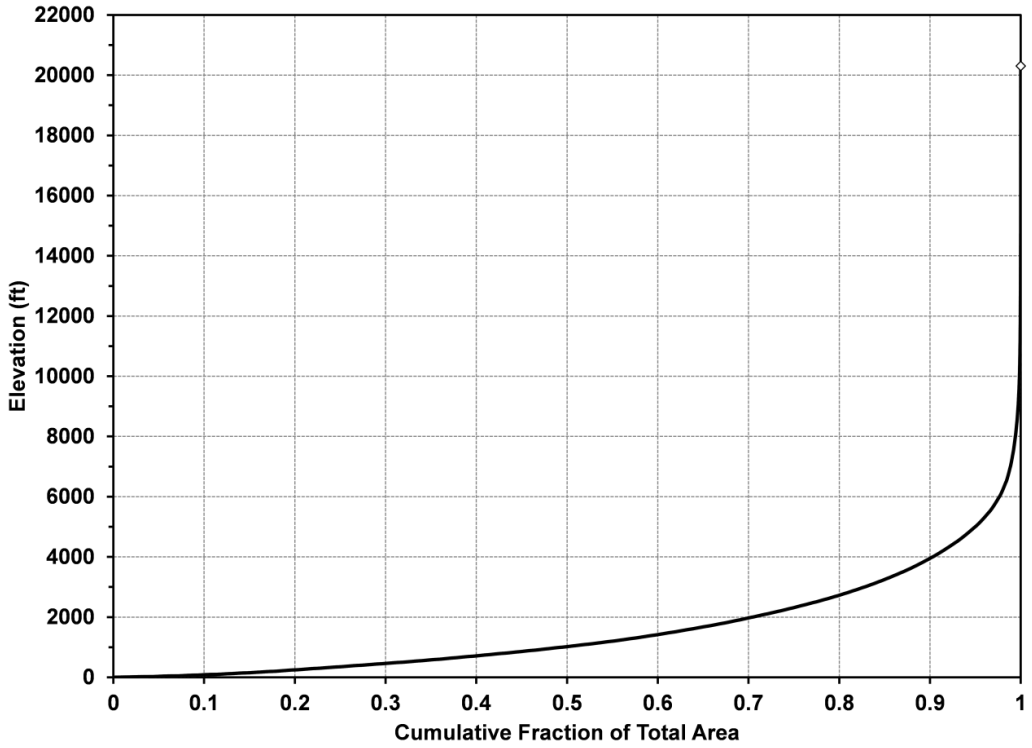

Figure 1: Hypsometric curve for Alaska showing the full range of the elevations from sea level to 20,320 ft (6194 m).

2.4 Gauge Undercatch

It has been known for quite some time (Larkin 1947) that we have not developed the precipitation gauge that exactly measures the true amount of precipitation (Goodison et al. 1998; Yang et al. 1998; Yang et al. 1999; Yang et al. 2000). Sevruk and Klemm (1989) illustrate most of the national gauges presently around the world. In most cases, the one exception being blowing snow conditions, all the precipitation gauges undercatch the actual precipitation amount. The average magnitude of the undercatch (when compared with the Double Fence Intercomparison Reference, or DFIR) at Annette Island in southeastern Alaska for the 24-hour annual maximum (1984–2008) for a gauge with an Alter shield was estimated to be 15%. A comparison study between gauges (Goodison et al. 1998) showed that the catch efficiencies varied; eventually the DFIR with a Tretyakov gauge was determined to have the highest catch efficiency. It was also determined prior to the mid-1940s (Larkin 1947) that wind shields on the U.S. 8-inch orifice gauges could significantly increase gauge catch. In the late 1940s, the use of Alter wind shields was initiated on some U.S. 8-inch orifice gauges used by the National Weather Service. The earliest we can document wind shields in Alaska is 1954 at Annette Island.

The two problems we faced on this project relative to gauge catch were, first, that at some of the sites (especially older ones) there were no wind shields initially, and second, that we used data from Canadian gauges along the eastern boundary of Alaska that have their own gauge catch characteristics when compared with the standard U.S. NWS 8-inch orifice gauge. We initially thought we could make undercatch corrections to the U.S. gauges for the two conditions of with and without wind shields. As indicated above, unfortunately, only in rare cases was there any documentation on when Alter shields were added to U.S. gauges.

Since this documentation was not available, we attempted an alternate approach. If Alter shields were added, we anticipated that there would be an increase in precipitation catch, and if we plotted cumulative annual precipitation versus time, we would detect a positive change in slope. We selected seven first-order stations (Anchorage, Barrow, Cold Bay, Fairbanks, Juneau, Ketchikan, and Nome) that were widely distributed over the state with a relatively long period of record, and plotted the results. The outcomes were not conclusive (Figure 2). Anchorage, Barrow, Fairbanks, and Ketchikan deviated little from a constant slope. During the period of record, Cold Bay and Juneau, which started around 1950, initially had a decrease in slope followed by an increase around the mid-1980s. Nome, although the station was started in 1908, was missing over 20 years of data (1930–1952); after 1952 the slope decreased briefly and then increased to the original value. Overall, this approach did not provide any insight into when Alter shields were added. Therefore, the precipitation data were not corrected for undercatch by wind.

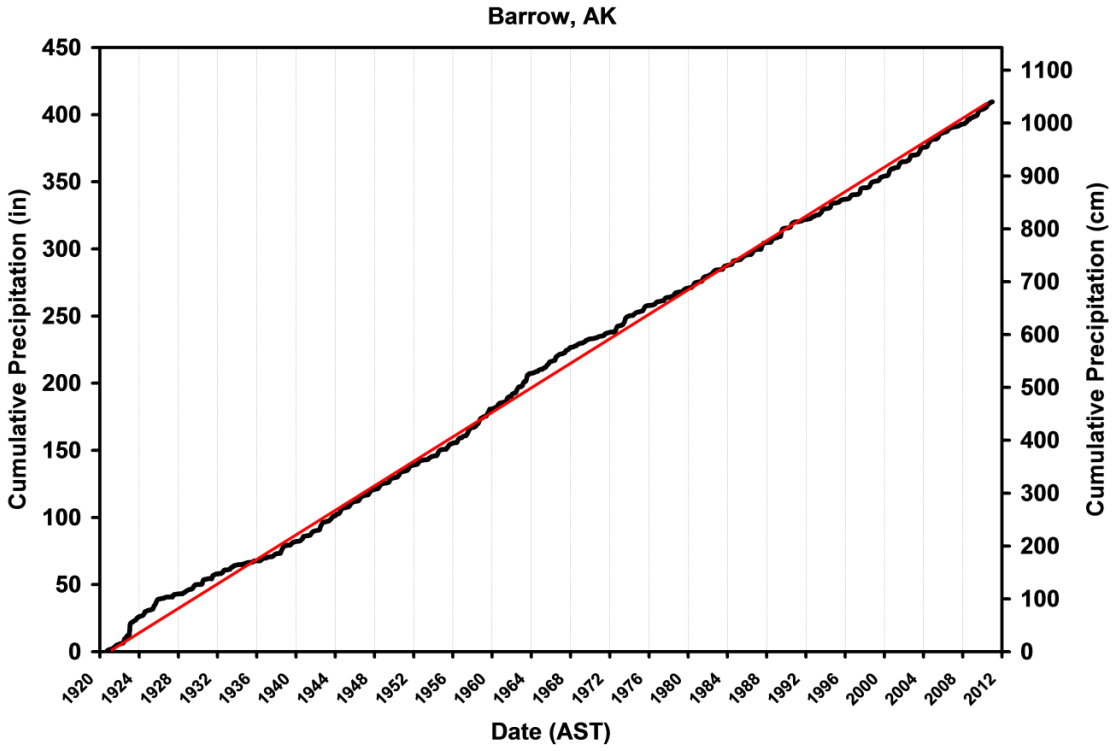

Figure 2: Cumulative curve for annual precipitation at the Barrow Post Rodgers Airport (50-0546) for the period of record. Note that there are three periods when the annual precipitation deviates slightly from a constant slope (straight line), but they are of short duration with no sustained long-term trend.

2.5 Length of Data Collection

As a rule of thumb, the NWS requires the station record length to be 30 years or longer for use in precipitation frequency analysis. The biggest advantage of the 2012 Alaska analysis versus the 1963 results is the additional 50 years of collected data. In 1963 the maximum record length was about 50 years, while in the most recent study, it was over 100 years. The average record length for stations used the 2012 study (Perica et al. 2012) was 32 years for daily stations (n = 396) and 18 years for durations less than 24 hours. Stations with as few as 5 years of data were included in

the 1963 study, while in the recent study, all stations with 15 years were retained (including some with as few as 9 to 10 years in remote areas with minimal data).

2.6 Missing Observations

The problem of missing data was ubiquitous throughout the recorded observations. Missing data are generally more common during the cold season than the warm season. Also, most annual precipitation maximums occur during rain events; therefore it is easier to tolerate missing data in the cold season. At several research sites (generally unmanned), daily and hourly precipitation data are collected only during the warm season (end-of-winter snow surveys are performed just prior to ablation to quantify the cumulative snow water equivalent on the ground). Numerous impediments exist at unmanned sites where cold season measurements are attempted, the largest being instrumentation robust enough for measuring solid precipitation; smaller ones are power, communications, environment, and wildlife. In the end, for the idf analysis it was acceptable if less than 33% of the wet season was missing. Wet seasons were delineated both by weighing the periods in which two-thirds of the annual maximum occurred at each station and by examining histograms of annual maximum for the one-day and one-hour durations in a region.

2.7 Climate Change

It is generally assumed when performing hydrologic frequency analysis that the data from the events are random, independent, and with no trends. In other words, the analysis is based on the assumption of a stationary climate (same mean and variance) over the period of data collection. The user of the idf is also assuming that these conditions prevail over the design time frame. Numerous environmental changes (warmer permafrost, reduced sea ice extent, vegetation changes, mass wasting of glaciers, etc.) have been documented for Alaska. Also, many of the Alaska station datasets are not long enough to exhibit statistical robustness. Perica et al. (2012) found for 12 hourly stations and 154 daily stations with a minimum record length of 40 years that positive trends were found in 8% of the stations, negative trends in 7% of the stations, and no trend in the remaining 80% of the stations (using parametric *t*-test and nonparametric Mann-Kendall test).

One should expect that positive trends (see Figure 2 as an example) in the precipitation data could also be triggered by the addition of Alter shields to the precipitation gauges due to increased catch. We originally thought that this may present itself as an approach to determining when wind shields were added at gauging sites due to the measured increased in catch. However, there was no consistent trend for the seven first-order stations examined (see section above titled "Gauge Undercatch") in detail. Although some stations showed an increasing slope around 1976, this was at the same time that Ebbesmeyer et al. (1991) documented a step-like change in 40 wide-ranging environmental variables for the Pacific Ocean and the Americas.

Presently, these data analyses do not appear to clearly yield statistically significant change in the magnitude of the annual precipitation maximums.

2.8 Data Quality

Evaluating the quality of data collected by others is always a challenge, especially in a region as vast and varying as Alaska. While we (Perica et al. 2012) did not attempt to address quality issues for all the precipitation data collected, all values (annual maxima of hourly and daily precipitation) used in the precipitation frequency analysis were scrutinized.

A large majority of the NWS precipitation stations are run by cooperators who volunteer their time. Many problems seemed to appear when the cooperator left the site (medical emergency, vacation, etc.) and another party collected the data in the cooperator's absence. For example, in some cases it appeared that daily readings of precipitation were not taken for one or more days; however, when the precipitation measurement was resumed, the cumulative amount of precipitation from the previous unmeasured days was reported. In some cases, there was an attempt to correct this on the original data work sheets, but often this problem was not identified at the time the data were collected. The problem for our precipitation frequency analysis is that these errors often show up as annual maximums for daily durations. So, prior to using the data, outliers (in our case, annual maxima that depart significantly from the trend of the other corresponding maximums in the dataset) had to be identified.

Both low and high outliers need to be identified as they can significantly affect the statistical parameters, especially for small datasets, which are common in the Alaska dataset.

2.9 Liquid versus Solid Precipitation/Temperature Segregation

One of the standard engineering practices is to use precipitation frequency estimates to predict peak runoff (also volume and complete hydrograph) predictions for the design of stream structures such as culverts in rural areas and storm drain structures in urban areas. In tropical areas, all precipitation events are rainfall with an immediate runoff response. At higher latitudes and high elevations, the possibility exists that annual maximum events are solid precipitation. The dilemma is that solid precipitation does not produce immediate runoff. In fact, there may be further accumulation of solid precipitation before it ablates and runoff is generated. Therefore, the rate of runoff is a function of the rate of melt and is quite different than the precipitation rate. Could we separate the annual maxima between liquid and solid precipitation?

Many of the stations in Alaska do not record the form of precipitation; however, for precipitation frequency estimation, this is an important piece of information. For each of the six climatic regions of Alaska, we identified a unique threshold temperature that separates solid and liquid precipitation. For those daily stations in each of the climatic regions that recorded air temperature and type of precipitation, we plotted a histogram of these events (Figure 3). On the *y*-axis, we plotted the ratio of the number of events at a given temperature divided by the total number of events (multiplied by 100 to get percent). On the *x*-axis, we plotted those temperatures at and above freezing where there is a transition from solid to liquid precipitation. The strategy was that if we can determine a threshold temperature where there is a transition from solid to liquid precipitation for each climatic region, we could apply that to the station data where the form of precipitation is not known. In addition to plotting the data for specific stations in Figure 3, the average for all of the stations plotted in Figure 3 for each climatic zone is shown as the far right bar in each grouping. In the far right panel at/around 36°F (2.2°C) for seven widely spaced stations, it is clear that there are more rain events than snow. In the far left panel (0°C, 32°F), it is clear that solid precipitation dominates. In this climatic region, the threshold temperature or transition between solid and liquid precipitation is 33°F (0.6°C).

In summary, using the average results (right bar in each panel), we see increasing threshold temperatures as we progress from higher to lower latitudes. For individual stations, this pattern is a little more confusing. Although the transition from liquid to solid is designated as a specific temperature, it is clear from Figure 3 that the two forms of precipitation can be found over a range of temperatures. This is similar to observations of Auer (1974).

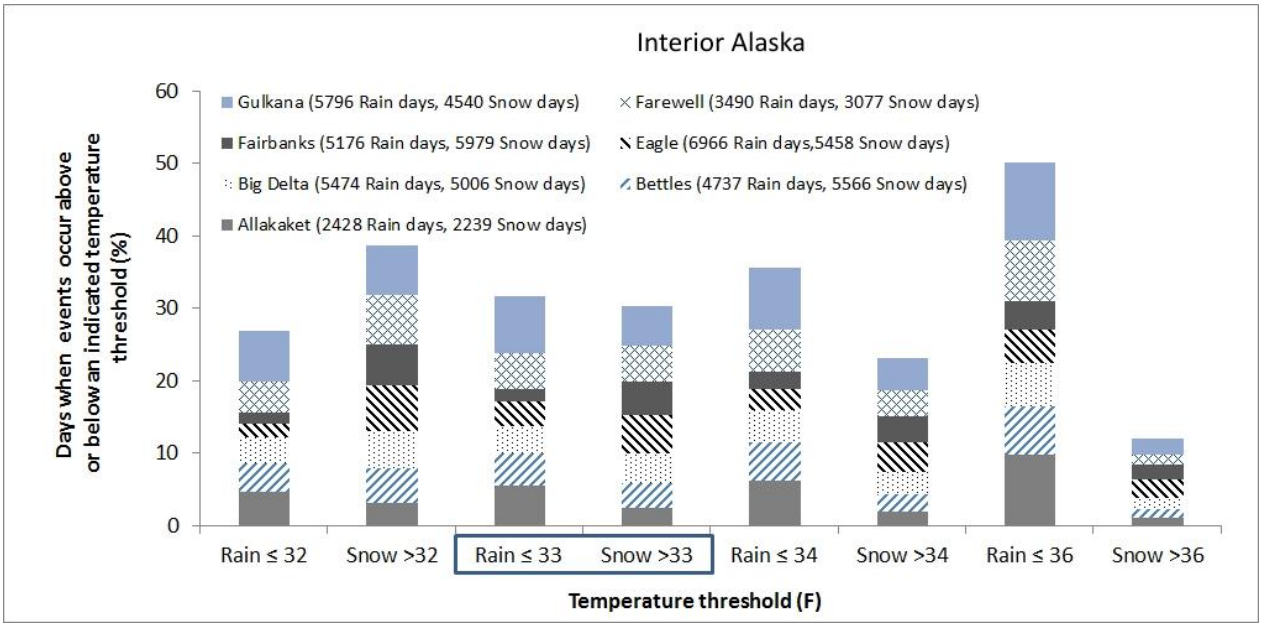

Figure 3: Plot of number of events (rain or snow) divided by total number of events for selected temperatures at and above freezing temperature. In this example, the threshold temperature is 33°F (~ 0.5°C); at or above that temperature, precipitation is more likely to be rainfall and below that temperature it is more likely to be solid.

3. CONCLUSIONS

Clearly, it is still a challenge for us to get good-quality precipitation data with adequate spatial cover; this is more so for solid precipitation. While it is an advantage for spatial coverage to have numerous parties (such as government agencies, private sector, universities) collecting precipitation, the quality of data between parties is not always compatible. We already know that all of the precipitation gauges undercatch the true amount, and each gauge type has different performance characteristics. Also, the use of unmanned gauges is always fraught with problems, for example, environment, wildlife, and power supply. The reason we have so many diverse groups collecting precipitation data in Alaska is that one or two groups cannot meet the precipitation data needs of all.

Would a meeting of all parties collecting precipitation data prove useful? Some agencies, like the National Weather Service or the National Resource Conservation Service, are specifically directed to collect precipitation over the long term. It is rare, however, for universities to collect long-term precipitation data. If any major overhaul of our precipitation data collection network in Alaska (or the USA) were to occur, it would require substantial resources. This reduces the likelihood of any major issues being addressed, such as replacing the type of precipitation gauges so that we can measure precipitation accurately. If data collection agencies were to convene a meeting, the first thing they should do is identify what the constraints are. Next, they should determine if the solutions are physically possible and financially feasible. Obviously, changes in our present precipitation network are going to be made in small steps, not generous ones. Many of the issues we have at the local scale in Alaska also exist at the international scale.

ACKNOWLEDGMENTS

The authors of this paper recognize the contributions made by the coauthors of Perica et al. (2012).

REFERENCES

Auer, A.H. Jr. 1974 The rain versus snow threshold temperatures. *Weatherwise* 27, 67.

Ebbesmeyer, C.C., Cayan, D.R., McLain, D.R., Nichols, F.H., Peterson, D.H. & Redmond, K.T. 1991 1976 step in the Pacific Climate: Forty Environmental Changes Between 1968–1975 and 1977–1984. *Proc. 7th Annual Pacific Climate (PACLIM) Workshop* (Betancourt, J.L. & Sharp, V.L., eds.), *April 1990*, California Department of Water Resources, Interagency Ecological Studies Program, Technical Report 26, pp. 115–126.

Goodison, B.E., Louie, P.Y.T. & Yang, D. 1998 *WMO Solid Precipitation Measurement Intercomparison.* World Meteorological Organization, Instrument and Observing Methods Report No. 67, WMO/TD Report No. 872, 212 pp.

Larkin, H.H. 1947 A comparison of the Alter and Nipher shields for precipitation gauges. *Bulletin American Meteorological Society* 28(4), 200–201.

Miller, J.F. 1963 *Probable Maximum Precipitation and Rainfall-Frequency Data for Alaska for Areas to 400 Square Miles, Durations to 24 Hours, Return Periods from 1 to 100 Years.* Technical Paper No. 47, U.S. Dept. of Commerce, Weather Bureau, U.S. Government Printing Office, Washington, DC, 69 pp.

Miller, J.F. 1965 *Two-to-Ten Day Precipitation for Return Periods of 2 to 100 Years in Alaska.* Technical Paper No. 52, U.S. Dept. of Commerce, Weather Bureau, U.S. Government Printing Office, Washington, DC, 30 pp.

Perica, S., Kane, D., Dietz, S., Maitaria, K., Martin, D., Pavlovic, S., Roy, I., Stuefer, S., Tidwell, A., Trypaluk, C., Unruh, D., Yekta, M., Betts, E., Bonnin, G., Heim, S., Hiner, L., Lilly, E., Narayanan, J., Yan, F. & Zhao, T. 2012 Precipitation-Frequency Atlas of the United States, Alaska. *NOAA Atlas 14 Volume 7 Version 2.0, NOAA,* National Weather Service, Silver Spring, MD., 45 pp.

Sevruk, B. & Klemm, S. 1989 *Catalogue of National Standard Precipitation Gauges.* World Meteorological Organization, Instrument and Observing Methods Report No. 39, WMO/TD-No. 313, 50 pp.

Yang, D., Goodison, B.E., Metcalfe, J.R., Golubev, V.S., Bates, R., Pangburn, T. & Hanson, C.L. 1998 Accuracy of NWS 8″ standard nonrecording precipitation gauge: Results and application of WMO intercomparison. *J. Atmospheric and Oceanic Technology* 15, 54–68.

Yang, D., Goodison, B.E., Metcalfe, J.R., Louie, P., Leavesley, G., Emerson, D., Hanson, C.L., Golubev, V.S., Elomaa, E., Gunther, T., Pangburn, T., Kang, E. & Milkovic, J. 1999 Quantification of precipitation measurement continuity induced by wind shields on national gauges. *Water Resources Research* 35(2), 491–508.

Yang, D., Kane, D.L., Hinzman, L.D., Goodison, B.E., Metcalfe, J.R., Louie, P.Y.T., Leavesley, G., Emerson, D.G. & Hanson, C.L. 2000 An Evaluation of the Wyoming Gauge System for Snowfall Measurement. *Water Resources Research* 36(9), 2665–2677.

Water Temperature Variations in Two Finnish Lakes (Kallavesi and Inari) in 1981–2010

Johanna Korhonen

Freshwater Centre, Finnish Environment Institute, Helsinki, FIN-00251, FINLAND
Corresponding author's email: johanna.korhonen@ymparisto.fi

ABSTRACT
Changes and variations of water temperature in lakes during the last three decades (1981–2010) are presented in this paper. The study includes data available from two dimictic lakes. The sites are located in central/eastern Finland (Lake Kallavesi) and in Lapland (Lake Inari). Bottom depths of the study sites are approximately at 40–45 m. Surface water temperature maximum usually occurs in late July, while water temperature maximum near the bottom occurs in late September. Some changes have been observed in water temperatures at different depths. Most of the changes were increases in water temperature of water layers not deeper than 20 m. The summer water temperatures of surface layers have risen in both lakes. In general, no changes near the bottom were observed. In Lake Kallavesi, surface water temperatures in wintertime have decreased. The observations of ice cover duration and surface water temperature near the shore are also compared with temperature profile measurements.

KEYWORDS
Finland; lakes; water temperature; variation; changes

1. INTRODUCTION
Water temperature has a big influence on the biological activity and growth of aquatic organisms in lakes. All aquatic species have preferred temperature ranges, which affects the abundance of each species. Temperature is also important because of its influence on water chemistry, which in turn affects biological activity.

The freezing and break-up records of Finnish lakes have revealed significant trends for later onset of ice cover and earlier melting (Korhonen 2002a, b; Korhonen 2005, 2006). Based on changes in ice cover duration and the length of the open-water period, some questions have been raised. Are there also changes in lake water temperatures and their variation at different depth levels in Finnish lakes? The average temperature profiles for Lakes Kallavesi and Inari were presented earlier by Korhonen (2002b); nevertheless, long-term changes were not discussed because only 20 years of data were available at that time. This paper will provide analysis for the same two lakes with 30-year datasets.

2. DATA AND METHODS

2.1 Observation Sites
Water temperature profiles are systematically monitored by the Finnish Environment Institute (SYKE) at ten sites in Finland. Some water temperature records in the database date back to the 1960s, but the homogeneity of all those time series cannot be proved. The metadata of observation site changes are sometimes poor. This study includes two observation sites with long

data histories and quite stable locations. The sites are situated in central/eastern Finland (Lake Kallavesi) and in Lapland (Lake Inari). Both lakes are rather big. Bottom depths of the study sites are approximately at 40–45 m, depending on the water level and small variations in the measuring site. The location of the observation sites are shown in Figure 1. Both lakes are regulated, but the regulation of Lake Kallavesi is somewhat moderate (water level variation 1–1.5 m), and it is not considered to have an effect on temperature or ice conditions. The regulation of Lake Inari is stronger, and the observed water level variation range is 2.5 m.

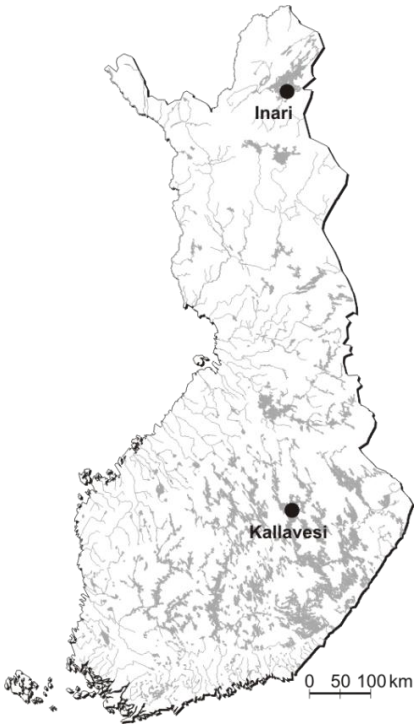

Figure 1: Location of lake observation sites of Lakes Kallavesi and Inari.

2.2 Measurement Method

Measurements are done manually with a digital thermometer attached to the cable. Before the 1990s, mercury thermometers were used. Observation locations are marked with buoys to ensure the same location every time. In the past, there was more variation of the measuring site. Water temperature is measured manually three times per month, every 10th, 20th, and 30th day of each month. The measurement interval is 1 m from the surface to a depth of 20 m, and 2 m from 20 to 50 m. Before the 1980s, the measurement interval was 5 m from the surface to the bottom. Therefore, precise detection of the thermocline is not possible from the data before the 1980s. There are gaps in measurements during early winter and late winter/early spring due to weak ice.

2.3 Data and Analysis Method

Data are available from the hydrology and water resources management data system of the Finnish Environment Administration. All data were analyzed for the period 1981–2010 for several different depths (near the surface, 5 m, 10 m, 15 m, 20 m, 30 m, 40 m, and near the bottom). Since the observations are done three times per month, the days between observations were interpolated. The gaps longer than a month were not interpolated if they were during the summertime. There are no long data gaps during 1981–2010 in Lake Kallavesi. For Lake Inari,

data of the years 1995 and 2001 are missing; also some couple of months gaps during other years. Monthly values were calculated from the interpolated daily values. Minima and maxima are the extremes of the exact measurement dates. The mean temperature of water column was also calculated for each measurement day. Mean values for different decades were additionally calculated and compared.

Trends were tested statistically with a non-parametric Mann-Kendall trend test with 5% significance level. (Kendall 1975; Mann 1945). Sen slopes for trends (Sen 1968) were calculated using the MAKESENS Excel program (Salmi et al. 2002).

3. RESULTS AND DISCUSSION

3.1 Annual Water Temperature Profile

Water temperature variations in dimictic Finnish lakes follow a yearly pattern. The isothermal mixing takes place during spring and fall. Lakes in Finland are ice-covered during winter and thermally stratified during summer. The mean annual water temperature at different depths for Lake Inari and Lake Kallavesi are presented in Figure 2 and 3, respectively.

The isothermal mixing period is longer in southern Lake Kallavesi, where it usually starts in autumn in the beginning of October and last until late November. In Lake Inari, the autumn mixing period lasts about a month (October). Reverse stratification takes place during the ice-covered winter period. Due to a longer mixing period, the water column cools more in Lake Kallavesi, resulting in cooler winter temperatures all the way from the surface to the bottom. The average bottom temperature during the winter is over 3°C in Lake Inari, while in Lake Kallavesi it is a bit over 2°C. The overturn period in spring is short in both lakes, and thermal stratification takes place during May in Kallavesi and in June in Inari. The surface water temperature maxima occur in late July; the average is over 19°C in Lake Kallavesi, and over 14°C in Lake Inari. The timing of the maximum moves later in deeper layers. The bottom water temperature maxima occur usually in late September just before the isothermal mixing starts. The annual temperature amplitude near the bottom is higher in Lake Kallavesi than in Lake Inari. The maximum water temperature near the bottom is over 10°C in Lake Kallavesi, while it is about 6°C in Lake Inari.

The thermocline is usually between 10 and 15 m in Lake Kallavesi, and between 20 and 25 m in Lake Inari. The difference between the depth of thermocline is caused by different optical properties of the lakes. The transparency of lake water in Lake Inari is higher than in Lake Kallavesi. The average visibility depth in Inari near the observation site is 5–7 m, while in Kallavesi it is 2–3 m.

Water temperatures near the lake bottom vary slowly. The main factor for the bottom temperatures during the winter is the autumn mixing and cooling period. A shorter mixing period results in warmer winter temperatures during the ice-covered period. In summertime, winds and mixing are the main forces driving the near-bottom water temperatures. Also, currents can bring cooler or warmer water. Strong stratification with calm weather type keeps the near-bottom temperatures low, but windy weather can make warmer surface water mix deeper.

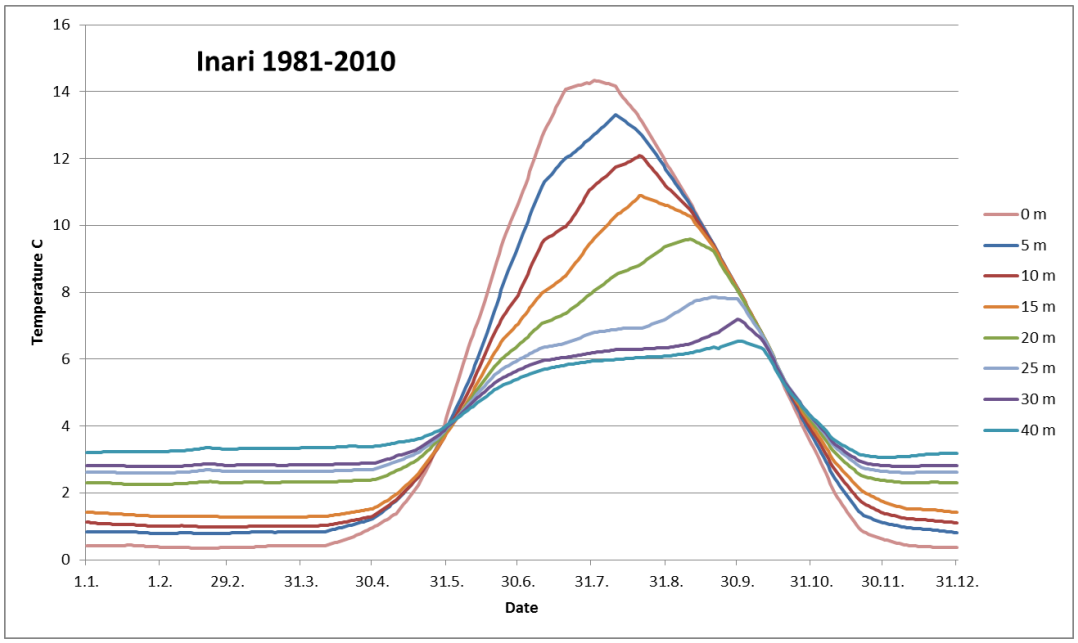

Figure 2: Average water temperature during the year at different depths in Lake Inari 1981–2010.

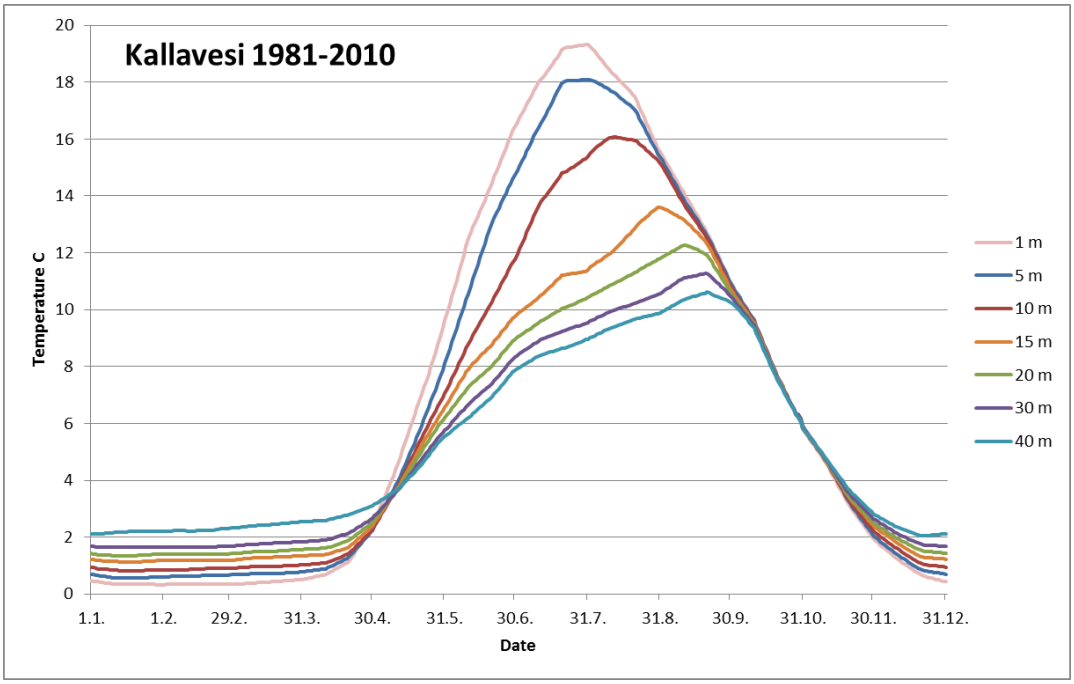

Figure 3: Average water temperature during the year at different depths in Lake Kallavesi 1981–2010.

3.2 Changes in Water Temperature at Different Depths during 1981–2010

Trends in monthly mean temperatures at different depths (near surface, 5 m, 10 m, 15 m, 20 m, 30 m, and 40 m, and near the bottom) and total water column were calculated.

For the annual mean of water column, no changes were found for Lake Kallavesi. The mean annual temperature for the water column in 1981–2010 was 5.8°C, varying from 4.5°C to 6.8°C. Monthly means of May and June have risen in Lake Kallavesi. The change in May and June was about +0.9°C during 30 years (+0.03°C/year). The mean annual temperature of water column in Inari was 4.4°C, varying from 3.7°C to 5.2°C. In Lake Inari, the mean annual water column temperature has risen +0.6°C during 30 years (+0.02°C/year). Monthly means of November have risen in Inari +0.9°C during 30 years (+0.03°C/year).

All statistically significant changes (Mann-Kendall, Sen slope <0.05) are presented in Table 1. In Lake Inari, the warming in late summer and autumn was observed in the surface layers (from the surface to 20 m). In Lake Inari, no changes in mean monthly temperatures were found between 20 m and the bottom. Also, in Lake Kallavesi, most of the changes have been observed in surface layers, not below 20 m. Early summer monthly temperatures have increased in the surface layers in Lake Kallavesi. In Lake Kallavesi, cooling of surface layers during the wintertime was also observed. This can be caused by delayed freezing and a longer cooling period during the autumn isothermal mixing. The magnitudes of changes were typically from 0.3°C to 1.0°C per decade.

Table 1: Statistically significant trends in water temperature profile in Lakes Kallavesi and Inari in 19812010.

Variable	Kallavesi	Inari
Mean annual water column temperature	no changes	+0.2 °C/decade (p<0.05)
Mean monthly temperature water column	May +0.4°C/decade (p<0.05) Jun +0.3°C/decade (p<0.05)	Nov +0.3°C/decade (p<0.05)
Mean monthly temperature near the surface	Jan −0.1°C/decade (p<0.01) Feb −0.1 °C/decade (p<0.001) Mar −0.1°C/decade (p<0.01) May +0.7°C/decade (p<0.05) Jul +1.1°C/decade (p<0.05) Aug +0.9°C/decade (p<0.01) Sep +0.4°C/decade (p<0.05)	May +0.3°C/decade (p<0.05) Aug +0.8°C/decade (p<0.01) Sep +0.4°C/decade (p<0.05)
Mean monthly temperature at 5 m	Jan −0.1°C/decade (p<0.05) Feb −0.2°C/decade (p<0.05) May +0.4°C/decade (p<0.05) Jul +0.8°C/decade (p<0.05) Aug +0.7°C/decade (p<0.05) Sep +0.4°C/decade (p<0.05)	Aug +0.9°C/decade (p<0.01) Sep +0.4°C/decade (p<0.05)
Mean monthly temperature at 10 m	May +0.4°C/decade (p<0.05) Jun +0.5°C/decade (p<0.05)	Aug +0.6°C/decade (p<0.05) Sep +0.4°C/decade (p<0.05) Nov +0.4°C/decade (p<0.05)
Mean monthly temperature at 15 m	May +0.4°C/decade (p<0.05) Jun +0.3°C/decade (p<0.05)	Sep +0.3°C/decade (p<0.05) Nov +0.5°C/decade (p<0.01)
Mean monthly temperature at 20 m	May +0.4°C/decade (p<0.05)	Nov +0.4°C/decade (p<0.05)
Mean monthly temperature at 30 m	no changes	no changes
Mean monthly temperature at 40 m	no changes	no changes
Mean monthly temperature at bottom (42-44m)	Feb −0.3°C/decade (p<0.05)	no changes

In Figures 4 and 5, mean monthly water column temperatures of different decades (1980s, 1990s, 2000s) are presented for both lakes. Changes between the 1980s and the 2000s are statistically significant in Lake Inari for August and November. In Lake Kallavesi, the changes between the 1990s and the 2000s for January–March are statistically significant ($p<0.05$).

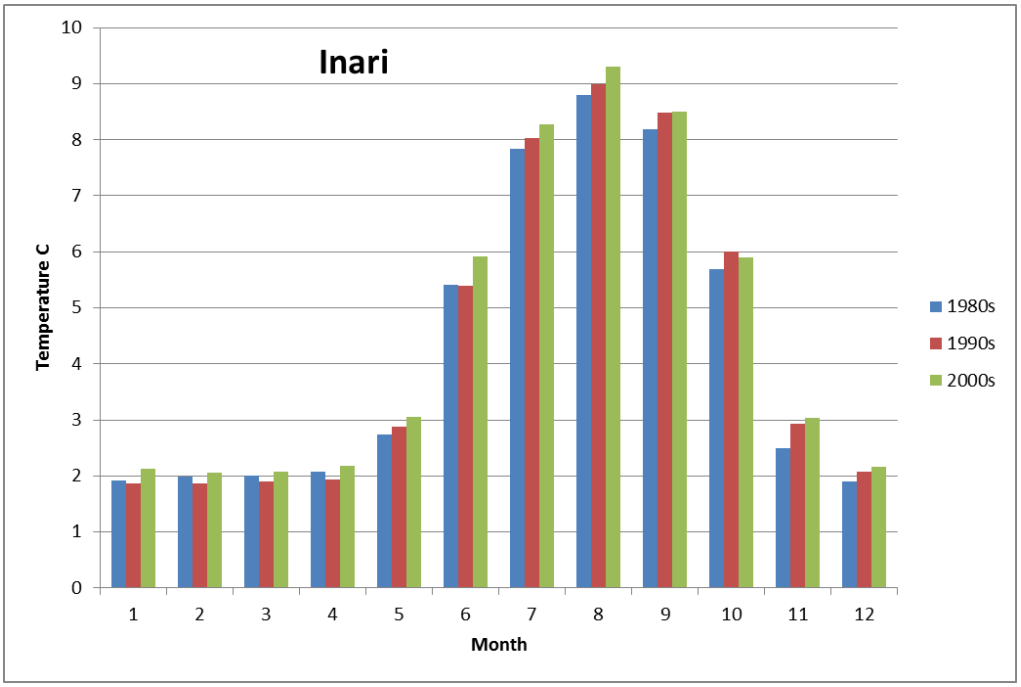

Figure 4: Mean monthly water column temperature in Inari during the 1980s, the 1990s, and the 2000s.

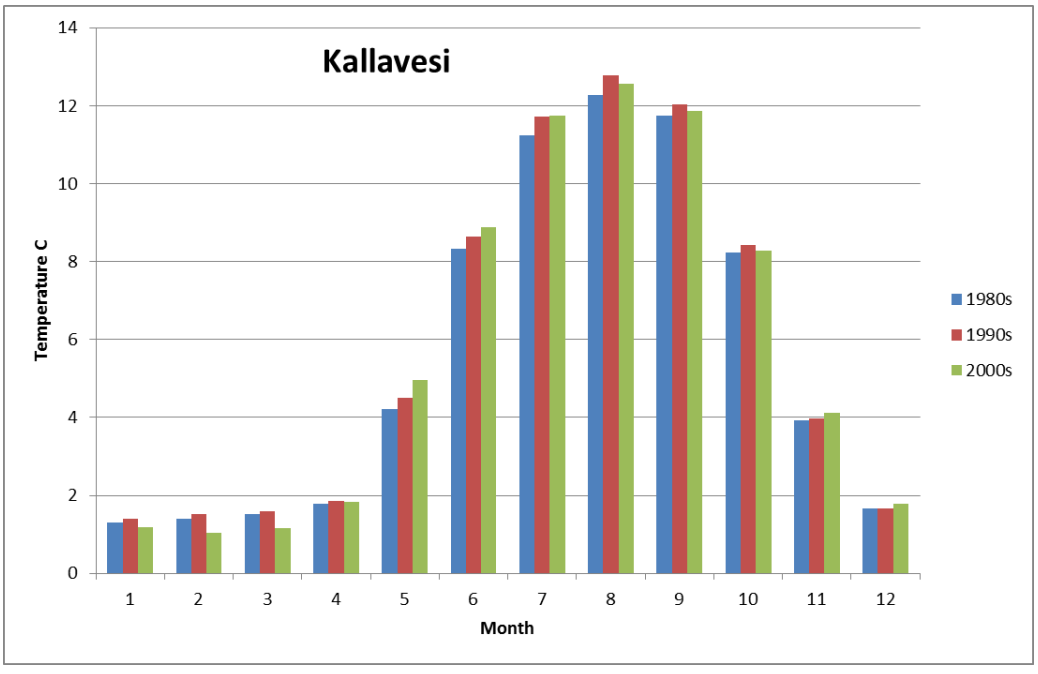

Figure 5: Mean monthly water column temperature in Kallavesi during the 1980s, the 1990s, and the 2000s.

3.3 Comparison with Changes in Ice Cover and Surface Water Temperature

3.3.1 Ice cover

During the period 1981–2010, no statistically significant trends were found for the maximum ice thickness for Lake Kallavesi or Lake Inari. In Lake Inari, changes in ice cover duration, ice break-up, or freeze-up dates were not statistically significant. In Lake Kallavesi, duration of ice cover had changed earlier (1 day per year, $p<0.05$) and the freeze-up later (0.8 day per year, $p<0.05$). Time series of freeze-up and break-up for Kallavesi and Inari are presented in Figures 6 and 7.

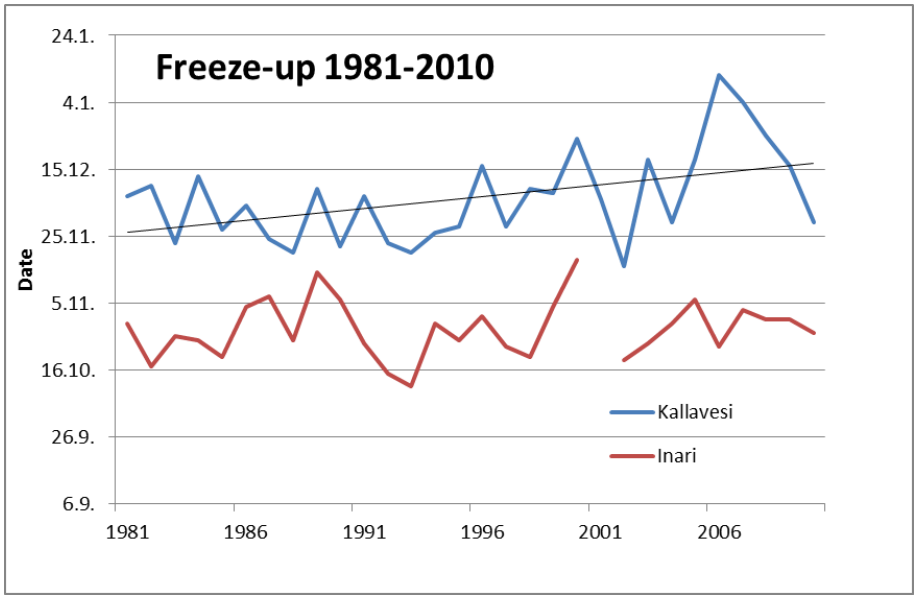

Figure 6: Lake ice freeze-up time series for Kallavesi and Inari in 1981–2010.

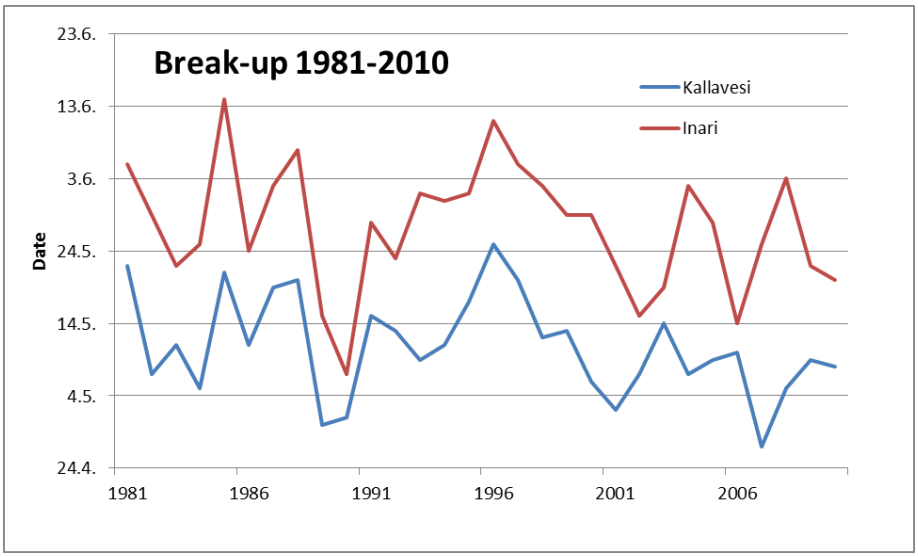

Figure 7: Lake ice break-up time series for Kallavesi and Inari in 1981–2010.

3.3.2 Surface water temperature near the shore

Both lakes have surface water temperature observation sites near the shore. The surface water temperature is measured daily in the morning during the open-water period. Trends for annual maximum, mean monthly (June, July, August), and number of days exceeding +10°C, +15°C, +18°C, and +20°C were calculated. For Lake Kallavesi, a statistically significant increase was found for August mean monthly temperature, and the number of days exceeding +10°C and +15°C. In Figure 8, mean monthly August surface water temperatures in 1981–2010 for both observation sites are presented. In Lake Inari, the same variables as in Lake Kallavesi have increased (August mean temperature and the number of days exceeding +10°C and +15°C) in the period of 1981–2010.

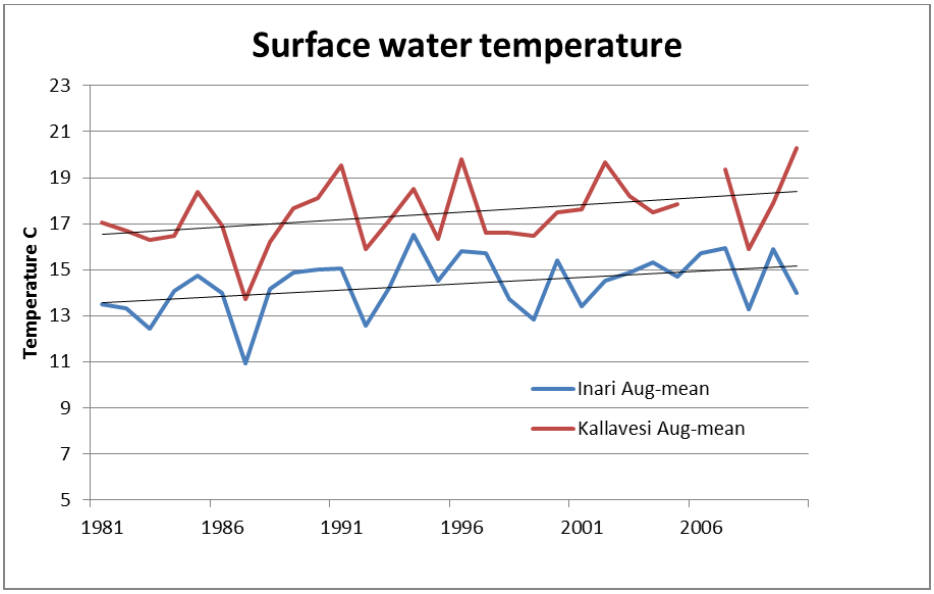

Figure 8: Mean August surface water temperature in Lakes Kallavesi and Inari in 1981–2010.

3.4 Correlation between Temperature Profiles and Ice Cover Time Series

The correlations with monthly mean water column temperatures and ice break-up and freeze-up were calculated. Trends of time series were eliminated before the Pearson correlation was calculated, in order to avoid correlation due to warming (anomaly to the mean). The ice break-up date correlated with May and June water column temperatures; early break-up resulted in higher water temperatures, naturally. The late autumn high water column temperatures correlated with late freeze-up. No other correlations were found. The correlation between break-up anomaly and anomaly of mean May water column temperature for Lake Kallavesi is shown in Figure 9.

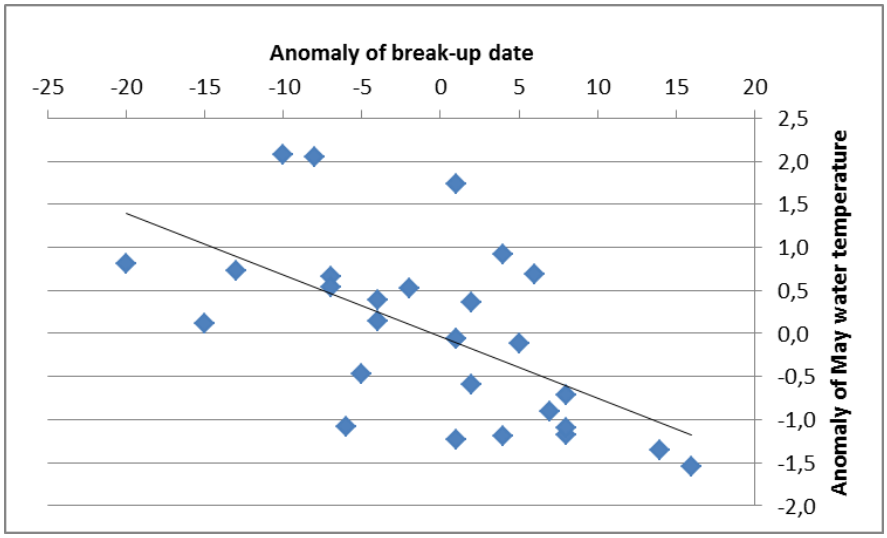

Figure 9: Correlation between anomaly of break-up date (difference between previous year) and anomaly of mean May water temperature (difference between previous year), Lake Kallavesi.

4. CONCLUSIONS

Lake water temperature profiles in 1981–2010 in two lakes (Kallavesi and Inari) in Finland were investigated in this study. The surface water maximum is usually observed in July, while near the bottom the maximum is much later in September. Some trends were detected for the water column mean temperatures (monthly) and monthly mean temperatures at different depths. Most of the changes have happened near the surface, not deeper than 20 m. In general, no trends were found for water temperatures near the bottom. In Lake Kallavesi, the spring and summer water temperatures have increased, and winter surface water temperatures have decreased. In Lake Inari, the water temperatures have increased in late summer and autumn. Typically, changes in water temperatures were 0.3°C to 1.0°C per decade, resulting in 1°C to 3°C increase in 30 years. Changes are in line with ice cover and surface water temperature (near the shore) changes in these lakes in the same time period.

REFERENCES

Kendall, M.G. 1975 *Rank Correlation Methods*. Charles Griffin, London.

Korhonen, J. 2006 Long-term changes in lake ice cover in Finland. *Nordic Hydrology* 37(4–5), 347–363.

Korhonen, J. 2002a Statistical analysis of water temperature observations in some Finnish lakes and rivers. In: Killingtveit, Å. (ed.), *XXII Nordic Hydrological Conference, Røros, Norway, 4–7 August.* Volume II. Røros, Nordic Association for Hydrology. NHP Report 47, 613–621.

Korhonen, J. 2002b Suomen vesistöjen lämpötilaolot 1900-luvulla. *The Finnish Environment 566.* 116 pp. (In Finnish, Summary in English: Water temperature conditions of lakes and rivers in Finland in the 20th century)

Korhonen, J. 2005 Suomen vesistöjen jääolot. *The Finnish Environment 751*. 145 pp. (In Finnish, Summary in English)

Mann, H.B. 1945 Nonparametric tests against trend. *Econometrica* 13, 245–259.

Salmi, T., Määttä, A., Anttila, P., Ruoho-Airola, T. & Amnell, T. 2002 Detecting trends of annual values of atmospheric pollutants by the Mann-Kendall test and Sen's slope estimate – The Excel template application MAKESENS. Finnish Meteorological Institute, Helsinki. *Publications on Air Quality* 31, 35 pp.

Sen, P.K. 1968 Estimates of the regression coefficient based on Kendall's tau. *Journal of the American Statistical Association* 63, 1379–1389.

Spatiotemporal Trends in Climatic Variables Affecting Streamflow across Western Canada from 1950–2010: A CROCWR Component

Hayley Linton[1*], Terry Prowse[1], Yonas Dibike[1], and Barrie Bonsal[2]

[1]*Department of Geography, University of Victoria/WCIRC, Victoria, BC, V8W 3R4, CANADA*
[2]*National Hydrology Research Centre, Saskatoon, SK, S7N 3H5, CANADA*
**Corresponding author's email: hayleylinton@gmail.com*

ABSTRACT
Changes to a watershed's hydrologic regime can affect local flora and fauna, but also human society in terms of agricultural productivity, municipal and industrial water supply as well as energy production. Understanding the ways climate change affects regional and continental scale water distribution is necessary for future water resources planning. A large portion of western Canada's water resources originates in mountainous regions where streamflow is driven by snow accumulation and melt, so any change to the climate of these regions can result in changes in runoff patterns. Understanding changes in runoff patterns depends upon understanding of the spatial and temporal changes in temperature, precipitation, snow accumulation, and snowmelt. Winter temperature increases indicate a shortening of the cold season, and decreases in winter precipitation indicate a reduced snowpack, which may contribute to smaller spring freshet peaks. Decreasing winter precipitation in the southern areas, along with precipitation increases during summer in the northern areas, indicates a possible northward shift of precipitation over time as well as a seasonal shift. This research is conducted as one portion of a larger hydroclimatic study titled Climatic Redistribution of Canadian Water Resources: Western Canada (CROCWR), which attempts to quantify redistribution of water resources across western Canada, including analysis of streamflow patterns in western Canadian and northern rivers and study of the synoptic patterns associated with climatic variability.

KEYWORDS
Climatology; hydrology; spatial analysis; trend analysis

1. INTRODUCTION
Climate change and variability can produce a variety of impacts on a watershed's hydrologic regime. Examining the linkages between hydrologic and climatic variables, such as temperature, precipitation, snow depth, and snowmelt, can also supply more information on why trends occur in river flow. Numerous changes have been linked to increasing air temperatures, including increasing atmospheric water vapour content and the resulting changes in precipitation patterns, snow cover reductions, melting of ice, and changes to runoff and soil moisture (Bates et al. 2008). Changes to regional water availability will affect many aspects of human society, from agricultural productivity and energy use to flood control, municipal and industrial water supply, and fisheries and wildlife management. A large portion of the river flow to the Canadian Arctic originates in the midlatitudes, some as mountain snowpack from the Northern Rocky Mountains. This freshwater inflow to the Arctic is an important factor in determining ocean convection in

the sub-Arctic seas, and any alteration to the Arctic or sub-Arctic hydrological cycle can lead to changes in the amount of freshwater reaching the Arctic Ocean, which may have implications for the global thermohaline circulation, Atlantic Ocean meridional overturning circulation, and thus global climate (Min et al. 2008; Holland et al. 2007). Much of the river flow in western Canada originates as mountain snowpack, particularly from the Northern Rocky Mountains, which form the headwaters of some of North America's largest river systems: the Mackenzie River, the Saskatchewan River, and the Columbia River (Pederson et al. 2011a, b). Climate variability and change are linked to the timing, volume, and extent of mountain snowpack and the associated snowmelt runoff; therefore, any changes in the extent and timing of snowpack and melt impact the volume and timing of snowmelt-dominated river flow on the continental to global scale (Stewart 2009). The spring freshet provides a significant contribution to annual streamflow of rivers originating in the Rocky Mountains and is comprised of a combination of snowmelt from accumulation of snow during winter and river ice breakup (Prowse et al. 2010). If mountain snowmelt and runoff occur earlier, it could result in a longer summer drought season and decreased summer and fall streamflow in dry regions, which may result in ecosystem stress due to lower flows and warmer stream and lake temperatures (Stewart 2009). Water is tremendously important for both society and nature, and understanding how a change in global climate could affect regional water supplies is essential for future water resources planning (Xu & Singh 2004; Kienzle et al. 2012).

This research aims to identify the temporal and spatial variations in hydroclimatic conditions across western Canada, including analysis of temporal trends and spatial variation both over time (from 1950–2010) as well as within the year. The study area for this research is western Canada. The study area is split into 32 watersheds, but these are amalgamated into 8 study regions for analysis (Figure 1). This study is part of a larger hydroclimatic study called Climatic Redistribution of Canadian Water Resources: Western Canada (CROCWR). The CROCWR project includes several hydroclimatic studies that attempt to explain the climatic redistribution of western Canadian water resources through analysis of streamflow patterns and trends in western Canadian rivers (Bawden et al. 2013), study of the synoptic patterns and teleconnections associated with climatic variability of the study area (Newton et al. 2013), and spatiotemporal analysis of climate variables affecting streamflow and water resource availability.

2. DATA AND METHODS

Watershed delineations were created based on a series of latitude-longitude points that correspond to hydrometric stations from Environment Canada's HYDAT database. ArcHydro was used to delineate the contributing areas for each hydrometric station. ArcHydro is an object-oriented model that is capable of establishing a topological network that includes flow direction, connectivity and upstream/downstream relationships of stream segments using a digital elevation model, a stream network, and points to distinguish watershed outlets (Fürst & Hörhan 2009). The ANUSPLIN-generated dataset used in this research covers the time period 1950–2010 and has a spatial resolution of 10 × 10 km, chosen for its high spatial resolution and temporal coverage (Hutchinson et al. 2009; McKenney et al. 2011). The dataset contains maximum and minimum temperature and precipitation, so snow accumulation and snowmelt were modeled using a temperature-index method. A temperature-index method was chosen due to data availability, the reliability of current data interpolation methods, and generally accurate model performance despite computational simplicity (Jost et al. 2012). Thin-plate trivariate splines are considered

superior to other common methods since they tend to produce the most accurate results (Xia et al. 2001). Due to varying topography and climatic regions in the study area, multiple snowmelt equations were employed in the snowmelt model. The simplified temperature-index equations used were taken from Maidment (1993), and vary based on atmospheric conditions, topography, geographical location, properties of the snow cover, and sometimes time of year. The equations utilize maximum and minimum temperature to calculate potential melt in millimeters, and then calculated values were compared to precipitation amounts to determine whether precipitation fell as rain or snow. Both snow accumulation and snowmelt are reported in millimeters of snow water equivalent.

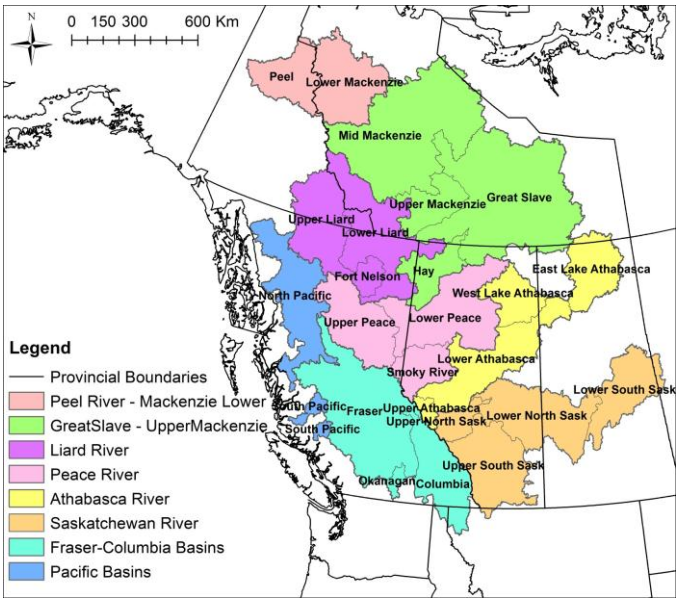

Figure 1: CROCWR study area with watersheds labeled by name and study regions identified by colour.

After calculating snow accumulation and snowmelt using the ANUSPLIN-generated dataset and degree-day snowpack model, pixel trajectory analysis was used to track temporal changes of each pixel through time, and map the results over the study area (Gralewicz et al. 2011). Trend analysis can be completed in a variety of ways, and digital change detection can be used to quantify temporal phenomena from multi-date imagery (Coppin et al. 2004). Each data point (10 × 10 km pixel) received a unique spatial and temporal identifier, and each point was analyzed individually for temporal trends. The Mann-Kendall (MK) test was used to calculate a trend value for each 10 × 10 km pixel; then the MK results were used to determine rate of change per decade (Mann 1945; Kendall 1975). Point surfaces of rate of change data were tested for spatial autocorrelation to determine hotspots of change, to provide better understanding of change patterns. Testing for positive autocorrelation can provide indications of clustering that deviates from the mean (Boots 2002). Spatial autocorrelation was tested using both Local and Global Moran's *I*, which indicate amount of significant clustering in the dataset and whether values are positively or negatively autocorrelated. The calculated values for both tests range from -1 to +1, and if the value is close to zero, there is very little spatial autocorrelation (Mitchell 2005). If the value is close to +1, it indicates clustering of similar values (positive autocorrelation), and if the value is close to -1, it indicates that nearby values are not similar (negative autocorrelation)

(Mitchell 2005). These tests are useful for determining hotspots of change, but not all areas that are significantly clustered contain statistically significant trend values.

For visual analysis, the point surfaces containing rate of change data were interpolated using inverse distance weighting (IDW). An IDW algorithm can interpolate data points on a grid into a continuous surface which can then be projected onto a two-dimensional Cartesian plane or base map (Dyer & Mote 2006). Inverse distance weighting is an exact interpolator used to create a surface where interpolated values are most influenced by the closest points, and less influenced by points farther away (O'Sullivan & Unwin 2010). Exact interpolation honours all data points so that the surface passes through all points of known value after interpolation is complete (Babish 2006). Interpolation methods, particularly simple methods like IDW, tend to work best and have the least error when used with datasets with even, dense sample distributions (Babish 2006). Parameters were chosen to minimize interaction between points, so that each pixel value would not be affected by neighbouring values. After interpolation, values with a significance level less than 10% were masked out of each raster dataset so that the only values remaining were significant. These values were then averaged by study region to obtain zonal means of rate of change for each month and each variable. All values stated in this paper are at the 10% significance level or better.

3. RESULTS AND DISCUSSION

3.1 Temperature

Maximum and minimum daily temperatures were averaged for the time period 1950–2010 across each of the 8 study regions, with maximum temperatures from -22.0°C to -5.0°C in the winter and 16.0°C to 24.0°C in the summer, and minimum temperatures from -32.0°C to -14.0°C in the winter and 5.0°C to 10.0°C in the summer. The greatest rates of change in maximum temperature occur during the winter months. January shows an increasing trend of 1.1°C/decade across the study area with a maximum of 1.9°C/decade occurring at higher elevations in the Upper Peace River and Peel River basins. February has experienced an increase of 0.7°C/decade across the study area, with a maximum of 2.3°C/decade at higher elevations of the Mackenzie River basin. January and February also show statistically significant clustering of values higher than the mean occurring in the Upper Peace, Upper Liard, Athabasca, and Peel River basins. April has also experienced a statistically significant increasing trend of 0.5°C/decade averaged across the study area, with a maximum of 1.0°C/decade in the Lower Liard and Lower Mackenzie River basins. These areas contain significant clustering of values higher than the mean. March shows statistically significant temperature increases of 0.5°C/ decade up to 1.3°C/decade in the Saskatchewan River basin. Global Moran's *I* values for all months exceed 0.94, indicating strong positive autocorrelation throughout the dataset. These values indicate warming throughout the spring months, potentially leading to an earlier melt season. Summer and autumn have experienced less warming than the remainder of the year. The majority of the trends in maximum temperature calculated for July, August, September, October, and November are not statistically significant. In most months, minimum temperature has experienced a greater rate of change than maximum temperature, particularly in January and February and in the more northern parts of the study area (Figure 2).

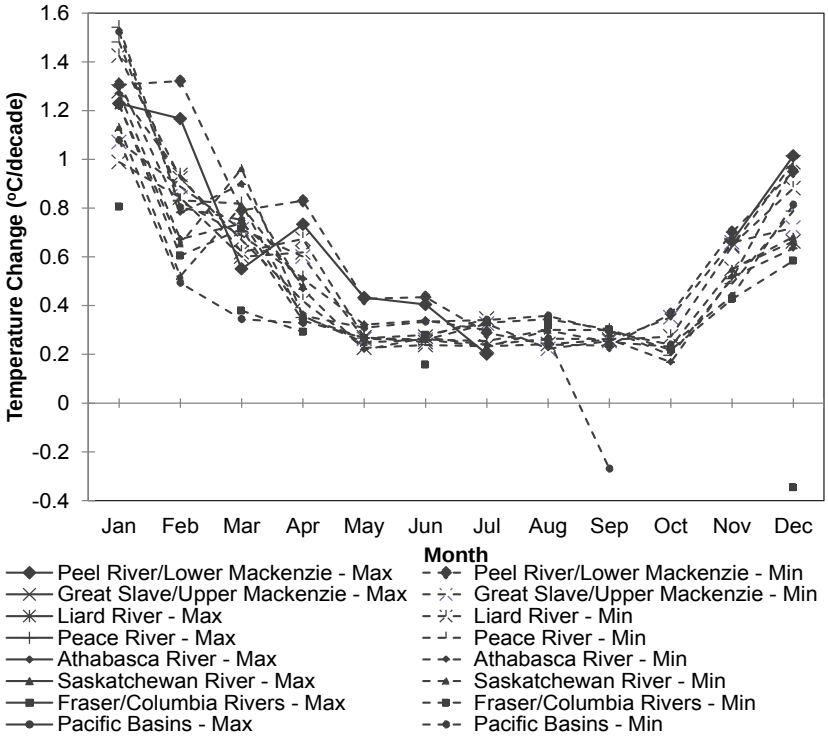

Figure 2: Rate of change for maximum and minimum daily average temperature. Results are statistically significant at 10% or better.

Minimum temperature has experienced statistically significant increases in most months, but the majority of temperature increases occur in the winter months. January and February have experienced increases of 1.3°C/decade and 0.8°C/decade averaged across the study area, with maximum rates of change of 3.3°C/decade and 2.4°C/decade, respectively (Figure 3). January shows statistically significant temperature increases across the entire study area, with the maximum values at higher elevations. February has experienced temperature increases across the northern half of the study area, with maximum values occurring at higher elevations. January and February also show statistically significant positive global autocorrelation across the study area as well as significant clustering of values higher than the mean in mountainous areas. Global Moran's *I* values for all months exceed 0.91, indicating strong autocorrelation throughout the year. Statistically significant temperature increases also occur throughout March and April, with most values between 0.8°C–1.0°C/decade across most of the study area. The increases in minimum temperature may contribute to an earlier melt season, but also may change the proportion of rainfall to snowfall in the study area. Summer and fall have experienced less warming than the remainder of the year. Many of the trends calculated for July, August, September, October, and November are not statistically significant.

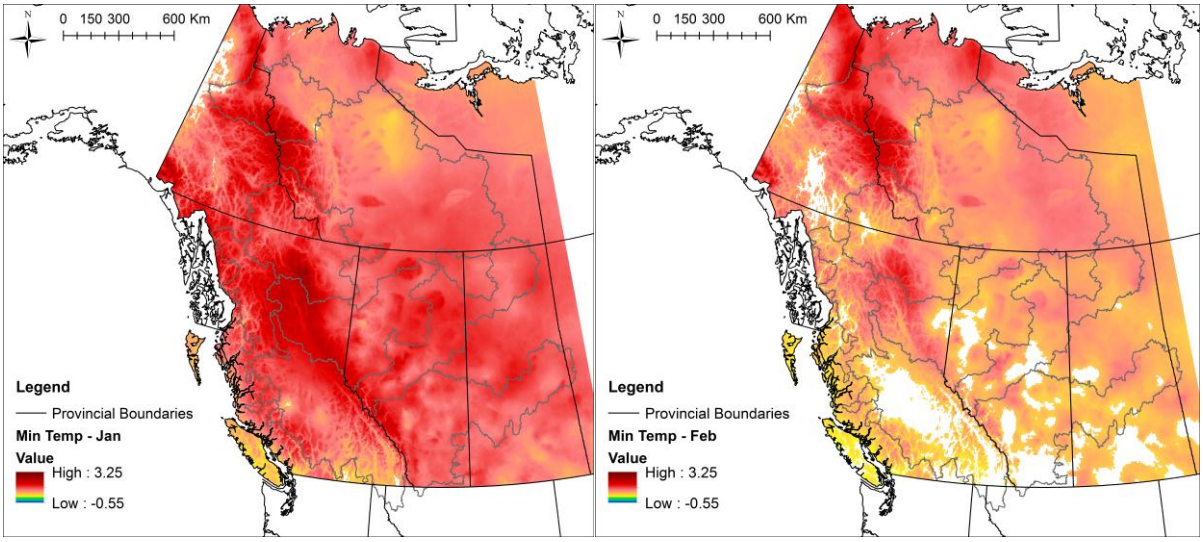

Figure 3: January (left) and February (right) minimum temperature trend results showing rate of change in °C/decade, from 1950–2010. Gray outlines show study region boundaries. Only trends significant at 10% or better are shown.

3.2 Precipitation

Precipitation patterns have experienced a combination of increasing and decreasing trends from 1950–2010 that are dependent on time of year and location (Figure 4). Summer precipitation has experienced statistically significant increases in the Upper and Lower Liard River basins and Fort Nelson area with rates of change up to 12.0 mm/decade. Spatial autocorrelation tests indicate statistically significant clustering of values higher than the mean in the Liard River region. Global Moran's *I* values range from 0.77 in January to 0.97 in July and August, indicating greater positive autocorrelation in the summer than in the winter. November precipitation has experienced decreases across most of the study area, with decreases of as much as -10 mm/decade in the Pacific region (Figure 5). December, January, and February have also experienced precipitation decreases across much of the study area, mostly in non-coastal regions, with values ranging from -1.5 to -2 mm/decade. This indicates that winter snowpack may be decreasing, particularly in prairie regions. In mountainous regions, particularly the Liard River basin, trend analysis shows that summer precipitation is increasing while winter precipitation is decreasing. This may lead to smaller snowpacks, a decreased spring freshet, and potentially higher streamflow during the summer months. The decreases in lower-latitude winter precipitation along with the increases in higher-latitude summer precipitation may indicate shifts toward precipitation occurring later in the year and more at higher elevations (Bawden et al. 2013).

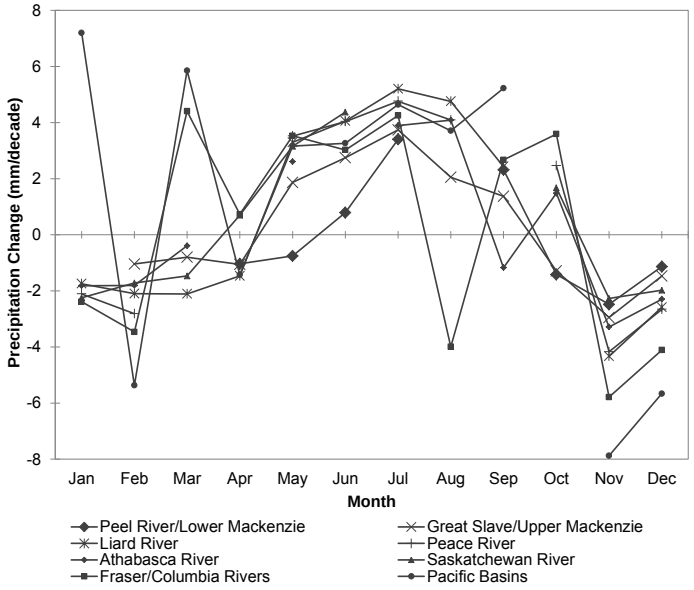

Figure 4: Rate of change of monthly total precipitation in mm/decade, from 1950–2010. Results are statistically significant at 10% or better.

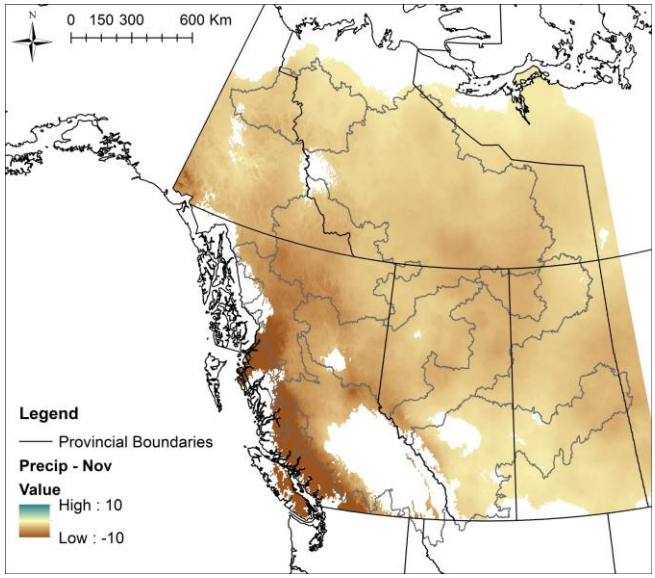

Figure 5: November precipitation trend results showing rate of change in mm/decade, from 1950–2010. Gray outlines show study region boundaries. Only trends significant at 10% or better are shown.

3.3 Snow Accumulation

Winter snow accumulation has experienced statistically significant decreases across most of the study area. November through April, snow accumulation has decreased by -1.5 to -2.5 mm/decade, particularly in the Liard, Peace, Athabasca, and Saskatchewan River basins

(Figure 6). The months of October through May show Global Moran's *I* values of 0.82–0.91, indicating strong spatial autocorrelation and clustering among calculated trends in these months. The Peel/Upper Mackenzie and Great Slave/Lower Mackenzie regions do not experience many decreasing trends except a trend of -2 mm/decade at higher elevations during April and May. These can likely be attributed to the decreasing precipitation trends identified in these areas. The largest decreases in snow accumulation are occurring during December, January, and February in coastal BC, with rates of change as low as -14.0 mm/decade. Reduced accumulation of snow in the winter months across much of the study area may lead to a decreased spring freshet. Small pockets of increasing trends have also been identified in the Fraser/Columbia region during November and March, despite most significant trends during these months being negative (Figure 7). These increasing trends range from 2.0–10.0 mm/decade at the highest elevations in the Rocky Mountains. Statistically significant precipitation increases in these areas during March, combined with increases in minimum temperature during these months may indicate a greater capacity for water vapor storage, thus increasing moisture content in the air, potentially leading to an increase in the accumulation of snow at these higher elevations.

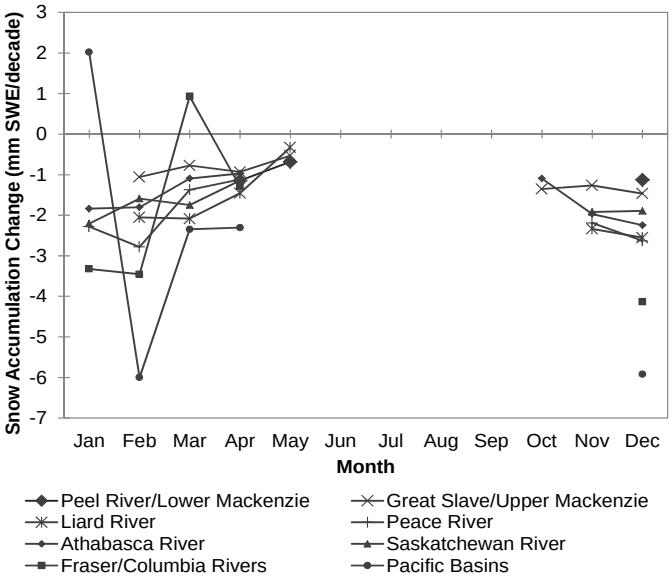

Figure 6: Rate of change of monthly snow accumulation in mm SWE/decade, from 1950–2010. Results are statistically significant at 10% or better.

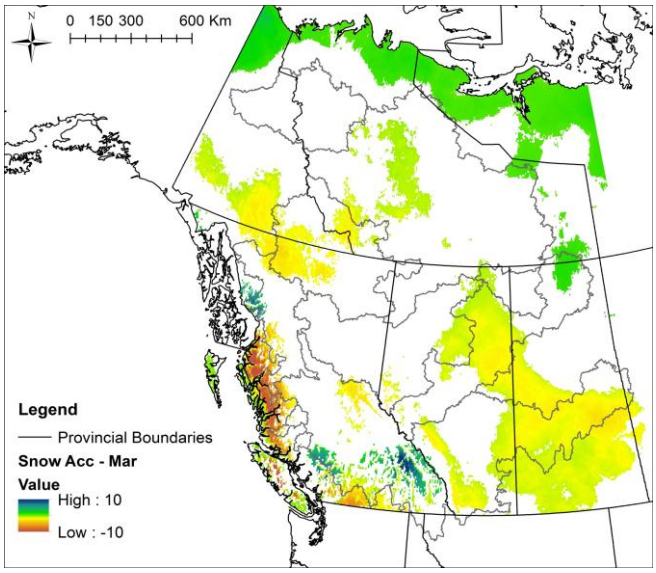

Figure 7: March snow accumulation trend results showing rate of change in mm SWE/decade, from 1950–2010. Gray outlines show study region boundaries. Only trends significant at 10% or better are shown.

3.4 Snowmelt

Snowmelt throughout the study area has experienced increasing trends January through April, with primarily decreasing trends occurring in May (Figure 8). The largest statistically significant snowmelt increases in March are located in the lower elevations of the Fraser/Columbia and Pacific regions, with average snowmelt increases of 1.5–3.0 mm SWE/decade, with maximum increases of as high as 22.0 mm SWE/decade. In April, some of the largest snowmelt increases occur in the Liard River basin, with an average increase of 6.4 mm SWE/decade. The Pacific region also shows significant snowmelt increases in April, with an average increase of 7.9 mm SWE/decade. These basins also experience significant spatial clustering. Areas of lower elevation in the Fraser/Columbia region experienced decreasing snowmelt during April, indicating that snowmelt in these areas is shifting earlier in the year, from April to March. May results indicate decreasing snowmelt in the Liard, Peace, Athabasca, and southern half of the Great Slave/Upper Mackenzie regions, with rates as low as -15.0 mm/decade. Areas that experienced significant increases in snowmelt during March and April also experienced significant decreases in snowmelt during May, with values as low as -32.0 mm/decade. Figure 9 displays areas experiencing snowmelt increases in April and snowmelt decreases in May, indicating that snowmelt is occurring earlier in the year, which is likely related to increased temperatures during these months, possibly resulting in an earlier onset of the spring freshet. The areas of higher elevation in the study area are also significantly clustered, indicating similar changes throughout this region. Increasing snowmelt in January in the Fraser and Okanagan basins, with increases between 2.0 and 3.0 mm/decade at the lower elevations, indicates an increase in mid-winter melt, which may contribute to decreased winter snowpack and a decreased spring freshet.

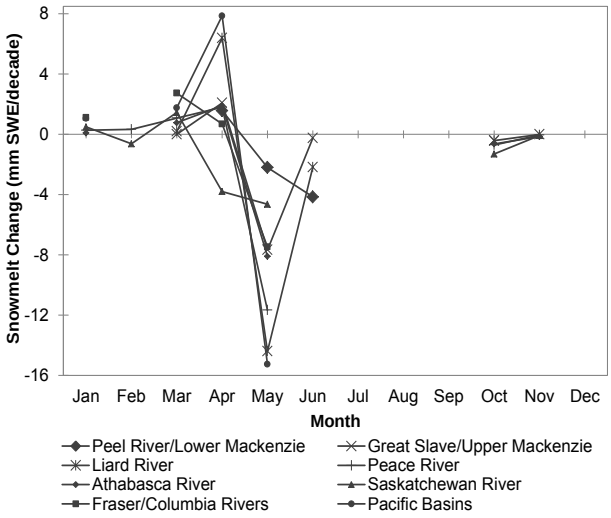

Figure 8: Rate of change of monthly total snowmelt in mm SWE/decade, from 1950–2010. Results are statistically significant at 10% or better.

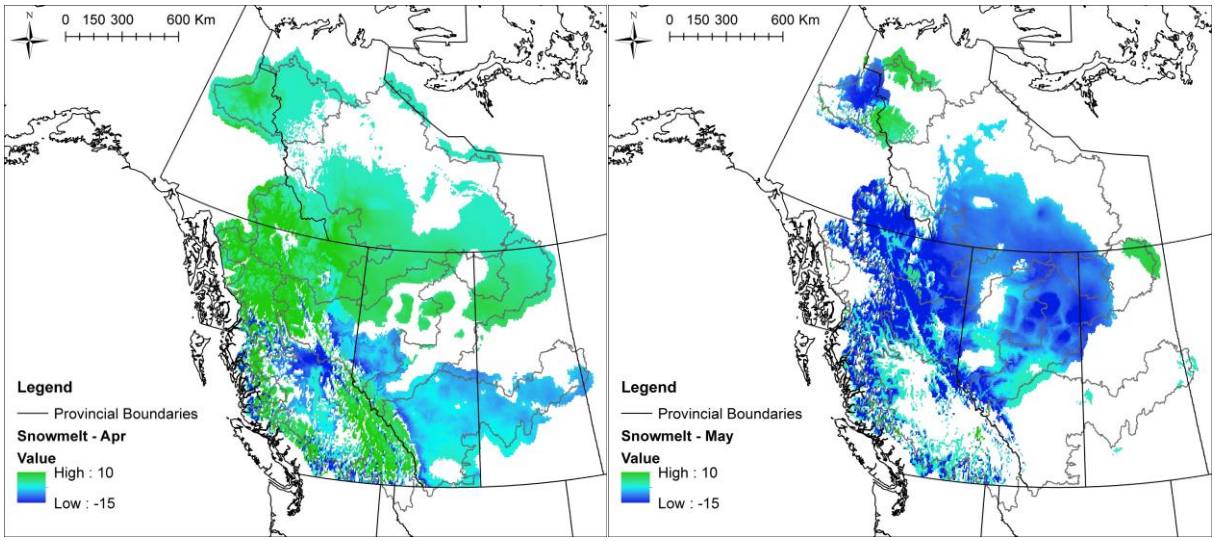

Figure 9: April (left) and May (right) snowmelt trend results showing rate of change in mm SWE/decade, from 1950–2010. Gray outlines show study region boundaries. Green indicates increasing snowmelt; blue indicates decreasing snowmelt. Only trends significant at 10% or better are shown.

4. CONCLUSION

Maximum and minimum temperatures appear to be increasing, particularly during the winter months, at northern latitudes, and at higher elevations. This may indicate that the cold season is becoming shorter in many parts of the study area. Increasing temperatures in the winter months

may also lead to more instances of mid-winter melt, particularly at more southern parts of the study area and at lower elevations. A shorter cold season will also lead to an earlier melt season and an earlier spring freshet. Spring freshets may also be decreased in volume due to higher instances of mid-winter melt and decreasing precipitation and snow accumulation during the winter months. The results also indicate a redistribution of precipitation toward summer months and northern latitudes. This may lead to increased summer streamflow at higher latitudes, with lower streamflow at lower latitudes due to a decrease in summer precipitation coupled with decreased winter snowpack that melts earlier in the year.

ACKNOWLEDGMENTS

H. Linton would like to thank her supervisory committee for the opportunity to work on this research project. The authors would like to acknowledge Natural Resources Canada for freely providing the data used in this project. Funding for this project is provided by Environment Canada and Natural Sciences and Engineering Research Council of Canada. A special thanks also to the CROCWWR team for their collaboration and assistance on this project.

REFERENCES

Babish, G. 2006 *Geostatistics Without Tears: A Practical Guide to Surface Interpolation, Geostatistics, Variograms, and Kriging.* Edition 2006.03. Environment Canada, Regina, SK, Canada.

Bates, B. et al. (eds.) 2008 Climate Change and Water: IPCC Technical Paper VI, Geneva: IPCC Secretariat.

Bawden, A.J., Burn, D.H. & Prowse, T.D. 2013 An analysis of spatial and temporal trends and patterns in western Canadian runoff: a CROCWR component. *Proc. of the Northern Research Basin Symposium, August 2013* (unpublished).

Boots, B. 2002 Local measures of spatial autocorrelation. *Ecoscience* 9(2), 168–176.

Coppin, P., Jonckheere, I., Nackaerts, K., Muys, B. & Lambin, E. 2004 Digital change detection methods in ecosystem monitoring: A review. *Int. J. Remote Sensing* 25(9), 1565–1596.

Dyer & Mote 2006 Spatial variability and trends in observed snow depth over North America. *Geophysical Research Letters* 33(16), 1–6.

Fürst, J. & Hörhan, T. 2009 Coding of watershed and river hierarchy to support GIS-based hydrological analyses at different scales. *Computers & Geosciences* 35(3), 688–696.

Gralewicz, N.J., Nelson, T.A. & Wulder, M.A. 2010 Spatial and temporal patterns of wildfire ignitions in Canada from 1980 to 2006. *Int. J. Wildland Fire,* doi: 10.1071/WF10095.

Holland, M., Finnis, J., Barrett, A. & Serreze, M. 2007 Projected changes in Arctic Ocean freshwater budgets. *Journal of Geophysical Research* 112.

Hutchinson, M.F. et al. 2009 Development and testing of Canada-wide interpolated spatial models of daily minimum-maximum temperature and precipitation for 1961–2003. *Journal of Applied Meteorology and Climatology* 48(4), 725–741.

Jost, G., Moore, R.D., Smith, R. & Gluns, D. 2012 Distributed temperature-index snowmelt modelling for forested catchments. *Journal of Hydrology* 420-421, 87–101.

Kendall, M.D. 1975 *Rank Correlation Measures*. Charles Griffin, London, UK.

Kienzle, S.W., Nemeth, M.W., Byrne, J.M. & MacDonald, R.J. 2012 Simulating the hydrological impacts of climate change in the upper North Saskatchewan River basin, Alberta, Canada. *Journal of Hydrology* 412, 76–89

Mann, H.B. 1945 Non-parametric tests against trend. *Econometrica* 13, 245–259.

Maidment, D.R. 1993 *Handbook of Hydrology*. McGraw-Hill, New York, USA.

McKenney, D. et al. 2011 Customized spatial climate models for North America. *Bulletin of the American Meteorological Society*, 1611–1622.

Min, S.-K., Zhang, X. & Zwiers, F. 2008 Human-induced Arctic moistening. *Science* 320(5875), 518–520.

Mitchell, A. 2005 *The ESRI Guide to GIS Analysis, Volume 2: Spatial Measurements & Statistics.* ESRI Press, Redlands, USA.

Newton, B.W., Prowse, T.D. & Bonsal, B.R. 2013 Synoptic climatological characteristics associated with water availability in western Canada: a CROCWR component. *Proc. of the Northern Research Basin Symposium, August 2013* (unpublished).

O'Sullivan, D. & Unwin, D.J. 2010 *Geographic Information Analysis*. 2nd ed. Wiley & Sons, Inc., Hoboken, NJ, USA.

Pederson, G.T., Gray, S.T. & Ault, T. 2011a Climatic controls on the snowmelt hydrology of the Northern Rocky Mountains. *Journal of Climate* 24(6), 1666–1687.

Pederson, G.T., Gray, S.T. & Woodhouse, C. 2011b The unusual nature of recent snowpack declines in the North American cordillera. *Science* 333, 332–335.

Prowse, T. Shrestha, R., Bonsal, B. & Dibike, Y. 2010 Changing spring air-temperature gradients along large northern rivers: Implications for severity of river-ice floods. *Geophysical Research Letters* 37(19), L19706.

Stewart, I.T. 2009 Changes in snowpack and snowmelt runoff for key mountain regions. *Hydrological Processes* 23, 78–94.

Xia, Y., Fabian, P., Winterhalter, M. & Zhao, M. 2001 Forest climatology: estimation and use of daily climatological data for Bavaria, Germany. *Agricultural and Forest Meteorology* 106(2), 87–103.

Scaling Runoff from Large to Small Catchments – Comparison of Theoretical Results with Measurements

Wolf-Dietrich Marchand* and Kjetil Vaskinn

Sweco Norge AS, Professor Brochs gate 2, 7030 Trondheim, NORWAY
**Corresponding author's email: wolf.marchand@sweco.no*

ABSTRACT
A large demand for renewable energy has directed focus on the planning of small hydropower plants. Such hydropower plants are usually located in small catchments without discharge measurements. In Norway, as in many other countries, most national stream gauging stations are located in relatively large catchments. A common solution for calculating the runoff from the power plant catchment is to find a gauged catchment with comparable characteristics (analogue catchment) and to scale the runoff series from the gauged catchment to the ungauged one. In most cases, this process means downscaling from a large catchment to a small catchment. To obtain environmentally friendly hydropower development, most power stations are licensed with a requirement for a certain environmental flow. If the power plant catchment is ungauged, this flow rate is usually calculated based on the scaled runoff series. Due to the difference in catchment size, and thus different runoff characteristics, the value for the environmental flow will often be higher compared with the values calculated based on data from flow measurements in the actual catchment. Measurement of the discharge will minimize the investment risk due to availability of more accurate values for average runoff, more correct runoff characteristics and environmental flow, as well as reduction of the risk for choosing a wrong analogue station. In the past ten years Sweco has collected runoff series in about 100 small catchments. A comparison of theoretically calculated values for runoff characteristics with that based on a selection of measurements is presented here.

KEYWORDS
Scaling runoff; ungauged catchments; environmental flow; small hydropower

1. INTRODUCTION
During the past decades, extensive development of small hydropower plants in Norway has taken place. Many of these plants are located in previously ungauged, small catchments. In order to estimate the expected power production and plan the turbine capacity, it is necessary to investigate the runoff from the catchment to the power plant. Both the amount of water and distribution over the year, the runoff regime, must be found.

The average annual runoff can be found from the official runoff map, which covers the whole country. However, the quoted accuracy of this map is ±25% (Beldring et al. 2002). Discharge measurements performed by Sweco indicate even more deviation between the real runoff and the map. Differences in the range of 30%–40% have been found at several locations.

A common method of estimating the runoff regime is to look for a gauged catchment in the area. The aim is to find an analogue station with similar characteristics, like catchments size, altitude, lake-percentage, etc., and to scale the runoff series from the gauged to the ungauged catchment.

Norway has a well-developed network of hydrological stations. However, the majority of the hydrological stations in the official network are located in large catchments. In most cases, the choice of the analogue station is a compromise between what is desirable and what is available. This means that it cannot be expected that the scaled runoff series represents the real runoff regime well in all cases.

The fact that both the estimated annual average runoff and the runoff regime are encumbered with significant uncertainty means that the hydrological basis for calculation of the estimated power production often is weak. To avoid unnecessary risk of a wrong decision in the investment phase, the Norwegian Water and Energy Directorate (NVE) is encouraging developers to perform their own discharge measurements in the river that is to be used for power production. Many professional investors follow that advice, and on behalf of them, Sweco has placed gauging stations in about 100 different locations (rivers) during the past ten years. Most of the stations are temporary, collecting data for a few years. A minimum of 2–3 years is recommended. Based on the collected data, the choice of the best analogue station can be supported and the runoff map can be verified. For verification of the runoff map, it is required to correct the measured short series for the amount of water in the measured years, whether they were wet or dry years, compared with a normal year. This is done by using the most representative analogue station in the area and comparing the runoff at that station in the respective years with the runoff in the normal period. The current normal period in Norway is 1961–1990. Also, the current valid runoff map refers to that period.

This study was performed to investigate possible differences when developing a power station just using runoff maps and analogue stations, compared with using additional measurements for the stream of interest. To do that, a selection of discharge measurements done by Sweco with a series of 3 to 8 years of data has been analyzed. The aim was both to find the differences and to illustrate how these results would affect a planned small hydropower plant.

2. METHODS

Important statistical variables of measured discharge series have been compared with those of measurements from analogue stations that had measurements in the same time period. The focus was on those variables that have an impact on the production of the power station.

One obviously important issue is the amount of flow. As a measure for that, the average flow from the actual measurements, scaled to the normal period, was compared with average runoff calculated from the runoff map.

Another major issue is the environmental flow. The environmental flow bypasses the power station. This means that the larger the environmental flow, the less power production there is. In Norway, typically the flow value Q_{95} (95% of the time the flow is larger than that value) is used as a basis for determining the environmental flow. It is common to differentiate between summer and winter season, to reflect natural variations. The mean values for $Q_{95,summer}$ and $Q_{95,winter}$ are calculated and used respectively as environmental flow summer and winter.

The impact on the suggested environmental flow, assumed to be Q95, was calculated by two different methods. The first method was based on scaling values from analogue catchments to the Sweco catchments. The second comparison regards a tool provided by the NVE: "Lavvann," which means low flow. This is an online Geographical Information System (GIS) tool. It calculates catchment statistics, as Q95, based on catchment characteristics and the official runoff

map 1961–1990. The latter period is the official actual "normal period" in Norway at the moment. The basics for the Lavvann tool are described in Hisdal (2005) and Væringstad & Hisdal (2005).

The described analyses were performed for 11 small catchments where Sweco had collected discharge data in connection with the development of small hydropower plants. The locations of the Sweco gauging stations, as well as their analogue NVE stations from the official countrywide hydrological network, are shown in Figure 1.

Figure 1: Overview of Norway with plotted locations of all gauging stations used.

Table 1 shows a list of all stations, the area of the measured catchment, the number of years used in the analysis, and the ratio of the area between the Sweco and their analogue stations.

Table 1: Overview of used gauging stations: Sweco stations and their corresponding analogue NVE stations.

Sweco station		Number of measured years	Analogue NVE station		Sweco to NVE area ratio
Station number	Area km^2		Station name	Area km^2	
1	5.3	7	Øye	138.4	26.3
2	5.6	3	Jordbrufjell	69.9	12.4
3	36.3	8	Storvatnet	48.0	1.3
4	172.7	4	Nervoll	653.4	3.8
5	9.8	8	Lavvatn	73.8	7.5
6	51.3	4	Krinsvatn	207.0	4.0
7	4.3	3	Lavvatn	73.8	17.2
8	24.1	4	Jordbrufjell	69.9	2.9
9	9.7	8	Lavvatn	73.8	7.6
10	28.4	3	Lavvatn	73.8	2.6

3. RESULTS AND DISCUSSION

As mentioned earlier, it is usually difficult to find analogue stations with a similar catchment size. This is also the case for most of the measured catchments. In all cases, the best analogue station in the area had a larger catchment than the measured one. The factor from measured to analogue is in the range 1.3 to 26.3, as shown in Table 1.

The results of the analysis of the available amount of water, the mean runoff, are shown in Table 2. The mean discharge of the analogue stations from short measurement period was scaled to the long period (equal to the "normal period" 1961–1990) for compensation of eventual dry or wet short measurement periods. The ratio from short to long period of the respective analogue NVE stations was used for scaling of the Sweco stations.

Table 2: Conversion of short-term mean runoff to long-term mean runoff for the "normal period" 1961 to 1990.

Sweco Station number	Sweco station short Qmean	NVE station short Qmean	NVE station long, 61-90 Qmean	factor short to long periode	Sweco station long, 61-90 Qmean	runoff map 61-90 Qmean	Difference runoff map to "measured"
	m3/s	m3/s	m3/s		m3/s	m3/s	%
1	0.491	9.69	8.467	0.873	0.429	0.521	-18
2	0.582	2.55	2.476	0.971	0.565	0.586	-4
3	3.553	5.20	5.721	1.100	3.908	3.755	4
4	8.008	32.54	27.889 [1]	0.857	6.864	7.687	-11
5	1.051	5.74	5.645 [2]	0.984	1.035	1.136	-9
6	3.160	12.41	12.523	1.009	3.189	3.048	5
7	0.361	5.03	5.645 [2]	1.122	0.406	0.353	15
8	0.744	2.95	2.476	0.841	0.626	1.239	-50
9	0.974	5.74	5.645 [2]	0.984	0.959	1.083	-11
10	3.672	6.07	5.645 [2]	0.930	3.415	2.396	43

[1] series starts at 1968, [2] series starts at 1964

Most of the NVE series covered the whole "normal period," except Nervoll, which started in 1968, and Lavvatn, which started in 1964. However, all stations were used equally. It was

assumed that the missing years, respectively 7 and 3 years in a 30-year period, will not change the average discharge value much. The calculated long-term mean values are compared with that found from the runoff map for the period 1961–1990.

The results show deviations from the runoff map from -50% to +43%. However, many of the stations had deviations in the range of ±11%. Three stations are in an acceptable range, within ±5%. Four stations are in the range of the quoted accuracy of the runoff map, ±25%. Two stations with deviations of -50% and +43% are far beyond the quoted accuracy.

Based on the series from Sweco and NVE, both measured in the same time period, values for Q95 were calculated. The results are presented in Table 3. The scaling factors from the analogue stations to the Sweco stations are shown in the same table. The factors are based on annual mean discharge for the whole period and measurements from both stations.

Table 3: Measured values for Q95 from Sweco stations and analogue NVE stations.

Measured runoff from Sweco station							Measured runoff from analogue NVE station							Scaling factor
Station number	Summer		Winter		Year		Station name	Summer		Winter		Year		
	Qmean	Q95	Qmean	Q95	Qmean	Q95		Qmean	Q95	Qmean	Q95	Qmean	Q95	based on
	m^3/s	m^3/s	m^3/s	m^3/s	m^3/s	m^3/s		m^3/s	m^3/s	m^3/s	m^3/s	m^3/s	m^3/s	Qmean,year
1	0.68	0.12	0.34	0.03	**0.49**	0.05	Øye	14.76	4.46	5.77	1.02	**9.69**	1.15	**0.051**
2	1.03	0.24	0.26	0.05	**0.58**	0.05	Jordbrufjell	4.10	0.47	1.20	0.21	**2.55**	0.27	**0.228**
3	5.14	0.29	2.25	0.12	**3.55**	0.14	Storvatnet	6.99	0.74	3.88	0.30	**5.20**	0.36	**0.683**
4	14.27	1.97	3.28	0.89	**8.01**	1.05	Nervoll	55.37	10.40	9.55	2.53	**32.54**	3.07	**0.246**
5	1.38	0.04	0.78	0.02	**1.05**	0.02	Lavvatn	7.72	0.35	4.28	0.24	**5.74**	0.26	**0.183**
6	2.29	0.08	3.88	0.28	**3.16**	0.13	Krinsvatn	9.52	0.31	14.80	1.47	**12.41**	0.64	**0.255**
7	0.62	0.08	0.18	0.01	**0.36**	0.01	Lavvatn	6.78	0.35	3.79	0.24	**5.03**	0.26	**0.072**
8	1.14	0.05	0.44	0.05	**0.74**	0.05	Jordbrufjell	4.96	0.54	1.38	0.23	**2.95**	0.28	**0.253**
9	1.68	0.20	0.45	0.06	**0.97**	0.06	Lavvatn	7.72	0.35	4.28	0.24	**5.74**	0.26	**0.170**
10	5.72	0.37	2.21	0.21	**3.67**	0.23	Lavvatn	8.44	0.29	4.46	0.33	**6.07**	0.32	**0.605**

The factors in Table 3 were used to scale the Q95 values from the analogue NVE stations to the Sweco stations. The scaled Q95 values are compared with the ones that were measured at the Sweco stations. This comparison is shown in Table 4, both for absolute values and as a percentage. The results indicate that the Q95 values from the analogue stations are larger than the ones from the Sweco stations for most catchments. The deviations are largest for seasonal values, in the range of -70% to +150% for the summer season and -31% to +165% for the winter season. Annual Q95 deviations range from -28% to 110%.

The next comparison regarding the NVE Lavvann tool is presented in Table 5. In many catchments, the Q95 calculated by Lavvann is lower (max -98%) than measured Q95 values. However, for a few catchments, the Lavvann values are much higher than the measured values, ranging up to 419%.

Table 4: Q95 differences between measured and scaled values.

Station number	Measurement Sweco station			Runoff from analogue NVE station scaled to Sweco station*					
	Summer	Winter	Year	Summer		Winter		Year	
	Q95	Q95	Q95	Diff.	Q95	Diff.	Q95	Diff.	Q95
	m3/s	m^3/s	m3/s	%	m^3/s	%	m^3/s	%	m^3/s
1	0.121	0.031	**0.046**	87	0.226	68	0.052	25	**0.058**
2	0.244	0.050	**0.050**	-56	0.107	-4	0.048	23	**0.062**
3	0.291	0.122	**0.138**	74	0.507	68	0.205	78	**0.246**
4	1.970	0.890	**1.050**	30	2.560	-30	0.623	-28	**0.756**
5	0.042	0.017	**0.023**	52	0.064	165	0.045	105	**0.048**
6	0.081	0.282	**0.126**	-3	0.079	33	0.374	30	**0.163**
7	0.080	0.007	**0.009**	-69	0.025	141	0.017	110	**0.019**
8	0.054	0.051	**0.053**	150	0.136	13	0.058	35	**0.071**
9	0.199	0.060	**0.060**	-70	0.059	-31	0.041	-27	**0.044**
10	0.372	0.213	**0.232**	-53	0.173	-7	0.199	-17	**0.193**
			average =	**14**		**44**		**36**	

* scaling factor based Sweco measurements and analogue station

Table 5: Q95 difference between measured values and results from NVE Lavvann.

Station number	Measurement Sweco station			Calculated with "NVE Lavvann" tool for Sweco station catchment*					
	Summer	Winter	Year	Summer		Winter		Year	
	Q95	Q95	Q95	Diff.	Q95	Diff.	Q95	Diff. Q95	Q95
	m3/s	m^3/s	m3/s	%	m^3/s	%	m^3/s	%	m^3/s
1	0.121	0.031	**0.046**	-4	0.116	-38	0.019	-59	**0.019**
2	0.244	0.050	**0.050**	-70	0.074	-98	0.001	-96	**0.002**
3	0.291	0.122	**0.138**	57	0.456	-5	0.116	7	**0.148**
4	1.970	0.890	**1.050**	-49	1.010	-62	0.338	-60	**0.416**
5	0.042	0.017	**0.023**	36	0.057	419	0.088	343	**0.103**
6	0.081	0.282	**0.126**	251	0.285	-31	0.194	69	**0.213**
7	0.080	0.007	**0.009**	-75	0.020	10	0.008	10	**0.010**
8	0.054	0.051	**0.053**	215	0.171	197	0.153	245	**0.182**
9	0.199	0.060	**0.060**	-22	0.155	-49	0.031	-36	**0.039**
10	0.372	0.213	**0.232**	45	0.541	-24	0.163	-1	**0.230**
			average =	**57**		**57**		**72**	

* The "NVE lavvann" tool calculation uses the official runoff map (1961-1990) and physical catchment parameters

4. CONCLUSIONS

The analysis of the available amount of water (mean annual runoff) shows that approximately half of the catchments have 9% to 50% less runoff than predicted by the runoff map. This is significant when considering if a hydropower plant is beneficial or not. At one of the stations, measured values indicate surplus water of 43%, which means that the installed turbine capacity would be much too low.

The Q95 is dependent on the runoff regime. It can be expected that large catchments with even runoff have higher Q95 values than small catchments with more dynamic runoff. This is verified by the findings in this study. More than half of the stations have much higher Q95 values scaled from the larger analogue catchments compared with the measured Q95 values. The deviation for

stations, where the scaled value is below the measured one, is much less. But since all the analogue catchments are larger than the measured ones, it is obvious that other catchment characteristics are influencing the results. Characteristics like lake-percentage, mean elevation, and gradient are not investigated here.

For most of the analyzed stations, the NVE Lavvann tool gives lower values for Q95, compared with measured values. However, deviations where Lavvann gives higher values are much larger than for the low values. Since the Lavvann tool is based on the runoff period 1961–1990 and the measured values are more up to date, it is difficult to make clear conclusions. The effect of higher values measured during the past years might be an effect of climate change. There is a general trend of more precipitation in the analyzed regions (Førland et al. 2000; Wilson et al. 2010; Lawrence & Hisdal 2011)

In general, the results from the analysis show that there is large uncertainty in the hydrological basis for planning of small hydropower stations. For half of the analyzed catchments, the power plant would get wrong installed capacity estimates, and the hydropower plant would probably not be beneficial at all. In many cases, the lower water amount and the too high environmental flow would superimpose and make the situation even worse.

One drawback in the analysis is that the "normal period" of data collection from 1961–1990 is too far in the past. NVE is currently working on a method to update the map more frequently. This analysis covered only 10% of the discharge series measured by Sweco. More series will be analyzed in the future. While time goes by, more long series will be available and a wider analysis with an updated runoff map could be done. It would also be of interest to apply some of the results of the presented work to some case project power plants.

ACKNOWLEDGMENTS

The author would like to thank the companies that own the rights for the discharge series, collected by Sweco, and that agreed to the use of the data series in this research study. These companies are Småkraft AS, Helgelandskraft AS, Selbu Energiverk, and Sjøfossen Energi. Further, the valuable help of all persons involved in the data collection is acknowledged. The students Irina and Ekaterina are accredited for help with data preparation. Another thank you is directed to the Norwegian Water and Energy directorate for the good work on collecting nationwide hydrological data and publishing runoff maps together with valuable analysis tools on the Internet.

REFERENCES

Beldring, S., Roald, L.A. & Voksø, A. 2002 *Runoff map for Norway* (in Norwegian). NVE report 2-2002. ISSN 1501-2840, Oslo, Norway.

Førland E., Roald L.A., Tveito O.E. & Hanssen-Bauer I. 2000 *Past and Future Variations in Climate and Runoff in Norway.* DNMI report no. 19/00 KLIMA, Norwegian Meteorological Institute, Oslo, Norway. Available online: http://www.nve.no/Global/Vann%20og%20vassdrag/Effekter%20av%20klimaendringer/pilolar4.pdf, 30 June 2013.

Hisdal H. 2005 *Regional Methods for Estimating Low Flow Characteristics* (in Norwegian). NVE report 7-2005. ISSN 1502-234X, Oslo, Norway, Available online: http://webby.nve.no/publikasjoner/rapport_miljoebasert_vannfoering/2005/miljoebasert2005_07.pdf, 30 June 2013.

Lawrence D. & Hisdal H. 2011 *Hydrological Projections for Floods in Norway Under a Future Climate*. NVE report 5-2011. ISSN 1502-3540, Oslo, Norway.

Væringstad T. & Hisdal H. 2005 *Estimation of Common Low Flow in Ungauged Catchments* (in Norwegian). NVE report 7-2005, ISSN 1502-234X, Oslo, Norway, Available online: http://webby.nve.no/publikasjoner/rapport_miljoebasert_vannfoering/2005/miljoebasert2005_06.pdf, 30 June 2013.

Wilson D., Hisdal H. & Lawrence D. 2010 Has streamflow changed in the Nordic countries? Recent trends and comparisons to hydrological projections. *Journal of Hydrology* 394(3–4), 26 November 2010, 334–346.

Sediment Transport to the Kangerlussuaq Fjord, West Greenland

Andreas Bech Mikkelsen[1,2*] and Bent Hasholt[1]

[1]*Department of Geosciences and Natural Resource Management, University of Copenhagen, Copenhagen, 1350, DENMARK*
[2]*Center for Permafrost, University of Copenhagen, Copenhagen, DENMARK*
**Corresponding author's email: abm@geo.ku.dk*

ABSTRACT
Sediment transport has been continuously monitored near the outlet of Watson River since 2007. Other major outlets to the Kangerlussuaq Fjord, measured during field campaigns in 2010, 2011, and 2012, focused on discharge and sediment concentration. The contribution from the ungauged subcatchments and the total amount of sediment delivered to the Kangerlussuaq Fjord is calculated, based on calculated sediment delivery and information from earlier investigations. The total annual load of sediment delivered to the fjord is approximately 30 million tons, corresponding to ~920 t km^{-2} y^{-1}.

KEYWORDS
Sediment transport; sediment; glacial erosion; Greenland; Kangerlussuaq

1. INTRODUCTION
Glacial erosion is one of the most powerful geomorphological agents (Hallet et al. 1996; Koppes & Montgomery 2009). Large parts of the landscapes in the circumpolar countries in North America, Europe, and Russia are formed by glacial erosion and the transportation and deposition of sediment originating from glacial erosion (Encyclopedia of Quaternary Science 2007). Interpretation of the layers of deposited sediment in lakes, fjords, and oceans has been used to evaluate the location and intensity of previous glacial activity (e.g., Gilbert 2000; Overeem & Syvitski 2010). Transport of ice rafted deposits (IRD) in the bottom sediments has been used as indication of calving glaciers. However, the validity of the interpretations heavily depends upon sufficient knowledge of the pathway of the sediment and the location of sinks between the source and the sediment deposit that is interpreted. Greenland is a major contributor of sediment to the adjoining ocean (Hasholt et al. 2005). The Greenland Ice Sheet (GrIS) and the surrounding ice-free margin provide opportunities to study land-forming processes similar to the conditions in the circumpolar countries during the Weichselian glaciation. Fjords are important parts of the marine coastal system, and they act both as transfer routes of the sediment and as sinks. The aim of this investigation is to locate sources of sediment and measure the output of sediment from different sources in a catchment draining to the fjord.

2. STUDY AREA
The mouth of the Kangerlussuaq Fjord is at the west coast of Greenland (Figure 1). The fjord is approximately 170 km long and 1 to 6 km wide. The outer part of the fjord is quite shallow, with depths of 30 to 50 m (Danish Nautical Charts). The inner part of the fjord consists of a 70 km long basin with depths up to nearly 300 m and mostly about 4 km wide. Well-developed deltas

are located at the outlet of Watson River, Umivit, and Sarfartoq. The tidal range varies temporarily from 2 to 4 m and causes tidal currents up to several meters per second in the shallow and narrow outer parts of the fjord (Nielsen et al. 2010).

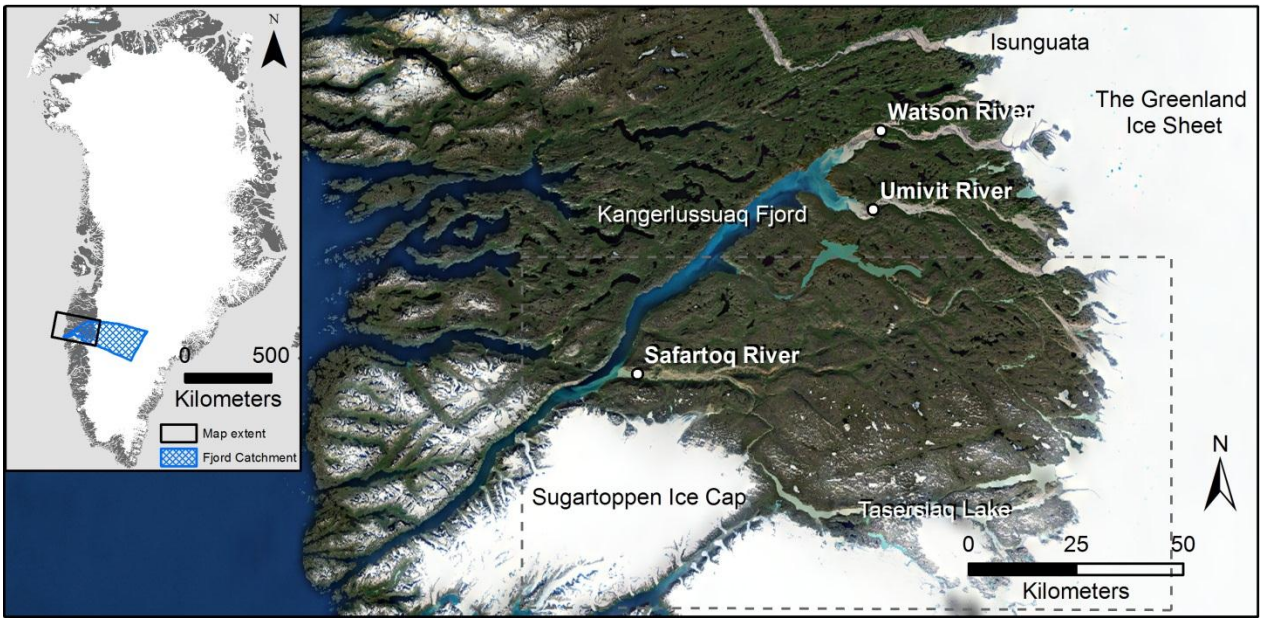

Figure 1: Insert top left is a map of Greenland with the location of the map extent for the main map marked with a rectangle and the catchment to the Kangerlussuaq Fjord shown with crossed pattern. On the main map, the monitoring sites and Kangerlussuaq Fjord are shown using a composite of Landsat images. The dashed grey rectangle corresponds to the extent of Figure 3.

During the Weichselian glaciations, the GrIS reached the present coastline. At 11,500 BP, the Taserqat stadium, the ice margin was located about 30 to 40 km from the mouth of the fjord, and through the next 2,300 years, the margin retreated to a location approximately 10 to 15 km upstream of Watson River—the Mt. Keglen stadium. Today the GrIS margin is located approximately 30 km further to the east. In the outer part of the fjord, the postglacial isostatic uplift is 140 m, while it is 40 to 50 m at the innermost part of the fjord (Ten Brink et al. 1974).

The drainage area of the fjord is 32,070 km^2 (Figure 1). Starting from the mouth north of the fjord, the drainage divide follows the direction of the fjord at a distance of approximately 5 km until the inner basin, where its distance increases up to 15 km, until the margin of the GrIS between Isunguata and Sandflugtsdalen. The divide is not well determined on the GrIS because of the very gentle slope. To the east, the basin is delimited by the main divide between the east and west coast of Greenland. The drainage divide south of the fjord extends 100 km from the fjord, and to the west it is located partly on the Sukkertoppen Ice Cap. It is observed that the drainage basin is asymmetric relative to the fjord so that a major part of the ice-free area drains to the southern coast of the fjord.

The geology of the area is characterized by an archaic block to the southeast, mainly gneiss and a zone of gneisses deformed by the Nagsugtoqidian orogeny closer to the fjord (Henriksen 2005). To the west, the present landscape is alpine with elevations up to more than 1000 m with local glaciers and the Sukkertoppen Ice Cap. To the east, the landscape is more gently undulating with elevations up to 600 m. The larger valleys including the fjord are carved by glacial erosion. Between the large valleys, the surface is covered by an abundance of lakes. To the west, the

vegetation is alpine. More abundant vegetation is found to the east. In the valleys, lush vegetation of dwarf brush and Salix is found, and more meager heath and grass vegetation is found on the hills.

Strong climatic gradients are observed in the drainage basin. To the west, a coastal oceanic zone is approximately 50 km wide. The average monthly temperature ranges from -13°C to +8°C, and the precipitation ranges from 600 mm to more than 1000 mm. The area between the coastal zone and the GrIS is continental with monthly temperatures ranging from -18°C to +11°C and precipitation that ranges from below 200 mm up to 400 mm. The GrIS has its own much colder climate and higher precipitation than the continental zone due to orography (Hasholt & Søgaard 1978).

The rivers are glacio-nival or nival according to Parde´ (in Beckinsale 1971); they are often frozen from October/November until April/May. Maximum discharge is recorded from June to August. Jökulhlaups occur in these glaciated areas (e.g., Russell et al 2011; Mikkelsen et al. 2013).

3. METHODS

3.1 Field Measurements

The sediment transport monitoring station (Figure 2) is located on a rock sill approximately 10 km east of the present delta of Watson River 10 m a.s.l. Discharge is determined through the runoff season by measuring the cross-section area and the corresponding average velocity. Discharge measurements have been used to construct a stage/discharge relationship, where data from a water level logger have been used to construct a continuous discharge record. Manual and automatic pump water samples are used for construction of concentration/discharge relationships or for calibration of turbidity sensors (Hasholt et al. 2012). When functioning, the calibrated readings from the turbidity sensors are used as a continuous record of sediment concentration. The discharge and sediment concentration at the outlet of Sarfartoq and Umivit were measured once a year in 2010, 2011, and 2012, when the locations were visited by boat from Kangerlussuaq. Discharge was measured by determining the cross-section area with an echo sounder and a GPS. The boat was used as a float, and the surface velocities were measured with a GPS at representative locations covering the entire cross sections measured. Surface velocities were converted to mean velocity by multiplying a factor 0.85. The sediment concentration was sampled both with a depth integrating water sampler and at the surface. The surface sample represents the wash load, while the near-bottom sample represents suspended load. Bed load is not measured.

Figure 2: The monitoring station at Watson River: 1. sensors (Solitech 10, OBS3+); 2. automatic pump sampler (ISCO); 3. datalogger box; 4. radar water level (Ott).

3.2 Calculation of Sediment Transport

Sediment transport from Watson River is calculated by multiplying the instantaneous discharge with the corresponding sediment concentration and summing for the whole period with discharge. The accuracy on a single sediment transport calculation is ±25%, while the accuracy on annual average is ±15%. A detailed description of the calculation procedures is found in Hasholt et al. (2012). At Umivit and Sarfartoq, the sediment transport at the time of measurement is found by multiplying the sediment concentration with the simultaneous discharge. The calculated transport is divided by the simultaneous transport from Watson River to determine the contribution from this source relative to the contribution from Watson River. It is assumed that the proportion is constant through time each year. The annual contribution is then found by multiplying the total seasonal output from Watson River with the proportion from each location. The sediment transport is divided by the area of the contributing drainage area to calculate the sediment delivery. The estimated accuracy by this procedure is ±30%.

From the determination of the total area draining to the fjord, we find that approximately 17% of the drainage basin has not been monitored. Areas of subcatchments are taken from Weidick and Olesen (1978); however, in this publication only subcatchments with a well-defined stream are included (Figure 3). Areas bordering the fjord are not included. Their drainage divides against other subcatchments are determined, and their areas are determined with a planimeter. The output of sediment to the fjord is calculated with a procedure for erosion prediction in ungauged basins described in Hasholt (2003). A sediment delivery rate (t km^{-2} y^{-1}) for each area is estimated based on experience from results found in areas with similar lithology, relief, glacier cover, sinks, and vegetation cover. The delivery rate from each area is multiplied by the area of the drainage basin.

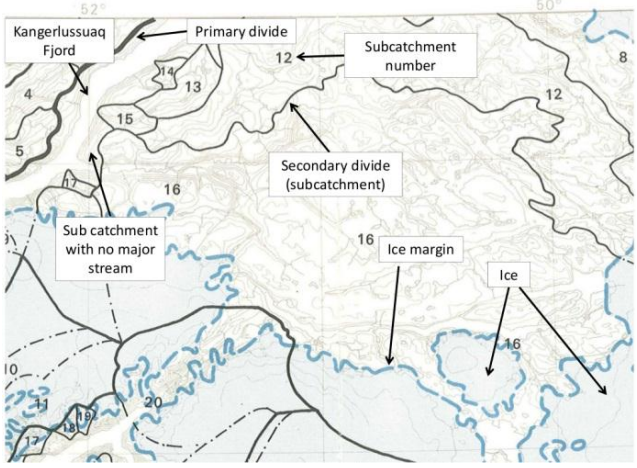

Figure 3: Map of subcatchments and areas without major streams draining to the fjord. Example from Weidick and Olesen (1978).

The actual output to the fjord is found by reducing the estimated delivery, depending on runoff, valley slope, sinks, and distance of major sediment sources from the fjord. By application of the method in gauged basins, the estimates based on the method were within ±50%–100% of measured sediment delivery.

4. RESULTS

The sediment output at the gauging station in Watson River is shown for each year in Table 1, and the seasonal variations of sediment transport are shown in Figure 4 for the two years with, respectively, minimum and maximum annual sediment transport. During five of the six years of observation (2007, 2008, 2010, 2011, and 2012), jökulhlaups occurred. These are not part of the normal seasonal variation, and delivered less than 2% of the total annual sediment transport in the years 2007, 2008, and 2010 (Mikkelsen et al. 2013) and even less in 2011 and 2012.

Table 1: Annual sediment transport in Watson River 2007–2012.

	Total annual sediment transport in Watson River ($t \times 10^6$)	**Max measured transport rate in Watson River ($t\ s^{-1}$)**	**Date for max. measured transport rate**
2007	7.1	3.6	31-08-07
2008	5.2	1.3	31-07-08
2009	4.8	1.6	16-07-09
2010	11.9	3.7	29-07-10
2011	10.0	3.5	17-07-11
2012	18.7	8.2	11-07-12

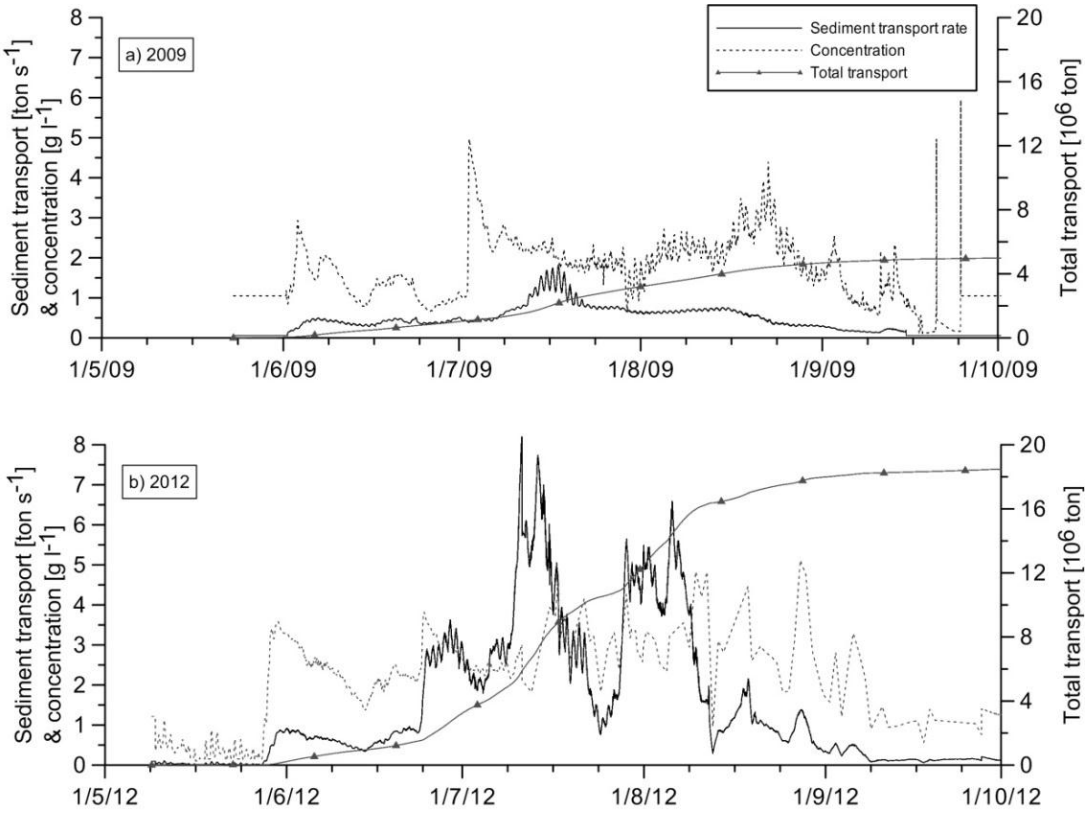

Figure 4: Examples of the measured sediment transport in Watson River.

In Table 2, the results from the subcatchments are shown together with total transport of sediment to the fjord. The calculated annual total amount of sediment delivered to the fjord is approximately 30 million tons. Hereof 87% is delivered to the deep inner basin of the fjord, and 13% to the shallow outer fjord. The three major sources—Watson, Umivit, and Sarfartoq—deliver 97% of the total transport to the fjord. Watson River and Umivit deliver 99% of the sediment to the inner basin. Sarfartoq delivers 78% of the sediment to the outer fjord, while the local glaciers and the southern coast deliver 20%, and only 2% originates from the northern coast.

Table 2: Sediment delivery to Kangerlussuaq fjord. Note that Watson River is not categorized under the north or the south coast.

	Area	**Share of total area**	**Average transport**	**Share of total trans-port**	**Min. total transport**	**Min. of total**	**Max. total transport**	**Max. of total**	**Average specific sediment transport**
	km^2	**%**	**$t\ y^{-1}$**	**%**	**$t\ y^{-1}$**	**%**	**$t\ y^{-1}$**	**%**	**$t\ km^2\ y^{-1}$**
North coast outer - no streams	207	0.6	72422	0.2	41384	0.3	103460	0.2	350
North coast inner - with streams	173	0.5	1733	0.0	1733*	0.0*	1733*	0.0*	10
North coast inner - no streams	193	0.6	19261	0.1	19261*	0.1*	19261*	0.1*	100
Watson River	**8059**	**25.1**	**9620000**	32.5	**4800000**	33.2	**18660000**	33.4	**1194**
South coast inner - no streams	261	0.8	19588	0.1	13059	0.1	26117	0.0	75
South coast inner - with streams	3308	10.3	54592.5	0.2	37641	0.3	71544	0.1	17
Umivit	**9814**	**30.6**	**16000000**	54.1	**8000000**	55.3	**31000000**	55.5	**1630**
Sarfartoq	**8879**	**27.7**	**3000000**	10.1	**1000000**	6.9	**5000000**	9.0	**338**
South coast outer - no streams	252	0.8	188632.5	0.6	125755	0.9	251510	0.5	750
South coast outer - with streams	925	2.9	589202.5	2.0	461471	3.2	716934	1.3	637
Total	**32070**	**100**	**29565432**	100	**14479310**	100	**55829565**	100	**922**
North coast total	573	1.8	93416	0.3					163
South coast total	23438	73.1	19852016	67.1					847

Although we know from the determination of the subcatchment areas that the three major sources only cover 83% of the total catchment area of the fjord, they deliver 97% of the total amount of sediment. They all originate from the GrIS, and their sediment originates primarily from glacial erosion. Sarfartoq delivers substantially less sediment per square kilometer, because a large amount of the sediment from the GrIS is trapped in the large Lake Tasersiaq. Sukkertoppen Ice Cap and local glaciers are the main sources of sediment to the outer fjord. The delivery of sediment to this fjord is strongly asymmetric; nearly all sediment is delivered from Watson River and sources located at the south coast. The contribution from ice-free areas is very

small; in particular, the contribution from the dry inner areas around the inner part of the fjord is low.

The character of the sediment that reaches the fjord depends on the location and size of sinks between the glaciated source area and the fjord. Watson River has sinks in the form of minor lakes close to the margin of the GrIS and 25–40 km long outwash plains in the valley bottoms. Similar conditions are found at Umivit. Therefore, the sediment that reaches the fjord is mainly silt and sand and a minor contribution of ice rafted material delivered in spring and autumn. At Sarfartoq, all coarse sediment from the GrIS is trapped in the large Lake Tasersiaq. The coarser sediments deposited in the delta here originate from the Sukkertoppen Ice Cap and local glaciers. The local glaciers along the outer part of the fjord can deliver coarse sediment directly into the fjord, as demonstrated by the location of terminal moraines at the coast of the fjord. No glaciers calve into the fjord.

5. DISCUSSION

Earlier measurements of sediment concentration are few. In mid-August of 1884, 0.118 g l^{-1} was recorded in Watson River and 0.77 g l^{-1} in Umivit by Jensen (1889) (in Weidick & Olesen 1978). In late July 1958, two measurements from Watson River were 1.470 and 1.510 g l^{-1} (Bauer et al. 1968b in Weidick & Olesen 1978). In 1976, measurements of concentration were made at several locations in the nonglaciated catchments; all were below 0.025 g l^{-1} (Hasholt & Søgaard 1978). Considering the large short-time variation in measured concentration, ±25%, the earlier results correspond reasonably well with results from the present investigation.

Covering such a large area with sediment transport monitoring stations is both economically and logistically impossible. To calculate total sediment output, therefore, it has been necessary to assume proportionality between the transport at Watson River and the outlets at Umivit and Sarfartoq. While the conditions at Umivit are quite similar to Watson River, it could be argued that the conditions at Sarfartoq are too different because of the trapping of sediment in Lake Tasersiaq and the moister climate nearer to the coast. However, as the discharge mainly originates from melting of ice driven by temperature, it is reasonable to assume similar runoff conditions most of the time at all glacier locations. Problems may occur if the point sampling is carried out during a jökulhlaup or a major rainstorm. This has not been the case; therefore, the assumption of proportionality is considered valid. The method for calculation of the sediment output applied from Hasholt (2003) could also be criticized; however, investigations from catchments on Disko Island further north in Greenland (Rasch et al. 2003) confirm that there is a strong correlation between output of sediment and glaciated area and that the steepness of the terrain influences the sediment delivery. In lack of other methods, the applied method is considered adequate.

It is seen from Watson River in Table 1 that sediment transport varies substantially from year to year; such information is not available from the other sources. The range in results from other sources in Table 2 is caused mainly from differences in the delivery estimates in the method from Hasholt (2003). Another problem is how much of the total load of sediment that is actually included in the monitoring and the calculation of the sediment transport. It is argued in Hasholt et al. (2012) that almost the total amount of sediment passing the monitoring station is monitored because all sediment finer than gravel size is brought in suspension, except a minor amount of bed load (<2%) during spring and fall, where the current velocities are too low to suspend it. This bed load cannot be monitored, and a contribution of 2% should be added to obtain the

"true" total load. Wash load is the fine suspended sediment that travels long distances and practically never settles at the bottom. At Umivit and Sarfartoq, the water samples taken in the water column represent wash load, suspended load, and suspended bed load (normally termed just suspended load). The water samples taken at the surface represent the wash load. The bed load cannot be measured here either. To get the "true" total load here, the unknown bed load must be added. From Hasholt (1976), the bed load in a proglacial river was found to be 20%–30% of the total load. From Turowski et al. (2010), it is seen that this percentage is realistic, but it is also stated that the determination of the proportion of bed load of total load is subject to large uncertainties. The total load at Umivit and Sarfartoq indicated here consists of a part calculated as above plus a theoretically based contribution of bed load. Concerning the overall uncertainty on the estimates from Umivit and Sarfartoq, the "missing" bed load has not been included in Table 2. This could be justified by the fact that bed load is mostly deposited in the delta areas before it reaches the fjord. However, if Table 2 is supposed to indicate the amount of sediment that goes "into" the fjord, then logically the unmeasured bed load from Watson River should be subtracted from Table 1, because it will be deposited in the delta area. This has not been done, implicating that the total load is slightly overestimated. Larger grain sizes may reach the fjord imbedded in ice (IRD); this can take place mainly during spring breakup and to a minor degree in the beginning of the freeze-up period, when ice frozen to the banks is released because of short thaw periods. There are no calving glaciers in this fjord now, but there may have been earlier. Ice rafted deposits are not measured.

It is shown that the three major sources—Watson River, Umivit, and Sarfartoq—deliver 97% of the total load, although their share of the total drainage area is only 83%. This emphasizes the importance of glacial erosion, in particular underneath the GrIS. The accurate catchment areas of rivers draining the GrIS will first be available when the topography underneath the ice is known. Catchment areas from Weidick and Olesen (1978) not including parts of the GrIS are considered accurate and are used in our calculations. However, areas of drainage basins including larger segments of the GrIS may be less accurate in Weidick and Olesen (1978). In Hasholt et al. (2012), we found a catchment area of 9743 km^2 for Watson River compared with 8059 km^2 found by Weidick and Olesen (1978). The difference is caused by the uncertainty in the determination of the drainage divide on the Greenland Ice Sheet, which recently has become less due to access to satellite-based altitude information. In Table 2, the Watson River specific sediment transport based on the area from Weidick and Olesen (1978) is 1194 t km^{-2} y^{-1}, while it is 987 t km^{-2} y^{-1} based on the area in Hasholt et al. (2012). See Hasholt et al. (2012) for further discussion of the problems with catchment delineation.

6. CONCLUSIONS

The average annual total load to the fjord is approximately 30 million tons. Three sources, Watson River, Umivit, and Sarfartoq, deliver 97% of the transported sediment. It is clearly demonstrated that the recent input of sediment to the fjord mainly originates from glacial erosion. The contribution of sediment from ice-free areas is very low, in particular from the dry zone along the innermost part of the fjord: less than 1%.

During the observation period, the contribution of sediment from catastrophic events (jökulhlaups and landslides) was very low, <2% of the annual transport in Watson River, where jökulhlaups have occurred. The sediment that reaches the fjord consists mainly of silt and clay

fractions and of sand deposited in the deltas. Larger grain sizes may reach the fjord as IRD during spring and fall. Contribution of IRD from calving is not found here.

The measured average annual amount of sediment delivered to the fjord from Watson River is 9.62×10^6 t, or 33% of the total transport. During the observation period, the output varied from 4.8×10^6 to 18.7×10^6 t. If the total annual sediment transport (29.6×10^6 t) is related to the entire catchment area (32,070 km^2), the average annual sediment delivery is 923 t km^{-2} y^{-1}.

ACKNOWLEDGMENTS

Our colleagues A. Kroon and T.J. Andersen are thanked for fruitful discussions of the manuscript. The project is supported by KVUG grant nos. 07-015998, 09-064628, and 2138-08-0003 and by FNU grant no. 272-07-0645. Further thanks for support from the Greenland Analogue Project (GAP) program, the Department of Geosciences and Nature Resource Management and the Center for Permafrost – CENPERM DNRF no. 100, funded by the Danish National Research Foundation.

REFERENCES

Beckinsale, R. 1971 *Introduction to Physical Hydrology*. Methuen & CO LTD, London. ISBN 416 68810 1.

Gilbert, R. 2000 Environmental assessment from the sedimentary record of high-latitude fiords. *Geomorphology* 32, 295–314.

Danish Nautical Charts number 1411, 1412, and 1413.

Hallet, B., Hunter, L. & Bogen, J. 1996 Rates of erosion and sediment evacuation by glaciers: A review of field data and their implications. *Global and Planetary Change* 12(1–4), 213–235.

Hasholt, B. 1976 Hydrology and transport of material in the Sermilik Area 1972. *Geografisk Tidsskrift* 75, 30–39.

Hasholt, B. 2003 Method for estimation of the delivery of sediments and solutes from Greenland to the ocean. Erosion prediction in ungauged basins: Integrating methods and techniques. *International Association of Hydrological Sciences (IAHS)* 279, 84–92.

Hasholt, B. & Søgaard, H. 1978 Et forsoeg paa en klimatologisk-hydrologisk beskrivelse af Holsteinsborg Kommune (Sisimiut). *Geografisk Tidsskrift-Danish Journal of Geography* 77, 72–92.

Hasholt, B., Bobrovitskaya, N., Bogen, J., McNamara, J., Mernild, S.H., Milburn, D. & Walling, D.E. 2006 Sediment transport to the Arctic Ocean and adjoining cold oceans. *Nordic Hydrology* 37(4–5), 413–432.

Hasholt, B., Mikkelsen, A.B., Nielsen, M.H. & Larsen, M.A.D. 2012 Observations of runoff and sediment and dissolved loads from the Greenland Ice Sheet at Kangerlussuaq, West Greenland, 2007 to 2010. *Zeitschrift fur Geomorphologie*.

Henriksen, N. 2005. *Grønlands geologiske udvikling. Geological Survey of Denmark and Greenland (GEUS)*, Copenhagen. 87-7871-163-0.

Koppes, M.N. & Montgomery, D.R. 2009 The relative efficacy of fluvial and glacial erosion over modern to orogenic timescales. *Nature Geoscience* 2, 644–647.

Mikkelsen, A.B., Hasholt, B., Knudsen, N.T. & Nielsen, M.H. 2013 Jökulhlaups and sediment transport in Watson River, Kangerlussuaq, West Greenland. *Hydrology Research* 44(1), 58–67.

Nielsen, M.H., Erbs-Hansen, D.R. & Knudsen, K.L. 2010 Water masses in Kangerlussuaq, a large fjord in West Greenland: The processes of formation and the associated foraminiferal fauna. *Polar Research* 29, 159–175.

Overeem, I. & Syvitski, J.P.M. 2010 Experimental exploration of the stratigraphy of fjords fed by glaciofluvial systems. *Geological Society, London, Special Publications* 344, 125–142.

Rasch, M., Nielsen, N., Christiansen, C., Balstrøm, T., Gilbert, R. & Desloges, J.R. 2003 Role of landscape parameters in riverine run-off and sediment and organic matter yeild on Disko Island, West Greenland. *Danish Journal of Geography* 103, 1–11.

Russell, A., Carrivick, L., Ingeman-Nielsen, T., Yde, J. & Williams, M. 2011 A new cycle of jökulhlaups at Russel Glaicier, Kangerlussuaq, West Greenland. *Journal of Glaciology* 57(202), 238–246.

Scott 2007 *Encyclopedia of Quaternary Science*.

Ten Brink, N. 1974 Glacio-isostasy: New data from West Greenland and geophysical implications. *Geological Society of America Bulletin* 85, 219–228.

Turowski, J.M., Rickenmann, D. & Dadson, S.J. 2010 The partitioning of the total sediment load of a river into suspended load and bedload: a review of empirical data. *Sedimentology* 57(4), 1126–1146.

Weidick, A. & Olesen, O. 1978 Hydrologiske bassiner i Vestgrønland. 1–160.

Synoptic Climatological Characteristics Associated with Water Availability in Western Canada: A CROCWR Component

Brandi W. Newton[1*], Terry D. Prowse[1], and Barrie R. Bonsal[2]

[1]*Water and Climate Impacts Research Centre, Environment Canada and University of Victoria, Victoria, BC, V8W 3R4, CANADA*
[2]*National Hydrology Research Centre, Environment Canada, Saskatoon, SK, S7N 3H5, CANADA*
**Corresponding author's email: bwnewton@uvic.ca*

ABSTRACT
Minor changes to seasonal temperature and precipitation regimes can result in substantial changes to the availability of water resources within large watersheds. To quantify the climatic redistribution of western Canadian water resources (CROCWR), a suite of atmospheric, hydroclimatic, and streamflow data is evaluated for spatial and temporal patterns and trends. This component of the CROCWR project focuses on the atmospheric drivers of climatic conditions in the watersheds originating on the leeward slopes of the Rocky Mountains. Dominant winter (Nov–Apr) and summer (May–Oct) synoptic-scale mid-tropospheric circulation patterns for 1950–2010 are classified using self-organizing maps. High-resolution gridded temperature and precipitation anomalies are calculated for each synoptic type, and clear patterns of above or below average temperature and precipitation emerge, including those patterns indicating a north–south gradient. Results indicate that the strength and position of a high-pressure ridge over the Pacific Ocean is associated with anomalously cool, wet conditions over the study region, while a high-pressure ridge over the continent, coupled with a low-pressure trough over the North Pacific Ocean, is associated with anomalously warm, dry conditions. Analysis of seasonal synoptic type frequencies and changes in frequencies over time are indicative of the magnitude of winter snowpack and distribution of summer water availability.

KEYWORDS
Synoptic climatology; hydroclimatology; water availability; self-organizing maps

1. INTRODUCTION
The headwaters of two major river systems in western Canada, the Mackenzie and Saskatchewan Rivers, are located on the leeward slopes of the Rocky Mountains. Together, these rivers represent a significant portion of the water resources in western Canada. The majority of annual discharge of these rivers originates as winter snowpack released from frozen storage during spring freshet. Summer water availability is a function of basin-wide precipitation, evapotranspiration, and, in some cases, contributions from glacier melt or controlled release of water from reservoirs at hydroelectricity generating facilities. Recent evidence has indicated an intensification of the hydrologic cycle (Huntingdon 2006; Déry et al. 2009) in addition to increases in temperature and changing patterns of precipitation (Zhang et al. 2000; Linton et al. *this issue*) and streamflow (Burn & Hag Elnur 2002; Rood et al. 2008; Bawden et al. *this issue*). The boundary between north- and east-flowing river systems lies in the midlatitudes at the border of the Athabasca and North Saskatchewan Rivers. Even minor shifts in the spatial patterns of

climatic variables can have substantial consequences for the distribution of water resources in western Canada and freshwater pathways to the Arctic Ocean.

Freshwater flux to the Arctic Ocean is important to numerous terrestrial and marine processes including density-based stratification driving circulation and sea ice formation (Arnell 2005; Lammers et al. 2001), and feedbacks to the global climate (Lewis et al. 2000). The primary source of freshwater to the Arctic Ocean is river discharge (Serreze et al. 2003), and the largest volumetric contribution to the north-flowing Mackenzie River originates in the midlatitude mountainous headwaters of the Liard, Peace, and Athabasca Rivers.

The Saskatchewan River basin (SRB) is located in a semiarid, agriculturally productive region, and ultimately drains into Hudson Bay. Droughts and periods of extreme precipitation are frequently occurring components of prairie hydroclimatology (Shabbar et al. 2011). Droughts have agricultural and economic (Stewart et al. 2011) consequences and affect terrestrial and aquatic health (Schindler & Donahue 2006). The SRB is heavily allocated, with irrigation representing the largest consumptive water use and hydroelectricity generation representing the largest non-consumptive use (Martz et al. 2007). Both agricultural and municipal water demands are highest during summer months (Schindler & Donahue 2006).

Mid-tropospheric circulation drives surface climate conditions through forcing of convergence or divergence in the air column associated with frontal movement and surface cyclogenesis (Holton 1979). Synoptic-scale circulation patterns have been shown to influence surface climate in western Canada (e.g., Lackmann et al. 1998; Shabbar et al. 2011). Patterns of atmospheric circulation patterns can be classified into dominant types to facilitate analysis with surface climate variables. This research identifies dominant synoptic circulation patterns as they relate to spatial patterns of temperature and precipitation, with a particular focus on winter snow accumulation and melt in the mountainous headwaters.

2. DATA AND METHODOLOGY

To create a catalogue of dominant synoptic types, daily winter (Nov–Apr) and summer (May–Oct) geopotential height (gph) data at 500 hPa for 1950–2010, obtained from NCEP/NCAR (Kalnay et al. 1996), are classified using SOM (Self-Organizing Map) Toolbox for Matlab (Vesanto et al. 2005). SOM is a neural network process based on competitive and cooperative learning that clusters and projects data onto a topologically ordered output array (Kohonen 2001), and has been found to offer several advantages over traditional classification methods including principal components analysis (Hewitson & Crane 2002; Reusch et al. 2005; Jiang et al. 2012). Each SOM is linearly initialized using the first two eigenvectors of each dataset, representing maximum variance. Training is accomplished using the batch training algorithm, presenting the entire dataset to the initialized SOM. During the training process, the best matching unit for each gph vector is determined by Euclidean distance, and neighbouring units are updated to a lesser extent, thus preserving topological relationships (Kohonen 2001). SOM quality is evaluated using topological error and quantization error, criteria that indicate topological ordering and assess fit between vectors and best matching units. The PNA index is a measure of circulation at 500 hPa over the North Pacific and North America, particularly representing the intensity and position of the Aleutian Low (Wallace & Gutzler 1981), and is used as a quality indicator for the winter (R = 0.73, significant at 0.01%) and summer (R = 0.32, significant at 0.01%) SOM classifications.

Analysis of surface climate variables is achieved by using gridded temperature and precipitation datasets in 10 km resolution created using an ANUSPLIN method described by McKenney et al. (2011). The ANUSPLIN thin-plate spline interpolation method accounts for changes in elevation and was determined to be robust compared with alternative datasets (Hutchinson et al. 2009; McKenney et al. 2011). Daily temperature anomalies are calculated as the deviation from the daily mean 1950–2010 and are mapped to the corresponding synoptic type. Precipitation anomalies associated with each synoptic type are calculated as a percentage of precipitation delivered to the area relative to the mean precipitation values, and are normalized to centre the mean precipitation value at 0.

3. RESULTS

3.1 Winter

Daily 500 hPa gph data are classified into 16 types on a 4 × 4 SOM array (Figure 1), and the frequency with which each type occurs is shown in Figure 2. The trajectory map, a function of the topological ordering of the SOM, represents the temporal evolution of atmospheric states (Figure 3). Synoptic type persistence represents the percentage of days the type remains the same on the following day (Figure 4). Synoptic Types 1 and 13 represent strong high-pressure ridges with persistence of 71% and 67%, respectively. Type 16 is also highly persistent at 68%, and is characterized by a strong trough of low pressure over Alaska and the North Pacific, and a ridge of high pressure over the western continent. There is a seasonal evolution of dominant synoptic types, where types located in the upper right corner occur primarily during the shoulder months (Nov and Apr), and types along the bottom row occur primarily during the winter months (Dec–Feb).

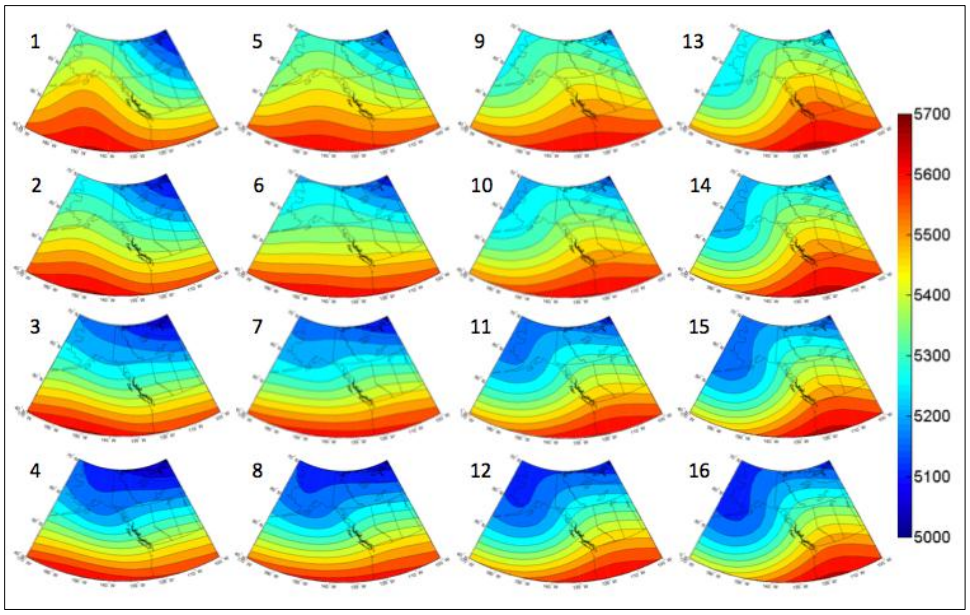

Figure 1: Daily winter (Nov–Apr) gph for 1950–2010 classified using SOM and used to assess surface climate variables across the entire study region.

8.8	5.5	5.8	7.8
5.9	4.0	4.9	6.4
6.1	4.4	4.7	6.4
7.2	6.6	6.5	9.1

Figure 2: Synoptic type frequency as percentage of total.

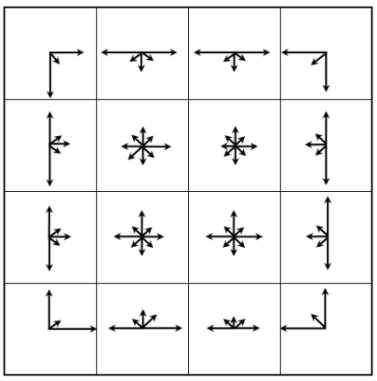

Figure 3: Trajectory map, where arrow length is proportional to pattern shifts.

71	45	48	67
41	28	32	46
39	26	28	41
62	42	39	68

Figure 4: Synoptic type persistence (%).

3.1.1. Surface climate analysis

Spatial distribution of precipitation anomalies associated with synoptic types is shown in Figure 5. To isolate winter snowpack in the Rocky Mountain headwaters, the primary source of annual streamflow, spatial averages of precipitation anomalies are calculated for each synoptic type for only the mountainous portion of south and north basins using a Rocky Mountain shapefile in ArcGIS (Table 1).

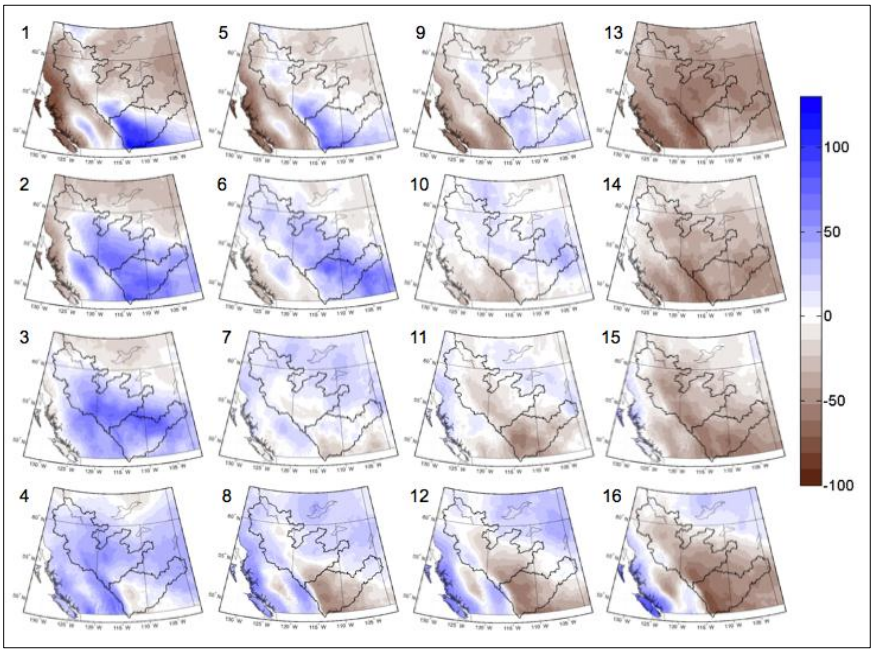

Figure 5: Precipitation anomalies associated with each synoptic type, calculated as percentage of precipitation delivered to each grid point referenced to 1950–2010 mean precipitation values, where 0 is equal to average precipitation.

Results indicate that synoptic Type 1 produces a strong north–south gradient of precipitation with low precipitation delivered to the Mackenzie basin and high precipitation delivered to the Saskatchewan basin. Opposite conditions are seen in precipitation patterns associated with Types

10 and 11, where the northern basins receive slightly above average precipitation and the southern basins receive below average precipitation. Results suggest the strength of the precipitation gradient is a function of the strength and position of the ridge over the Pacific Ocean.

Table 1: Average precipitation anomalies (%) in mountain headwaters, referenced to 1950–2010 mean precipitation values, where 0 is equal to average precipitation.

Synoptic type	1	2	3	4	5	6	7	8	9	10	11	12	13	14	15	16
Mackenzie River	-25	5	25	33	-7	18	14	24	-6	5	1	10	-38	-16	-16	-10
Saskatchewan River	45	57	56	54	29	8	7	11	-3	-26	-31	6	-56	-65	-51	-36

Temperature anomaly patterns associated with northerly meridional flow over the study region (Types 1-3 and 5-6) are subject to cold air advection from the Arctic, resulting in below average temperatures (Figure 6). Patterns of above average temperatures are those associated with a ridge axis immediately above and to the west of the study region (Types 10-16). Temperature is associated with timing of snow accumulation and melt, which can be approximated with the timing of the 0°-isotherm (Bonsal & Prowse 2003). To evaluate timing and snow accumulation and melt, averages of temperature anomalies are calculated for each synoptic type for the mountainous regions of the north and south basins (Table 2). Several of these patterns are associated with north–south temperature anomaly gradients. Type 8 is associated with below average temperatures in the north and above average temperatures in the south, where Type 9 is associated with below average temperatures in the north and above average temperatures in the south.

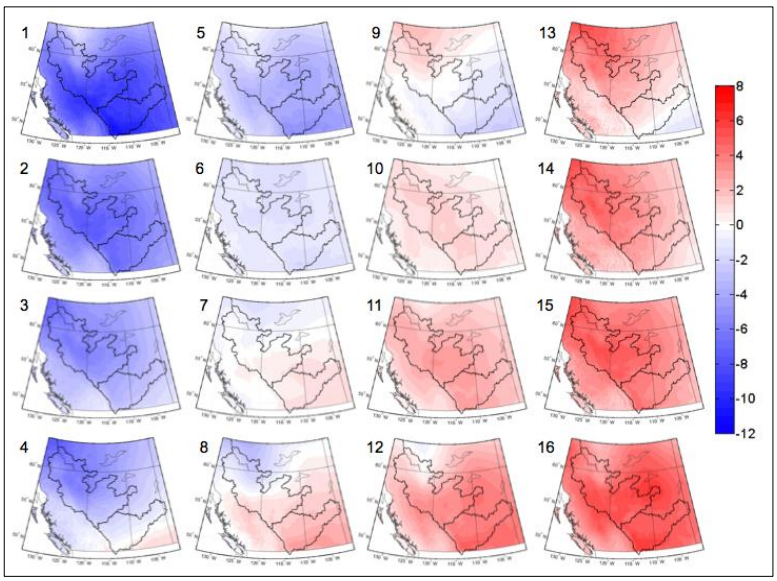

Figure 6: Temperature anomalies (°C) associated with each synoptic type, calculated as mean daily departure from 1950–2010 average values for each grid point.

Table 2: Average temperature anomalies (°C) in mountain headwaters.

Synoptic type	1	2	3	4	5	6	7	8	9	10	11	12	13	14	15	16
Mackenzie River	-6.5	-6.6	-5.2	-4.6	-2.0	-0.9	0.1	-0.2	0.9	1.4	2.6	2.3	3.7	4.7	5.1	4.8
Saskatchewan River	-9.8	-5.5	-2.5	-0.7	-3.9	-0.7	0.7	1.7	-0.8	1.3	2.6	3.7	1.7	3.3	4.3	5.3

Isolating precipitation anomalies for the mountainous region of the north and south basins facilitates analysis to determine which synoptic types are associated with high/low precipitation; thus, a high/low frequency of these types is expected to result in above/below average snowpack. Below average temperatures accompanying above average precipitation have the potential to extend the snow accumulation season if the frequency of these types is high during the onset of the accumulation season (Nov) and spring freshet (Mar–Apr). Conversely, a high frequency of below average precipitation and above average temperatures can shorten the snow accumulation season through delaying the onset of snow accumulation, increasing the potential for mid-winter melt or rain on snow events, and initiate an early spring freshet. For the Saskatchewan River headwaters, a high snowpack is expected during winters with a high frequency of Types 1-5, and a low snowpack is expected during winters with a high frequency of Types 10, 11, and 13-16. For the Mackenzie River headwaters, a high snowpack is expected during winters with a high frequency of Types 3-4 and 6-8, while a low snowpack is expected with a high frequency of Types 1 and 13-15.

3.1.2. Synoptic trend analysis

Changes in synoptic type frequency are evaluated using the Mann-Kendall (MK) non-parametric test for trend (Mann 1945; Kendall 1975). Types 2 (-33%), 3 (-33%), 4 (-42%), and 8 (-30%) have significantly decreased, and Types 9 (150%), 13 (90%), and 14 (59%) have significantly increased over the study period (1950–2010), significant at the 10% level. These results suggest a decrease in weak ridging over the Pacific Ocean and zonal flow and an increase in strong ridging over the western continental region. These trends contribute to the tendency toward above average temperatures and below average precipitation for both the Saskatchewan basin and Mackenzie headwater basins, resulting in lower average snowpack and a shorter snow accumulation season.

3.2 Summer

Daily summer (May–Oct) 500 hPa gph data are classified into 12 types on a 4 × 3 SOM array (Figure 7). Type 4 is indicative of a highly persistent split flow blocking high-pressure pattern, with a persistence of 85% and frequency of 20%. However, Type 4 occurs almost exclusively during July and August (Figure 8). Type 9 is also highly persistent (83%), and occurs primarily during May and October. As several summer synoptic types display a strong seasonal dependency, persistence, frequency, and trajectory are not representative of expected monthly frequencies or temporal evolution of synoptic types.

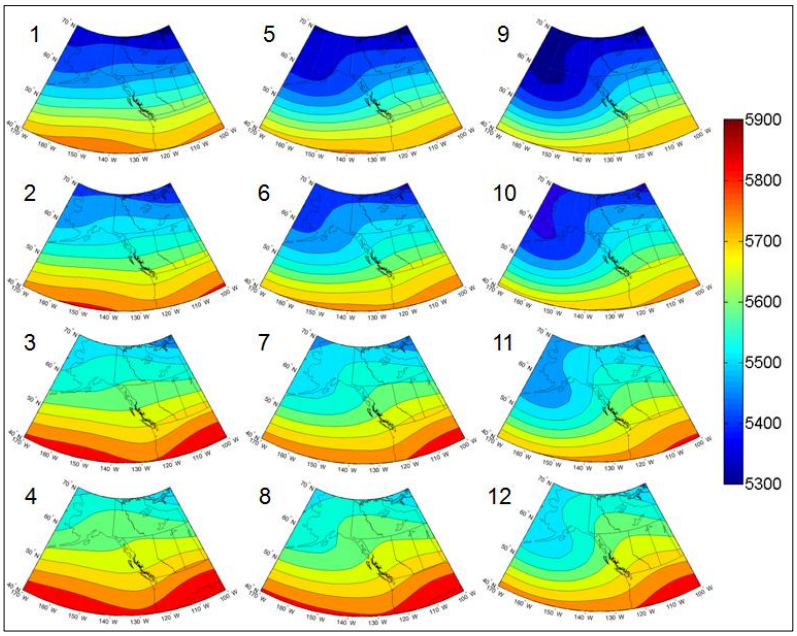

Figure 7: Daily summer (May–Oct) gph for 1950–2010 classified using SOM and used to assess surface climate variables across the entire study region.

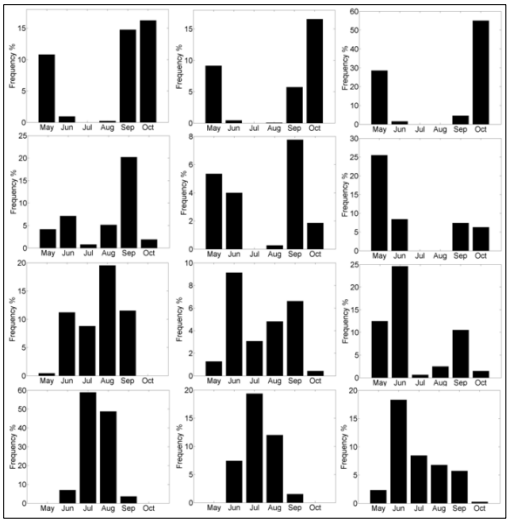

Figure 8: Summer synoptic type frequency by month, indicating a strong seasonal evolution of dominant types.

3.2.1. Surface climate analysis

Spatial distribution of precipitation anomalies associated with summer synoptic types are shown in Figure 9. Summer precipitation is influenced by meso-scale convective processes in addition to synoptic-scale circulation (Raddatz & Hanesiak 2008). As a result, the relationship between circulation and precipitation is less cohesive than winter results. Several north–south gradients are apparent (i.e., Types 1 and 10), as well as patterns with drier (Type 12) or wetter (Type 7) conditions in the centre of the study region than the south and north.

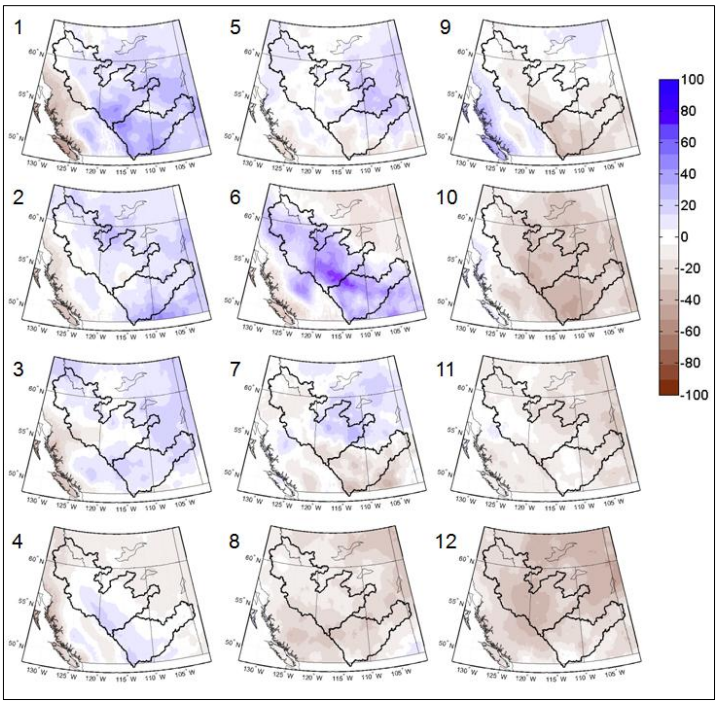

Figure 9: Precipitation anomalies associated with each synoptic type, calculated as percentage of precipitation delivered to each grid point referenced to 1950–2010 mean precipitation values.

In the far north, summer shoulder season temperatures (May and Oct) may be associated with late onset freshet and early onset freeze-up. Figure 10 shows spatial distribution of temperature anomalies associated with summer synoptic types. Types 1-3 and 5 are associated with fairly uniform below average temperatures across all basins. Types 8, 10, and 11 are associated with above average temperatures. Cooler south-warmer north temperature gradients are shown in Types 4, 8, and 12, while warmer south-cooler north gradients are seen in Types 6, 7, and 9.

Negative precipitation anomalies are indicative of low water availability during times of high demand, and potential drought conditions. Positive temperature anomalies may exacerbate dry conditions through increased evapotranspiration. Drier than average conditions in the Saskatchewan basin are expected during summer seasons with a high frequency of Types 7-12. Drier than average conditions in the Liard, Peace, and Athabasca basins are expected during summer seasons with a high frequency of Types 8-12.

Wetter than average conditions in the southern prairies are expected during summers with a high frequency of Types 1-6, particularly Types 1 and 6, which are an average of 33% and 36% above average precipitation, respectively. These types are also associated with below average temperatures; thus evapotranspiration is expected to be lower and soils are expected to retain moisture. Wetter than average conditions are expected for the northern basins during summers with an increased frequency of Types 1-3 and 5-6, which are associated with both above average precipitation and below average temperatures.

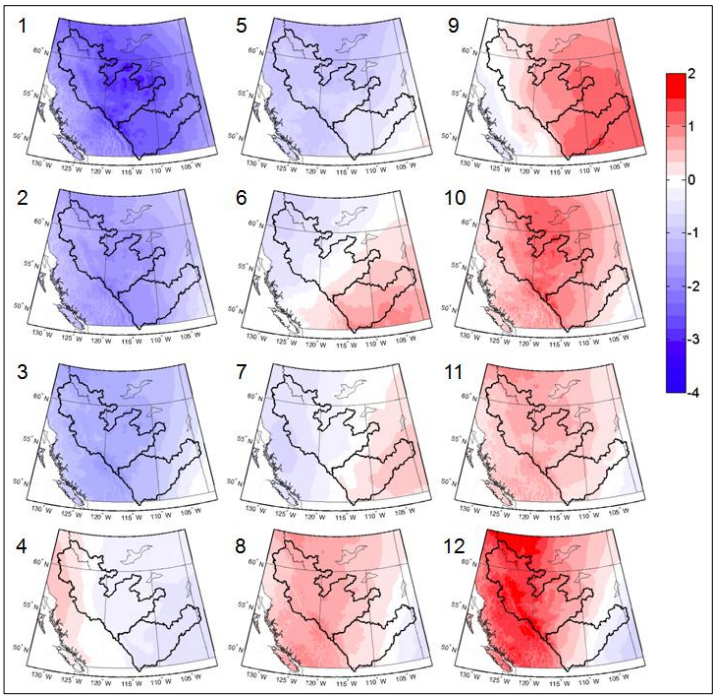

Figure 10: Temperature anomalies (°C) associated with each synoptic type, calculated as mean daily departure from 1950–2010 average values for each grid point.

3.2.2. Synoptic trend analysis

Mann-Kendall trend results indicate that Type 4 (38%) has significantly increased and Types 9 (-27%) and 10 (-32%) have significantly decreased over the 1950–2010 period (sig. 5%). This indicates an increase in split flow high-pressure blocking pattern over the western continental region, confined to the July–August period, given the summer dependency of Type 4. This increase is associated with an increase in precipitation and a slight decrease in temperature for the Peace, Athabasca, and Saskatchewan basins and slight decrease in precipitation and slight increase in temperature in the Liard basin. Results also indicate a decrease in strong low-pressure troughs over Alaska accompanied by south–north meridional flow over the western continent. Type 9 has a strong presence in May and October, and Type 10 has a strong presence in May; therefore, this decrease is expected to affect shoulder season circulation. These trends suggest decreases in low-precipitation/high-temperature climatic conditions, with a greater impact in the Saskatchewan basin compared with the Mackenzie headwater basins.

4. CONCLUSIONS

Mid-tropospheric circulation, classified into 16 winter (Nov–Apr) and 12 summer (May–Oct) synoptic types using SOM, are used in hydroclimatic analysis to determine the impacts of synoptic-scale circulation on Rocky Mountain snowpack and snowmelt, and basin-wide summer water availability. Results indicate that above average precipitation and below average temperature are associated with a ridge of high pressure over the North Pacific Ocean, advecting cold Arctic air over the study region. Conversely, a ridge of high pressure over the western continent effectively blocks the intrusion of cold Arctic outbreaks, and is associated with above average temperatures and below average precipitation in the study region. Results from this

research, combined with additional CROCWR project results support a climatic redistribution of precipitation and shifting patterns of water availability that is essential for future water management strategies.

ACKNOWLEDGMENTS

This research was funded by the Natural Sciences and Engineering Research Council of Canada. Support for this project was provided by the Water and Climate Impacts Research Centre, Environment Canada, the University of Victoria, and the CROCWR project team.

REFERENCES

Arnell, N.W. 2005 Implications of climate change for freshwater inflows to the Arctic Ocean. *Journal of Geophysical Research* 110, D07105.

Bawden, A.J., Burn, D.H. & Prowse, T.D. 2013 An analysis of spatial and temporal trends and patterns in western Canadian runoff: A CROCWR component. *Proc. of the Northern Research Basin Symposium, August 2013* (unpublished).

Bonsal, B.R. & Prowse, T.D. 2003 Trends and variability in spring and autumn 0°C-isotherm dates over Canada. *Climatic Change* 57, 341–358.

Burn, D.H. & Hag Elnur, M.A. 2002 Detection of hydrologic trends and variability. *Journal of Hydrology* 255, 107–122.

Déry, S.J., Hernández-Henríquez, M.A., Burford, J.E. & Wood, E.F. 2009 Observational evidence of an intensifying hydrological cycle in northern Canada. *Geophysical Research Letters* 36, L13402.

Hewitson, B.C. & Crane, R.G. 2002 Self-organizing maps: applications to synoptic climatology. *Climate Research* 22, 13–26.

Holton, J.R. 1979 *An Introduction to Dynamic Meteorology,* 2nd ed. Academic Press, Inc., NY.

Huntington, T.G. 2006 Evidence for intensification of the global water cycle: Review and synthesis. *Journal of Hydrology* 319, 83–95.

Hutchinson, M.F., McKenney, D.W., Lawrence, K., Pedlar, J.H., Hopkinson, R.F., Milewska, E. & Papadopol, P. 2009 Development and testing of Canada-wide interpolated spatial models of daily minimum-maximum temperature and precipitation for 1961–2003. *Journal of Applied Meteorology and Climatology* 48, 725–741.

Jiang, N., Cheung, K., Luo, K., Beggs, P.J. & Zhou, W. 2012 On two different objective procedures for classifying synoptic weather types over east Australia. *International Journal of Climatology* 32, 1475–1494.

Kalnay, E., Kanamitsu, M., Kistler, R., Collins, W., Deaven, D., Gandin, L. & Joseph, D. 1996 The NCEP/NCAR 40-year reanalysis project, *Bulletin of the American Meteorological Society* 77, 437–471.

Kendall, M.G. 1975 *Rank Correlation Measures*. Charles Griffin, London.

Kohonen, T. 2001 *Self-Organizing Maps*. Springer, New York.

Lackmann, G.M. & Gyakum, J.R. 1998 Moisture transport diagnosis of a wintertime precipitation event in the Mackenzie River basin. *Monthly Weather Review* 126, 668–691.

Lammers, R.B., Shiklomanov, A.I., Vörösmarty, C.J., Fekete, B.M. & Peterson, B.J. 2001 Assessment of contemporary Arctic river runoff based on observational discharge records. *Journal of Geophysical Research* 106, D4: 3321–3334.

Lewis, E.L. 2000 *The Freshwater Budget of the Arctic Ocean*. Kluwer Academic Publishers, Dordrecht.

Linton, H., Prowse, T., Dibike, Y. & Bonsal, B. 2013 Spatiotemporal trends in climatic variables affecting streamflow across western Canada from 1950-2010: A CROCWR component. *Proc. of the Northern Research Basin Symposium, August 2013* (unpublished).

Mann, H.B. 1945 Non-parametric tests against trend. *Econometrica* 13, 245–259.

Martz, L., Bruneau, J. & Rolfe, J.T. (eds.) 2007 Climate *Change and Water, SSRB Final Technical Report*. University of Saskatchewan, Saskatoon, Saskatchewan

McKenney, D.W., Hutchinson, M.F., Papadopol, P., Lawrence, K., Pedlar, J., Campbell, K. & Owen, T. 2011 Customized spatial climate models for North America. *Bulletin of the American Meteorological Society* 9212, 1611–1622.

Raddatz, R.L. & Hanesiak, J.M. 2008 Significant summer rainfall in the Canadian Prairie Provinces: modes and mechanisms 2000–2004. *Int. Journal of Climatology* 28, 1607–1613.

Reusch, D.B., Alley, R.B. & Hewitson, B.C. 2005 Relative performance of self-organizing maps and principal component analysis in pattern extraction from synthetic climatological data. *Polar Geography* 293, 188–212.

Rood, S.B., Pan, J., Gill, K.M., Franks, C.G., Samuelson, G.M. & Shepherd, A. 2008 Declining summer flows of Rocky Mountain rivers: Changing seasonal hydrology and probably impacts on floodplain forests. *Journal of Hydrology* 349, 397–410.

Schindler D.W. & Donahue W.F. 2006 An impending water crisis in Canada's western prairie provinces. *PNAS* 10319, 7210–7216.

Serreze, M.C., Bromwich, D.H., Clark, M.P., Etringer, A.J., Zhang, T. & Lammers, R. 2003 Large-scale hydro-climatology of the terrestrial Arctic drainage system. *Journal of Geophysical Research* 108, D2, 8160.

Shabbar, A., Bonsal, B.R. & Szeto, K. 2011 Atmospheric and oceanic variability associated with growing season droughts and pluvials on the Canadian Prairies. *Atmosphere-Ocean* 1, 1–17.

Stewart, R., Pomeroy, J. & Lawford, R. 2011 The drought research initiative: A comprehensive examination of drought over the Canadian Prairies. *Atmosphere-Ocean* 494, 298–302.

Vesanto, J., Himberg, J., Alhoniemi, E. & Parhankangas, J. 2000 *SOM toolbox for Matlab 5*. Helsinki University of Technology, Rep. A57.

Wallace, J.M. & Gutzler, D.S. 1981 Teleconnections in the geopotential height field during the Northern Hemisphere winter. *Monthly Weather Review* 109, 784–812.

Zhang, X., Vincent, L.A., Hogg, W.D. & Niitsoo, A. 2000 Temperature and precipitation trends in Canada during the 20th century. *Atmosphere-Ocean* 383, 395–429.

Winter Streamflow Generation in a Subarctic Precambrian Shield Catchment

Christopher Spence[1*], Shawne A. Kokelj[2], Steve V. Kokelj[3], and Newell Hedstrom[1]

[1]*National Hydrology Research Centre, Environment Canada, Saskatoon, SK, S7N 3H5, CANADA*
[2]*Water Resources Division, Aboriginal Affairs and Northern Development Canada, Yellowknife, NT, X1A 2B3, CANADA*
[3]*Northwest Territories Geoscience Office, Yellowknife, NT, X1A 2R3, CANADA*
**Corresponding author's email: chris.spence@ec.gc.ca*

ABSTRACT
There have been widespread increases in winter streamflow across the circumpolar north since the mid to late 1900s. However, the physical processes that result in winter runoff generation are not well understood. The objective of this research was to determine the runoff generation processes and pathways of cold season streamflow, and to compare and contrast them with those of spring freshet in a study catchment in the subarctic Canadian Shield in which winter streamflow regime changes have been documented. Traditional hydrometric methods were used in conjunction with models and hydrochemistry to estimate runoff sources and pathways. Results suggest runoff generation processes do not necessarily differ between spring and winter runoff events. The timing at which pre-event and event water contributes and runoff pathways activate and deactivate is different. Runoff during the spring freshet is dominated by pre-event water that has not been exposed to the subsurface. Most notably, isotopic chemistry reveals that 80% of high cold season streamflow is from new precipitation. Only 29% of cold season streamflow was exposed to the subsurface. In Precambrian Shield landscapes, or even where there may be a large fraction of lakes, late autumn rainfall can increase lake storage to ample levels that can provide high amounts of winter runoff. Where autumn rainfall has been increasing, precipitation and surface water should be considered as a source of enhanced winter streamflow in these types of landscapes. These results have implications for how widespread environmental changes in the circumpolar north, notably those of aquatic chemistry and permafrost decay, should be interpreted and predicted.

KEYWORDS
Streamflow; runoff generation; climate change; subarctic; Precambrian Shield; stable isotopes

1. INTRODUCTION
One of the clearest hydrological changes in a rapidly changing circumpolar north has been increases in winter streamflow since the mid to late 1900s (Walvoord & Striegl 2007; Déry et al. 2009). Broad investigative scales of most studies required investigators to infer proposed mechanisms driving enhanced winter streamflow (thawing permafrost, more efficient runoff from land scarred by forest fires, and wetter conditions) (Smith et al. 2007; St. Jacques & Sauchyn 2009). Modelling exercises provide insight (Bense et al. 2009; Bosson et al. 2012), but there remains a notable knowledge gap of the physical processes by which water reaches the stream during these periods of enhanced winter streamflow. This research investigates runoff generation processes in the Precambrian Shield, a common landscape in northern Canada,

Greenland, Scandinavia, and Russia, where winter streamflow changes have been documented (Smith et al. 2007; St. Jacques & Sauchyn 2009; Déry et al. 2009; Spence et al. 2011). This region is somewhat underrepresented in the literature because most studies have focused on widely available large-scale data from the Ob, Yenisey, Lena, Yukon, and Mackenzie Rivers, with only the last containing any significant portion of Precambrian Shield. It is also important to elucidate the processes responsible for enhanced winter streamflow in specific regions for proper interpretation and prediction of impacts and feedbacks among changing environmental conditions and northern circumpolar streamflow regimes, particularly river chemical loads (Frey & McClelland 2009; Jones & Reinhart 2010) and permafrost dynamics (Kokelj & Burn 2005). The goal of this research was to identify the predominant processes, source areas, and runoff pathways during the production of enhanced winter streamflow and determine if differences exist between periods of enhanced winter streamflow and the spring freshet or typical winter baseflow.

2. STUDY CATCHMENT

Baker Creek is a typical shield stream characterized by lakes connected by short channels that drains water from ~165 km^2 of subarctic Precambrian Shield into Great Slave Lake in Canada's Northwest Territories (62°30′8″N, 114°24′25″W) (Figure 1). The shield landscape is characterized by a mosaic of exposed granitic and metamorphic bedrock (Baker Creek basin fraction of 40%) and areas of thin unconsolidated till and lacustrine deposits (Baker Creek basin fraction of 37%). Baker Creek is in the discontinuous permafrost zone. Soils averaging 1.5 m in depth derived from glaciolacustrine clays, outwash, and organic deposits are typically underlain by permafrost, whereas bedrock and well-drained areas with sandy overburden are typically not (Wolfe 1998). Ice-rich permafrost is generally restricted to fine-grained deposits that comprise only a small portion of the landscape. Three hundred and forty nine perennial lakes occupy 23% of the Baker Creek basin. The region has short cool summers (17°C in July) and long cold winters (-27°C in January). Annual unadjusted precipitation averages 281 mm, with 54% of that falling as snow. Snow cover exists from October until May. Convective cells produce much of the summer precipitation, producing high inter-annual variability, especially in July and August. The weather becomes cool and damp in autumn when periodic synoptic conditions allow for persistent travel of cyclones over the region (Spence & Rausch 2005).

In most years, the largest flux of water from the basin is during the spring freshet, and the streamflow regime of the basin has traditionally been characterized as subarctic nival, as this melt dominates the annual hydrograph of Baker Creek (Figure 2). However, the synoptic conditions described by Spence and Rausch (2005) have become so common since the late 1990s that fall and winter runoff events now regularly exceed the spring freshet in magnitude, leading to a shift to a combined nival/pluvial streamflow regime and higher winter streamflow (Spence et al. 2011). Between 1972 and 1996, the spring freshet months of May and June and the winter months of October to March contained 76% and 8% of Baker Creek annual yield, respectively. After 1997, these values changed significantly to 50% and 20%, respectively, with no significant change in annual yield. The occurrence of these winter runoff events, and shifts in the streamflow regime, makes Baker Creek an ideal location at which to investigate winter runoff generation processes.

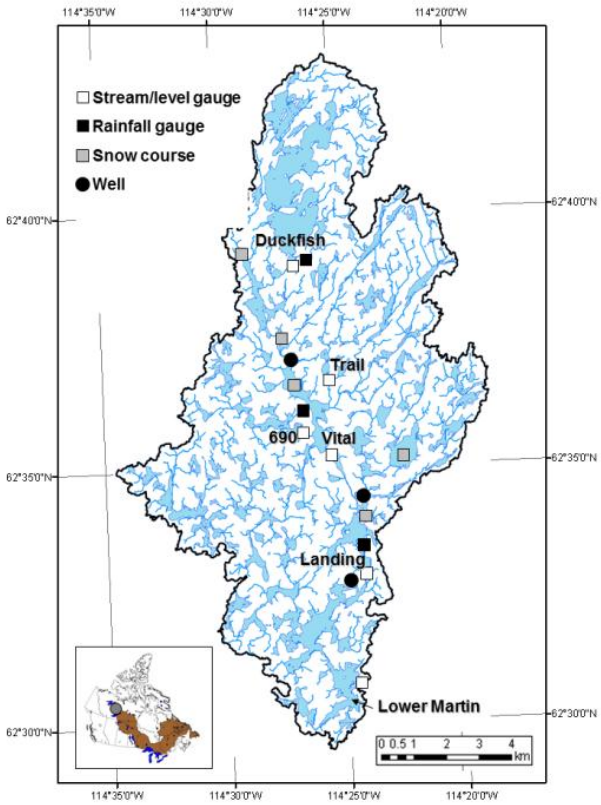

Figure 1: Map of the Baker Creek research catchment showing the drainage network, names of important lakes, and relevant instrumentation.

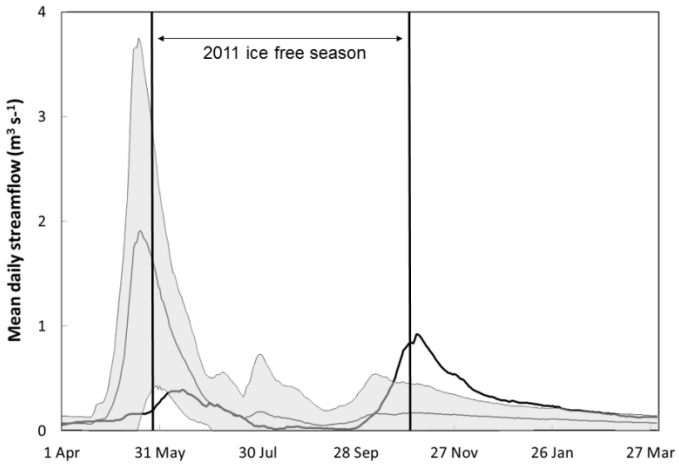

Figure 2: Annual hydrograph of Baker Creek below Lower Martin Lake. Average streamflow (19XX–20XX) is denoted by the grey line, bounded by one standard deviation in the grey shade; 2011 streamflow is denoted by the thick black line.

3. METHODOLOGY

To evaluate historical winter streamflow in the basin and compare and contrast it with characteristics of the spring freshet, discharge records for Baker Creek at the outlet of Lower

Martin Lake from 1972–2011 were acquired from the Water Survey of Canada (http://www.wateroffice.ec.gc.ca/index_e.html). Recession coefficients (t^*), defined with:

$$Q_t = Q_0 \cdot \exp^{(-t/t^*)} \quad (1)$$

where t is time (days), Q_0 is streamflow at time 0 and Q_t is streamflow at time t, were used to differentiate proportional differences in runoff source areas. Larger values of t^* are associated with larger source areas transferring storage to streamflow (Carey & Woo 2001). Winter recession coefficients were calculated before and after 1997, the breakpoint year for the upward shift in winter streamflow in Baker Creek is documented by Spence et al. (2011).

During wet periods, a greater proportion of lakes in the catchment contribute to streamflow for a longer duration than during dry conditions (Spence 2006). The contributing lake area during spring freshet and winter periods from 1972–2011 was estimated with a relationship found between contributing lake area and t^*. This relationship was attained by implementing a sequential bucket model simulating the network of lakes along the main stem of Baker Creek. This model assumes water is only removed from the lakes by surface outflow, and downstream lakes only receive inflow from upstream lakes. Streamflow was calculated iteratively through time, for a combination of increasing numbers of contributing lakes and from full conditions until outflow exhausts detention storage in each lake. The resulting recession curves were used to calculate t^* using Eq. (1), and compared against the input contributing lake area.

The 2011/2012 water year at Baker Creek was dominated by two major streamflow events: the spring freshet and a winter runoff event (Figure 2). The portion of pre-event and event water and the nature of runoff pathways for both spring and winter runoff events during this water year were determined using a three-component hydrograph separation technique following Hinton et al. (1994), using a stable isotope of water (oxygen-18, ^{18}O) and a conservative geochemical tracer applicable to Canadian Shield watersheds (magnesium, Mg^{2+}) (Wels et al. 1991). These two constituents exhibit distinct concentrations in upstream lakes, rainfall, snow, and groundwater, and are not co-linear. Enrichment of water with ^{18}O in lakes and groundwater after rainfall permits the portion pre-event water to be identified in the hydrograph, while entrainment of Mg^{2+} by groundwater allows the identification of that portion of streamflow that was exposed to subsurface pathways.

Concentrations of Mg^{2+} in precipitation were obtained from the closest Canadian Air and Precipitation Monitoring Network (CAPMoN; http://www.ec.gc.ca/natchem/) atmospheric chemistry station at Snare Rapids while samples for isotope analysis were collected from rainfall gauges and snow courses in the watershed. Stream water was sampled just downstream of the Water Survey gauge, in upstream lakes and from groundwater wells in representative locations prior to and biweekly, or as logistics and access to the steam allowed during each event. Samples for ^{18}O isotope analysis were collected unfiltered and unpreserved in 25 ml HDPE bottles and capped tightly to avoid evaporation and stored at room temperature. Samples were analyzed at the National Hydrology Research Centre in Saskatoon, Canada using spectroscopy following the methods described by Lis et al. (2008). Isotopic composition is expressed in terms of $^2H/^1H$ and $^{18}O/^{16}O$ ratios and represented by delta notation (δ) in units per mill (‰) relative to Standard Mean Ocean Water (SMOW). Concentrations (mg/l) of magnesium (Mg^{2+}) were determined using ion chromatography at the Taiga Environmental Laboratory in Yellowknife, Canada.

Uncertainty in the hydrograph separation was estimated following the methods of Genereux (1998).

Field measurements also included water levels at five lakes on major Baker Creek tributaries and near-surface ground thermal and soil moisture conditions at several sites in or nearby the Baker Creek catchment (Figure 1). These terrestrial sites included (A) two hillslope Brunisol soil columns of ~2 m thickness capped with shallow and thin organic soils; (B) two soil columns of ~1.5 m thickness composed entirely of humic peat above bedrock; and (C) two wetland soil columns with ~0.5 m of humic peat over impervious glaciolacustrine clays. Soil observation sites (A) and (C) were underlain by permafrost, but (B) soil columns were underlain by bedrock and too shallow to contain permafrost. Because of the high thermal conductivity of the Precambrian bedrock, it is unlikely that permafrost was present anywhere in the subsurface at (B) sites. Each of these soil columns was instrumented with site-specific calibrated ECH_2O-TE soil moisture and temperature probes installed horizontally at the soil surface, 0.25 m, and 0.4 m depth recorded half-hourly. These were installed to gain an understanding of the time required for winter freeze-back and the depth of the active layer of the soil column, as an indication of the possible runoff pathways during the spring freshet and fall and winter.

4. SOURCE WATER AND RUNOFF PATHWAYS

The average winter recession coefficient from 1972–1996 was 37 days, but this increased threefold to 103 days during the period 1997–2009. This implies that larger stores of water have been available to support winter streamflow during this latter period. The increase in winter t^* in Baker Creek was not associated with dry years (t^* = 34) when a potential driver such as meltwater from thawing permafrost would have been most evident. The experimental model implies t^* increases with contributing lake area following:

$$t^* = 8x10^{-6} A_L + 31.113 \quad (2)$$

Configuring the routing model with a lake the same size as the one immediately above the Water Survey gauge results in a t^* of 43 days; comparable to observed conditions in Baker Creek prior to 1997. The sequence of Vital, Landing, Martin, and Lower Martin Lakes has been observed as the area contributing to streamflow in late winter hgh streamflow conditions. If these lake areas are applied to Eq. (2), t^* increases to over 150 days, comparable in magnitude to that observed in the stream since 1997. This suggests that when late season rainfall generates enough runoff to permit growth in the contributing area to the outlet, lake surface storage alone can account for the observed increases in t^* and be the source water of enhanced winter streamflow in the watershed.

Snowmelt of 45.2 mm and 10.4 mm of rainfall between 4 and 11 May triggered the spring freshet of 2011. Streamflow rose from 0.1 m^3s^{-1} to a peak of 0.39 m^3s^{-1} on 13 June (Figure 3). An additional 90.2 mm of rain fell before the end of the event. The fraction of event water during early phases of the freshet was 0.13, but this increased steadily to 0.4 by peak spring streamflow. The fraction of event water steadily increases to 0.8 by the end of the event, which by this time would be a combination of snow and summer rain. The fraction of streamflow exposed to subsurface pathways remained steady at 0.2 throughout much of the event.

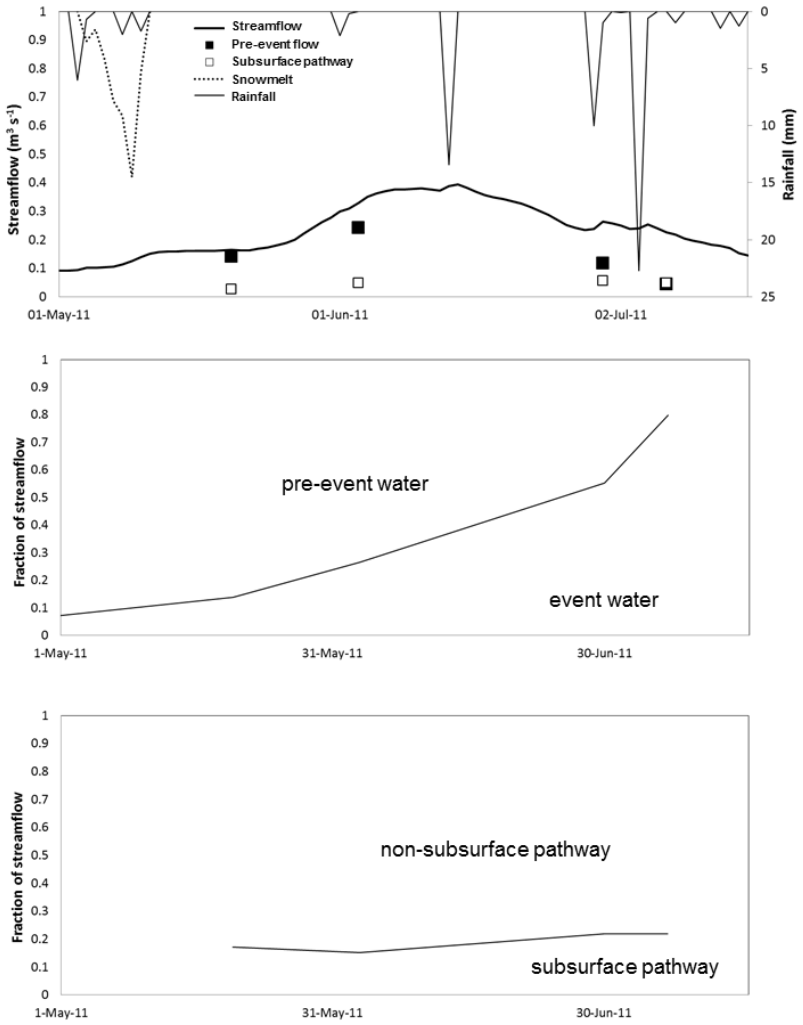

Figure 3: Spring freshet hydrograph separation.

Rainfall of 44 mm fell over a prolonged period of 39 days from 18 September to 27 October 2011 (Figure 4). This rainfall increased streamflow to a peak of 0.93 m^3s^{-1} on 4 November, just after complete formation of lake ice cover in the basin. Streamflow receded steadily through to 25 April 2012, when the next spring freshet began. The runoff ratio for the event was 0.81. In contrast to the spring freshet, the fraction of event water was very high during the rising limb (0.9). This suggests that event water was able to contribute to streamflow quite quickly. The fraction exposed to the subsurface approached 0.5 during this phase of the event. Event rainfall dominates the hydrograph well into March. The volume of streamflow that was pre-event water and that exposed to the subsurface was similar from December to mid-January. After January, pre-event water dominated the hydrograph, but it was not water that was exposed to subsurface pathways.

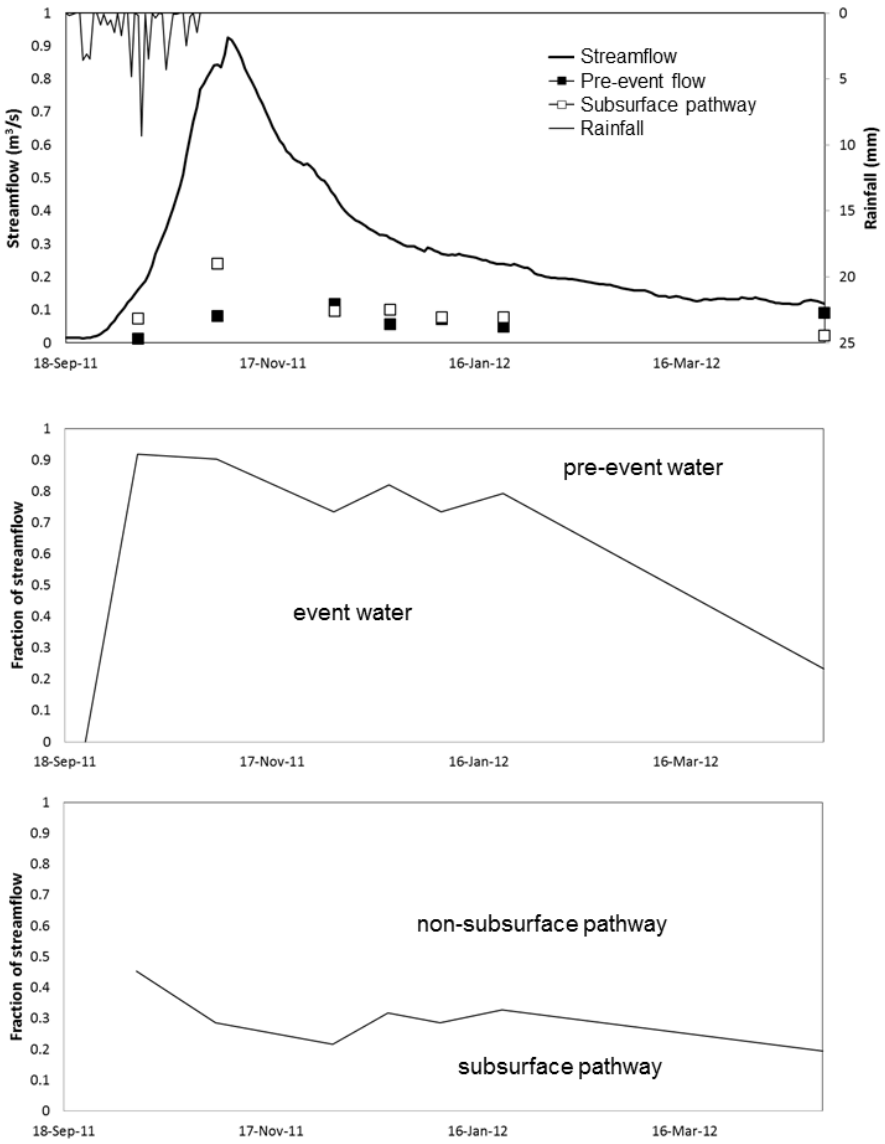

Figure 4: Winter hydrograph separation.

Most of the error in the hydrograph separation is in identifying the fraction associated with subsurface pathways (Table 1). Overall, the groundwater Mg^{2+} and ^{18}O concentrations were dissimilar from the other sources of water, notably the pre-event lake water (C_{og} = 18 mg/l and -18.7‰; C_{ol} = 3.5 mg/l and -14.7‰). However, there were wide variations in groundwater chemistry among all the sites, which increased the resulting uncertainty. The standard deviation of Mg^{2+} was 2.9 mg/l with a range from 10 to 20 mg/l and ^{18}O varied from -16.3‰ to -21.8‰. The presence of this type of uncertainty in the hydrochemistry analysis demonstrates the importance of using hydrochemical techniques in partnership with other methodologies. In this instance, corroborating model results also suggest lake surface storage maintains streamflow during the recession of winter runoff events, and adds confidence to the results of the hydrograph separation.

Table 1: Statistics and uncertainty associated with tracer data for 1 Nov 2011. This day exhibits the greatest uncertainty associated with estimates of streamflow fraction during either the winter or spring event. W is the uncertainty around the estimate, and W_f is the percentage of total uncertainty associated with each tracer.

Water	Tracer	Mean	σ	n	W (90%)	W_f
Event water	^{18}O (‰)	-11.3	0.05	2	0.15	0.18
	Mg^{2+} (mg/l)	0.01	0.01	31	0.01	0.003
Pre-event lake water	^{18}O (‰)	-14.7	0.6	2	1.72	0.14
	Mg^{2+} (mg/l)	3.5	0.4	3	0.78	2.8
Pre-event groundwater	^{18}O (‰)	-18.7	1.6	6	2.38	27.9
	Mg^{2+} (mg/l)	18.0	2.9	6	4.28	68.0
Stream water	^{18}O (‰)	-12	0.6	1	1.85	0.01
	Mg^{2+} (mg/l)	3.9	0.8	1	2.44	0.03

5. STREAMFLOW GENERATION PROCESSES

Pre-event water dominated the rising limb of the spring hydrograph, but as the summer and hydrograph recession progressed, event water became increasingly predominant. The low fraction of spring streamflow exposed to groundwater pathways and the frozen soils suggests that infiltration was limited, pathways were shallow, and hillslope runoff was generated by Hortonian processes. However, the low spring event runoff ratio (0.08) and high pre-event fraction in spring streamflow at peak flow both imply that much of the snowmelt runoff generated in the basin did not reach the outlet and could have been intercepted by headwater lakes with large storage deficits. In this scenario/situation, the low observed fraction of water exposed to groundwater pathways could be merely the inability of this water to reach the basin outlet, rather than an indication of the physical processes active on the hillslopes, which tend not to be Hortonian even during periods when soils are frozen (Spence & Woo 2003). Many of the tributaries to Baker Creek had stopped contributing streamflow by mid-June, so the only areas hydrologically connected to the basin outlet were lakes in lower positions in the watershed, essentially resulting in a runoff generation process analogous to precipitation on saturated areas for summer rain. In contrast, the largest source of water to the winter streamflow event was precipitation. The fraction exposed to subsurface pathways was comparable to the fraction of land cover with significant soil cover, and with the high runoff ratio, this indicates that most of the watershed contributed to the event. Therefore, runoff generation processes were likely a combination of fill-and-spill runoff generation processes and precipitation on saturated areas (i.e., lakes and exposed bedrock at storage capacity) proportional to the distribution of land cover on which these processes occur.

A slow rate of soil freezing implies terrestrial runoff pathways might remain hydrologically connected to the basin outlet during winter. Mean air temperatures were below freezing by 26 October 2011, but ground temperatures at 0.4 m depth remained above freezing until 18 January 2012 (Figure 5). Unfrozen soils, above permafrost acting as an aquiclude, could accommodate the lateral transfer of soil water well into winter. This appears to have been important during the period from early December to the end of January when both the pre-event portion and that exposed to subsurface pathways were comparable (0.25). The predominant runoff generation process in early winter then could be characterized as subsurface stormflow. After soil columns freeze, the pre-event portion of streamflow remains similar (0.77), but the portion that was

exposed to the subsurface decreases to less than 0.2. As subsurface sources decline in late winter, the remaining streamflow was generated from detention storage of pre-event water in lakes.

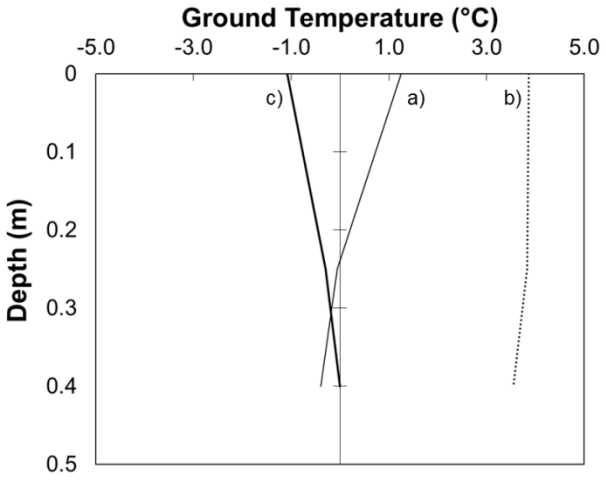

Figure 5: Shallow ground temperature profiles in a Brunisol soil column on (a) 12 May 2011, (b) 1 October 2011, and (c) 18 January 2012.

6. CONCLUDING REMARKS

Enhanced winter streamflow involves an expansion of source areas for streamflow beyond what would be observed during typical winter baseflow. Modelled and observed recession coefficients imply an expansion in surface storage (i.e., lakes) hydrologically connected to the basin outlet alone can be the source of higher winter flows in a lake-rich Precambrian shield watershed. This enhanced winter streamflow can be generated by a diversity of processes in a subarctic Precambrian Shield landscape. In this study, the majority of winter flow was derived from rainfall on lakes and areas of exposed bedrock hydrologically connected to the basin outlet. Half of the initial portion of the receding limb was event water exposed to subsurface pathways, through saturation overland flow and fill-and-spill runoff generation processes. The results imply the source of enhanced winter flow over time has not been from permafrost thaw, because the portion exposed to subsurface pathways decreases through late winter as soils freeze and streamflow recedes. Late winter flow is comprised of pre-event lake surface storage. Many previous large-scale studies have inferred the causes and impacts of higher circumpolar winter streamflow. These are important studies to gauge global effects of environmental change in the circumpolar North. However, to properly adapt to change and make informed water resource development decisions in a changing environment, proper understanding of predominant geophysical processes is important.

REFERENCES

Bense, V.F., Ferguson, G. & Koot, H. 2009 Evolution of shallow groundwater flow systems in areas of degrading permafrost. *Geophys. Res. Lett.* 36, L22401, doi: 10.1029/2009GL039225.

Bosson, E., Sabel, U., Gustafsson, L.G., Sassner, M. & Destouni, G. 2012 Influences of shifts in climate, landscape, and permafrost on terrestrial hydrology. *J. Geophys. Res.* 117, D05120, doi: 10.1029/2011JD016429.

Carey, S.K. & Woo, M.K. 2001 Slope runoff processes and flow generation in a subarctic, subalpine catchment. *Journal of Hydrology* 253, 110–129.

Dery, S.J., Hernández-Henriquez, M.A., Burford, J.E. & Wood, E.F. 2009 Observational evidence of an intensifying hydrological cycle in northern Canada. *Geophys. Res. Lett.* 36, L13402, doi: 10.1029/2009GL038852.

Frey, K.E. & McClelland, J.W. 2009 Impacts of permafrost degradation on arctic river biogeochemistry. *Hydrological Processes* 23, 169–182.

Genereux, D. 1998 Quantifying uncertainty in tracer based hydrograph separation. *Water Resources Research* 34, 915–919.

Hinton, M.J., Schiff, S.L. & English, M.C. 1994 Examining the contributions of glacial till water to storm runoff using two- and three- component hydrograph separations. *Biogeochemistry* 26, 67–88.

Jones, J.B. & Reinhart, A.J. 2010 The long-term response of stream flow to climatic warming in headwater streams in interior Alaska. *Can. J. Forest Res.* 40, 1210–1218.

Kokelj, S.V. & Burn, C.R. 2005 Geochemistry of the active layer and near-surface permafrost, Mackenzie Delta region, Northwest Territories, Canada. *Can. J. Earth Sci.* 42, 37–48.

Lis G., Wassenaar L.I. & Hendry M.J. 2008 High precision laser spectroscopy D/H and $^{18}O/^{16}O$ measurements of microliter natural water samples. *Analytical Chemistry* 80, 287–293.

Smith, L.C., Pavelsky, T.M., MacDonal, G.M., Shiklomanov, A.I. & Lammers, R.B. 2007 Rising minimum daily flows in northern Eurasian rivers: A growing influence of groundwater in the high-latitude hydrological cycle. *J. Geophys. Res.* 112, G04S47, doi: 10.1029/2006JG000327.

Spence, C. 2006 Hydrological processes and streamflow in a lake dominated water course. *Hydrological Processes* 20, 3665–3681.

Spence, C., Kokelj, S.V. & Ehsanzadeh, E. 2011 Precipitation trends contribute to streamflow regime shifts in northern Canada. In: Yang, D., Marsh, P. & Gelfan, A. (eds.), *Cold Region Hydrology in a Changing Climate,* IAHS Publ. No. 346, 3–8.

Spence, C. & Rausch, J. 2005 Autumn synoptic conditions and rainfall in the subarctic Canadian Shield of the Northwest Territories, Canada. *International J. Climatology* 25, 1493–1506.

Spence, C. & Woo, M.K. 2003 Hydrology of subarctic Canadian Shield: Soil filled valleys. *Journal of Hydrology* 279, 151–166.

St. Jacques, J.M. & Sauchyn, D.J. 2009 Increasing winter baseflow and mean annual streamflow from possible permafrost thawing in the Northwest Territories, Canada. *Geophys. Res. Lett.* 36, L01401, doi: 10.1029/2008GL035822.

Walvoord, M.A. & Streigl, R.G. 2007 Increased groundwater to stream discharge from permafrost thawing in the Yukon River basin: Potential impacts on lateral export of carbon and nitrogen. *Geophys. Res. Lett.* 34, L12402, doi: 10.029/2007GL030216.

Wels, C., Cornett, R.J. & Lazerta, B.D. 1991 Hydrograph separation: A comparison of geochemical and isotopic tracers. *Journal of Hydrology* 122, 253–274.

Wolfe, S.A 1998 *Living with Frozen Ground: A Field Guide to permafrost in Yellowknife, Northwest Territories*. Geological Survey of Canada Misc. Report 64, 71 pp.

Water Balance Calculation over Surface Water Storage in the Dry Interior Climate of the Athabasca River Region in Western Canada: A CROCWR Component

G. S. Walker[1*], T. D. Prowse[1,2], Y. B. Dibike[2], and B. R. Bonsal[3]

[1]*Water and Climate Impacts Research Centre (W-CIRC), Department of Geography, University of Victoria, Victoria, BC, V8W 3R4, CANADA*
[2] *W-CIRC, Environment Canada, University of Victoria, Victoria, BC, V8W 3R4, CANADA*
[3] *National Hydrology Research Centre, Environment Canada, Saskatoon, SK, S7N 3H5, CANADA*
**Corresponding author's email: walkerg@uvic.ca*

ABSTRACT
The volume of water stored on the earth's surface is controlled in part by global climate. As average temperatures increase, the water cycle is expected to intensify, increasing average global water vapour, precipitation, and evaporation, and altering the spatial and temporal distribution of Earth's water. As part of a broader study assessing the Climatic Redistribution of Canada's Water Resources: Western Canada (CROCWR: WC), this paper evaluates the impacts that changing climatic inputs and outputs from a catchment will have on the remainder water balance term—water stored in lakes and reservoirs. While regional climate models (RCMs) can be used to project possible future climate conditions, the water balance of small lakes cannot be assessed directly through RCMs as the models do not include small-scale heat storage. Therefore, a thermodynamic lake model, MyLake, is used to model the water balance representative of lakes of different depths in the Athabasca River catchment of northern Alberta, Canada. Climate variables from the North American Regional Reanalysis (NARR) dataset for the baseline period of 1979–1999 are used to correct the biases of the corresponding climate variables from an ensemble of RCMs, which are then used to run MyLake for current and future periods. The project will help clarify how climate change may alter the water balance, affecting flood cycles and drought frequencies, specifically in hydroclimatic regimes sensitive to climate extremes such as a dry high-latitude interior climate in western Canada.

KEYWORDS
Water balance; Athabasca River; regional climate model; precipitation; evaporation

1. INTRODUCTION
It is recognized that global climate warming is causing an intensification of the hydrologic cycle (i.e., Huntington 2006; Prowse 2009). This intensification results not only in an increase in globally averaged precipitation, evaporation, and mean water vapour, but also in dramatic changes to the temporal and spatial distribution of the planet's water, in the form of extreme events (Meehl et al. 2007). At local and regional scales, a change in the occurrence and intensity of extreme precipitation and evaporation events can have significant consequences, such as on natural and anthropogenic storage of freshwater on the land surface. This paper uses current and future modeled climate scenarios and an offline lake model, MyLake, to evaluate how future changes in the regional patterns of precipitation and evaporation will affect surface freshwater in the high-latitude dry interior climate of northern Alberta, Canada.

2. STUDY SITE

The Athabasca River watershed is located in the interior plains of northern Alberta, Canada, a dry high-latitude climate in the major cold-region portion of North America (Alberta Environment 2013; Dibike et al. 2011a). The study region (the "Athabasca River region") is the downstream, northern portion of the watershed (see Figure 1), located in the lee of the Canadian cordillera, south of the discontinuous permafrost zone of the Canadian subarctic (Peters et al. 2006) and north of the Palliser Triangle, the driest part of the Canadian prairies (Dale-Burnett 2012). The region experiences high natural hydro-climatic variability, with long cold winters, short cool summers and highly variable precipitation that peaks in July and is largely delivered by high-intensity, short-duration convective storms (Environment Canada 2013). This hydro-climatically variable, drought-prone climate increases the impacts that any changes in precipitation and temperature regimes would have on the region.

Figure 1: Image of western Canada; the box shows the Athabasca region in northern Alberta and the Fort McMurray and Fort Chipewyan study sites (Google Earth 2013).

2.1 Study Basins

The specific study sites for this project each consist of a theoretical 1st order lake basin with dimensions based on average sizes of naturally occurring or anthropogenic (existing or proposed) lakes in the region. The "intermediate-depth" and "deep" basins are theoretically located near Fort McMurray, AB (56.72°N, 111.37°W) and the "shallow" basin is theoretically located 220 km further north near Fort Chipewyan, AB (58.77°N, 111.13°W), on the edge of the PAD. Table 1 shows the surface area and depth of each study basin, which are described in more detail below.

The shallow basin is representative of a shallow perched (elevated) lake in the Peace-Athabasca Delta (PAD), of which there are over 1000 less than 1.5 m deep. These perched basins are only connected hydrologically when the Peace River stage rises higher than that of the delta lakes and flow reverses into the delta (Peters et al. 2006). The intermediate-depth is representative of End Pit Lakes (EPLs). End Pit Lakes (EPLs) are artificial lakes designed to store and promote the degradation of toxic residual organic compounds found in tailings disposed of by the oil sands industry (Golder Associates Ltd. 2011). Located in oil sands post-mining pits, these lakes are designed to be reclamation tools that are expected to become permanent fixtures in the post-oil sands landscape (Golder Associates Ltd. 2006; Westcott & Watson 2007). Modeling efforts by Golder Associates Ltd. (2006) have determined that the ideal EPL should be at least 50 m deep

with a small surface area around 1–4 km^2 in order to remain stratified, keeping the contaminated materials from mixing with the clean freshwater cap. The deep basin is representative of off-stream storage of freshwater by industry. Water requirements of the oil sand mines do not vary much over a year, whereas the river has seasonal cycles of flows (Westcott 2007). To protect the river's aquatic ecosystem, regulations are being developed that may require water license holders to offset their withdrawals from the river at certain times with stored water (Ohlson et al. 2010).

Table 1: Study basin sizes are based on similar lakes in the Athabasca River region.

Study Basin	Depth	Surface Area	Represents	Theoretical Location
Shallow	1.5 m	20 km^2	PAD perched basins	Fort Chipewyan. AB
Intermediate-depth	50 m	4 km^2	End Pit Lakes	Fort McMurray, AB
Deep	100 m	50 km^2	Off-stream industrial storage	Fort McMurray, AB

3. METHODS

3.1 Water Balance Method

To evaluate the impact of changing climate on water resources, the nature of both current, and projected future, hydrologic cycle in a watershed is assessed (Kane & Yang 2004). Calculating the *water balance* is one way to quantify the water in all hydrologic phases within a defined catchment (Deitch et al. 2009). In this study, the current and future water balance will be calculated for 1st order study catchments based on the water balance equation,

$$P - E = \Delta S,$$

where P = precipitation, E = evaporation, and ΔS = change in freshwater storage. *Storage* refers to the water held on the landscape for longer than the temporal scale of the model, in this case the water held in the theoretical lakes that encompass the entirety of each study catchment.

The simple water balance equation was chosen based on the goal of the proposed study as well as the scale of the study catchments. Stream inflow and outflow are excluded from the equation, since the study basins are of first order and therefore have only negligible inputs and outputs from the land and streams. This is especially true within the shallow study basin representative of the PAD, where the low relief means negligible intermediate flows between basins (Nielsen 1972). Leaving inflows and outflows out of the equation also serves to not conflate the effects of climate change on streamflow as opposed to on water storage. Furthermore, the mesoscale of the proposed regional modeling allows the exclusion of more specific parameters representing temporally or spatially large-scale processes, such as groundwater fluxes, soil moisture fluxes, and sublimation and condensation.

3.2 Current and Future Climate Data

Meteorological climate data required to model the water balance includes cloud cover fraction, relative humidity, surface pressure, wind speed, temperature and precipitation. These climate variables for both the current (1971–1999) and future (2041–2069) periods were extracted from regional climate models (RCMs) nested within atmosphere-ocean global climate models (AOGCMs) provided by the North American Regional Climate Change Assessment Program (NARCCAP). The NARCCAP models simulate climate over the United States and most of Canada with observations at a 50 km resolution every three hours. The models were run using

the Intergovernmental Panel on Climate Change (IPCC) SRES A2 emissions scenario for the 21st century, chosen since it was one of the IPCC's "marker" scenarios (Mearns et al. 2009; UCAR 2007). The A2 scenario family is characterized by an increasing human population, high greenhouse gas emissions, and slow adaptation to new technologies and mitigation strategies, relative to other SRES scenarios (Nakicenovic et al. 2000).

Data for all six climate variables were extracted for the current and future periods from the nine closest grid cells to Fort Chipewyan (shallow study basin) and Fort McMurray (intermediate-depth and deep study basins), from four of the available twelve AOGCM-nested RCMs (model selection based on data availability; see Table 2). Wind speed data were calculated as the hypotenuse of vertical and horizontal *u* and *v* wind variables, and relative humidity was calculated from specific humidity, using pressure, temperature and partial pressure of water vapour (Nievinski 2009). The data were then averaged temporally and spatially to create a daily dataset for current and future representing approximately 8750 km^2 surrounding each of the study basins.

Table 2: Four AOGCM-nested RCMs were used in this study, as indicated by the acronyms in the body of the table.

	Regional Climate Models (RCMs)	
Atmosphere-Ocean Global Climate Models (AOGCMs)	Canadian Regional Climate Model (**CRCM**)	Regional Climate Model version 3 (**RCM3**)
Community Climate Model v.3 (**CCSM3**)	**CRCM_CCSM**	----
Canadian Global Climate Model v.3 at the T47 spatial resolution (**CGCM3**)	**CRCM_CGCM3**	**RCM3_CGCM3**
Geophysical Fluid Dynamics Laboratory Climate Model 2.1 (**GFDL**)	----	**RCM3_GFDL**

3.2.1 Bias correction

Climate model outputs cannot be used to obtain realistic outputs from secondary models without some sort of prior bias correction (Piani et al. 2010). Since changes in the variability and extremes of climate variables are being examined, the often used "delta method" of bias correction in which modeled changes between current and future climate are applied to the observed climate may not be appropriate for this analysis (Lenderink et al. 2007). Instead, absolute future climate simulations are used, with bias correction to correct any systematic model errors by scaling the output variables. An interpolated average monthly bias correction factor is used, The ensemble modeling approach used in this analysis also smoothes out bias from each of the NARCCAP models and provides a range of results to study a range of responses of the water balance to climate change (Randall et al. 2007).

Bias correction factors for all six climate variables (cloud cover, relative humidity, surface pressure, wind speed, temperature and precipitation) from each of the four NARCCAP models were created by comparing the long-term daily mean for each month from the current model data (1979–1999) to the same average over the same time period from the North American Regional Reanalysis (NARR) dataset, which is considered representative of the true current climate (Mesinger et al. 2006). Climate variables corresponding to those used from the NARCCAP models were extracted from the twelve NARR grid points closest to Fort McMurray and Fort Chipewyan and averaged temporally and spatially to get daily datasets covering approximately 6650 km^2 centered on the two study basin locations.

The bias correction factors were calculated by dividing the monthly NARCCAP means by the monthly NARR means, or subtracting the NARCCAP mean from the NARR mean, in the case of temperature, resulting in a value that represents the difference between the climate as it actually occurred and the values produced by the NARCCAP models. The precipitation bias correction factors were calculated based on wet days only (>0.01 mm/day). The bias correction factors were then applied to the full daily datasets of the current and future climate variables from each model. A multiplicative function was used for all variables except temperature, which used an additive function in order to ensure that the daily minimum never exceeds the daily maximum (Ahmed 2011; Lenderink et al. 2007; Teutschbein & Seibert 2010). The equations used for bias correction are as follows, where NARR represents observed climate and NARCCAP is the simulated climate.

For temperature, $T_{BiasCorrected} = T_{NARCCAP} + (T_{NARR} - T_{NARCCAP})$, (1)

where the correction factor is $T_{CF} = T_{NARR} - T_{NARCCAP}$. (2)

For cloud cover, relative humidity, surface pressure, wind speed, and precipitation ("Var"),

$Var_{BiasCorrected} = Var_{NARCCAP} \div \left(\frac{Var_{NARR}}{Var_{NARCCAP}}\right)$, (3)

where the correction factor is $Var_{CF} = \left(\frac{Var_{NARR}}{Var_{NARCCAP}}\right)$. (4)

3.3 Evaporation Modeling

Current global and regional climate models do not include modeling of land surfaces that include water bodies more than a few meters deep (Meehl et al. 2007). Radiative and turbulent fluxes, which represent the link between the earth's surface and the atmosphere, are impacted by the storage of heat within deep water (Henderson-Sellers 2006; Swayne et al. 2005). If these are not modeled correctly, estimations of evaporation, wind forcing, and energy fluxes will be affected (Swayne et al. 2005). This study addresses the heat storage problem by modeling evaporation for the study catchments using an offline specialized model, MyLake.

3.3.1 MyLake

MyLake is a one-dimensional, process-based, comprehensive lake model that simulates the vertical distribution of lake water temperature. The model takes into account the effects of heat storage and ice-cover dynamics on the components of the water balance (Saloranta & Andersen 2004), and therefore can be used to estimate evaporation in catchments with significant surface water storages such as the three study basins. The model has been shown to produce accurate water temperature profiles for a variety of Northern Hemisphere lakes and is therefore deemed applicable to the study site of northern Alberta (see Dibike et al. 2011a; Dibike et al. 2011b; Saloranta & Andersen 2007; Saloranta et al. 2009).

The MyLake simulations for the three study basins were run at the model's fixed daily (24 hour) timestep, using bias corrected daily meteorological climate input data on cloud cover (%), surface pressure (hPa), relative humidity (%), surface temperature (°C), precipitation (mm/day), and windspeed (m/s,) from the CRCM CCSM, CRCM CGCM3, RCM3 CGCM3 and RCM3 GFDL NARCCAP models, as described above. Each MyLake scenario (four climate models for each of the three study basins) was run for the communal date ranges of January 1, 1971–November 30, 1999, for the current period, and January 1, 2041–November 30, 2069, for the

future (the last Decembers were excluded due to missing data). The only exception is that cloud cover data from the CRCM CCSM model were used for both the RCM3 CGCM3 and RCM3 GFDL model runs. For each study basin, a depth and a starting surface area was assigned (see Table 1), and a series of horizontally homogeneous vertical layers were defined, each being 0.5 m thick with a surface area decreasing to zero at the bottom layer (except for the shallow 1.5 m basin, which only decreases from 20 km^2 to 5 km^2).

3.3.2 MyLake's estimation of evaporation

Evaporation was calculated by MyLake, using Matlab's Air-Sea toolbox to calculate sensible and latent heat fluxes from the meteorological input data and the depth of the lake (USGS 2013). First, the heat of vaporization (*Le*) [J/kg] over the lake is calculated using:

$$Le = (2.501 - 0.00237 * Ts) * 10^6; \quad (5)$$

where *Ts* is the water surface temperature [°C], and 2.501 is the energy [MJ/kg] needed to convert liquid water to vapour at 0°C, modified as the air temperature changes (Oke 1987).

The latent heat flux (H_l) [W/m^2] into the lake is then calculated using *Le*, by:

$$H_l = rho * Le * U_{star} * Q_{star}; \quad (6)$$

where $rho = 100 * Pa/gas\_const\_R * Tv$, using air pressure (*Pa)*, the gas constant for dry air ($gas\_const\_R = 287.1$ J/kg/K), and the air virtual temperature (*Tv*).

$U_{star} = cdnhf * S$ (7) is based on the velocity friction scale [m/s] and calculated using wind speed, surface drag and gustiness values. $Q_{star} = cqnhf * Dq$ (8) is calculated using air pressure and humidity values as well as surface temperature. See Fairall et al. (1996) and Smith (1988) for more details.

Webb et al. (1980) proposed a correction to the calculation of latent heat flux to account for the slightly higher velocity of ascending versus descending parcels of air. This "Webb effect" is corrected by adding a small mean vertical velocity to the latent heat (H_l) to keep the net dry mass flux equal to zero (Fairall et al. 1996). The Webb correction (H_{l_webb}) is calculated by:

$$H_{l\_webb} = rho * Le * W * Q; \quad \text{(Fairall et al. 1996: Eq. 22, p. 3751) (9)}$$

where *rho* is a constant, *Le* is the heat of vaporization, both described above, *W* is calculated using the velocity friction (U_{star}) and humidity (Q_{star}) scales, as well as the temperature scale (T_{star}), and *Q* is the specific humidity of air.

The Webb correction is added to the latent heat flux, resulting in a corrected latent heat flux for the lake (Fairall et al. 1996):

$$Hl\_webb\_corrected = Hl + Hl\_webb \quad (10)$$

Finally, evaporation is calculated by dividing the available heat flux in the lake by the heat of vaporization required to evaporate freshwater:

$$Evaporation = Hl\_webb\_corrected \,/\, Le; \quad (11)$$

resulting in units of $kg * s^{-1} * m^{-2}$, which can be converted to an evaporation rate in standard $mm * d^{-1}$ units using the density of water (10^3 kg/m^3) to replace 1 kg/m^2 of water with a 1 mm-deep layer of water.

4. PRELIMINARY RESULTS AND DISCUSSION

4.1 Bias Correction Factors

Bias correction was required on all climate variables, since the null hypothesis—that there was no difference in the mean of the NARCCAP modeled data and the mean of the NARR data—was rejected for surface pressure, wind speed, relative humidity and temperature. Figure 2 shows the resulting bias correction factors.

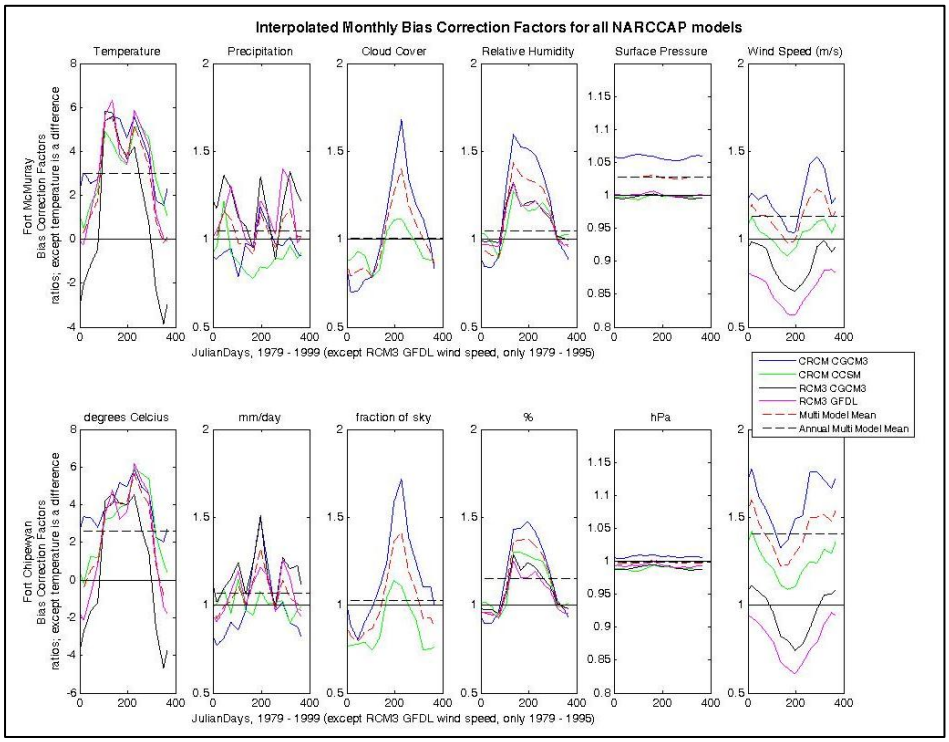

Figure 2: Bias correction factors for the NARCCAP models (CRCM CGCM3, CRCM CCSM, RCM3 CGCM3, and RCM3 GFDL), the multi-model mean for each variable, and the single value multi-model mean over all years for each variable.

At the Fort McMurray study site the bias correction factors range from the largest decrease on the corresponding climate variable of 0.57 (wind, RCM3 GFDL) to the largest increase of 1.68 (cloud, CRCM CCSM), across all models, for all variables except temperature. The average annual multi-model mean (see dashed, horizontal lines in Figure 2) for precipitation was 1.05, cloud cover 1.0, pressure 1.03, relative humidity 1.15, wind speed 1.13, making the average multiplicative correction factor at Fort McMurray across all models and all variables except temperature 1.08. For temperature at Fort McMurray, the bias correction ranges from subtracting 3.84°C (RCM3 CGCM3) from the current and future data records, to adding 6.34°C (RCM3 GFDL) to the data records, with the average correction factor across the year being an increase of 2.98°C across the models.

At the Fort Chipewyan study site the bias correction factors range from the largest decrease on the corresponding climate variables of 0.61 (wind, RCM3 GFDL, same as at Fort McMurray) to the largest increase of 1.77 (wind, CRCM CGCM3; same model, different variable than Fort McMurray), across all models, for all variables except temperature. The average annual multi-model mean for precipitation was 1.07, cloud cover 1.02, pressure 0.99, relative humidity 1.15

and for wind speed was 1.4, making the average multiplicative correction factor at Fort Chipewyan across all models and all variables except temperature 1.13. For temperature at Fort Chipewyan, the bias correction ranges from subtracting 4.66°C (RCM3 CGCM3, as at Fort McMurray) to adding 6.18°C (RCM3 GFDL, as at Fort McMurray), and the average correction factor across the year was an increase of 2.62°C. Therefore, the multiplicative bias correction factor is slightly less at Fort McMurray than the correction required at Fort Chipewyan, whereas the average temperature correction at Fort McMurray is slightly less than at Fort Chipewyan.

Based on the bias correction factors, the cloud cover and pressure variables are best modeled (least correction) by the ensemble of NARCCAP climate models, and the temperature variable was the least accurate simulation (most correction). While further analysis is required, initial inspection of the bias correction factors leads to the conclusion that the CRCM CGCM3 model is the most accurate simulation of the current climate and the RCM3 CGCM3 model is the least accurate simulation of the current climate.

4.2 Current and Future Evaporation

Average daily evaporation was modeled by MyLake using bias corrected climate data from NARCCAP for the current (1971–1999) and future (2041–2069) periods. See Figure 3 for results from both periods overlain to show differences. For all three lake depths, evaporation is projected to be higher in the future during the summer months (May–August; Julian days 122 to 244) than in the current period. In the summer, the rising limb is earlier and rises to a higher peak for all depths of lake, the greatest difference being over the shallow lake at Fort Chipewyan. Future evaporation rates remain higher throughout the summer months and then begin to match the current period more closely in the fall (Julian days 245–365), finally matching or falling slightly below current evaporation in the spring (Julian days 0–121). While the range of climate models in the current and future periods overlap each other, the multi-model means clearly show the prediction of greater future evaporation in the summer, and less in the winter, than in the current period.

4.3 Current and Future Water Balance

The simulation of the current and future water balances are shown in Figure 4. Precipitation is predicted to stay at a similar scale in the late 21st century as it was in the late 20th century, while future evaporation is expected to be higher in the summer months and similar or lower in the winter months than current patterns, as described above. The difference between incoming precipitation rates and outgoing evaporation rates above the shallow, intermediate depth, and deep lakes studied is shown by the current and future change in storage values, also seen in Figure 4. It is expected that slightly less loss of water volume will occur in the fall, winter, and spring months (approximately Julian days 0–121 and 245–365) than in the summer months, when higher temperatures in the future drive higher evaporation than currently occurs. This subjective analysis is the first step in comparing the current and future water balances. Future work will contain a more detailed analysis of the response of the Fort McMurray and Fort Chipewyan water balances to future climate.

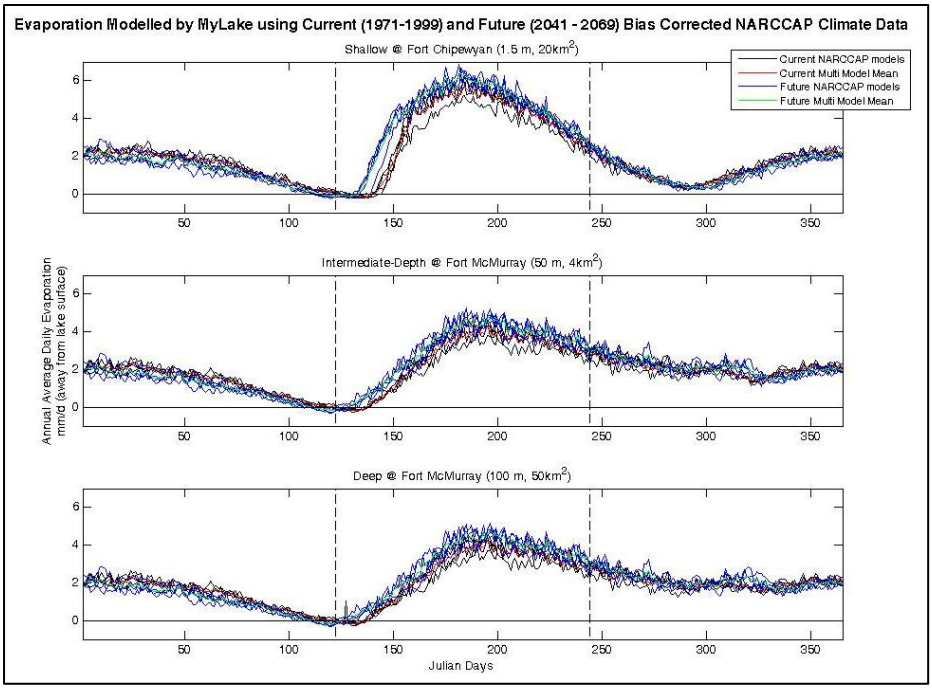

Figure 3: Evaporation in the current (1971–1999) and future (2041–2069) periods from MyLake, based on bias corrected climate data from four NARCCAP models (CRCM CCSM, CRCM CGCM3, RCM3 CGCM3 and RCM3 GFDL). Summer is delineated by dashed vertical lines at May 1st (Julian day 122) and August 31st (Julian day 244).

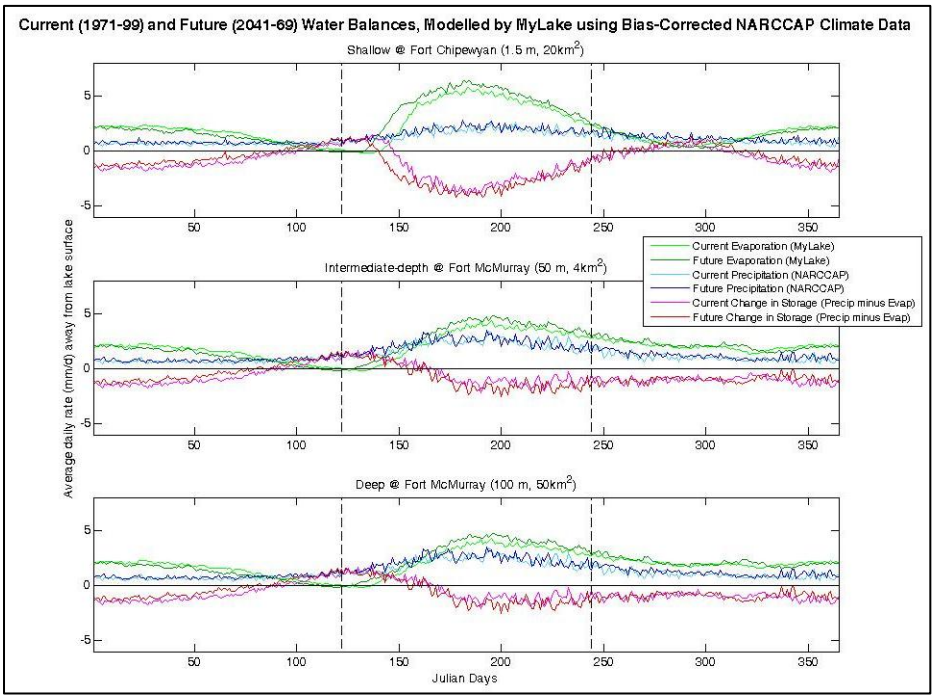

Figure 4: Water balance over the shallow, intermediate-depth, and deep study basins. The change in storage was calculating by subtracting the evaporation (mm/d away from the lake surface) from the precipitation amount (mm/d). Vertical lines delineate summer as in Figure 3.

5. CONCLUSION AND FUTURE WORK

The water balances modeled using bias-corrected regional climate model data to run the MyLake lake model show that if climate changes from the current late 20th century patterns to the patterns predicted by the ensemble of NARCCAP climate models run using the IPCC's A2 SRES future scenario for the late 21st century, there will be changes in the amount of evaporation leaving all depths of lakes in the dry interior climate of northern Alberta, Canada. This paper summarizes the initial work required to correct for model bias in the NARCCAP climate variables and to model the water balances for the current and future period. Future work will include a more in-depth analysis of the evaporation and water balance average annual results, as well as an analysis of extreme events throughout the full data record. This will provide information on how the intensification of the water cycle due to climate change may impact freshwater stored on the earth's surface in western Canada, and will compliment other work being done to assess changes in the water cycle under the Climatic Redistribution of Canada's Water Resources: Western Canada (CROCWR: WC) project.

REFERENCES

Ahmed, K.F. 2011 *Bias Correction and Downscaling of Climate Model Outputs Required for Impact Assessments of Climate Change in the U.S. Northeast*. Masters Thesis, University of Conneticut. Paper 212, http://digitalcommons.uconn.edu/gs_theses/212.

Dale-Burnett, L. 2012 Palliser Triangle. *The Encyclopedia of Saskatchewan*. Retrieved May 1, 2012 from http://esask.uregina.ca/entry/palliser_triangle.html.

Deitch, M.J., Kondolf, G.M. & Merenlender, A.M. 2009 Surface water balance to evaluate the hydrological impacts of small instream diversions and application to the Russian River basin, California, USA. *Aquatic Conservation: Marine and Freshwater Ecosystems* 19, 274–284.

Alberta Environment and Sustainable Development 2013 Bedrock Geology. Retrieved June 5, 2013, from http://environment.alberta.ca/02189.html.

Dibike, Y.B., Prowse, T.D., Bonsal, B.R., De Rham, L.P. & Saloranta, T.M. 2011a Simulation of North American lake-ice cover characteristics under contemporary and future climate conditions. *Int. J. of Climatology*. Available online: wileyonlinelibrary.com, doi: 10.1002/joc.2300

Dibike, Y.B., Prowse, T.D., Saloranta, T.M. & Ahmed, R. 2011b Response of Northern Hemisphere lake-ice cover and lake-water thermal structure patterns to a changing climate. *Hydrological Processes* 25, 2942–2953.

Environment Canada 2013 Canada's National Climate Data and Information Archive. Retrieved May 20, 2013, from http://climate.weatheroffice.gc.ca/climateData/canada_e.html.

Fairall, C.W., Bradley, E.F., Rogers, D.P., Edson, J.B. & Young, G.S. 1996 Bulk parameterization of air-sea fluxes for Tropical Ocean-Global Atmosphere Coupled-Ocean Atmosphere Response Experiment difference relative analysis. 101, 3747–3764.

Golder Associates Ltd. 2006 *Phase II 2005/2006 Pit Lake Work Plan*. For the Cumulative Envrionmental Management Association (CEMA) Reclamation Working Group, contract #2004-0017 (pp. 15).

Golder Associates Ltd. 2011 *Draft Report: CEMA Oil Sands Pit Lake Model*. For the Cumulative Environmental Management Association (CEMA) Reclamation Working Group, report number 09-1336-1008, Calgary, AB (pp. 86).

Google Earth 2013 Google Earth version 5.1.3533.1731, build date Nov 12, 2009.

Henderson-Sellers, A. 2006 Improving land-surface parameterization schemes using stable water isotopes: Introducing the "iPILPS" initiative. *Global and Planetary Change* 51, 3–24.

Huntington, T. 2006 Evidence for intensification of the global water cycle: Review and synthesis. *Journal of Hydrology* 319, 83–95.

Kane, D.L. & Yang, D. 2004 Overview of water balance determinations for high latitude watersheds. *Northern Research Basins Water Balance Workshop held in Victoria, BC, March 2004.* IAHS-AISH Publication 290, 1–12. Victoria, BC.

Lenderink, G., Buishand, A. & Van Deursen, W. 2007 Estimates of future discharges of the river Rhine using two scenario methodologies: Direct versus delta approach. *Hydrology and Earth System Sciences* 11, 1145–1159.

Mearns, L.O., Gutowski, W.J., Jones, R., Leung, L.-Y., McGinnis, S., Nunes, A.M.B. & Qian, Y. 2009 A regional climate change assessment program for North America. *EOS* 90, 311–312.

Meehl, G.A., Stocker, T.F., Collins, W.D., Friedlingstein, P., Gaye, A.T., Gregory, J.M., Kitoh, A. et al. 2007 Global Climate Projections. In: Solomon, S., Qin, D., Manning, M., Chen, Z., Marquis, M., Averyt, K.B., Tignor, M. et al. (eds.), *Climate Change 2007: The Physical Science Basis. Contribution of Working Group I to the 4th Assessment Report of the Intergovernmental Panel on Climate Change* (pp. 100). Cambridge University Press, Cambridge, UK, and NY, USA.

Mesinger, F., DiMego, G., Kalnay, E., Mitchell, K., Shafran, P.C., Ebisuzaki, W., Jović, D. et al. 2006 North American regional reanalysis. *Bulletin of the American Meteorological Society* 87, 343–360.

Nakicenovic, N., Alcamo, J., Davis, G., Vries, B. de, Fenhann, J., Gaffin, S., Gregory, K. et al. 2000 *Special Report on Emissions Scenarios. A Special Report of Working Group III of the International Panel on Climate Change (IPCC).* (N. Nakicenovic & R. Swart, eds.) (pp. 599). Cambridge University Press, Cambridge, UK.

Nievinski, F.G. 2009 *Humidity conversion*, Appendix IV in *Ray-tracing Options to Mitigate the Neutral Atmosphere Delay in GPS*. Masters of Science in Engineering Thesis, Department of Geodesy and Geomatics Engineering Technical Report No. 262, University of New Brunswick, Fredericton, New Brunswick, Canada (pp. 232).

Ohlson, D., Long, G. & Hatfield, T. 2010 *Phase 2 Framework Committee Report. Final report of the Phase 2 Framework Committee (P2FC)* (p. 238).

Oke, T.R. 1987 *Boundary Layer Climates* (2nd Ed., pp. 435). Routledge, NY.

Peters, D.L., Prowse, T.D., Marsh, P., Lafleur, P.M. & Buttle, J.M. 2006 Persistence of water within perched basins of the Peace-Athabasca Delta, Northern Canada. *Wetlands Ecology and Management* 14, 221–243.

Piani, C., Haerter, J.O. & Coppola, E. 2010 Statistical bias correction for daily precipitation in regional climate models over Europe. *Theoretical and Applied Climatology* 99, 187–192.

Prowse, T.D. 2009 Introduction: hydrologic effects of a shrinking cryosphere. *Hydrological Processes* 23, 1–6.

Randall, D.A., Wood, R.A., Bony, S., Colman, R., Fichefet, T., Fyfe, J., Kattsov, V. et al. 2007 Climate Models and Their Evaluation. In S. Solomon, D. Qin, M. Manning, Z. Chen, M. Marquis, K.B. Averyt, M. Tignor et al. (eds.), *Climate Change 2007: The Physical Science Basis. Contribution of Working Group I to the 4th Assessment Report of the Intergovernmental Panel on Climate Change* (pp. 74). Cambridge University Press, Cambridge, UK, and NY, USA.

Saloranta, T. & Andersen, T. 2004 *MyLake (v.1.1): Technical Model Documentation and User's Guide*. NIVA Report 4838. (pp. 44). Oslo, Norway.

Saloranta, T. & Andersen, T. 2007 MyLake—A multi-year lake simulation model code suitable for uncertainty and sensitivity analysis simulations. *Ecological Modelling* 207, 45–60.

Saloranta, T.M., Forsius, M., Järvinen, M. & Arvola, L. 2009 Impacts of projected climate change on the thermodynamics of a shallow and a deep lake in Finland: model simulations and Bayesian uncertainty analysis. *Hydrology Research* 40, 234–248.

Smith, S.D. 1988 Coefficients for sea surface wind stress, heat flux, and wind profiles as a function of wind speed and temperature, *J. Geophys. Res.: Oceans* 93, 467–472.

Swayne, D., Lam, D., MacKay, M., Rouse, W. & Schertzer, W. 2005 Assessment of the interaction between the Canadian Regional Climate Model and lake thermal–hydrodynamic models. *Environmental Modelling & Software* 20, 1505–1513.

Teutschbein, C. & Seibert, J. 2010 Regional climate models for hydrological impact studies at the catchment scale: A review of recent modeling strategies. *Geography Compass* 4, 834–860.

U.S. Geological Survey. 2013 SEA-MAT: Matlab Tools for Oceanographic Analysis. Air-Sea Toolbox. Retrieved April 22, 2013, from http://woodshole.er.usgs.gov/operations/sea-mat/index.html

University Corporation for Atmospheric Research (UCAR) 2007 North American Regional Climate Change Assessment Program (NARCCAP). Retrieved March 6, 2012, from www.narccap.ucar.edu/

Webb, E.K., Pearman, G.I. & Leuning, R. 1980 Correction of flux measurements for density effects due to heat and water vapour transfer. *Quarterly Journal of the Royal Meteorological Society* 106, 85–100.

Westcott, F. 2007 *Oil Sands End Pit Lakes: A Review to 2007*. Clearwater Environmental Consultants Inc. Project 2006-32 (pp. 42).

Westcott, F. & Watson, L. 2007 *End Pit Lakes Technical Guidance Document.* Prepared by Clearwater Environmental Consultants Inc. for the Cumulative Environmental Management Association (CEMA) End Pit Lakes Subgroup (pp. 51).

Forest Disturbance Effects on Snow and Water Yield in South-Central British Columbia

Rita Winkler[1*], Dave Spittlehouse[2], Sarah Boon[3], and Barbara Zimonick[4]

[1]*BC Ministry of Forests, Lands and Natural Resource Operations, Kamloops, BC, V2C 2T7, CANADA*
[2]*BC Ministry of Forests, Lands and Natural Resource Operations, Victoria, BC, V8W 9C2, CANADA*
[3]*Department of Geography, University of Lethbridge, Lethbridge, AB, T1K 3M4, CANADA*
[4]*Zimonick Enterprises, Kamloops, BC, V2C 5K6, CANADA*
**Corresponding author's email: rita.winkler@gov.bc.ca*

ABSTRACT
Long-term studies at Upper Penticton Creek and Mayson Lake in British Columbia's southern interior are quantifying hydrologic response to natural disturbances and to logging. At Upper Penticton Creek, interannual variability in weather exceeded logging effects until 50% of the treatment watersheds had been clearcut. Then spring high flows occurred earlier, April water yield increased, and June to July yield decreased, in part a result of snowmelt from high elevation clearcuts synchronizing with melt from lower elevations. Over an eight-year period post mountain pine beetle (MPB) attack at Mayson Lake, canopy transmittance in a young pine stand increased by 24%, with the largest change occurring in year four. Snow accumulation was most affected by interannual variability in weather, with changes related directly to MPB attack measurable by year five, when most needles had fallen. The influence of forest cover was greatest in the year of least snowfall, with 41% and 56% lower April 1 snow water equivalent in the pine and mixed species stand than in a clearcut, respectively. As young pine canopy was lost, the timing of snowpack depletion advanced so that by year six, snow disappeared at the same time as in the clearcut. A similar lag in snow response was observed in a nearby burned stand. The results of these projects will improve operational evaluation of hydrologic response to forest disturbance, including retention of beetle-killed stands and salvage logging.

KEYWORDS
Snow; water yield; mountain pine beetle; fire; logging

1. INTRODUCTION
Streamflow from most southern-interior watersheds in British Columbia (BC) is generated by mid- to high-elevation spring snowmelt. Much of this region is forested with lodgepole pine (*Pinus contorta* Dougl.), Engelmann spruce (*Picea engelmannii* Parry), and subalpine fir (*Abies lasiocarpa* (Hook.) Nutt., and is subject to forest cover changes from fire, insect infestations, and logging. Since 1994, 17.5 million ha of lodgepole pine-dominated forest in BC were attacked by mountain pine beetle (MPB), and large areas were salvage harvested. Extensive changes in forest structure, combined with the potential for logging operations to expand into higher elevation forests, raise concern regarding the effects on snow accumulation and ablation, and the potential for associated changes in snowmelt-generated streamflow volume and timing.

Coniferous forest canopy attributes are well correlated with snow accumulation and melt (Varhola et al. 2010), the interrelationships varying with weather, elevation, and aspect (Ellis et al. 2010). Changes in snow accumulation are related to changes in canopy interception and

sublimation losses, while changes in ablation rates result from changes in the short- and long-wave energy balances (Boon 2009; Varhola et al. 2010). Following insect attack in mature stands, increases in SWE of 11% to 21% have been measured, and snowpack depletion has been observed up to one week earlier (Pugh & Small 2011; Winkler et al. 2012).

Changes in snow accumulation and ablation rates, together with changes in summer evaporation, in clearcut areas, generally result in larger spring peak flows and higher annual flows (Stednick 1996; Moore & Wondzell 2005). A comparison of four snow-dominated watersheds in BC and Colorado (Green & Alila 2012) found that once 33%–40% of the watershed had been clearcut, the magnitude of peak flows of a given frequency increased over the full range of return periods. The frequency of peak flows of a given magnitude increased by at least two to three times, depending upon watershed characteristics such as elevation and aspect distribution, size, and slope gradient.

Long-term forest watershed research in interior BC has largely focused on forest-snow interactions and the effects of small (20 ha) distributed clearcuts on water supplies, as well as the mitigative effects of forest regrowth. With extensive post-MPB forest mortality, the focus has changed to understand the consequences of extensive disturbance and the benefits of dead stand retention versus clearcut salvage logging. Additionally, the threat of increased fire occurrence under a changing climate has resulted in a need for post-fire snow data (Westerling et al. 2003). Upper Penticton Creek (UPC) and Mayson Lake (ML) provide the longest records of environmental variables, including snow and water yield, in the southern interior. We combine data from both sites to quantify the effects of natural disturbance (MPB and fire) on snow processes and the potential effects of logging on water yield.

This paper summarises the effect of 50% clearcut logging on water yield and snow accumulation and ablation at UPC. At ML, we describe snow response to natural disturbance for eight years post-MPB attack and five years post-wildfire relative to clearcutting. The results of this research will provide information useful to forest planners and hydrologists assessing the potential consequences of various forest management options on water supplies.

2. STUDY AREA AND METHODS

2.1 Study Sites

Upper Penticton Creek and ML are located on the Thompson-Okanagan Plateau, in the southern interior of BC (Figure 1); UPC is 26 km northeast of Penticton (49°39′N, 119°24′W, 1600–2140 m a.s.l.) in the Engelmann spruce – subalpine fir biogeoclimatic zone, Okanagan dry cold variant (BC FLNRO 2008). This area receives an average annual precipitation of 700 mm, of which approximately 60% falls as snow and has a mean annual temperature of 1.8°C (January average minimum -10.5°C; July average maximum 19.5°C). Mayson Lake is approximately 50 km northwest of Kamloops (51°13′N, 120°24′W, 1270 m a.s.l.) in the Montane Spruce zone, North Thompson dry mild variant, has an annual average precipitation of 560 mm, of which approximately 45% falls as snow, and has a mean annual temperature of 2.5°C (January average minimum -11.7°C; July average maximum 22.4°C).

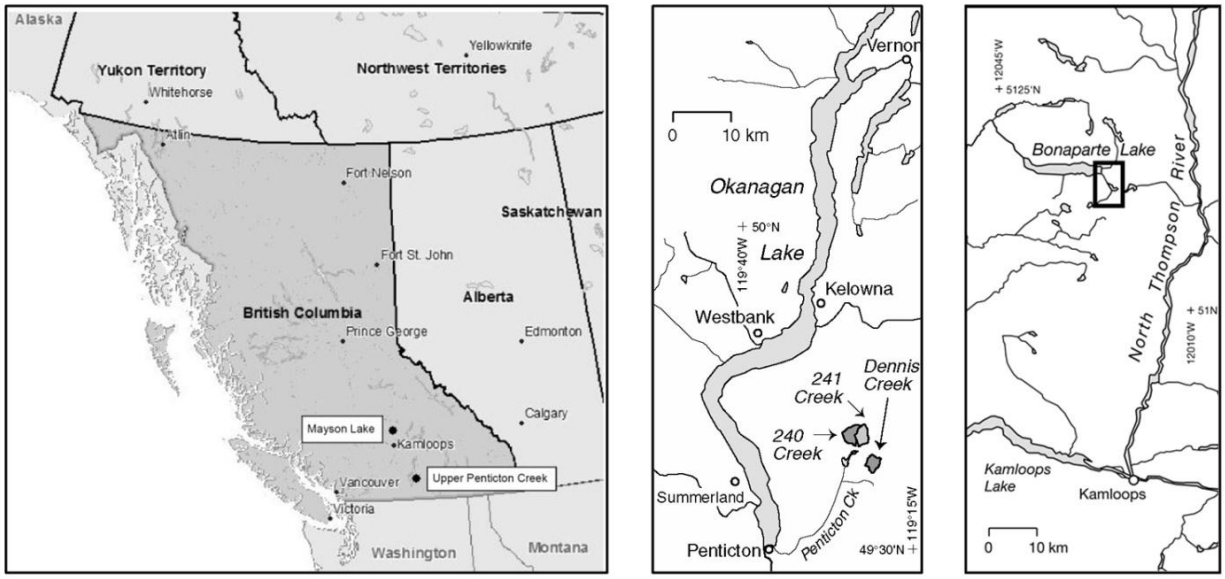

Figure 1: Location of the Upper Penticton Creek watershed experiment (middle) and Mayson Lake research site (right).

The three watersheds comprising the UPC experiment—240, 241, and 242 Creeks—are approximately 5 km^2 in size with gentle to steeply sloping terrain. The area is underlain by coarse-grained granitic rock covered by glacial till and overlain by glacio-fluvial sand and gravel in the lower reaches. Soils are coarse sandy-loam over loamy-sands, low in clay and high in coarse fragments, have a low water-holding capacity, and are well drained. Forest cover is predominantly lodgepole pine in the 240 and 241 Creek watersheds and mixed stands of Engelmann spruce, subalpine fir, and pine in the 242 Creek watershed. Mature trees are >120 years old and up to 26 m tall. The 240 and 241 Creek watersheds have a southerly orientation, and the 242 Creek watershed has a westerly orientation.

The UPC watershed experiment follows a paired watershed before-after control-impact design. No logging occurred between 1985 and 1995 (control period). Logging began during the winter of 1995 in both the 241 and 242 Creek watersheds. Clearcutting was done incrementally with three- to five-year intervening monitoring periods. After final logging in 2007, 50% of both the 241 and 242 Creek watersheds had been clearcut; the 240 Creek watershed remained an uncut control. Pre-logging relationships between the control and treatment streams were used to predict post-logging yield at UPC. Predicted yield was compared with actual flows to determine the magnitude of change.

The MPB study sites at ML are located on gently rolling terrain within 3 km of each other and represent forest cover typical of the region: young (~35 years old) thinned and pruned lodgepole pine (YP), mature mixed Engelmann spruce, subalpine fir and lodgepole pine (MM), and a recent clearcut (CC) (Winkler et al. 2005). In 2006, the main canopy of YP was 12.7 m tall, evenly spaced (1000 stems per hectare – sph) with a canopy transmittance of 27%. In contrast, MM was denser (3631 sph; canopy transmittance 18%), and trees forming the main canopy were much larger (23.4 m tall; basal area 50 m^2/ha vs. 18 m^2/ha in YP). Most lodgepole pine trees >14 cm in diameter at the study sites, and in the region, were attacked by MPB in 2005. Over the study period, 58% of the pine trees in YP and 20% in MM lost all needles and fine canopy material. A detailed description of these sites can be found in Winkler et al. (2012). The burned

site, which was similar to MM prior to the fire, and a nearby clearcut are about 5 km from the MPB sites.

2.2 Data Collection and Analysis

Weather data were collected in clearcut and forest sites at both study locations. Variables include incident and reflected shortwave radiation (LiCor LI200; Eppley B&W pyranometer), air temperature and humidity (2 m) (Vaisala HMP35C), wind speed (3 m) (MetOne 013 cup anemometer; RM Young wind monitor), snow temperature (Type K thermocouples at 0, 0.2, and 0.5 m depth), snow surface temperature (Apogee infrared radiometer), snow depth (Campbell Scientific Inc. SR50A), and rainfall (tipping buckets; and also a standpipe gauge at UPC). Data were recorded on Campbell Scientific Inc. 10X and CR1000 data loggers scanning every minute providing hourly and daily summaries.

Daily and hourly streamflow at UPC is measured by the Water Survey of Canada (http://www.wsc.ec.gc.ca/applications/H2O/index-eng.cfm). Complete records are available for all three streams from 1996 to 2011 (2012 pending), and have been summarised as monthly, annual (October 1 to September 30), and seven-day maximum and minimum water yields.

Snow water equivalent (SWE) was measured at 32 stations arranged in 10–15 m grids in a low (1600 m) and high (1950 m) clearcut and lodgepole pine forest pair of sites at UPC and at each site at ML. Measurements were made within a 1 m radius of each station marker using a standard Federal snow tube. Surveys began on March 1, were repeated on or near April 1, and then continued weekly to biweekly through the melt season. The date of snow depletion was calculated using the average ablation rate measured in the last sampling period with snow cover. Snow water equivalent post-MPB attack was measured from 2006 to 2012; these data are complemented by surveys completed in the same stands prior to attack (2003–2005). This paper includes snow surveys completed at UPC from 2001 to 2012.

Hemispherical photographs were taken at every second snow station at each site under completely overcast skies, near the same date in spring 2007–2012, using a Nikon 4500 camera with a FC-E8 fisheye lens converter at ~1.3 m above the snow surface. Photos were taken and analysed by the same person throughout the study to minimise user bias, using Gap Light Analyser 2.0. The April 1 to May 15 time period was used in determining canopy transmittance, as detailed in Winkler et al. (2012).

Data summaries and statistical analyses were completed using SYSTAT 11, with statistical significance for all tests set to $\alpha = 0.01$. Snow data were not normally distributed in all years, and variances were not equal; thus differences between years and sites were tested using the non-parametric Kruskall-Wallis test.

3. RESULTS AND DISCUSSION

At UPC and ML, precipitation falls mainly as snow from late October until mid-May or mid-April, respectively. By April 1, SWE in the open ranges from 250 to 350 mm at UPC and 200 to 250 mm at ML. The snowpack is usually depleted by early June at UPC and mid-May at ML. At both locations, average daily air temperatures increase from -7°C in January to +5°C during the melt period. Average daily wind speeds vary by less than 10% between years, averaging 2 m/s with maxima of 8 to 12 m/s during the melt period. Solar radiation during melt averages 19.5 $MJ/m^2/d$ at UPC and 17.2 $MJ/m^2/d$ at ML, where melt occurs a month earlier.

At UPC, annual water yield from 240, 241, and 242 Creeks ranges from 0.8 to 3 million m^3/yr from each watershed; 30%–60% of total annual precipitation. The highest daily flows occur in May during mid- to high-elevation snowmelt and can reach 1.5 m^3/s. August through April low flows, sustained by groundwater and rain, are often less than 0.01 m^3/s.

3.1 Changes in Water Yield Following Clearcut Logging

During the pre-treatment period (1986–1995), water yields in 240 Creek (control) were well correlated with yield measured in both 241 and 242 Creeks for annual, April, June to August, October, and maximum and minimum 7-day values (r^2>0.80 and p<0.01) (Table 1). May, September, and maximum daily water yields in 240 Creek were also well correlated with yield in 241 Creek. Water yield measured post-50% clearcut logging was compared with that predicted using the pre-treatment relationships; results are summarised in Table 1.

Table 1: Changes in water yield following clearcut logging of 50% of the area in the 241 and 242 Creek watersheds relative to the unlogged control (240 Creek) at Upper Penticton Creek (shading indicates p<0.01).

	Correlation (r^2) with 240 Cr Pre-Disturbance		Average (SD) Percent Difference from Predicted	
	241 Cr	242 Cr	241 Cr	242 Cr
Percent Logged	**0**	**0**	**50**	**50**
Years of Survey (n)	10	10	4	11
Annual (Oct-Sep) Yield	0.98	0.92	7 (6)	5 (14)
Monthly Yield				
Apr	0.95	0.91 (E)	36 (52)	104 (97)
May	0.91	0.14	28 (26)	
Jun	0.99	0.96	-28 (7)	-20 (11)
Jul	0.93	0.93	-3 (40)	-28 (12)
Aug	0.98	0.59	-12 (18)	
Sep	0.93	0.56	4 (82)	
Oct	0.94	0.87 (E)	62 (32)	8 (28)
Max Daily Yield	0.91 (P)	0.36	7 (8)	
Max 7-Day Yield	0.96	0.84	4 (11)	12 (23)
Min 7-Day Aug-Oct Yield	0.91	0.65	-24 (53)	

P = polynomial, E = log X and log Y, other relationships are linear

In 242 Creek, April water yield increased by >100% from that predicted yield, while in 241 Creek, May water yield increased by 28% over predictions. June water yields decreased by 28% and 20% in 241 and 242 Creeks, respectively. July water yields were also reduced (28%) in 242 Creek. Differences between predicted and actual yield for other periods were not significant.

At UPC, daily streamflow begins to increase in early April in response to snowmelt. At low elevation, April 1 SWE averaged 328 mm (SD = 88) in the clearcut, an increase of 12% (range 0 to 38%) from that in the lodgepole pine forest. In the large south-facing high-elevation clearcut, April 1 SWE averaged 318 mm (SD = 91) or 12% less (range -12% to 9%) than in the adjacent forest. However, as shown in Figure 2, high-elevation snow losses occur prior to this date; thus a portion of the pack has already been depleted. The snowpack completely disappeared on average 10 and 13 days earlier in the clearcut than in the forest at low and high elevations, respectively.

In 2010, snow in the high elevation clearcut disappeared 23 days earlier than in the forest. This was also the year of the largest post-50% logging peak flow event.

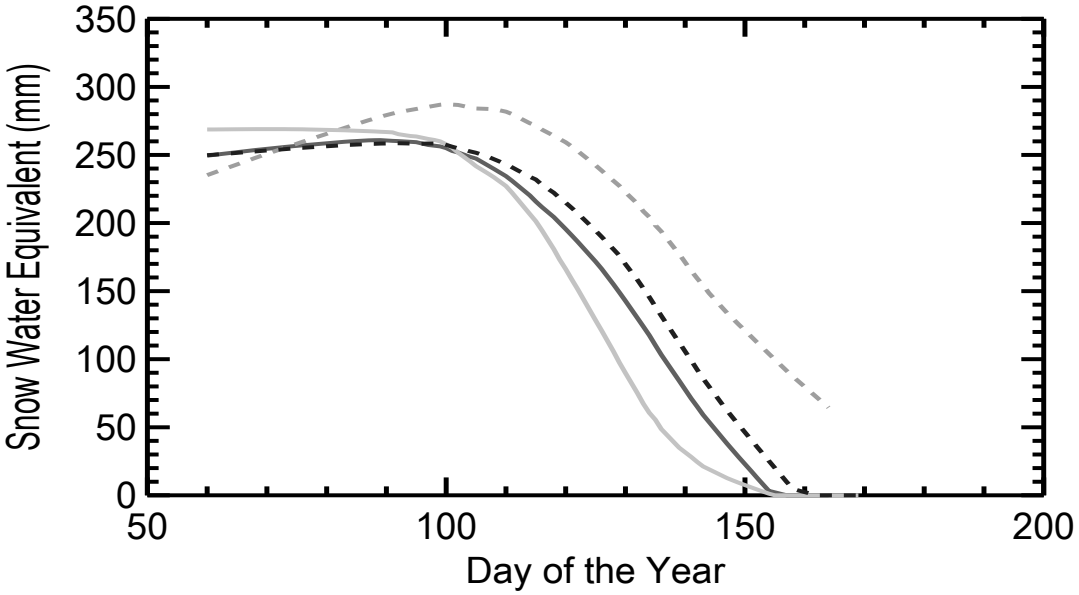

Figure 2: Average snow accumulation and ablation measured since 1995 in a low-elevation clearcut (black, solid) and forest (black, dashed) and in a high-elevation clearcut (grey, solid) and forest (grey, dashed) at Upper Penticton Creek.

Peak streamflows at UPC generally occur during the second half of May. On average by this time, snow in the upper elevation clearcut has been depleted by ~50%. This synchronizes melt contributions from high-elevation openings with melt runoff from low elevations and contributes to the increased spring streamflow magnitudes observed post-50% logging.

Previous studies have also reported significant changes in streamflow from snow-dominated watersheds once >30% of the area was clearcut (Stednick 1996; Moore & Wondzell 2005; Green & Alila 2012). At Camp Creek, in the Okanagan basin, April water yield increased significantly, and the timing of peak flow was significantly advanced relative to the control (Moore & Scott 2005). Using field data and model-derived datasets for three locations in BC and the Fool Creek watershed in Colorado, Green and Alila (2012) found an 11%–35% increase in peak flows once 33%–40% of the watersheds had been clearcut, with the timing of peak flows advanced by up to one week as a result of synchronization of melt from upper and lower elevations.

3.2 Changes in Forest Cover and Snow Following Natural Disturbance

Canopy condition following the 2005 MPB attack at ML changed gradually over a period of three years. Pine trees remained green in 2006, but by spring 2007, 55% of the trees (95% of the main canopy) in YP were red. Heavy needle loss occurred in 2009. By 2011, 58% of the trees (96% of the main canopy) were grey, having lost most needles and other fine canopy material. The green trees, including pine and other species, were mostly in the understory. In MM, 76% of the trees were green in 2006, and the remainder was snags of trees killed in previous insect attacks. By 2011, 53% of the main canopy in MM was grey; however, trees in the understory remained green. With tree mortality and needle loss, canopy transmittance in YP increased from

27% in 2007 to 51% in 2013 (Figure 3). In MM, canopy transmittance remained at 18% over the study period. Tree condition, litter, and canopy transmittance to 2012 are detailed in Winkler et al. (2012).

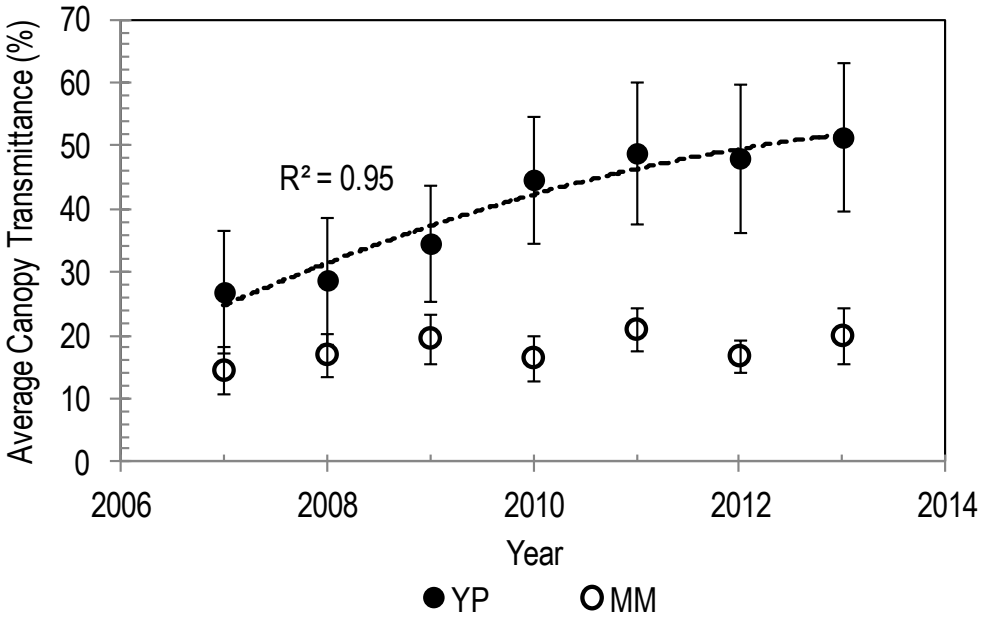

Figure 3: Changes in canopy transmittance with tree condition in a young pine (YP) and mature mixed species (MM) stand after attack by mountain pine beetle at Mayson Lake.

Prior to needlefall (2003–2008), April 1 SWE averaged 31% lower in YP and 35% lower in MM than in CC (Figure 4). The largest difference between the forested sites and CC at ML (46% and 56% less in YP and MM, respectively) occurred in 2010, the year of lowest snowfall. Larger differences in forest versus open SWE during low snow years have also been reported by others (Hedstrom & Pomeroy 1998; Jost et al. 2007; Boon 2011). In the year of highest needlefall (2009), SWE in YP was only 15% less than that in CC. In 2010 and 2011, SWE in YP was 46% and 27% less than in CC, within the range of pre-attack differences. In 2012 and 2013, the difference between YP and CC was only 18% and 14%, respectively. These results suggest a considerable lag between insect attack and snow response. Pugh and Small (2011) also only observed changes in snow accumulation once the trees had reached the "grey" phase.

Prior to MPB attack, snow disappeared a maximum of six days earlier in YP than in CC, as a result of reduced SWE and differences in the short- and long-wave radiation balances as described by others (Pomeroy et al. 2009; Pugh & Small 2011). From 2011 on, snow disappeared from both sites at the same time (Figure 4), whereas snow disappeared from MM ~5–10 days later than in CC.

At the burned site, where pre-disturbance forest cover was similar to MM (transmittance 18%), canopy transmittance increased to 87% by the fourth year after the fire. In the first year post-fire, April 1 SWE in the burn was similar to that in the forest and significantly lower than that in a nearby clearcut. In western Alberta, Burles and Boon (2012) found that maximum SWE increased >50% four years post-wildfire, and the snowmelt period was shortened by 9–15 days as a result of an ~30% increase in shortwave radiation and sensible heat energy fluxes. At ML,

differences in April 1 SWE between the burn and forest were highest in years three and four post-fire (77% and 63%, respectively). Average ablation rates were significantly different in the burn than in the forest in all years post-fire, ranging from 31% to 93% higher; however, the largest difference was measured in year five (Winkler 2011). These results suggest that, similar to insect attack-related defoliation, snow accumulation response to forest cover loss following a moderate burn may be delayed until needles and fine canopy material are lost and burned stems topple.

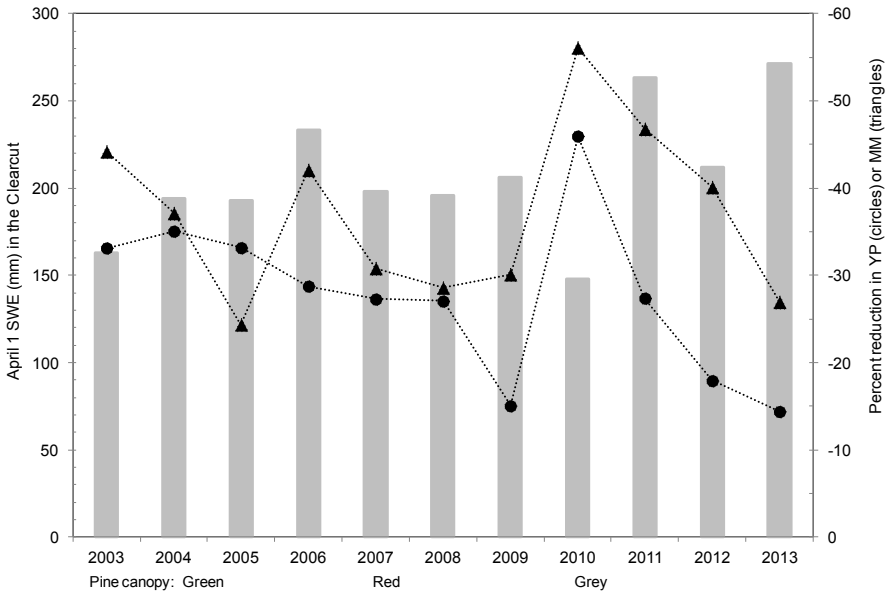

Figure 4: Differences in April 1 snow water equivalent in a young pine stand (YP) and a mature mixed species stand (MM) relative to a clearcut (CC) for 11 years pre- and post-mountain pine beetle attack at Mayson Lake.

The relationships between forest to clearcut ratios of April 1 SWE (FOSWE) or ablation rates (FOAR) and canopy transmittance at ML are shown in Figure 5. With the exception of 2010 lowest snowfall, canopy transmittance explained over 70% of the variability in FOSWE and FOAR. This result is similar to previous work, where green forests (4–23 m tree heights) showed a 6% reduction in April 1 SWE for every 10% increase in crown closure (Winkler & Roach 2005). Although Figure 5 also highlights the influence of interannual weather variability, expanding these relationships geographically to include a range of sites throughout the southern interior may provide useful indices of relative hydrologic response under varying forest cover conditions, including following natural disturbance and salvage logging.

When compared with changes in snow following clearcutting, natural disturbances such as MPB and fire in south-central BC result in an intermediate snow response. Retention of attacked and moderately burned stands, until most canopy material has been lost, could mitigate the immediate effects of salvage clearcut logging, reducing the increase in water available to generate spring runoff and possibly delaying the timing of runoff relative to clearcuts.

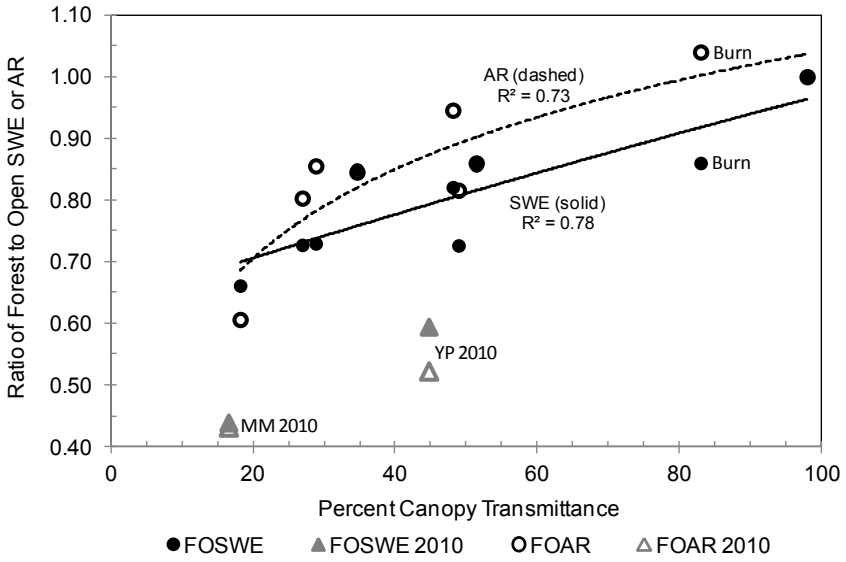

Figure 5: Changes in the ratios of forest, and burn, to clearcut April 1 snow water equivalent (FOSWE) and ablation rate (FOAR) with increasing percent canopy transmittance at Mayson Lake from 2007 to 2013, excluding the lowest snow year 2010 (shown in grey for the young pine [YP] and mature mixed [MM] stands).

4. CONCLUSIONS

Research at UPC and ML shows a significant change in snow accumulation and ablation with clearcut logging, though the magnitude of change varies with elevation and forest cover type. Earlier snowmelt in extensive clearcuts and synchronization of melt between high-elevation clearcuts and low elevations has advanced the timing of spring high flows, significantly increasing April water yield and decreasing that in June and July. Post-MPB and post-wildfire snow surveys at ML indicate that disturbance has a delayed and intermediate effect on snow accumulation and melt relative to green mature forest and clearcuts. Relationships between variables describing the forest canopy, such as canopy transmittance and canopy cover, may provide useful forest planning indices to assess differences between retention of naturally disturbed stands and salvage logging.

ACKNOWLEDGMENTS

This research was funded by the BC government, and forestry operations were completed by Weyerhaeuser Canada Ltd. The authors gratefully acknowledge Ralph Adams, Karen Baleschta, Derek Carlson, Tim Giles, David Maloney, Patrick Martin, Todd Redding, Jean Roach, Brian Gautier, Michael Ryan, Rob Scherer, and Gary Van Emmerick who helped with instrumentation, snow surveys, forest inventory and database maintenance throughout these projects.

REFERENCES

BC Ministry of Forests, Lands and Natural Resource Operations (BC FLNRO). 2008 *Biogeoclimatic Ecosystem Classification Subzone/Variant District-Scale Field Maps*. Available online: http://www.for.gov.bc.ca/hre/becweb/resources/maps/FieldMaps.html, 12, June 2013.

Boon, S. 2011 Snow accumulation following forest disturbance. *Ecohydrology*, doi: 10.1002/eco.212.

Boon S. 2009 Snow ablation energy balance in a dead forest stand. *Hydrol. Process.* 23(18), 2600–2610.

Burles, K. & Boon, S. 2011 Snowmelt energy balance in a burned versus a healthy forest stand, Crowsnest Pass, Alberta, Canada. *Hydrol. Process.*, doi: 10.1002/hyp.8067.

Ellis, C.R., Pomeroy, J.W., Essery, R.L.H. & Link, T.E. 2010 Effects of needle-leaf forest cover on radiation and snowmelt dynamics in the Canadian Rocky Mountains. *Can. J. Forest Res.* 41, 608–620.

Green, K. C. & Alila, Y. 2012 A paradigm shift in understanding and quantifying the effects of forest harvesting on floods in snow environments. *Water Resour. Res*, 48(10), doi: 10.1029/2012WR012449.

Hedstrom, N.R. & Pomeroy, J.W. 1998 Measurements and modelling of snow interception in the boreal forest. *Hydrol. Process.* 12(10–11), 1611–1625.

Jost, G., Weiler, M., Gluns, D.R. & Alila, Y. 2007 The influence of forest and topography on snow accumulation and melt at the watershed-scale. *J. Hydrol.* 347, 101–115.

Moore, R.D. & Wondzell, S.M. 2005 Physical hydrology in the Pacific Northwest and the effects of forest harvesting – A review. *J. Am. Water Resour. Assoc.* 41, 753–784.

Pomeroy, J.W., Marks, D., Link, T., Ellis, C., Hardy, J., Rowlands, A. & Granger, R. 2009 The impact of coniferous forest temperature on incoming longwave radiation to melting snow. *Hydrol. Process.* 23(17), 2513–2525.

Pugh, E. & Small, E. 2011 The impact of pine beetle infestation on snow accumulation and melt in the headwaters of the Colorado River. *Ecohydrology*, doi: 10.1002/eco.239.

Stednick, J.D. 1996 Monitoring the effects of timber harvest on annual water yield. *J. Hydrol.* 176, 79–95.

Varhola, A., Coops, N.C., Weiler, M. & Moore, R.D. 2010 Forest canopy effects on snow accumulation and ablation: An integrative review of empirical results. *J. Hydrol.* 392, 219–233.

Westerling, A.L., Gershunov, A., Brown, T.J., Cayan, D.R. & Dettinger, M.D. 2003 Climate and wildfire in the western United States. *Bulletin of the American Meteorological Society* 84(5), 595–604.

Winkler, R. 2011 Changes in snow accumulation and ablation after a fire in south-central British Columbia. *Streamline Watershed Management Bulletin* 14(2), 1–7.

Winkler, R. & Roach, J. 2005 Snow accumulation in B.C.'s southern interior forests. *Streamline Watershed Management Bulletin* 9(1), 1–5.

Winkler, R., Boon, S., Zimonick, B. & Spittlehouse, D. 2012 Snow accumulation and ablation response to changes in forest structure and snow surface albedo after attack by mountain pine beetle. *Hydrol. Process.*, doi: 10.1002/hyp.9574

Winkler, R.D., Spittlehouse, D.L. & Golding, D.L. 2005 Measured differences in snow accumulation and melt among clearcut, juvenile, and mature forests in Southern British Columbia. *Hydrol. Process.* 19(1), 51–62.

Ecohydrology of Boreal Forests: The Role of Water Content

Jessica M. Young (formerly Cable)* and W. Robert Bolton

International Arctic Research Center, University of Alaska Fairbanks, Fairbanks, AK, 99775, USA
**Corresponding author's email: jmcable@alaska.edu*

ABSTRACT
Plant water storage is not typically included in hydrological models, but the amount of water can be significant and may impact soil moisture levels. The boreal forest has two primary ecosystem types that have different permafrost conditions, and each differ in its potential to impact soil moisture via plant storage. The first is dominated by large deciduous trees, and the soil does not have permafrost. The second is dominated by small coniferous trees, and the soil is underlain by permafrost. Prior work has shown that the deciduous trees have significantly higher water flux rates than the coniferous trees. The primary question we address in this paper is, How do the water contents of each vegetation type differ? Field and modeling work revealed that the deciduous trees have significantly higher water contents, and they take up a large portion of snowmelt water prior to leaf out. The deciduous trees clearly have significant potential to affect soil moisture, particularly during the critical period of snowmelt. This is the first study to illuminate this process.

KEYWORDS
Discontinuous permafrost; boreal ecohydrology; plant water storage; soil water storage.

1. INTRODUCTION
Water stored in vegetation is typically part of the error term in hydrological models, as it is considered negligible. In ecophysiological studies, vegetation water storage is an important component of plant water status, as it supports photosynthesis and transpiration during periods of low water availability. Plant water storage can reduce the chance of hydraulic failure, such as cavitation, during dry periods. This ability to store water depends upon xylem anatomy, and trees are typically able to store more water than small herbaceous plants (which may not have as great of a need to store water, given their small stature). For plant water storage to have a significant effect on hydrology, the vegetation would have to be large, like trees, and have a widespread distribution. Thus, this study focuses on the water content of trees within watersheds rather than small plants.

In the boreal forest, hydrological processes are mediated by soil storage capacity in areas that are underlain by permafrost. As the seasonal thaw depth increases over the summer, the storage capacity of the soil increases. Precipitation events or snowmelt water tends to push existing moisture stored in the soil laterally out of the system and into streams. However, in non-permafrost areas of the boreal forest, the soils tend to store much less water. Without the impermeable permafrost layer, water has the capacity to infiltrate the soils, effectively recharging deep soil layers, with less impact on streamflow. However, the role of plant water uptake, storage, and flux to the atmosphere has not been well evaluated in Interior Alaska boreal systems. This may be particularly important to quantify the snowmelt period, as snowmelt water

greatly increases streamflow in areas with and without permafrost. Any changes in snowmelt runoff could impact water flow in this critical period of time.

The vegetation in permafrost and non-permafrost areas is drastically different, which may contribute to differences in the plant water storage component of the hydrologic cycle. Permafrost areas are dominated by small-statured black spruce trees (*Picea mariana*). Permafrost-free areas are dominated by larger deciduous trees (birch [*Betula neoalaskana*] and aspen [*Populus tremuloides*]). Ongoing work by Cable (Young) and Bolton has shown that the water flux rates of the two vegetation types are extremely different. Deciduous vegetation has an order of magnitude higher flux rate than the coniferous vegetation. The primary question we address in this paper is, How do the water contents of each vegetation type differ? We hypothesize that—given the higher flux rates of deciduous vegetation—the water contents of the deciduous vegetation will be higher than the coniferous vegetation. Using field and modeling approaches, we explored inter- and intra-annual variability in water contents and the effects of hillslope position (high vs. low locations on hillsides), as the drainage properties of the soil should differ based on hillside position.

2. METHODS

In 2011, four field sites were established within the same watershed as part of a larger project at Caribou Poker Creek Research Watershed near Fairbanks, Alaska. Two sites are located on a north-facing slope, and two sites are located on a south-facing slope. The north-facing slopes have near-surface permafrost (at ~50 cm depth), a thick moss and organic layer (~30 cm), and black spruce (*Picea mariana*) overstory, and the understory is a mixture of birch shrub species (*Betula sp.*). The south-facing slopes do not have permafrost, and the soils are fairly rocky. The overstory is composed of birch and aspen trees (*Betula neoalaskana* and *Populus tremuloides*), and the understory is composed largely of birch (*Betula sp.*) shrubs. On each aspect, one site is located high on the hillside and one site is low on the hillside. At each site, meteorological stations were established, measuring air temperature (°C), relative humidity (%), net radiation (W), soil temperature (°C) and moisture (%) at 5 cm and 40 cm depths (in organic and mineral soil, respectively). Granier sap flux sensors were installed in 5 trees in 2011 and in 5 additional trees in 2012. Snow depth and density measurements were made at each site during the snowmelt period, and snow water equivalent (SWE) was calculated.

We used the TDR (time domain reflectometry) approach to measure tree water content. Two welding rods (3.18 mm diameter, 10 cm long) were installed 2 cm apart into trees (the number of trees increased from 5 in 2011 at all four sites, to 23 in 2013 at the south facing and 15 at the north facing). The rods were installed to a depth of 8 cm, so as to imbed the rods in the sapwood of the tree. Time domain reflectometry measurements were made with a TDR 100 (Campbell Scientific) by putting cable testers on each rod. Thus, the measurements were manual, not automated. Measurements were conducted ~1–2 weeks each summer from snowmelt ablation to senescence (~March–September).

To calibrate the data, a birch and a black spruce tree were cut down during the wettest time of year (March–April), and we cut out four equal-length segments of wood (25 cm long). Two welding rods were installed into each segment. Every week for approximately 4 months, a TDR measurement and weight (g) of each segment was made until each dried out. The volume of each segment was determined by immersing it in a pool of water and measuring the water volume

displacement. The TDR waveform coefficients were converted to volumetric water content using these data. This equation was used to convert all the field TDR data to volumetric water content.

We used a Bayesian modeling approach to explore the effects of climate (vapor pressure deficit, air temperature, RH) and soil environmental conditions (soil moisture and temperature) on water content. We focused our analysis on data from 2012, as this is the most complete year of data to date. We also calculated the percentage of snowmelt water taken up by the trees for 2013. The Bayesian approach was used because uncertainty in all sources of data (meteorological, TDR, water flux, etc.) could be accounted for and propagated throughout the model. Further, produced are mean and uncertainty estimates for the coefficients associated with the climate and soil environmental effects on tree water content.

3. SUMMARY OF RESULTS AND DISCUSSION

Data summary – Tree water content was always significantly higher for deciduous trees than coniferous trees. The deciduous trees had very high water content during the snowmelt period (>100%), and upon leaf out, the water contents declined slightly. Water contents at the low site were slightly greater than the high site. The coniferous trees always had low water contents (<50%). For both tree types, once the growing season began (e.g., post-leaf out for the deciduous trees), tree water content did not vary. There was inter-annual variability in terms of when the peak water uptake period occurred, which likely depended on the timing of snowmelt. For example, the peak water uptake period was both longer and later in 2013 compared with 2012 because of the later snowmelt period in 2013.

Modeling results – The Bayesian model fit the data very well, explaining >90% of the variability in the data for 2012. We found that higher tree water content occurs with warm and wet soils, and dry air. However, these effects are only significant for the deciduous trees, as the coniferous tree water content data were relatively invariant. Also, these effects differ depending on hillside position and whether or not the leaves were out. We also found that, in 2013, a large fraction of snowmelt water was taken up by deciduous trees during the period between snowmelt and leaf out.

Deciduous tree water content likely plays a significant role in boreal hydrology by removing water from the system. The water is then stored and fluxed to the atmosphere. Storage in trees appears to be a significant part of the hydrologic cycle and should not be overlooked in models, particularly given that a large fraction of snowmelt water is taken up by the deciduous trees. The effect of tree water storage on plant physiological and forest processes is not yet clear, but likely reduces the effects of drought on photosynthesis and production. This is one of the first studies to show the dynamics of tree water content of deciduous and coniferous trees in the boreal forest of Interior Alaska, and the potential significance for hydrology.

ACKNOWLEDGMENTS

This research was supported by NSF OPP grant #0852078, NSF Hydrology grant #1114457, and DOE SciDAC grant #DE-SC0006913.

Seasonal Stream Regimes and Water Budgets of Hillslope Catchments, Polar Bear Pass and Cape Bounty, Nunavut

Kathy L. Young[1*], Melissa J. Lafrenière[2], Scott Lamoureux[2], Anna Abnizova[1], and Elizabeth A. Miller[1]

[1]*Dept. Geography, York University, Toronto, ON, M3J IP3, CANADA*
[2]*Dept. Geography, Queen's University, Kingston, ON, K7L 3N6 CANADA*
**Corresponding author's email: klyoung@yorku.ca*

ABSTRACT
In a recent study, Derksen and Brown (2012) demonstrated a rapid reduction in snow cover extent in arctic regions, even faster than the loss of sea ice and predictions by climate change models. Mineral and oil and gas development is accelerating in high arctic regions, and a solid understanding of shifting water resources is now required. This paper seeks to evaluate whether this rapid decline in snow cover extent is matched by changes in the seasonal stream regime of several small hillslope catchments on Bathurst and Melville Islands, and the resulting impact of these possible shifts on the spring/summer water budgets. Paired catchments (West and East) at the Cape Bounty Arctic Watershed Observatory (CBAWO) on Melville Island (74.9°N, 109.5°W) have been studied from the pre-snowmelt season to early August since 2003. They are low-rolling tundra catchments and are between 8.0 and 11.6 km^2 in area. Likewise, within the Polar Bear Pass watershed, Bathurst Island (75.7°N, 98.7°W), two hillslope basins; one larger (Windy Creek, 4.2 km^2) than the other (Landing Strip Creek, 0.2 km^2) have been investigated since 2007. In both areas, detailed snow surveys were conducted each spring, and streamflow estimates were made using the midsection velocity method. A nival-type regime continues to dominate in these basins, but runoff ratios are variable between catchments, across islands, and from year-to-year. In comparison with past streamflow studies across the Queen Elizabeth Islands, an earlier response to peak discharge and start of flow for these hillslope streams cannot yet be confirmed.

KEYWORDS
Canadian High Arctic; climate variability/change; streamflow; water budgets; water resources

1. INTRODUCTION
Like much of the circumpolar Arctic, Canada's High Arctic islands are now experiencing a changing climate, and evidence for these changes intersects across the terrestrial cryosphere. While warming in the Western Arctic has been ongoing for the last 20–30 years, this warming did not start until about 1993 in the Eastern Canadian Arctic, but so far has been continuing (Smith et al. 2010). Environmental manifestations of this warming include warming of permafrost and deepening of the active layer, the drying, shrinkage, and loss of ponds and lakes sometimes with a shift in ecological diversity (Smol & Douglas 2007a, b) ,and a dramatic loss of glacial ice which is now considered irreversible (Lenaerts et al. 2013). Recently, Derksen and Brown (2012) have documented the rapid decline in snow cover extent across pan-arctic regions (April, May, June), with this reduction occurring most dramatically from 2005 onwards.

Snow is critical for high arctic ecosystems; it replenishes ponds, lakes, and desiccated wetlands. Meltwater from hillslope catchments deliver water, nutrients, and sediments from upland terrain into these low-lying zones. Past studies in the Queen Elizabeth Islands (QEIs) (e.g., Wedel et al. 1977; Woo 1983; Woo 2000 and others) indicate streamflow regimes are dominated by nival regimes (snowmelt), with rainfall normally playing a secondary role in both streamflow generation and basin water budgets. Hydrological, paleological, and biogeochemical studies were initiated around 2003 in small paired hillslope catchments at the Cape Bounty Arctic Watershed Observatory (CBAWO), Melville Island (74.9°N, 109.5°W). Similarly, since June 2007, Polar Bear Pass (PBP), Bathurst Island (75.7°N, 98.7°W) has been the focus of both wetland and hillslope hydrology studies. In this particular study, we assess the impact of recent warming (since 2005) and a reduction in snow cover extent as described by Derksen and Brown (2012) on both streamflow response and water budgets in these small hillslope catchments. We are particularly interested in exploring whether (1) we are now seeing a shift in the stream regime; specifically, can we document a departure from a *Nival* to a *Mixed* or *Pluvial*-type of flow regime; and/or (2) if we are observing a decline in snow cover extent, is this translating into earlier streamflow, and an earlier and higher peak Q; and finally (3) in terms of seasonal water budgets, can we observe differences in the allocation of water resources between catchments, islands, and years, and how do these estimates compare to earlier basin studies in this region and elsewhere. Such basic knowledge on the water resources of this oft forgotten zone adjacent to the Northwest Passage is of critical importance to the environmental sustainability of this area, growing industrial services, and the nearby Inuit community of Resolute Bay.

2. MAIN STUDY AREAS

2.1 Polar Bear Pass

Polar Bear Pass (PBP) is located in the middle of Bathurst Island about 146 km northwest of Resolute Bay (Figure 1). The Pass consists of a large, low-gradient wetland about 94 km^2 in area. It is made up of two large lakes, about 4000 ponds, comprising 30% of the area, and wet meadow and patches of dry ground (Abnizova et al. submitted). It is bounded by low-rolling hills running east-west rising to 150–200 m a.s.l. These hills are notched by stream valleys (upwards of 50), which drain the upland areas of both snowmelt and rainwater (Young et al. 2013). Two typical hillslope stream catchments draining into the low-lying wetland were the focus of this study: Landing Strip Creek (LSC) – 0.2 km^2, and Windy Creek (WC) – 4.2 km^2 (Figure 2a, b). Polar Bear Pass is considered a biological oasis, though a comparison of its climate with Resolute Bay (Young & Labine 2010) suggests that it can also be considered to have a polar desert climate, long cold winters, and short cool summers. The region is underlain by continuous permafrost, and active layers average 0.3–0.5 m in boggy, wet soils, while dry polar desert ridges can reach upwards of 1 m in warmer years (e.g., 2010, 2012).

Landing Strip Creek (unofficial name) is a first-order creek, typical of others in the Pass (see Figure 2a). It has a south-facing slope and is sparsely vegetated, comprising polar desert soils (porosity = 0.50, organic content <4%). The upper part of the catchment is bowl-shaped and a lingering late-lying snow bed forms along the upper ridge. Ground thaw here can reach 1.0 m. The main channel is narrow and steep, and waters drain into a lush wet meadow with tundra ponds (porosity = 0.93) (Young et al. 2010). Windy Creek is the larger catchment (4.2 km^2) and has 3 main tributaries. The east-west tributary (Moss Creek) has an extensive organic layer 10–160 mm in thickness over gravelly ground, and a late-lying snow bed typically lies along the

north-facing slope. The main channel of Windy Creek branches above Moss Creek, with one tending northeast to southwest while the other is northwest- to southeast-facing. The rocky channel length is 2.73 km, and the average slope is 3.9°. Polar desert soils comprise most of the basin, though pockets of ice-rich polygonal terrain occur (Young et al. 2010). Shallow frost tables occur here. Detailed topographic maps for these two catchments can be found in Young et al. (2010).

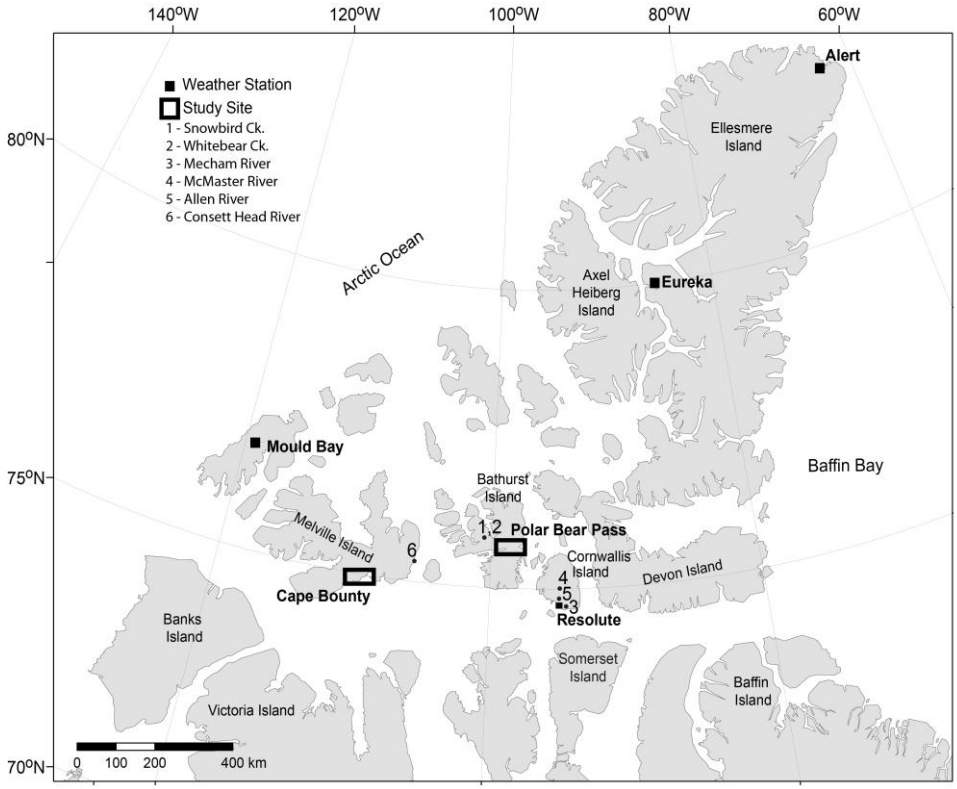

Figure 1: Map of the Queen Elizabeth Islands showing the location of the main study sites of Polar Bear Pass, Bathurst Island, and Cape Bounty Arctic Watershed Observatory, Melville Island. Locations of the main government weather stations and previous watershed studies are also indicated. More details about these catchments can be found in Appendix 1. Note that the Mould Bay weather station now consists of an AWS.

2.2 Cape Bounty

The Cape Bounty Arctic Watershed Observatory is located on the southcentral coast of Melville Island (Figure 1). Paired basins have been the focus of study since 2003. Similar to PBP, these catchments are underlain by continuous permafrost and have a maximum active layer of less than 1 m. The sparsely vegetated catchments are composed of low-relief hills (<120 m a.s.l); prostrate tundra is typical on the uplands, while wet sedge meadows exist in low-lying areas. The area can be considered to have a polar desert climate, with annual precipitation approaching 111 mm and July temperatures of 4°C (1971–2000) at Mould Bay, the nearest government weather station (Stewart & Lamoureux 2011). Both catchments are south-facing and have tributaries that feed a main channel draining into lakes, but the West River catchment (8.0 km^2) has a steeper gradient and deeper gullies and channels than the East River catchment (11.6 km^2). This usually results in more snow for the western basin (Stewart & Lamoureux 2011). Detailed topographic maps of these basins can be found in Stewart and Lamoureux (2011).

3. METHODOLOGY

The theoretical framework for this research is the catchment water budget:

$$P(Sn+Rain)-E-Q = \Delta S+\xi \quad (1)$$

where *P* is precipitation (Snow + Rain), *E* is evaporation loss, *Q* is discharge (runoff), ΔS is the change in storage, and ξ is the error term. In seasonal catchment water budgets, rarely is ξ estimated separately from ΔS (see Kane & Yang 2004; Young & Woo 2004a,b), and this is the case for this study too; that is, all gauge measurements and analytical and human errors can potentially reside on the right side of the equation (ΔS+ξ). Woo (2012, p. 504) remarks that oftentimes this is an unavoidable circumstance of fieldwork in such remote and difficult terrain where "it is not easy to close the water balance." He further suggests that "some level of uncertainty has to be accepted, but within specified limits of tolerance, the results should enable qualitative assessment of the hydrologic status of the basin."

3.1 Polar Bear Pass

At Polar Bear Pass (PBP) end-of-winter snow surveys (late May) were conducted to assess the snow amount (SWE, mm) in each one of these basins. Methodology followed after Woo (1997) and consisted of a series of transects across varying terrain types making up the catchments. Snow depth was typically made every 10 to 50 m along long transects (plateau) and every 2 to 5 m across shorter ones (valley bottoms, ponds). Except for ponds, each snow depth measurement was typically the average of 4 measurements. Snow density using an MSC snow rod was made at the start and end of each transect, with more frequent sampling along long transects >1 km. Daily snowmelt for the terrain types in the catchments (plateau, valley, slope) was estimated using a surface energy budget snowmelt model (Woo & Young 2004) that was previously deemed applicable to this site (Young et al. 2010; Assini & Young 2012; Young et al. 2013) and elsewhere (Woo & Young 2004; Young 2008). Meteorological inputs to the model (air temperature, relative humidity, solar radiation, precipitation, wind speed, and pressure) were available at an automatic weather station in the middle of the wetland (CAWS) and were complemented by climate data from the Plateau AWS near the cabin. Both of these AWSs are within 1 km of each other. More details about the model used can be found in both Woo and Young (2004) and Young et al. (2010). Snowmelt estimates were compared with direct measurements of surface snow ablation following after Heron and Woo (1978) at varying terrain comprising the catchments (pond, plateau, late-lying snowbed, wet meadow). Here a marked line (~2 m long) was held taut by two dowels placed in the snowpack. Ten measurements from the middle of the line to the snowpack at intervals of 10 cm were made daily and then averaged. These measurements together with 5 surface density measurements, each snow sample being 200 cm^3, allowed the surface snow water equivalent to be determined (mm). In mid-June snow cover distribution in the catchments was validated with low-level aerial photography via a helicopter.

Summer precipitation (rainfall and snow, mm) areally weighted for each catchment was quantified with a recording precipitation gauge at the AWSs. This was supplemented by manual rain gauges at each catchment (see Young et al. 2010 for more details). The Priestley-Taylor (P–T) approach (Priestley & Taylor 1972) was used to assess evaporation from the wet meadow and saturated ground following snowmelt using an $\alpha = 1.26$. For moist and drying ground, the α term was adjusted to near-surface soil moisture conditions (0–15 cm) using the algorithm developed by Marsh et al. (1981) for polar desert terrain. Near-surface volumetric soil moisture was determined in both wet meadows and polar desert using either continuously measuring Campbell

Scientific TDR probes or Echo probes geared into Campbell Scientific loggers. These hourly estimates were confirmed by regular volumetric soil moisture measurements with a handheld Theta probe (see Young et al. 2010 for more details). Occasionally (e.g., 2008), due to missing data for polar desert terrain—either net radiation (Q*), ground heat flux (Qg), or soil moisture data—evaporation was quantified using the empirical approach described by Stewart and Rouse (1976). This approach calls for inputs of solar radiation and air temperature and was originally developed for subarctic areas. Undoubtedly, this likely led to some error in our evaporation estimates for polar terrain. Like snowmelt, evaporation estimates were areally weighted for each catchment based on terrain type, and climate data for evaporation estimates came from both the Plateau AWS and the CAWS (see Young & Labine 2010; Young et al. 2010 for additional details).

Seasonal runoff from each catchment was captured near its exit, and standard techniques were used to make estimates of this discharge. Stage was monitored by recording water level sensors with Hobo pressure transducers (±3.0 mm) or Ecotones (±25.4 mm). Frequent direct measurements of stilling well stages were made with a metric ruler (±5.0 mm). These estimates confirmed continuous stage measurements, and/or were used to correct stage when values drifted. Direct discharge measurements at both low and high flows were made to develop reliable stage-discharge curves for each year. Oftentimes, due to shifting conditions in the channel, two equations were developed: one for an ice-filled channel and another for an ice-free channel. These equations with an R^2 typically >0.80 were then used to adjust the water stage into a continuous discharge record. Streamflow estimates can amount to 10%–15% error on average (Young et al. 2010). Further details on the current metering equipment deployed at each site can be found in Young et al. (2010). Determination of terrain areas in each catchment (±5%) is described in Young et al. (2010). As mentioned above, these areas were used to areally weight daily snow, evaporation, and rainfall for both LSC and WC basins. Exceedance probability diagrams were produced of both snowmelt and post-snowmelt streamflow. Hydrograph separation between these periods (snowmelt vs. post-snowmelt) was made subjectively by extending the recession limb of the last major snowmelt pulse to the *x*-axis marking time.

The right side of the equation ($\Delta S + \xi$) was the residual in this study, and as mentioned earlier, all of the errors can reside in this term(s). Storage can include snow storage in lingering snowpacks, soil moisture, ground ice, and groundwater storage. Like previous studies here and elsewhere, uncertainty in our basin estimates likely falls between 15% and 20%, given the remote location of this study and limitations with snowmelt, streamflow, and evaporation estimates. In particular, any errors in terrain unit areas will be reflected in precipitation, snowmelt, and evaporation estimates. For instance, it is well known that water can cross boundaries both on the surface and below the ground due to a variable snow cover distribution and an evolving frost table. Melt-out of unaccounted late-lying snow or ground ice can lead to overestimates in the runoff ratio (Q/P) (Young & Woo 2004 a, b; Woo 2012).

3.2 CBAWO

Similar to PBP, a terrain-based snow survey is routinely conducted at CBAWO in late May or early June prior to melt. The methodology differs slightly than the one developed for PBP. Here 21 snow survey transects were set up across each basin. Each transect comprised ten depth measurements and a single snow density measurement. Mean SWE (mm) was estimated for each transect and then spatially averaged for each catchment based on terrain type (channel, slope, and plateau) (Lamoureux et al. 2006). At the meteorological stations (n = 3), air temperature was

measured at a 1.5 m height with Onset Hobo H8 loggers (±0.4°C) or a Humirel HTM2500 sensor logged with an Unidata Prologger at MainMet (±0.2°C), with precipitation measured with a Davies tipping bucket gauge (0.2 mm). Incoming solar radiation at MainMet was monitored with a Davies industrial sensor (5%) and soil moisture with Decagon Echo 10 cm probes (5%) and Onset U12 loggers. Hydrometric stations were located near the outlet of both East and West Rivers. Stage was recorded with Onset U20 water level loggers (±2 mm) at 10-minute intervals. Streamflow was estimated with a Swoffer impellor meter usually every second day during the season, and rating curves (stage/discharge) for the catchment routinely exceed an R^2 of 0.80 (Lamoureux et al. 2006). In the absence of Qg and net radiation (Q*) data for some years, evaporation was estimated using the empirical approach by Stewart and Rouse (1976). The previous study by Young et al. (2010) showed that it was applicable for polar desert terrain.

4. RESULTS AND DISCUSSION

There is now a pressing need for reliable streamflow and water budget information in arctic environments, especially from catchments with a range of scales and physiography (Spence et al. 2005). Spence et al. (2005) argue that new theories and modeled data cannot be tested if suitable datasets are not available. These researchers hypothesize that the sparse network of the Water Survey of Canada makes it difficult to predict streamflow in ungauged basins, particularly ones of interest to industry (Spence et al. 2005).

In terms of industry in high arctic watersheds, details on the potential for flooding (timing, magnitude) are required for safe oil and gas pipeline installations across stream valleys, while mining extraction processes require secure water supplies too. Due to the high cost of diesel to generate electrical power, there is also a growing desire to assess the potential of many arctic streams for hydro-electric power (HEP), especially in Nunavut. Runoff also transfers nutrients and sediments into ponds, lakes, rivers, and streams, and ultimately these waters empty into nearby arctic coastal waters. To date, there is a particular interest in the delivery of DIC/DOC into a range of water bodies and its role in the global carbon cycle (Abnizova et al. 2012; Holmes et al. 2012; Lewis et al. 2012). Information on the timing and availability of water, and knowledge of hazards (both floods and droughts) are also required by local Inuit who have concerns about water supplies to their local water reservoirs, and the potential for destruction of infrastructure (sewage/water pipelines; for example, Pangnirtung, spring 2008). Larger urban communities have immediate water issues too. Arctic cities like Iqaluit and its inhabitants need to consider household water supplies, sewage considerations, and urban industrial needs (hospitals, schools).

4.1 Type of Streamflow Regime

Figure 2 provides details on the recent seasonal streamflow regimes from PBP and CBAWO, and the exceedance probabilities of streamflow during the snowmelt and post-snowmelt periods. Clearly, a nival regime still exists for these hillslope streams where the bulk of the runoff is generated by snowmelt. Peak streamflow was produced by snowmelt at PBP with rainfall never leading to runoff exceeding 5 mm/d. This streamflow pattern differed for CBAWO, where in 2007 and 2009 the greatest peaks were generated by rainfall, with the West River exhibiting higher peaks than the East River. Kane et al. (2009) indicate that in the Alaska Arctic, for small and medium-sized basins (<200 km^2) floods of record are usually caused by rainfall rather than snowmelt. Other studies in the High Arctic confirm the importance of summer rains in generating peak flows (e.g., Cogley & McCann 1976; Woo & Guan 2006). Figure 3 indicates

that climatic conditions are comparable for PBP and CBAWO, which suggests that differences in their runoff patterns may be linked to local site conditions (i.e., basin topography, soils, ground ice).

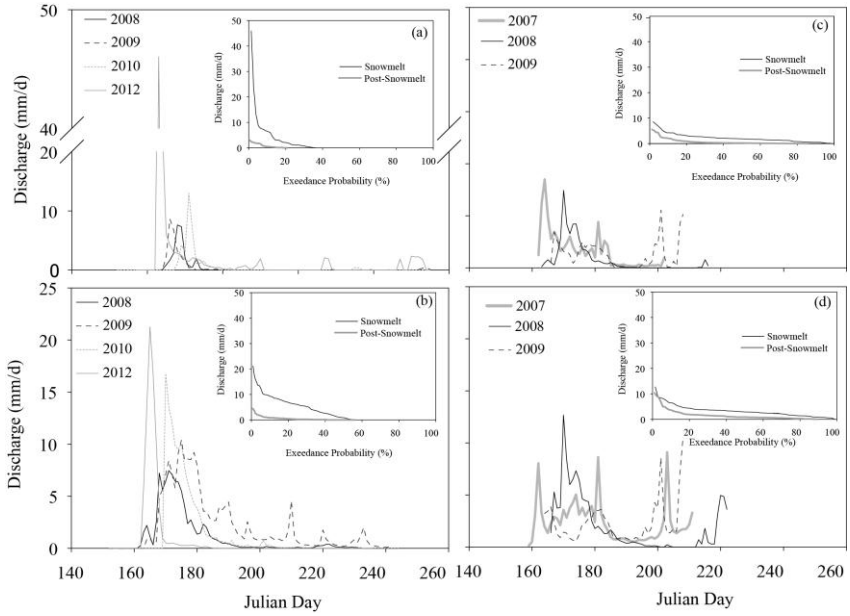

Figure 2: Seasonal streamflow regimes (mm/d) at Polar Bear Pass: (a) Landing Strip Creek (LSC), (b) Windy Creek (WC), and at CBAWO: (c) East River, and (d) West River. Inset diagrams show the exceedance probability of streamflow for the snowmelt and post-snowmelt periods.

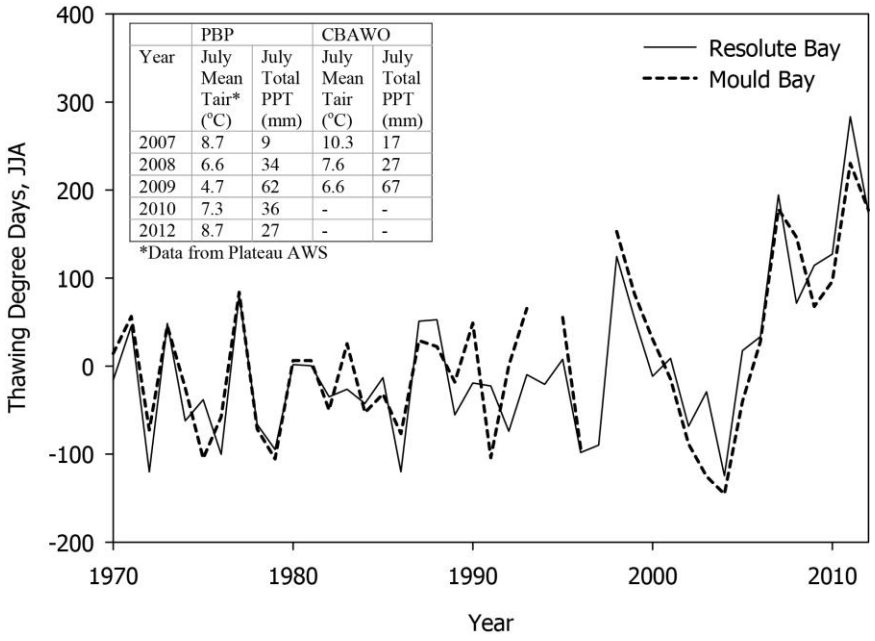

	PBP		CBAWO	
Year	July Mean Tair* (°C)	July Total PPT (mm)	July Mean Tair (°C)	July Total PPT (mm)
2007	8.7	9	10.3	17
2008	6.6	34	7.6	27
2009	4.7	62	6.6	67
2010	7.3	36	-	-
2012	8.7	27	-	-

*Data from Plateau AWS

Figure 3: Thawing degree day anomaly (June, July, and August) for Resolute Bay (solid line) and Mould Bay (dashed line). Note the steep warming since 2005. Inset table shows July average air temperature and precipitation totals for PBP and CBAWO.

4.2 Day of Peak Snowmelt Q

Day of peak discharge generated from snowmelt for the study sites (Figure 4) is compared with previous streamflow studies across Bathurst, Melville, and Cornwallis Islands (prior to 1985), and available Water Survey of Canada data from Cornwallis Island (i.e., the Allen and Mecham Rivers, see Appendix 1 for further details on these sites). Generally, peak discharges at PBP and CBAWO occur before Julian Day (JDay) 180 (~June 29). In comparison, earlier catchment studies in the 1970s/1980s peaked after JD185 (~July 4), though there are occurrences where peak discharge occurred much earlier (e.g., McMaster and Mecham Rivers). Consequently, due to this overlap in timing we cannot yet suggest that peak discharges are occurring earlier across Bathurst and Melville Island. Aside from LSC, the relative magnitude of peak discharge at PBP and CBAWO sites are similar to previous studies. An extreme runoff value for LSC in 2012 arises from its small size (0.2 km^2) and the rapid drainage of its channel after a slush flow was breached. Others have reported on the flashy response in hydrographs due to slush flows (e.g., Braun et al. 2000).

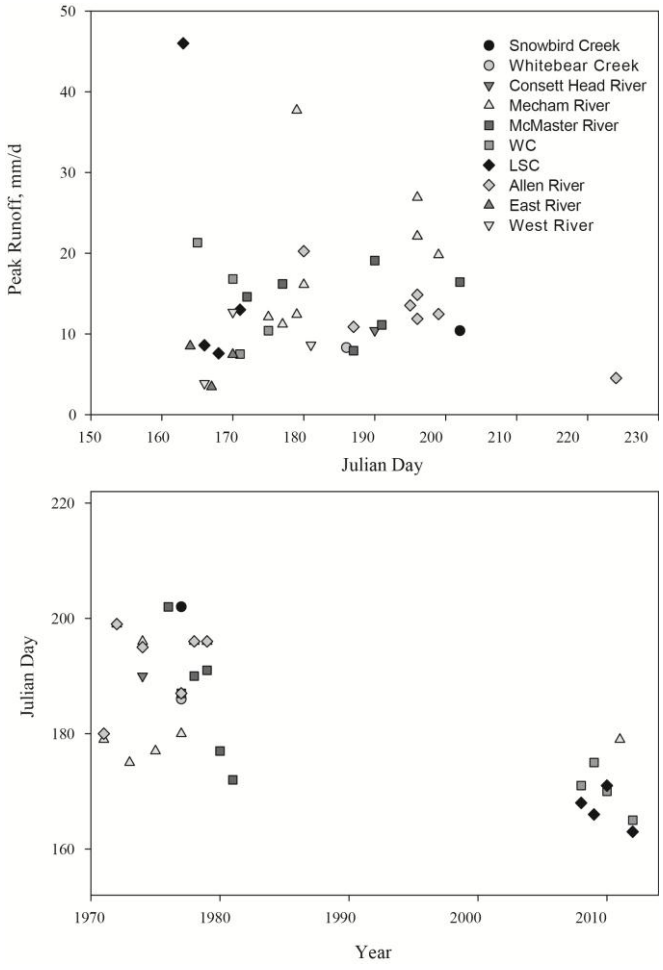

Figure 4: Comparison of peak runoff from the study sites (PBP, CBAWO) in relation to past streamflow studies across the QEIs (Melville, Bathurst, and Cornwallis) and Water Survey of Canada data from Cornwallis Island. Diagrams show (a) peak runoff (mm/d) in relation to Julian Day for sites and (b) Julian Day of peak runoff in relation to the year of record.

4.3 Onset of Snowmelt Runoff

For most years, the initiation of snowmelt runoff for these catchments is earlier than previous studies (Figure 5), and this is likely in response to the recent warming in this region (see Figure 3). A regional trend toward an earlier start to snowmelt runoff has been observed in Eurasian Arctic rivers, which is attributed to an upward trend in air temperature (Tan et al. 2011). However, given that there is still some overlap in timing with older streamflow studies in this region, it is not yet possible to confirm that a strong signal exists for an earlier start to runoff at PBP and CBAWO.

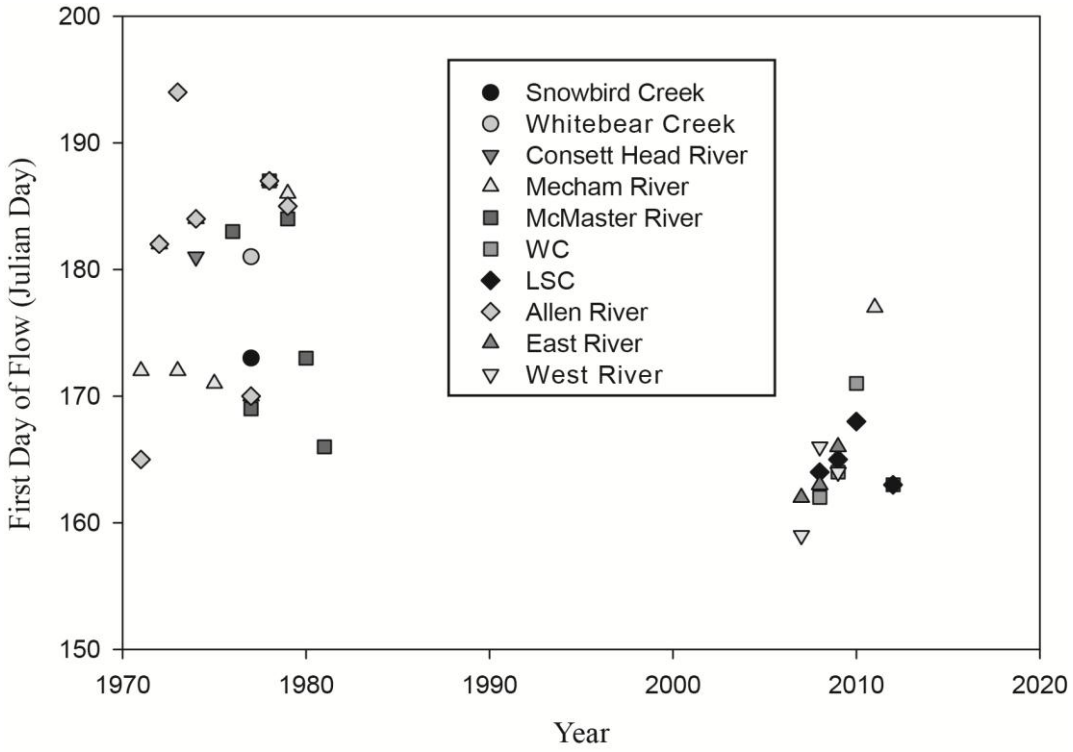

Figure 5: Initiation of runoff versus year for the study sites (PBP, CBAWO) in relation to past streamflow studies across the QEIs (Melville, Bathurst, and Cornwallis Islands.

4.4 Seasonal Water Budgets (PBP and CBAWO)

Figure 6 shows the seasonal water budgets for WC and LSC (PBP) (a, b) from 2008–2010, 2012, and the East and West Catchments of CBAWO from 2007–2009 (c, d). Runoff ratios (Q/P %) are also shown in the diagrams.

At the study hillslope creeks at PBP, there was more rainfall than snow in 2008 and 2009. Streamflow was variable from year-to-year with higher flows being maintained in 2009, a cool and rainy season. The storage term differed between the catchments and remained variable. Negative storage persisted at WC over the years, implying that water is being taken out of storage and contributing to runoff. This might be accommodated by snowmelt from residual snowbeds, either lying in the lee of slopes or in the stream valleys. Ground ice melt might also supplement flow. The presence of shallow frost tables in ice-rich zones (vegetated polygons) can limit infiltration, helping to shed rainfall into the stream channel (Young et al. 2010). Runoff ratios are generally less than 1 (100%), except for in 2009.

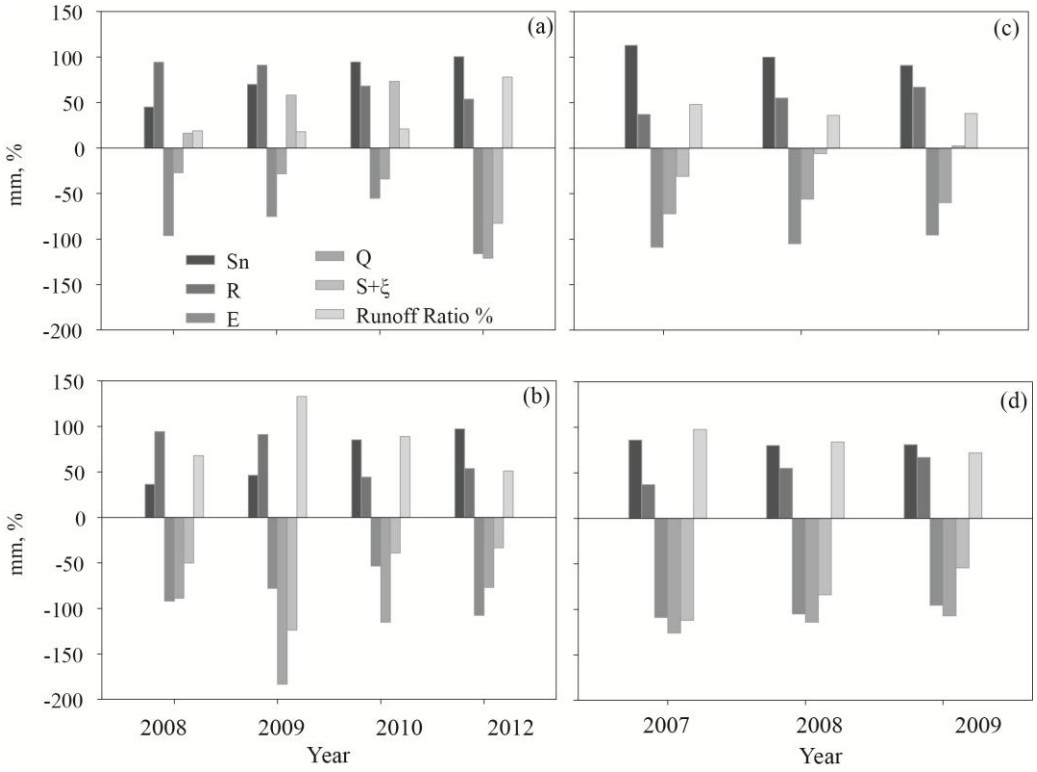

Figure 6: Seasonal water budgets for PBP (2008–2010, 2012): (a) LSC; (b) WC and CBAWO (2007–2009); (c) East River; (d) West River. Also shown are the seasonal runoff ratios (Q/P %).

At CBAWO, more snow than rainfall is accounted for in the catchment. Evaporation losses exceeded runoff in the East River but not the West River. Slopes are generally south-facing in the East Basin which may encourage higher evaporation losses (McLeod 2008, unpublished MSc). Storage was negative in both catchments, but levels were slightly more negative in the West River. Runoff ratios in both catchments were less than 100%, with the East River never exceeding 50%.

4.5 Average Water Budgets (PBP, CBAWO, and Others)

Table 1 considers the average water budgets from all study sites in comparison with information from two long-term arctic runoff studies: the McMaster River Basin and Imnaviat Creek. Some notable observations can be made. First, there is less snow in these study catchments than that measured in the McMaster Basin, while rainfall receipt is much higher than recorded at McMaster River (mid 1970s to early 1980s). Rainfall at Imnaviat Creek (Low Arctic) still has much higher levels than these basins. Evaporation losses while higher than McMaster River are still much lower than Imnaviat Creek.

Runoff at study sites is lower than both McMaster River and Imnaviat Creek, and average change in storage is much more variable, differing between sites and across islands. As mentioned above, at PBP, LSC shows a positive storage (water is being held), while WC has a large negative storage, implying additional inputs of water into the system. Similarly, while both the East and West basins show negative storages, the West Basin's is greater, and like WC this difference might be attributed to deep snow in channels and late-lying snowbeds, locations in the

basin where snow is often underestimated during annual snow surveys (McLeod 2008, unpublished MSc).

Table 1: Average water budgets (units, mm) for study sites and two long-term arctic watersheds.

Water Budget Term	WC, PBP, 4.2 km^2 2008-2012	West River Basin, 8.0 km^2 CBAWO 2007-2009	McMaster River*, 33 km^2, 1976-1981	LSC, PBP, 0.2 km^2, 2008-2012	East River Basin, 11.6 km^2 CBAWO 2007-2009	Imnaviat Ck**, 2.2 km^2 1986-1989
Sn	66.3 (29.5)	82.3 (3.2)	147 (39)	77.5 (25.3)	101.3 (11.1)	120 (33)
R	70.9 (25.6)	53.0 (15.1)	43 (18)	76.9 (19.3)	53 (15.1)	241 (45)
E	-82.8 (23.0)	-103.1 (7.0)	-38 (9)	-85.7 (26.3)	-103.1 (7.0)	-179 (40)
Q	-116.1 (47.6)	-115.7 (9.6)	-158(29)	-52.6 (45.7)	-62.7 (8.3)	-181 (56)
$\Delta S+\xi$	-62 (42.1)	-83.5 (28.8)	-1 (23)	+16.2 (70.3)	-11.5(17.4)	1 (32)
Runoff Ratio	0.85	0.84	0.84	0.34	0.41	0.46

*Source: Woo 1983, as found in Young and Woo 2004; ** Source: Kane et al. 1992, as found in Young and Woo 2004, NRB Water balance, IAHS Pub. 290; ( ) Standard Deviation

Interestingly, the runoff ratios are similar between WC, the West River and McMaster River catchment, while LSC, East River, and Imnaviat Creek have similar runoff ratios. The reasons for these patterns are not yet entirely clear and deserve further attention. Understanding the processes controlling the streamflow regimes at these sites is critical if we are to ever estimate streamflow in other ungauged stations across the QEIs, especially ones draining into the Northwest Passage.

5. CONCLUSIONS

(1) The hillslope creeks at Polar Bear Pass, Bathurst Island, and Cape Bounty, Melville Island, are still exhibiting a nival-type regime, though high discharge peaks are being generated by summer rainfall at Cape Bounty.

(2) It is not yet possible to identify an earlier onset in snowmelt runoff and peak snowmelt discharge at these catchments in comparison with previous streamflow studies. Additional years of monitoring are required, and an expansion of the Water Survey of Canada hydrometric network in the QEIs is encouraged.

(3) Variations in streamflow and water budgets between catchments and across islands deserve further attention, to better understand the processes controlling these patterns.

ACKNOWLEDGMENTS

This research was supported by the Natural Science and Engineering Research Council, Canada (individual grants to K.L. Young, M.J. Lafrenière, and S. Lamoureux) as well as grants from Arctic-Net NCE, the Federal Government of Canada International Polar Year Program. We are grateful for the excellent logistical support from the Polar Continental Shelf Program and the

Northern Student Training Program. We would like to thank our many students over the years who have diligently worked in the field to collect these data. We are inspired by their dedication and enthusiasm for the Canadian High Arctic.

REFERENCES

Abnizova, A., Miller, E.A, Young, K.L. & Shakil, S. Seasonal variability in hydrological and physico-chemical characteristics of small water bodies across a High Arctic wetland, Nunavut Canada. *Arct. Antarct. and Alpine Res*. Submitted April 20, 2013.

Abnizova, A., Young, K.L. & Lafrenière, M.J. 2012 Pond hydrology and dissolved carbon dynamics at Polar Bear Pass wetland, Bathurst Island, Nunavut. *Ecohydrol*., doi: 10.1002/eco.1323, published online Oct. 11, 2012.

Assini, J. & Young, K.L. 2012 Snowcover and snowmelt of an extensive High Arctic wetland: spatial and temporal seasonal patterns. *Hydrol. Sci. J.* 57(4), 738–755.

Braun, C., Hardy, D.R., Bradley, R.S. & Retelle, M.J. 2000 Streamflow and suspended sediment transfer to Lake Sophia, Cornwallis Island, Nunavut Canada. *Arctic and Alpine Res*. 32(4), 456–465.

Cogley, J.G. & McCann, S.B. 1976 An exceptional storm and its effects in the Canadian High Arctic. *Arctic Alpine Res*. 8, 105–110.

Derksen, C. & Brown, R. 2012 Spring snow cover and extent reduction in the 2008–2012 period exceeding climate model projections. *Geophys. Res. Lett*. 39, L19404, doi: 10.1029/2012GL053387.

Holmes, R.M., McClelland, J.W., Peterson, B.J., Tank, S.E., Bulygina, E., Eglinton, T.I., Gordeev, V.V., Gurtovaya, T.Y., Raymond, P.A., Repeta, D.J., Stapes, R., Striegl, R.G., Zhulidov, A.V. & Zimov, S.A. 2012 Seasonal and annual fluxes of nutrients and organic matter from large rivers to the Arctic Ocean and surrounding seas. *Estuar. Coast*. 35, 369–382, doi: 10.1007/s12237-011-9386-6.

Heron, R. & Woo, M.K. 1978 Snowmelt computations for a high arctic site. *Proc. of the 35th Eastern Snow Conference*, Hanover, New Hampshire, USA, 162–172.

Kane, D.L. Hinzman, L.D., Woo, M.K. & Everett, K.R. 1992 Arctic hydrology and climate change. In: *Arctic Ecosystems in a Changing Climate, An Ecophysiological Perspective*, Chapin III, F.S., Jefferies, R.L., Reynolds, J.F., Shaver, G.R., Svoboda, J. & Chu, E.W. (eds.), 35–55. Academic Press, New York USA.

Kane, D.L. & Yang, D. 2004 Overview of water balance determinations for high latitude watersheds. *IAHS Publ.* 290, 1–12.

Kane, D.L., Youcha, E.K. & Trochim, E.D. 2009 Estimating design flows for catchments in the Alaskan Arctic. *17th International Northern Research Basins Symposium and Workshop, Iqaluit-Pangnirtung-Kuujjuaq, Canada, August 12–18, 2009.*

Lamoureux, S.F, McDonald, D.M., Cockburn, J.M.H., Lafrenière, M.J., Atkinson, D.M. & Treitz, P. 2006 An incidence of multi-year sediment storage on channel snowpack in the Canadian High. *Arctic* 59(4), 381–390.

Lenaerts, J.T.M., van Angelen, J.H., van den Broeke, M.R., Garnder, A.S., Wouters, B. & van Meijaard, E. 2013 Irreversible mass loss of Canadian Arctic archipelago glaciers. *Geophys. Res. Lett.* 40, 870–874.

Lewis, T., Lafrenière, M.M. & Lamoureux, S.F. 2012 Hydrochemical and sedimentary responses of paired high arctic watersheds to unusual climate and permafrost disturbance, Cape Bounty, Melville Island, Canada. *Hydrol. Process*. 26, 2003–2018.

Marsh, P., Rouse, W.R. & Woo, M.K. 1981 Evaporation at a High Arctic site. *J. of Appl. Meteorol.* 20, 713–716.

McLaren, P. 1981 River and suspended sediment discharge into Byam Channel, Queen Elizabeth Islands, Northwest Territories, Canada. *Arctic* 34(2), 141–146.

McClelland, J.W., Stieglitz, M., Pan, F., Homes, R.M. & Peterson, B.J. 2007 Recent changes in nitrate and dissolved organic carbon export from the upper Kuparuk River, North Slope, Alaska. *J. Geophys. Res.-Biogeosci.* 112, G04S60, doi: 10.1029/2006JG000371.

McLeod, B. 2008 *The Influence of Snowcover Distribution and Variable Melt Regimes on the Transport of Nutrients from Two High Arctic Watersheds*. Unpublished MSc thesis, Department of Geography, Queen's University, pp. 157.

Priestley, C.H.B. & Taylor, R.J. 1972 On the assessment of surface heat flux and evaporation using large-scale parameters. *Mon. Weath. Rev*. 100, 81–92.

Raymond, P.A. McClelland, J.W., Homes, R.M., Zhulidov, A.V., Mull, K., Peterson, B.J. Striegl, R.G., Aiken, G.R. & Gurtovaya, T.Y. 2007 Flux and age of dissolved organic exported to the Arctic Ocean: A carbon isotopic study of the five largest arctic rivers. *Glob. Biogeochem. Cyc.* 21, GB4011, doi: 10.1029/2007GB002934.

Smith, S.L., Romanovsky, V.E. Lewkowicz, A.G., Burn, C.R., Allard, M., Clow, G.D., Yoshikawa, K. & Throop, J. 2010 Thermal state of permafrost in North America: A contribution to the International Polar Year. *Perm. and Perigl. Process*. 21, 117–135.

Smol J.P. & Douglas M.S.V. 2007a Crossing the final ecological threshold in high Arctic ponds. *Proc. of the Nat. Acad. of Sci.* 104, 12395–12397.

Smol J.P. & Douglas M.S.V. 2007b From controversy to consensus: making the case for recent climatic change in the Arctic using lake sediments. *Frontiers in Ecol. and the Environ*. 5, 466–474.

Spence C., Pomeroy, J.W. & Pietroniro, A. 2005 *Prediction in Ungauged Basins: Approaches for Canada's Cold Regions.* Canadian Water Resources Association. Cambridge.

Stewart, K.A. & Lamoureux, S.F. 2011 Connections between river runoff and limnological conditions in adjacent High Arctic lakes: Cape Bounty, Melville Island, Nunavut. *Arctic* 64(2), 169–182.

Stewart, R.B. & Rouse, W.R. 1976 Simple models for calculating evaporation from dry and tundra surfaces. *Arct. and Alp. Res*. 8(3), 263–276.

Tan, A., Adam, J.C. & Lettenmaier, D.P. 2011 Change in spring snowmelt timing in Eurasian Arctic rivers. *J. Geophys. Res.-Atmos*. 116, D03101, doi: 10.1029/2010JD014337.

Water Survey of Canada. Historical Hydrometric Data. Available online: www.wsc.ec.gc.ca. Last visited June 2013.

Wedel, J.H., Thorne, G.A. & Baracos, P.C. 1977 Site intensive hydrologic study of a small catchment on Bathurst Island. Hydrological regimes, Freshwater Project No. 1. Environment Canada, Inland Waters Directorate, Western and Central Region, Ottawa, Canada.

Woo M.K. 1983 Hydrology of a drainage basin in the Canadian High Arctic. *Ann. Assoc. Am. Geogr*. 73, 577–596.

Woo M.K. 1997 A guide for ground based measurement of the arctic snow cover. Canadian Snow Data CD, Meteorological Service of Canada, Downsview, Ontario.

Woo, M.K. 2000 McMaster River and Arctic hydrology. *Phys. Geog*. 21, 466–484.

Woo, M.K. 2012 *Permafrost Hydrology*. Springer, London.

Woo, M.K. & Young, K.L. 2004 Modelling arctic snow distribution and melt at the 1-km grid scale. *Nordic Hydrol*. 35(4), 295–307.

Woo, M.K. & Guan XJ. 2006 Hydrological connectivity and seasonal storage change of tundra ponds in a polar oasis environment, Canadian High Arctic. *Perm. & Perigl. Process*. 17, 309–323.

Young, M.K. 2008 Role of snow in the hydrology of a High Arctic riparian wetland. *Hydrol. Res*. 39(4), 277–286.

Young, K.L. & Woo, M.K. 2004a Queen Elizabeth Islands: water balance investigations. *IAHS Publ*. 290, 152–163.

Young, K.L. & Woo, M.K. 2004b Queen Elizabeth Islands: problems associated with water balance research. *IAHS Publ.* 290, 237–248.

Young, K.L. & Labine, C. 2010 Summer hydroclimatology of an extensive low-gradient wetland: Polar Bear Pass, Bathurst Island, Nunavut Canada. *Hydrol. Res*. 41(6), 492–502.

Young, K.L., Assini, J., Abnizova, A. & DeMiranda, N. 2010 Hydrology of hillslope-wetland streams, Polar Bear Pass, Nunavut, Canada. *Hydrol. Process*. 24, 3345–3358.

Young, K.L., Assini, J., Abnizova, A. & Miller, E. 2013 Snowcover and melt characteristics of upland/lowland terrain: Polar Bear Pass, Bathurst Island, Nunavut, Canada. *Hydrol. Res*. 44(1), 2–20.

Appendix 1. Detailed information on streamflow studies mentioned in text.

Basin	Area (km^2)	Location (Lat., Long.)	Years of Record	Source
Snowbird Ck.	61.1	76°N, 101°W	1977	Wedel et al. 1977
Whitebear Ck.	8.5	76°N, 101°W	1977	Wedel et al. 1977
Mecham River	86.8	74.7°N, 94.8°W	1971-1975 1977-1979 2011	Water Survey of Canada (www.wsc.ec.gc.ca
McMaster River	33	75°N, 95°W	1976-1981	Data courtesy of M.K. Woo
Allen River	448	74.8°N, 95.1°W	1971-1974 1977-1979	Water Survey of Canada (www.wsc.ec.gc.ca
Consett Head River	117	75.4°N, 105°W	1974	McLaren 1981

Symposium

Abstracts

River Flow Transformation Processes in the Lena River Delta, Russia

Nikolay I. Alekseevsky, Denis N. Aibulatov, Ludmila V. Kuksina*,
and Antonina A. Chetverova

Dept. of Hydrology, Faculty of Geography, Moscow State University, Moscow, 119991, RUSSIA
**Corresponding author's email: ludmilakuksina@gmail.com*

ABSTRACT

Water and sediments inflow to the Lena River delta is characterized by temporal variability in streamflow. Water flow fluctuations have three large cycles: low-water period (1938–1957); average-water period (1958–1987); and high-water period (1988–2006). In suspended sediment yield fluctuations, there are two periods: low (1967–1987) and high (1988–2004). Substantial flow transformation occurs downstream from the head of the delta. The main sediment transport is into the Trofimovsky and Bykovsky channels, and the minimum one is into the Oleneksky and Tumatsky channels. The maximum flow is in the direction of the Sardahsky channel. The Bykosvky and Trofimovsky channels are characterized by average conditions of streamflow. Flooding of the delta is typical where it fans out, and in the eastern part of the Lena River delta. The maximum width of the delta floodplain is 6–8 km. This area, which is situated closer to the delta sea edge, is flooded less than areas where the delta fans out. The Lena River delta is characterized by a decrease in water surface spectral radiance in the channels and, as a consequence, by a decrease of water turbidity, which is estimated at 20%–40% in the section from the delta channel sources to the river mouths. The maximum decrease of water turbidity characterizes the smallest channels. Significant decrease of turbidity in large channels occurs only in coastal waters. In the direction of the channels' deltas, dissolved-matter flow also changes. Depending on the type of chemical element, its content growth (or decrease or no change) has a connection with the conditional rivers' orders.

KEYWORDS

Lena River delta; substantial flow; transformation

Hydrological Analysis of Catchments in the National Petroleum Reserve – Alaska Prior to Petroleum Development

Christopher D. Arp[1*] and Matthew Whitman[2]

[1]*Water and Environmental Research Center, University of Alaska Fairbanks, Fairbanks, AK, USA*
[2]*Arctic Field Office, Bureau of Land Management, Fairbanks, AK, USA*
**Corresponding author's email: cdarp@alaska.edu*

ABSTRACT

The lands of the Arctic Coastal Plain (ACP) of northern Alaska are covered with thermokarst lakes and drained thermokarst lake basins (DTLB) set atop continuous permafrost and drained by beaded streams. Besides fundamental ecological services, this hydrologic landscape provides essential habitat for migratory waterbirds and fishes of importance for subsistence harvest as well as water supply for industrial activities. These hydrologic functions are particularly relevant in the National Petroleum Reserve – Alaska (NPR-A), where development needs to be carefully balanced with other societal values of arctic ecosystems. Here, we report on baseline hydrologic monitoring of five catchments in the northeastern NPR-A (Fish Creek Watershed) with planned oil development. Catchments range from 24 to 64 km^2 with average lake area of 20% and DTLB area of 38%, and have varying levels of planned development ranging from no roads or infrastructure (reference sites) to permanent roads, drilling pads, and lake water extraction. Discharge and climate monitoring from 2009–2011 shows that total annual runoff ranged from 35 to 69 mm, with an average runoff ratio of 0.38. Hydrograph separation indicated that average snowmelt runoff ratios were 0.55 and summer runoff ratios were 0.24, with considerable interannual and inter-catchment variability. Similar to observations in larger ACP watersheds, lake extent and particularly DTLB extent appear to determine spatial variability in runoff response. This suggests that future development activities that modify lake and DTLB storage and drainage processes should be carefully monitored to ensure adequate streamflow for summer fish passage and maintenance of overwintering habitat.

KEYWORDS

Arctic; hydrology; catchments; monitoring; development; lakes

Macrodispersion of Groundwater Contaminants in Discontinuous Permafrost

Michelle L. Barnes* and Dave L. Barnes

Water and Environmental Research Center, University of Alaska Fairbanks, Fairbanks, AK, USA
**Corresponding author's email: mlbarnes2@alaska.edu*

ABSTRACT

The objective of this study is to characterize the macrodispersion processes of groundwater contaminants in discontinuous permafrost. Permafrost acts as an impermeable barrier that impedes flow of groundwater and influences contaminant transport. Discontinuities in the permafrost yield the potential for interaction between the subpermafrost and the suprapermafrost waters such as upward and downward flow. The sulfolane plume site in North Pole, Alaska, a region characterized by discontinuous permafrost, has been selected as a case study. Sulfolane is a slightly polar, highly soluble compound with very low sorption properties. The preliminary findings of this study have aided regulatory and private agencies in understanding contaminant transport of the sulfolane plume and in configuring contaminant transport models. The atypical aspect ratio of the plume and the detection of sulfolane concentrations below the permafrost layer at depths up to 305 feet are indicative of macrodispersion processes. Data collected from monitoring wells in the North Pole region for sulfolane concentrations, stable isotopes, groundwater elevation, and temperature have been used to characterize the macrodispersion processes of groundwater contaminants in discontinuous permafrost. Fluctuations in groundwater elevation indicate surface water influence from both the Tanana River and the Chena Slough. Temperature profiles identify areas of potential discontinuities. Preliminary stable isotope analysis identifies a difference between subpermafrost and suprapermafrost waters, and has the potential to serve as an identifier of areas of discontinuities.

KEYWORDS

Discontinuous permafrost; groundwater; contaminant macrodispersion

Arctic Water Change: Limitations and Opportunities for Its Detection and Predictability

Georgia Destouni[1,2]

[1]*Department of Physical Geography & Quaternary Geology, Stockholm University, SWEDEN*
[2]*Bert Bolin Centre for Climate Research, Stockholm University, SWEDEN*
Corresponding author's email: georgia.destouni@natgeo.su.se

ABSTRACT

This study reports results from an interdisciplinary research project aiming to identify hot spots and knowledge gaps of hydrological change in the Arctic, and related knowledge advancement needs and opportunities. The aims have been addressed by interdisciplinary research in a suite of arctic studies, including benchmarking monitoring assessments, long-term hydroclimatic record interpretations, and model developments and applications. The main research questions and results include:

1. What are the main gaps in and needs for hydrological monitoring to detect Arctic change? The main findings are (a) that arctic river basins with the largest expected climatic changes have the most declining and least dense hydrological monitoring; and (b) that the generally large gaps and declines in arctic hydrological monitoring are particularly limiting for detection of changes in hydrological transport of climate-relevant substances, nutrients, and pollutants to the Arctic Ocean and permafrost-related hydrological and ecosystem changes.
2. What are the main drivers and impacts of hydroclimatic change in the Arctic? The main findings are that (a) not only glacial meltwater, but also glacier-independent river flow from the Pan-Arctic drainage basin to the Arctic Ocean has accelerated and may contribute considerably to sea level rise; (b) glacier-independent river flows have increased more than associated precipitation, likely due to water storage changes in permafrost and/or groundwater; and (c) permafrost thawing and associated changes in water availability, flow, and transport are detectable in hydrological monitoring records of arctic catchments, and are predictable by different available modeling frameworks.

KEYWORDS

Arctic catchments; hydroclimatic change; monitoring; modeling; permafrost hydrology; hydrological transport

Response of Water Bodies in the Northwest Part of Russia to Climate Changes and Anthropogenic Impacts

N. N. Filatov[1*], T. V. Efremova[1], A. P. Georgiev[1], L. E. Nazarova[1], N. I. Pal'shin[1], and L. A. Rukhovets[2]

[1]Northern Water Problems Institute, Karelia, RUSSIA
[2]St. Petersburg Institute of Economy and Mathematics, Russian Academy of Science, RUSSIA
**Corresponding author's email: nfilatov@rambler.ru*

ABSTRACT

The response of the hydrological regime and biota of different lakes of the northwest part of Russia to climate changes and anthropogenic impacts are investigated. Over the last 20 years, climate warming resulted in a shift of climatic seasons. In all water bodies of the region, the duration of the ice-free period, water temperatures, and "biological summer" period increased. The continuing tendency of warming should lead to transformation of the hydrological regime of medium- and small-sized dimictic lakes into monomictic and great reorganizations in their ecosystems. As a result of these changes, there is an increased share of thermophilic fish species in catches, while that of cold-resistant forms decreased. According to modeling, further warming may result in a decrease in plankton biomass, particularly during the autumn period. The dominant algal species in largest lakes (*Aulacosira islandica*) has an optimum of water temperature below 8°C. The water bodies of the region are characterized by more notable response of their ecosystems to variations in anthropogenic loading than to climate changes. An important issue is to provide the justification of rational use and conservation of water and biological resources in northern Russia under intense resource development in the Arctic and in subarctic regions.

KEYWORDS

Climate change; anthropogenic impact

The Interaction of Atmospheric, Hydrologic, Geomorphic, and Ecosystem Processes on the Arctic Coastal Plain

Larry D. Hinzman[1*], Cathy J. Wilson[2], Joel C. Rowland[2], Susan S. Hubbard[3], Margaret S. Torn[3], William J. Riley[3], Stan D. Wullschleger[4], David E. Graham[4], Liyuan Liang[4], Richard J. Norby[4], Peter E. Thornton[4], and Alistair Rogers[5]

[1]*International Arctic Research Center, University of Alaska, Fairbanks, AK, USA*
[2]*Los Alamos National Laboratory, Los Alamos, NM, USA*
[3]*Lawrence Berkeley National Laboratory, Berkeley, CA, USA*
[4]*Oak Ridge National Laboratory, Oak Ridge, TN, USA*
[5]*Brookhaven National Laboratory, Upton, NY, USA*
**Corresponding author's email: ldhinzman@alaska.edu*

ABSTRACT

The complex interplay of physical, chemical, and biological processes interacts to such a degree that it is not possible to understand future trajectories without developing more fully holistic perspectives of the complete system. The components of the Arctic are interrelated through a complex network of linkages, feedbacks, and multidependent interactions. Theoretically, a change in one variable in a part of the system can initiate a cascade of effects throughout the system, and these connections need to be understood and quantified to achieve a level of predictability. In arctic regions, the interactions of surface mass and energy fluxes are complicated by the presence of permafrost and the important role of microtopography. These both affect and are mediated by dynamic atmospheric, geomorphological, and ecosystem processes such as nonuniform snow distribution, lake formation and drainage, wetland succession, thermokarst and erosion, and hydrological dynamics highly variable on different temporal and spatial scales.

Especially in northern regions, soil moisture is important not only as a hydrological storage component, but also as a result of its strong influence on the hydrological cycle through controls on energy fluxes such as evaporative heat flux, phase change in thawing of permafrost, and effects on thermal conductivity. With projected increases in surface temperature and decreases in surface moisture levels that may be associated with global warming, it is likely that the active layer thickness will increase, leading to subtle but predictable ecosystem responses such as vegetation changes.

Spatially distributed model simulations are being conducted across a range of scales. Preliminary results indicate macro-topographic gradients greatly impact the importance of lateral versus vertical fluxes. Microtopographic differences affect the small spatial-scale differences in snow distribution, soil moisture, and runoff rates, but have less impact on flux direction. Permafrost in arctic regions exerts a significant influence on soil moisture through controls on snow cover, vegetation, and drainage, and through differential degradation due to inhomogeneous ground ice distribution. In relatively flat areas where the frozen layer is near the surface, the soil moisture contents are usually quite high. These areas have relatively high evapotranspiration and sensible heat transfer, but quite low conductive heat transfers due to the insulative properties of thick organic soils. As in more temperate regions, watershed morphology exerts strong controls on hydrological processes; however, unique to arctic watersheds are complications arising from

short-term active layer dynamics and longer-term permafrost dynamics. In permafrost lowlands, degradation of near-surface regularly and irregularly distributed ground ice may substantially enhance microtopographic gradients, impacting hydrologic flow. In addition, hydrologic flow patterns are seasonally highly variable due to strongly varying water supply and connectivity throughout the thaw season.

The Arctic, an area of low rainfall and evapotranspiration, is generally an area of abundant wet tundra, wetlands, ponds, and lakes. The limited precipitation is held near the surface. This situation is, in part, due to the presence of permafrost near the surface and where there is limited lateral flow due to modest topography. Vegetation also plays a role. Mosses tend to act as rectifiers, conducting heat to the atmosphere when it is cool and wet, and slowing heat uptake under warm, dry conditions when their thermal conductivity is lower. Shrubby vegetation can both increase the depth of snow and decrease the albedo and snow-free period compared with *graminoid* vegetation. Increases in the active layer depth can cause a lowering of the suprapermafrost water table. Sufficient increase in the active layer can cause thermokarst erosion, tending to drain surrounding areas, often increasing the decomposition rate of soil organic matter, and speeding the loss of carbon from the landscape.

The impact of increasing temperature and decreasing soil moisture on net ecosystem carbon flux is a complex interaction of nonlinear processes. Optimal water content for maximal soil respiration falls in intermediate soil water contents. Decreasing soil moisture can increase or decrease soil respiration, decomposition, and mineralization depending on the state of water content in the soil.

KEYWORDS
Permafrost hydrology; landscape evolution; thermokarst; arctic ecosystems; carbon dynamics

Sensitivity of Yukon Hydrologic Response to Climate Warming: A Case Study for Community and Sectoral Climate Change Adaptation

J. R. Janowicz[1*], J. W. Pomeroy[2], and S. Carey[3]

[1]*Water Resources Branch, Yukon Department of Environment, CANADA*
[2]*Centre for Hydrology, University of Saskatchewan, CANADA*
[3]*School of Geography and Earth Sciences, CANADA*
**Corresponding author's email: Richard.Janowicz@gov.yk.ca*

ABSTRACT

The climate of Yukon Territory has fluctuated considerably over the last century, with increasing temperatures and precipitation resulting in permafrost degradation. Studies have shown that climate change has produced alterations to the Yukon hydrological cycle. Annual peak streamflows within the last three decades have decreased within regions of significant permafrost, while winter low flows have increased. Breakup timing on major rivers has advanced by one week over the last century, while breakup severity has generally increased. There is also an apparent trend of increasing peak flows and water levels within Yukon's glacial regime. This study includes a detailed sensitivity assessment of hydrological response to climate warming and associated permafrost thawing using the Cold Regions Hydrological Model (CRHM) at the Wolf Creek research basin, followed by the application of CRHM to other Yukon regions and communities to provide the necessary climate warming sensitivity information to develop sectoral adaptation strategies. The sectors included in the study are mining, hydroelectric, transportation, oil and gas, agriculture, forestry, tourism and recreation, and municipal. Using a range of climate change scenarios, assessments have been carried out in Yukon's four hydrological regions. Model outputs include projected changes to magnitude, timing, and interaction of water balance components (precipitation, evapotranspiration, runoff, and storage). Projected changes to hydrological response (extreme and drought events, annual and seasonal flows) are summarized allowing for the development of adaptation strategies and options, which may include improving flood forecasting and warning systems, infrastructure design modification, land zoning changes, and changes to policy, regulation, and legislation.

KEYWORDS

Climate change scenarios; hydrologic response; water balance; Cold Regions Hydrological Model

Thermokarst Lake Change in Western Siberia: From Spatiotemporal Landscape Dynamics to Hydrological Reflections

Johanna Mård Karlsson[1,2*], Steve W. Lyon[1,2], and Georgia Destouni[1,2]

[1]*Department of Physical Geography & Quaternary Geology, Stockholm University, SWEDEN*
[2]*Bert Bolin Centre for Climate Research, Stockholm University, SWEDEN*
**Corresponding author's email: johanna.maard@natgeo.su.se*

ABSTRACT

Recent warming in the Arctic has triggered changes in the cryosphere, including warming and degradation of permafrost. These changes have a direct influence on the terrestrial hydrology of the Arctic and, more specifically, on the presence and distribution of thermokarst lakes in arctic regions, as such lakes are by definition tightly coupled to the existence and condition of subsurface permafrost. In this study, remotely sensed imagery was used to assess changes in both the size and size distribution of thermokarst lakes for three time periods within the Nadym (48,000 km^2) and Pur (95,100 km^2) River basins in western Siberia, aiming to understand landscape dynamics in a thermokarst lake-rich region. Results show variability in the size and distribution of thermokarst lakes within the two river basins. Over the three periods from 1973 through 1987–1988 to 2007–2009, there is clear predominance for size decrease in the smaller (<~50 ha) lakes relative to the larger lakes. The period between 1973 and 1987–1988 emerges as an intense phase, during which more and larger lakes experienced complete drainage compared with the period between 1987–1988 and 2007–2009. There is a latitudinal gradient in lake change such that lake areas decrease or lakes completely disappear with increasing latitudes. This dynamic nature of permafrost thawing and thermokarst lake development/drainage occurs concurrently with detectable hydrological change in this Siberian landscape, with smaller catchments exhibiting a stronger and clearer change signal than larger ones.

KEYWORDS

Permafrost; thermokarst lakes; hydrological cycles and budgets; catchments; climate change

An Assessment of Suspended Sediment Transport in Arctic Alaska Rivers

Erica Lamb[1*], Horacio Toniolo[1], Doug Kane[1], and William Schnabel[1]

[1]Water and Environmental Research Center, University of Alaska Fairbanks, Fairbanks, AK, USA
**Corresponding author's email: elamb3@alaska.edu*

ABSTRACT

Rivers of Arctic Alaska have hydrologic and sedimentologic regimes that can differ dramatically from those of temperate rivers. Long, severe winters and the presence of permafrost affect the dynamic of rivers that can be frozen for over seven months of the year. In addition, the majority of spring runoff may occur while ice is still present in the river channel, producing sediment transport patterns and overall sediment yields that can differ from expected values. A lack of data in this region that is temporally or spatially dense, as well as remote and difficult research conditions, compounds the problem of being able to fully assess the suspended sediment regimes of Arctic Alaska rivers. The Anaktuvuk, Itkillik, and Chandler Rivers originate in the Brooks Range of Alaska and flow north, joining with the Colville River in the foothills and coastal plain. With an increasing human presence in all three watersheds, it has become imperative to study these rivers and increase our understanding of sediment transport in the Arctic, as well as the unique controls on sediment transport that exist in these northern watersheds. To meet this goal, a field campaign was conducted over two summers, with suspended sediment samples collected at regular intervals on all three rivers. Sampling techniques included automated Isco samplers, depth integrated samplers, and bed sediment distribution measurements as well as numerous discharge measurements for correlation. Suspended sediment concentration (SSC) rating curves developed for the Anaktuvuk and Chandler Rivers over the two-year study period revealed a strong correlation between SSC and discharge. Suspended sediment discharge was also analyzed, showing that over 90% of suspended sediment transport occurred during the spring melt period for the flow year in 2011.

KEYWORDS

Arctic Alaska rivers; suspended sediment yield; sediment transport patterns

Greenland Freshwater Runoff. Part I: A Runoff Routing Model for Glaciated and Nonglaciated Landscapes (HydroFlow)

Glen E. Liston[1*] and Sebastian H. Mernild[2]

[1]Cooperative Institute for Research in the Atmosphere, Colorado State University, Fort Collins, CO, USA
[2]Glaciology and Climate Change Laboratory Center for Scientific Studies/Centro de Estudios Cientificos (CECs), Valdivia, CHILE
**Corresponding author's email: glen.liston@colostate.edu*

ABSTRACT

A gridded linear-reservoir runoff routing model (HydroFlow) was developed to simulate the linkages between runoff production from land-based snow and ice melt processes and the associated freshwater fluxes to downstream areas and surrounding oceans. HydroFlow was specifically designed to account for glacier, ice sheet, and snow-free and snow-covered land applications. Its performance was verified for a test area in southeast Greenland that contains the Mittivakkat Glacier, the local glacier in Greenland with the longest observed time series of mass-balance and ice-front fluctuations. The time-evolution of spatially distributed grid-cell runoffs required by HydroFlow were provided by the SnowModel snow-evolution modeling system, driven with observed atmospheric data, for the years 2003 through 2010. The spatial and seasonal variations in HydroFlow hydrographs show substantial correlations when compared with observed discharge coming from the Mittivakkat Glacier area and draining into the adjacent ocean. As part of its discharge simulations, HydroFlow creates a flow network that links the individual grid cells that comprise the simulation domain. The collection of networks that drain to the ocean produced a range of runoff values that varied most strongly according to catchment size and percentage and elevational distribution of glacier cover within each individual catchment. For 2003–2010, the average annual Mittivakkat Glacier region runoff period was 200±20 days, with a significant increase in annual runoff over the 8-year study period, both in terms of the number of days (30 d) and in volume (54.9 × 106 m3).

KEYWORDS

Runoff routing model; HydroFlow; snow; Greenland

Interactions between Vegetation, Snow, and Permafrost Active Layer

Philip Marsh[1*], Xiaogang Shi[1], Stefano Endrizzi[2], Jennifer Baltzer[3], and Trevor Lantz[4]

[1]*National Hydrology Research Centre, Environment Canada, Saskatoon, SK, CANADA*
[2]*University of Zurich, Zurich, SWITZERLAND*
[3]*Wilfrid Laurier University, Waterloo, ON, CANADA*
[4]*University of Victoria, Victoria, BC, CANADA*
**Corresponding author's email: philip.marsh@outlook.com*

ABSTRACT

The proliferation of tall shrubs across Arctic tundra ecosystems has been well documented. However, our ability to model resulting changes in snow, permafrost, and hydrology is limited, especially where the development of shrub patches is expected to dominate shrub expansion. This paper will report a combination of field observations and modeling that investigate the role of shrub patches on snow accumulation and melt, and active layer thickness and therefore water storage and runoff. Field observations were carried out at a single shrub patch, approximately 50 m across, in the Trail Valley Creek research basin located 50 km north of Inuvik, NWT. Observations include end of summer frost table depth, and snow depth and density over the winter of 2012 and 2013. Modeling will utilize the GEOtop hydrological model, linked to a blowing snow model. Preliminary observations show that (1) the shrub patch results in increased snow depths, with snow over 1.5 m deep in the centre of the shrub patch compared with less than 0.5 m away from the shrubs; (2) the active layer depth is also deeper in the centre of the shrub patch with depths of approximately 1 m, versus less than 0.5 m away from the shrubs; and (3) the centre of the shrub patch is topographically lower than outside the patch, suggesting that active layer deepening has resulted in ground subsidence. GEOtop will be used to explore the interrelated factors of shrub occurrence, snow accumulation and melt, surface energy balance, and active layer formation.

KEYWORDS

Snow; permafrost; hydrology; shrubs

Greenland Freshwater Runoff. Part II: Distribution and Trends, 1960–2010

Sebastian H. Mernild[1*] and Glen E. Liston[2]

[1]*Glaciology and Climate Change Laboratory Center for Scientific Studies/Centro de Estudios Cientificos (CECs), Valdivia, CHILE*
[2]*Cooperative Institute for Research in the Atmosphere, Colorado State University, Fort Collins, CO, USA*
**Corresponding author's email: smernild@gmail.com*

ABSTRACT
Runoff magnitudes, the spatial patterns from individual Greenland catchments, and their changes through time (1960–2010) were simulated in an effort to understand runoff variations to adjacent seas and to illustrate the capability of SnowModel (a snow and ice evolution model) and HydroFlow (a runoff routing model) to link variations in terrestrial runoff with ocean processes and other components of Earth's climate system. Significant increases in air temperature, net precipitation, and local surface runoff lead to enhanced and statistically significant Greenland ice sheet (GrIS) surface mass balance (SMB) loss. Total Greenland runoff to the surrounding oceans increased 30%, averaging 481±85 km^3 yr-1. Averaged over the period, 69% of the runoff to the surrounding seas originated from the GrIS, and 31% came from outside the GrIS from rain and melting glaciers and ice caps. The runoff increase from the GrIS was due to an 87% increase in melt extent, 18% from increases in melt duration, and a 5% decrease in melt rates (87%+18%+5=100%). In contrast, the runoff increase from the land area surrounding the GrIS was due to a 0% change in melt extent, a 108% increase in melt duration, and an 8% decrease in melt rate. In general, years with positive Atlantic multidecadal oscillation (AMO) index equaled years with relatively high Greenland runoff volume and vice versa. Regionally, runoff was greater from western than eastern Greenland. Since 1960, the data showed pronounced runoff increases in west Greenland, with the greatest increase occurring in the southwest and the lowest increase occurring in the northwest.

KEYWORDS
Greenland; ice sheet and glaciers; runoff; modeling; SnowModel/HydroFlow; climate change and AMO

Climatic Redistribution of Canada's Western Water Resources (CROCWR)

T. D. Prowse[1*], B. R. Bonsal[2], D. H. Burn[3], Y. B. Dibike[1], T. Edwards[4], R. Ahmed[1], A. J. Bawden[3], H. C. Linton[1], B. W. Newton[1], and G. S. Walker[1]

[1]*Water and Climate Impacts Research Centre, Environment Canada and University of Victoria, Victoria, BC, V8W 3R4, CANADA*
[2]*National Hydrology Research Centre, Environment Canada, Saskatoon, SK, S7N 3H5, CANADA*
[3]*Civil & Environmental Engineering, University of Waterloo, Waterloo, ON, N2L 3G1, CANADA*
[4]*Earth and Environmental Sciences, University of Waterloo, Waterloo ON, N2L 3G1, CANADA*
**Corresponding author's email: terry.prowse@ec.gc.ca*

ABSTRACT

The recent IPCC "Climate Change and Water" technical report stresses that future climate will accelerate the hydrologic cycle. For some regions, this will mean enhanced access to water resources, but because the effects will not be spatially uniform, other regions will have reduced access. In simplest terms, accessibility can be gauged by changes in precipitation or flow patterns, both of which have already significantly changed over the last few decades and are projected to experience more change in the near future. Most such analyses have been conducted at relatively coarse-resolution spatial scales, but do show strong gradients in North America and for Canada, particularly in the west—an area of highly contrasting hydroclimatic regimes. In addition to spatial redistribution of water resources, a temporal redistribution is projected to occur, most significantly at the seasonal scale. In recognition of a need to conduct more detailed and higher-resolution assessments of such water redistribution that makes the results more useable by water managers and policy makers, a multicomponent integrated study entitled CROCWR (Climatic Redistribution of Canada's Western Water Resources) was initiated. This study focuses on (a) the rationale for initiation of CROCWR; (b) its major analytical components including trends in controlling atmospheric patterns and conditions, surface hydroclimatology, and regional flow patterns; and (c) some of the integrated preliminary results. Of particular interest is the trend for higher-latitude regions to become "water-rich" in contrast to middle-southern latitudes becoming more "water-poor." Discussion focuses on the potential implications of such a north–south contrast.

KEYWORDS

Climate; water resources; western Canada; hydrology; redistribution

Permafrost Thaw Induced Changes to Surface Water Systems: Implications for Streamflow

W. L. Quinton[1*] and J. L. Baltzer[2]

[1]*Centre for Cold Regions and Water Science, Wilfrid Laurier University, CANADA*
[2]*Department of Biology, Wilfrid Laurier University, CANADA*
**Corresponding author's email: wquinton@wlu.ca*

ABSTRACT

This study was conducted in the wetland-dominated southern margin of continental permafrost at Scotty Creek, NWT, Canada, over the period 2001–2010. In this region, permafrost is discontinuous and occurs predominately below tree-covered peat plateaus. The southern margin of continental permafrost is experiencing unprecedented rates of permafrost thaw, yet the effect of this thaw and the resulting ecosystem changes on northern water resources are poorly understood. The objectives of this study are to (a) demonstrate changes in annual stream runoff in the lower Liard River valley; (b) propose a new conceptual framework for describing the flow and storage of water in peat plateau-bog-fen complexes that dominate the southern margin of discontinuous permafrost; c) estimate primary runoff from the plateaus using the Cold Regions Hydrological Model and relate to basin runoff; and (d) evaluate the impact of changing primary runoff of basin discharge. A distinction between primary and secondary runoff pathways that supply the basin drainage networks was identified and incorporated into a new conceptual model that describes the flow and storage of water in the wetland-dominated terrains at the southern margin of permafrost. A strong, positive correlation between primary runoff from plateaus and basin discharge was demonstrated, indicating that with the representation of other flow and storage processes, such secondary runoff, and the routing of water through connected bogs and channel fens, hydrograph simulation for basins with thawing permafrost plateaus is attainable.

KEYWORDS

Permafrost thaw; peatlands; streamflow; ecohydrology

The Ecohydrology of Thawing Permafrost Plateaus

W. L. Quinton[1*] and J. L. Baltzer[2]

[1]*Centre for Cold Regions and Water Science, Wilfrid Laurier University, CANADA*
[2]*Department of Biology, Wilfrid Laurier University, CANADA*
**Corresponding author's email: wquinton@wlu.ca*

ABSTRACT

The southern margin of permafrost is experiencing unprecedented rates of thaw, yet the effect of this thaw on northern water resources is poorly understood. The hydrology of the active layer on a thawing peat plateau in the wetland-dominated zone of discontinuous permafrost was studied at Scotty Creek, Northwest Territories (Canada), from 2001 to 2010. Two distinct and seasonally characteristic levels of unfrozen moisture were evident in the 0.7 m active layer. Overwinter moisture migration produced a zone of high ice content near the ground surface. The runoff response of a plateau depends on which of the three distinct zones of hydraulic conductivity the water table is displaced into. The moisture and temperature of the active layer steadily rose with each year, with the largest increases close to the ground surface. Permafrost thaw reduced subsurface runoff by (1) lowering the hydraulic gradient, (2) thickening the active layer, and, most importantly, (3) reducing the surface area of the plateau. By 2010, the cumulative permafrost thaw had reduced plateau runoff to 47% of what it would have been had there been no change in hydraulic gradient, active layer thickness, and plateau surface area over the decade.

KEYWORDS

Permafrost thaw; ecohydrology; peatlands; boreal

Meteorology for Hydropower Production Scheduling

Knut Sand[1*] and Thor Erik Nordeng[2]

[1]*Statkraft Energi AS, NORWAY*
[2]*The Norwegian Meteorological Institute, NORWAY*
**Corresponding author's email: knut.sand@statkraft.com*

ABSTRACT

More than 95% of all energy production in Norway originates from hydropower. High-quality inflow forecasting is therefore important for production planning of hydropower and marked operation. In order to improve inflow forecasting for hydropower reservoirs, both for the short and long term, Statkraft has recently completed a three-year strategic research and development program in cooperation with the Norwegian Meteorological Institute. For short-term forecasting, a new method has been developed for estimation of probability distribution for precipitation in catchments with Norwegian (rugged) topography with resolution of 1–4 km^2. Also, tests have been performed of different snow algorithms applied in the coupled HARMONIE-SURFEX model (atmosphere-land model). Long-term forecasting is based on stochastic modeling. Long historical records of temperature and precipitation are crucial in order to estimate the statistical range for reservoir inflow. A considerable effort has been made to reconstruct digital precipitation and temperature data back to 1930 over selected parts of Norway. In addition, a study of predictability of seasonal (3 months) forecasts for temperature, air pressure, and precipitation has been carried out. This study concluded that significant predictability was found in the seasonal forecasts for temperature and pressure, but not as much for precipitation. Another focus of the program has been on how to deal with future climate scenarios in hydrological modeling. This project has included studies of bias correction methods for RCM data, estimation of uncertainty of runoff scenarios, a classification framework for weather types, and which GCM/RCM combinations give the best results for estimation of runoff.

KEYWORDS

Hydropower; meteorology; hydrology; forecasting

Delineation of Snow Patterns in Northern Alaska

Anna M. Wagner[1*], Christopher A. Hiemstra[1], and Matthew Sturm[2]

[1]*Cold Regions Research and Engineering Laboratory (CRREL), Fairbanks, AK, USA*
[2]*University of Alaska Fairbanks, Fairbanks, AK, USA*
**Corresponding author's email: Anna.M.Wagner@usace.army.mil*

ABSTRACT

Deep and shallow areas of snow repeat from year to year due to perennial, reliable, consistent interactions among topography, vegetation, and weather. While mean snow depth varies from year to year, relative differences remain fixed in most landscapes. If snow patterns can be consistently identified, understood, and classified using observations, remote sensing, and models, an untapped potential exists to expand and improve the accuracy of snowpack assessments. As part of the SnowNet project (http://ipysnow.net/), snow depths have been measured annually from 2010 to present at three different scales (1 km^2 to 21 km^2) just north of the Brooks Range in Alaska. A total of about 17,000 snow measurements were taken in 2010, and the number of measurements culminated in 2012 at 32,000. Over the same area, coincident snowmelt sequences from satellite imagery (e.g., Worldview 2, Quickbird, Geoeye, Landsat) were also collected. Snow distribution modeling using SnowModel, a distributed snow accumulation and ablation model, was also performed. Observations, imagery, and simulations show the repeatability of snow patterns at all scales. The spatial match between modeled (SnowModel) snow and the satellite imagery during snowmelt in spring is remarkable. Our results indicate that snow patterns represent a promising technique for understanding and predicting snow cover distributions to a much greater degree than what is being used to date.

KEYWORDS

Snow patterns; snow modeling; remote sensing

Winter Low Flow in the Mackenzie River Basin

Ming-ko Woo* and Robin Thorne

School of Geography and Earth Sciences, McMaster University, CANADA
**Corresponding author's email: woo@mcmaster.ca*

ABSTRACT

Winter low flow of northern rivers refers to the diminished discharge occurring between the time of rapid flow reduction in the freeze-up period and the arrival of spring freshet when the flow takes an abrupt rise. Owing to the large extent of the Mackenzie River basin (area 1.8 million km^2) in Canada, the duration of winter low flow season as defined (i.e., between freeze-up and breakup) varies considerably within the basin, and November to March is here considered as the winter flow season to give a common time frame that enables between-basin comparison. Several hydroclimatic conditions influence winter flows to varying degrees. The presence of snow and ice cover decouples river flow processes from atmospheric water gains and losses, and the formation of river ice increases channel storage at the expense of discharge. Groundwater sustains baseflow, and outflow released from lake storage can considerably augment winter flow below large lakes. Streamflow generally increases down the river as more water is gathered from an enlarged drainage network. The discharge from Williston Lake reservoir, regulated for hydropower generation, eliminates winter low flow along the Peace River and the effect propagates down the Mackenzie River basin. The flow of the Peace accounts for about 40% of total winter flow of the Mackenzie River.

KEYWORDS

Low flow; groundwater discharge; lake storage; river ice; regulated flow; Mackenzie River